CONVECTIVE FLOW AND HEAT TRANSFER ANALYSIS BY USING THERMAL LATTICE BOLTZMANN METHOD

Ph.D. THESIS

by

GANGAWANE KRUNAL MADHUKAR

DEPARTMENT OF CHEMICAL ENGINEERING
INDIAN INSTITUTE OF TECHNOLOGY ROORKEE
ROORKEE – 247 667 (INDIA)
DECEMBER, 2014

CONVECTIVE FLOW AND HEAT TRANSFER ANALYSIS BY USING THERMAL LATTICE BOLTZMANN METHOD

A THESIS

Submitted in partial fulfilment of the requirements for the award of the degree of

DOCTOR OF PHILOSOPHY

in

CHEMICAL ENGINEERING

by

GANGAWANE KRUNAL MADHUKAR

DEPARTMENT OF CHEMICAL ENGINEERING
INDIAN INSTITUTE OF TECHNOLOGY ROORKEE
ROORKEE – 247 667 (INDIA)
DECEMBER, 2014

INDIAN INSTITUTE OF TECHNOLOGY ROORKEE
ROORKEE

CANDIDATE'S DECLARATION

I hereby certify that the work which is being presented in this thesis entitled "**CONVECTIVE FLOW AND HEAT TRANSFER ANALYSIS BY USING THERMAL LATTICE BOLTZMANN METHOD**", in partial fulfilment of the requirements for the award of the Degree of Doctor of Philosophy and submitted in the Department of Chemical Engineering of the Indian Institute of Technology Roorkee is an authentic record of my own work carried out during a period from **July, 2010 to December, 2014** under the supervision of Prof. Surendra Kumar, *Emeritus Fellow* and Dr. Ram Prakash Bharti, *Assistant Professor*, Department of Chemical Engineering, Indian Institute of Technology Roorkee.

The matter presented in this thesis has not been submitted by me for the award of any other degree of this or any other Institute.

(GANGAWANE KRUNAL MADHUKAR)

This is to certify that the above statement made by the candidate is correct to the best of our knowledge.

(Ram Prakash Bharti)
Supervisor

(Surendra Kumar)
Supervisor

Date: 07.04.15

The Ph.D. Viva-Voce Examination of **Mr. Gangawane Krunal Madhukar**, Research Scholar, has been held on **April 7, 2015**.

Chairman, SRC

Signature of External Examiner

This is to certify that the student has made all the corrections in the thesis.

07/04/15
Signature of Supervisors

Head of the Department

Acknowledgments

It is a great pleasure to thank many peoples who have been part of my education as teachers, friends and colleagues and made this thesis possible.

It is difficult to overstate my gratitude to my Ph.D thesis supervisors, Professor Surendra Kumar and Dr. Ram P. Bharti. I would like to express my deep and sincere gratitude to them for their invaluable support, suggestions, guidance, freedom, encouragement and infinite patience throughout this thesis work. I cannot forget their kind help and cooperation in bringing me to this position. Their teachings and advices were indispensable for whatever I have been able to do today.

I express my deep sense of gratitude to Dr.(Mrs.) Shashi, Associate Professor, Chemical engineering department, IIT Roorkee for her guidance, encouragement and support.

I wish to thank to Mr. Harikrishnan Narayanan for useful discussions in understanding basics of C++ programming language.

My gratitude to my lab-mates, Dr. Mohd. Danish, Dr. Mohd. Jaffar,Dr. (Mrs.) Nisha Katiyar, Deepak Sahu, Sathyanarayan Murthy, Brajesh Kumar, Yogendra Pal, Payal, Ashutosh Mugdil for friendly working environment in lab and making my experience something, which I will cherish forever.

Special thanks to all my friends for helping me through difficult times, and for all their emotional support entertainment and caring they provided. I feel fortunate to have support of them with me and making my stay at IIT Roorkee, a memorable. I would never forget the company of you all. Thank you PhD group (Anil, Partha, Ravikant, Nilambar, Soumitra, Amit Sir, Vinod, Vijay), M.Tech group (Anand, Bhalchandra, Praful, Sujit). I thank you all, whom I could not mention at this time, anonymously.

I would also like to thank, Ms. Swati Sabale (Pune) for her immense care, help and support, without it I would have been lost.

I wish to thank Department of Chemical Engineering for providing me opportunity to carry out my research work and to use the departmental facilities. My sincere thanks to MHRD for providing me the institute fellowship for completing this thesis.

Above all, I thank the Almighty for giving me the strength to bear the hardships during the difficult phases of the work.

Finally, I would like to express my reverence and great admiration for my parents and family, to whom I owe everything. They have been all the strength, inspiration and guiding force for all my life and I have tried to meet their expectations.

Most of people do not stop to read the acknowledgement, since you did, Thanks to you.

(Krunal M. Gangawane)

ABSTRACT

Over the years, great extent of research efforts are devoted towards the investigation of hydrodynamic characteristics of thermally driven flows and transport processes, due to their fundamental and pragmatic significance. Thermally (or buoyancy) driven flows are widely encountered in diverse fields of nuclear reactor systems, meteorology, geophysics, energy storage and conservation, fire control, and chemical, food, and metallurgical industries, as well as in the conventional fields of the fluid and heat transfer processes (Roy and Basak, 2005).

Among others, investigation of natural convection heat transfer in closed, as well as open, ended cavities is considered as an important research field due to the wide ranges of the industrially important applications namely chemical vapor deposition (Spall, 1996), cooling devices in electronic equipment (Bilgen and Muftuoglu, 2008; Hsu and Wang, 2000; Du et al., 1998), polymer and material processing (Hsiao, 2007; Habib et al., 2005), solar collectors (Hobbi and Siddiqui, 2009), electronic card arrays (Manca and Nardini, 2010) and domestic refrigerators, oven (Skok et al., 1990). It is not to be mentioned that the flow and heat transfer in cavity is also considered as one of the bench marking problem in the development and testing of numerical and computational fluid dynamics solver. An ideal representation of natural convection heat transfer is generally based on the thermal conditions on the cavity walls, i.e., one wall maintained isothermally at higher temperature while other walls are either kept isothermally at lower temperature or maintained adiabatically or open to the ambient. In chemical and process industries, however, such ideal conditions deviate due to the practical and measurement limitations and they, in turn, leads to the non-linear heating/cooling of the cavity walls. It, therefore, necessitates the investigation of the partially/non-linearly heated cavities and their influences on the natural convection characteristics. In spite of their wide occurrence in the ranges of practical/industrial applications, very limited results are available for cavity having varied

combinations of partial heating arrangements (Varol et al., 2008; Aghajani Delavar et al., 2011; Sankar et al., 2011; Nikbakhti and B., 2012; Jmai et al., 2013). Thus, in this work, an attempt have been made to fulfill the gap available in literature for convective heat transfer in enclosures. The natural convection heat transfer in enclosure (closed as well as open ended) is, therefore, studied herein for laminar range of Rayleigh number (heat intensity parameter for buoyancy driven flows), Prandtl numbers, heating size and locations. Further attempts are also made to investigate the magneto-hydrodynamic (MHD) effects on natural convection heat transfer in partially heated square cavity.

Similarly, the flow and heat transfer across bluff bodies in particular cylinders and spheres, is considered as one of the fundamental as well as classical problem in the area of fluid mechanics. Owing to its fundamental and practical significance, the flow across bluff bodies (cylinder of circular and non-circular cross-sections and spheres) have been explored well over the centuries, for instance, see (Zdravkovich, 1997a,b; Chhabra, 1996, 1999; Dhiman et al., 2006a,b, 2007; Bharti et al., 2007). The review of the available literature suggests that the flow across circular cylinders have been explored in greater details in comparison of rectangular cylinders (**?**Sharma and Eswaran, 2005; Dhiman, 2006; Bharti et al., 2007; Dhiman et al., 2007; Sahu, 2010), etc. It is, however, greatly acknowledged that the flow characteristics of square cylinders, i.e., gross engineering parameters such as drag coefficient, Nusselt number, wake size, etc., are often used in the designing of cooling towers, antennas, chimneys, support structures, high rise buildings, etc (Chatterjee et al., 2009; Sharma et al., 2012). Though reasonable amount of information is available for flow past bluff bodies other than circular cylinder, it is neither extensive and comprehensible. The available literature encompasses the influence of wall blockage on flow and thermal characteristics have been explored, but for the limited range of blockage ($\beta \leq 1/8$) and/or aspect ratio ($AR \leq 6$). The present work aims to extend the literature knowledge for the wide ranges of both blockage and aspect ratios of a rectangular cylinder. In particular, the influences of wall blockage and aspect ratio on forced convection flow and heat transfer from rectangular cylinders have been investigated numerically for the wide ranges of the flow governing parameters.

Over the past decades, the lattice Boltzmann method (LBM) has been established as a promising numerical tool of computational fluid dynamics (CFD) for solving various problems of complex fluid flows and heat transfer. The lattice Boltzmann method has derived from Boolean variables based lattice gas automata (LGA). It is, therefore, considered as an alternative numerical tool to conventional CFD numerical tools, which are based on the macroscopic continuum equations (Mishra et al., 2005; Mishra and Roy, 2007; Mishra

et al., 2008; Mondal and Mishra, 2009). The lattice Boltzmann method basically solves a kinetic and discrete velocity based Boltzmann equation (in statistical physics) (Succi et al., 1989; Chen and Doolen, 1998). The LBM has been successfully applied in the varieties of complex fluid flows involving porous structures (Succi et al., 1989; Kao et al., 2007), magneto-hydrodynamic (Chen et al., 1991a; Sheikholeslami et al., 2012), non-Newtonian rheology Delouei et al. (2014); Nazari and Ramzani (2014), reaction-diffusion (Dawson et al., 1993), diffusion-dispersion (Mohamad et al., 2009), suspension flows (Sankaranarayanan et al., 2002), compressible flows (Yu and Zhao, 2000), multiphase flows (Chen et al., 1991b), nanotube effect (Jafari et al., 2014) etc. The advantages of the LBM are simplicity of coding and algorithm, ease in application of boundary conditions (thus, suitable for complex fluid flow problems), ease of parallel computing, an adroitness estimation of pressure field as compared to conventional CFD tools, etc (Chen and Doolen, 1998).

Keeping in mind the simplicity and efficiency, aforementioned investigations have been carried out by using lattice Boltzmann method (LBM) based computational flow solver, developed in C++ programming language in the present work. The flow and thermal field in LBM can be simulated by using three approaches, viz., multispeed, double distribution function (DDF) approach and passive scalar (or simplified DDF). In the present work, passive scalar- thermal lattice Boltzmann method (PS-TLBM) based on simplified double distribution function model (He et al., 1998; Peng et al., 2003b) is used to solve field equations.

The basic validation of the present LBM code is ascertained through the standard benchmark problems of 2D lid driven cavity (Ghia et al., 1982b) and flow between parallel walls. For validation of flow through channel, the comparison of analytical solution of the fully developed velocity profile along vertical axis of channel is carried out. The comparison of present results with available for both cases shows close agreement, thus lending the credibility in the reliability and accuracy of the numerical results developed by in-house LBM code.

Further, optimum grid size is chosen by carrying out grid independence for all considered problems herein. For the problems of flow past a rectangular cylinders, the proper choice of domain parameters (upstream length, downstream length, etc.) is very important as it has influence on the accuracy of the solution. Thus, systematic study is carried out for the selection of these parameters.

In this work, the extensive results elucidating the influence of flow governing parameters on the local and global flow and thermal characteristics of flow problems (briefed in

TABLE 1: Flow problems considered in this work with their ranges of parameters.

Sr. No.	Problem	Physical parameters
1.	Differentially heated cavity*	$0.71 \leq Pr \leq 100$ $10^4 \leq Ra \leq 10^6$
2.	Partially-differentially heated cavity*	$10^4 \leq Ra \leq 10^6$ $Pr = 0.71; \quad L_h = L_c = 1/2$
3.	Magneto-hydrodynamic partially heated cavity*	$Pr = 1; \quad 10^3 \leq Ra \leq 10^5$ $0 \leq Ha \leq 120; \theta = 0^o, 45^o, 90^o$ $1/6 \leq L_c \leq 1; \quad L_h = 1/2$
4.	Partially heated open ended cavity*	$0.71 \leq Pr \leq 7; \quad 10^3 \leq Ra \leq 10^6$ L_l=Middle, top, bottom $L_h = 1/4, 1/2, 3/4$
5.	Square cavity with built-in heated square block*	$0.71 \leq Pr \leq 10$ $10^4 \leq Ra \leq 10^6$ $H_s = 0.15H$
6.	Flow past rectangular cylinder#	$5 \leq Re \leq 40; \quad 1/8 \leq \beta \leq 1/20$ $Pr = 1; \quad AR = 1, 2, 4, 6$

**: Natural convection, #: Forced convection, θ: Angle of magnetic field, L_l : Heating location, L_h : Heater size, AR: aspect ratio of rectangular cylinder (width/height), $\beta(b/H)$: Blockage ratio, b: side of square, H: Height of channel, H_s: height of square cylinder*

next paragraphs) are obtained by using the in-house developed PS-TLBM solver. In particular, dependence of local characteristics (streamlines, vorticity, pressure, isotherm profiles) and gross engineering parameters (individual and total drag coefficients, local and average Nusselt numbers, etc.) on the flow and geometrical parameters (Reynolds number, Rayleigh number, Prandtl number, heater and cooler size, heating location, Hartmann number etc.) are presented. The ranges of conditions used in various problem is detailed in Table 5.1.

A brief description of the problems considered herein is presented below.

1. Natural convection in differentially heated square cavity: Effect of Prandtl and Rayleigh numbers

The influence of wide range of Prandtl numbers on natural convective heat transfer in differentially heated closed cavity have been elucidated by using thermal lattice Boltzmann method (TLBM) for laminar range of Rayleigh number. Natural convection effect increases with the increase in Prandtl number (Pr) for all values of the Rayleigh number (Ra) due to the increasing dominance of viscous forces over the inertial forces. As thermal diffusion is inversely proportional to Prandtl number, velocity is more diffused than thermal energy. The average Nusselt number (dimensionless heat transfer coefficient) of

isothermal wall is seen to increase with increasing value of both the Prandtl and Rayleigh numbers.

2. Natural convection in partially-differentially-simultaneously heated/cooled square cavity

The influence of one wall of cavity exposed to contrast (i.e., both hot and cold) thermal conditions on natural convective heat transfer have been explored. The one wall of cavity is equally exposed to hot and ambient conditions and other wall exposed to ambient. The flow governing parameters used for numerical experimentation are Rayleigh number in laminar range with heater size, $L_h = \frac{1}{2}$ with air ($Pr = 0.71$) as a working fluid. The results indicated the formation of convection cell near lower part of mixed heated wall of cavity is observed for $Ra \geq 10^4$, as low temperature fluid retained in that region. The size of convection cell increases with the increase in Rayleigh number (Ra). The average Nusselt number ($\overline{Nu}$) and overall Nusselt number ($\widehat{Nu}$) value show linear increase with Rayleigh number.

3. Magneto-hydrodynamic natural convection in partially heated square cavity

In this problem, the influence of cooler size, Hartmann number, Rayleigh number and angle of magnetic field direction on natural convection heat transfer in differentially as well as partially heated cavity is elucidated. The cavity considered is partially heated at middle location ($1/4 \leq L_h \leq 3/4$) at one wall while other wall is partially cooled for different cooling length (L_c). The other part of vertical walls except heated/cooled are kept at adiabatic thermal condition. The top and bottom walls are also maintained adiabatically. It is observed that temperature contours move towards partially heated wall, which increases the temperature gradients, hence, enhancing the rate of heat transfer (average Nusselt number values). Also the rate of heat transfer increases with both Hartmann and Rayleigh number, while the angle of magnetic field has marginal influence on heat transfer rate.

4. Natural convection in partially heated open ended square cavity

The natural convection heat transfer analysis in a partially heated open ended square cavity have been carried out to elucidate the influence of heater size and heating location. First, effect of three heating locations (middle, top, bottom) and heater size ($L_c = 1/4, 1/2, 3/4$) for Pr=0.71 and, secondly, effect of Prandtl number ($0.71 \leq Pr \leq 7$) on partially heated open ended cavity (heated at the middle location of vertical wall), on heat transfer characteristics are analyzed herein. Linear dependence of the average Nusselt number ($\overline{Nu}$) on the Rayleigh number is observed, irrespective of the heating locations and heater size. However, average Nusselt number ($\overline{Nu}$) shows a proportional

dependence for the bottom and middle locations and inversely proportional dependence for the top heating location on the heater size, i.e., an increasing value of L_h enhanced $\overline{Nu}$ for the bottom and middle locations and deteriorated $\overline{Nu}$ for the top heating location. Over the range of Rayleigh number, middle partial heating location shows higher heat transfer rate followed by bottom and top heating locations.

The results also indicated the strong influence of Prandtl numbers on rate of heat transfer. As expected, the average Nusselt number values increased with both Prandtl and Rayleigh number. Finally, a closure relationship between average Nusselt number with Prandtl and Rayleigh numbers have developed in standard form.

5. Natural convection in square cavity with built-in square block

In this problem, the vertical walls of square cavity is exposed to the ambient (T_c) with horizontal walls maintained at adiabatic condition. A heated square block (T_h) is placed at the center of cavity. The natural convection characteristics have been explored for range of fluids ($0.71 \leq Pr \leq 10$). It is observed that the heated block has significant effect on the nature of flow inside cavity. The circulation of fluid between active wall causes formation of plume over the top wall of square block. The Prandtl number variation causes significant change in structure of the plume. With the increase in Prandtl number the length of plume decreases. Moreover, the increase in Prandtl number causes isotherms patterns to be more confined towards the heated walls. The circulation of fluid between cold cavity walls with heated square block is decipited in the form of streamlines. The Prandtl number has remarkable influence on the size of this quasi-motionless region, i.e., increasing in Prandtl number decreases the size of this region.

6. Wall effects on forced convection flow and heat transfer from channel built-in rectangular cylinder

The effect of wall confinement on the momentum and heat transfer characteristics of a channel built-in rectangular cylinder ($1 \leq AR \leq 6$) for blockage ratios ($1/8 \leq \beta \leq 1/20$), Reynolds numbers ($5 \leq Re \leq 40$) and Prandtl number ($Pr = 1$) have been explored. The results indicated that the increase in blockage ratio causes marginal increase in re-circulation length for considered range of Reynolds number. The drag coefficient values are found to be in inverse proportion with blockage ratio and Reynolds number. Furthermore, for a fixed Reynolds number, increase in blockage ratio causes crowding of isotherms in the vicinity of cylinder. Higher surface pressure coefficient (C_P) values are obtained for front face of cylinder at low blockage ratio. Thus, increasing blockage ratio reduces C_P values along the cylinder surface. Linear increase in average Nusselt number ($\overline{Nu}$) is observed with Reynolds number and lower blockage ratio. Thus, increase in blockage ratio impedes

rate of heat transfer. The Colburn heat transfer factor j_H is strongly dependent on blockage ratio. Finally, an empirical correlations relating total drag coefficient (C_D) and average Nusselt number ($\overline{Nu}$) with blockage ratio (β) and Reynolds number (Re) have been developed for its possible use in engineering design purpose. It is observed that drag as well as average Nusselt number have linear dependence on aspect ratio of rectangular cylinder.

In summary, the detailed insights of the natural and forced convection flow and heat transfer have been gained and presented for wide ranges of flow governing parameters and geometrical parameters. In addition, the present study also successfully developed and utilized the passive scalar thermal lattice Boltzmann method (PS-TLBM) with acceptable level of accuracy.

Contents

List of Figures

List of Tables

Nomenclature

B	magnetic field, N.S/C.m
b	size of cylinder, m
BGK	Bhatnagar-Gross-Krook
BH	Bottom heating
c	lattice speed, $=dx/dt$, m/s
C_D	drag coefficient, dimensionless
C_{DF}^N	normalized friction drag coefficent, dimensionless
C_{DP}^N	normalized pressure drag coefficent,dimensionless
C_{DF}	friction drag coefficent, dimensionless
c_p	specific heat capacity, J/(kgK)
C_{DP}	pressure drag coefficient, dimensionless
Da	Darcy number, dimensionless
DDF	Double distribution function
e_k	particle velocity at link k, m/s
f	distribution function for flow field
F_k	bouyancy force, N
FVM	Finite element method
f_k^{eq}	equilibrium distribution function for flow field, dimensionless
FVM	Finite volume method
g	distribution function for thermal field
g_k^{eq}	equilibrium distribution function for thermal field, dimensionless
Gr	Grashof number, dimensionless
g_y	acceleration due to gravity, m^2/s

H	height of enclosure, m
h_1	length of bottom end of heater from bottom-left corner (0,0) of cavity, dimensionless
h_2	length of top end of heater from bottom-left corner (0,0) of cavity, dimensionless
Ha	Hartmann number, dimensionless
J	Joule parameter, dimensionless
j_H	The Colburn factor of heat transfer, dimensionless
$\hat{k}$	opposite lattice link direction of k
L	length of enclosure, m
Le	Lewis number, dimensionless
L_h	length of heater, $=l_H/H$, dimensionless
l_h	length of heater, m
L_{hc}	heating location,, dimensionless
LBM	lattice Boltzmann Method
Nu	local Nusselt number
MH	Middle heating
n_h	number of heaters, dimensionless
$\overline{Nu}$	average Nusselt number
$\overline{Nu}_{Overall}$	Overall average Nusselt number of square cylinder, dimensionless
P	pressure, dimensionless
Pe	Peclet number, dimensionless
Pr	Prandtl number, dimensionless
P_s	surface pressure along square cylinder, Pa
QUICK	Quadratic upstream interpolation for convective kinematics
AR	aspect ratio, $=L/H$, dimensionless
a_r	aspect ratio of rectangular cylinder (b/H), dimensionless
Ra	Rayleigh number, dimensionless
Re	Reynolds number, dimensionless
Re_m	Magnetic Reynolds number, dimensionless
SIMPLE	Semi Implicit method for pressure linked equations

SAINTS	Software for arbitrary integration of NavierStokes equation with Turbulence and Porous Media Simulator
T	temperature, K
T_c	ambient temperature, K
TH	Top heating
t	lattice time,s
TLBM	thermal Lattice Boltzmann Method
Δt	lattice time step, s
ΔT	temperature difference, K
$\overline{T}$	reference/average temperature, K
U_{avg}	average velocity at inlet, m/s
U_{max}	maximum velocity at inlet, m/s
V	characteristic velocity, m/s
$U_{x,y}$	velocity components, dimesionless
X, Y	horizontal and vertical coordinates, dimensionless
U_x, U_y	velocity component, dimensionless, dimensionless
w_k	weight function for k^{th} lattice link, dimensionless

Greek symbols

α	thermal diffusivity, m^2/s
β	blockage ratio (b/H), dimensionless
β	coefficient of thermal expansion, K^{-1}
$\delta_{min}, \delta_{max}$	minimum and maximum % deviation, dimensionless
ϵ	porosity of the medium, dimensionless
Γ_e	thermal energy diffusion coefficient, dimensionless
Γ_m	momentum diffusion coefficient, dimensionless
κ	thermal conductivity, W/(m.K)
μ	dynamic viscosity, kg/m.s
ν	kinematic viscosity, m^2/s
ϕ	inclination angle, degree
ρ	density, kg/m^3
σ	Electrical conductivity, kg/m^3

τ_ν	relaxation parameter for flow field, m^2/s
θ	temperature, dimensionless
θ_c	ambient temperature, dimensionless
τ_g	relaxation parameter for thermal field, m^2/s
θ_h	hot wall temperature, dimensionless
T_h	hot wall temperature, K
ψ	stream function, m^2/s
ψ_{min}	minimum value of stream function, m^2/s
ψ_{max}	maximum value of stream function, m^2/s

Subscripts

c	cold
hc	center of heating
e	energy
h	Hot
k	lattice link direction
m	momentum
min, max	minimum, maximum
x, y	direction in x and y coordinates

Superscripts

eq	equilibrium
N	normalized values

List of publications

Refereed International Journals

1. Gangawane, K. M., Bharti, R. P. and Kumar, S. (2015). Two dimensional lattice Boltzmann simulation of natural convection in differentially heated square cavity: Effect of Prandtl and Rayleigh numbers. The Canadian Journal of Chemical Engineering. 93: 766-780.

2. Gangawane, K. M., Bharti, R. P. and Kumar, S. (2014). Lattice Boltzmann analysis of natural convection in a partially heated open ended enclosure for different fluids. Journal of the Taiwan Institute of Chemical Engineers. In Press. DOI: 10.1016/j.jtice.2014.11.020.

3. Gangawane, K. M., Bharti, R. P. and Kumar, S. (2016). Lattice Boltzmann analysis of effects of heating location and size on natural convection in partially heated open ended enclosure. Heat Transfer Engineering. In Press: 36(6): 1-47.

4. Gangawane, K. M., Bharti, R. P. and Kumar, S. (2014). Lattice Boltzmann analysis of natural convection in an open ended cavity with partially heated wall: Effect of heating location. The Korean Journal of Chemical Engineering. In press.

5. Gangawane, K. M., Bharti, R. P. and Kumar, S. (2014). Lattice Boltzmann analysis of natural convection in a partially heated open ended enclosure for different fluids: Effect of heating location. Under Preparation.

Conferences

1. Gangawane, K. M., Bharti, R. P. and Kumar, S. (2014). Lattice Boltzmann computation of forced convection heat transfer from heated built-in square cylinder: Effect of wall confinement. Proceeding of 5th International and 41th national conference on fluid mechanics and fluid power (FMFP-2014), IIT Kanpur, India, December 12-14, 2014.

2. Gangawane, K. M., Bharti, R. P. and Kumar, S. (2013). Lattice Boltzmann simulation of natural convection in a partially differentially heated square enclosure. Proceeding of 22nd National and 11th International ISHMT-ASME Heat and Mass Transfer Conference, IIT Kharagpur, India, December 28-31, 2013.

3. Gangawane, K. M., Bharti, R. P. and Kumar, S. (2013). Thermal Analysis of natural convection in an enclosure containing heated square body by Thermal Lattice Boltzmann Approximation. Proceeding of International Conference on Advances in Chemical Engineering (ACE 2013), IIT Roorkee, India, February 22-24, 2013.

4. Gangawane, K. M., Bharti, R. P. and Kumar, S. (2012). Thermal analysis of natural convection in differentially heated shallow cavities at different Rayleigh numbers by lattice Boltzmann approximation. Proceeding of International Conference on Sustainable Technologies for Energy and Environment in Process Industries and Indo-US Joint International Conference on Energy and Environment, Dr. B. R. Ambedkar National Institute of Technology, Jalandhar, India, December 28-31, 2012.

5. Gangawane, K. M., Bharti, R. P. and Kumar, S. (2012). Thermal lattice Boltzmann method: A review. Proceeding of Conference on Technological Advancements in Chemical and Environmental Engineering (TACEE 2012), BITS Pillani, India, March 23-24, 2012.

To my family

Chapter 1

INTRODUCTION

Though, the heat transfer fundamentals have been studied over the centuries, its development is still one of the developing research area in the field of the applied thermal science. Among the three modes of heat transfer (conduction, convection and radiation), the convective heat transfer mechanics is abundantly found in domestic as well as industrial applications. The study of heat transfer enhancement is given prime importance due to its prime significance in the chemical and process industries. The heat transfer by convection correlates two basic fields, namely, heat transfer and fluid mechanics. Thus, the study of convective heat transfer problems is based on fundamental principles of heat transfer and fluid mechanics (Bejan, 2003).

Over the past decades, the use of computers for solving problems of engineering fields have witnessed tremendous increase, particularly the problems of fluid flow and heat transfers, which are abundantly observed in the areas of automobile industry, power sector, aerospace, hydrology, etc. The reasons which are responsible for the rapid growth in the use of computers for solving engineering problems are necessity of speedy solution with moderate to high accuracy, very high cost involved in the laboratory experiments, etc (Murlidhar and Sundararajan, 2003). The availability of high speed computers has constituted the quick and cheap solution of such problems and the solution of complex problems

can be obtained at very less time. A brief discussion on the fundamental approaches for the solution of fluid flow and heat transfer problems is presented in the preceeding section.

1.1 Fundamental approaches for the solution of fluid mechanics-heat transfer problems

For the solution of the problems of the fluid mechanics and heat transfer, generally three appraoches are available. It can be seen from Figure 1.1, the physical problem can be solved via three ways, viz., experimental, theoretical and numerical/CFD (Anderson, 1995). In order to illustrate the comparison between them let us consider an example of determination of pressure coefficient on the surface of circular cylinder as reported by Anderson (1995). In experimental investigation, first a circular cylinder of desired

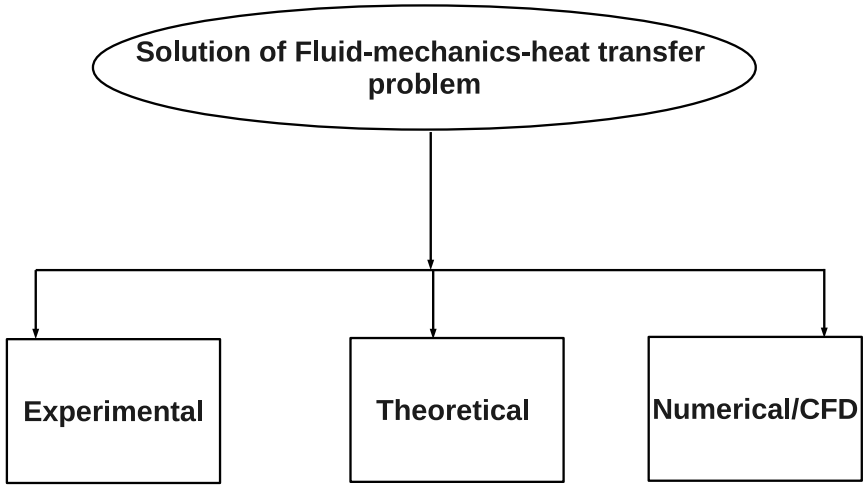

FIGURE 1.1: Different approaches of solving thermo-hydrodynamic problem.

dimension need to be designed and manufactured. The model should have provision for pressure estimation along the wall of circular cylinder, along with capability of producing required free-stream conditions in the test section. The match of flow conditions in wind tunnel can prove troublesome. Once the model and the wind tunnel flow conditions finalized, the actual testing can be started. The test time should be kept minimum as it requires maximum energy. Once the measurements are over, the wind tunnel correlation

factors should be applied to the raw data and final useful results should be obtained. Thus the experimental results are realistic answer to the problem but with the greater cost (Anderson, 1995).

In theoretical approach, assumptions are made to simplifying the problem. A general assumption is Newtonian fluid of perfect gas. This approach is useful in preliminary design of system and reasonable answers of problem can be obtained.

From the inception of the powerful computers, the development of computational/numerical methods have emerged as a strong way to explore and analyze the physical insights of complex flow and heat transfer phenomenon (Mohamad, 2011). For an instance, the development of finite element method (FEM) took pace in 1950's followed by finite difference (FDM) and finite volume method (FVM) impressed the worldwide researchers from 1980's to solve partial differential equations (PDE), in order to investigate the fluid flow and heat transfer characteristics. In conventional approaches, the Navier-Stokes equations are used to describe the fundamental physics of flow and heat transfer. In computational fluid dynamics (CFD), basically there are two approaches for solving field equations, i.e., continuum and discrete. The solution of conservation of energy, mass, and momentum for an infinitesimal control volume by using partial differential equations are required in the continuum approach (finite difference, finite volume, finite element, etc), which is macroscopic scale. While the discrete approach uses the medium made of small particles such as, atom, molecules, etc. such that these particles collide with each other. For solution of such discrete domain lattice Boltzmann method (mesoscale) and molecular dynamics (Microscopic) are used (Mohamad, 2011; Sukop and Throne, 2005). Figure 1.2 illustrates the various ways of solution of field equations.

1.2 CFD numerical methods

The most popular CFD methods can be discretized on the basis of its problem solution approach, like macroscopic tools (finite difference, finite volume and finite element), mesoscopic (lattice gas automata, lattice Boltzmann method) and microscopic (Monte Carlo simulation). The brief discussion of all these methods are given below.

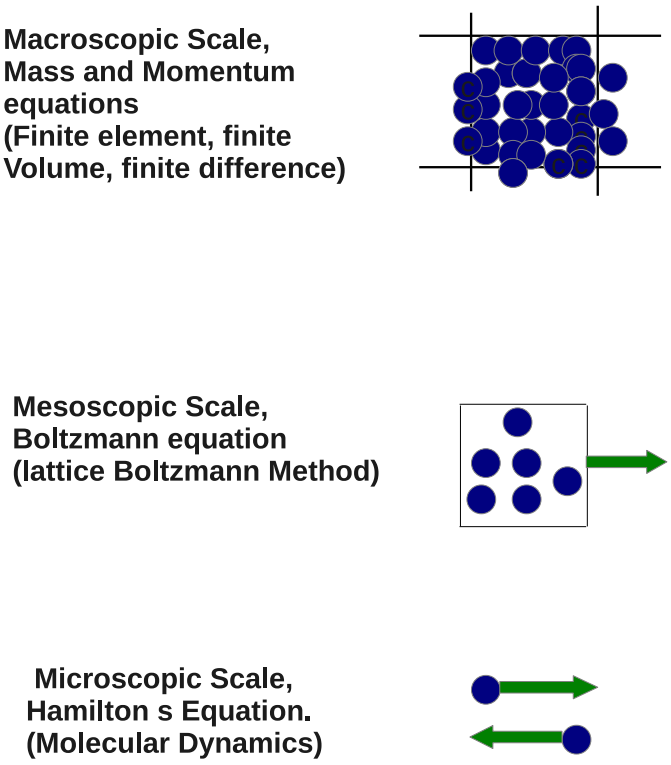

FIGURE 1.2: Various numerical/computational approaches of solving field equations.

1.2.1 Macroscopic numerical methods

This are conventional CFD tools. In these methods, macroscopic continuum equations are discretized over a considered physical domain of problem of consideration.

1.2.1.1 Finite difference method (FDM)

It is first numerical method developed for solution of partial differential equation. It was first used by Euler, probably in the year of 1768 (Blazek, 2001). The fundamental idea of FDM is to employ a Taylor series expansion for the discretization of the derivatives of the flow variables. The discretizations by finite difference method is done by using three ways, namely, central, forward and backward finite difference approach.

The advantages of FDM include its simplicity, possibility to obtain high-order approximations and thereby achieving high-order accuracy of the spatial discretisation, etc. The drawbacks are low application range as requires a structured grid, can not be applied to the body-fitted curve, etc (Blazek, 2001; Anderson, 1995).

1.2.1.2 Finite element method (FEM)

The development of finite element method was took place in 1956 for structural analysis. After a decade, researchers started to utilize the finite element method for the numerical solution of field equations in continuous medium. However, after 90's only FEM were successfully applied for the solution of Euler's and Navier-Stokes equations. In FEM, the physical domain is divided into triangular (2D) and tetrahedral (3D) elements. Thus generation of unstructured grid is required. Depending on the element type and the required accuracy, a certain number of points at the boundaries and/or inside an element is specified, where the solution of the flow problem has to be found. The total number of points multiplied with the number of unknowns determines the number of degrees of freedom. Furthermore, the so-called shape functions have to be defined, which represent the variation of the solution inside an element. In practical implementations, linear elements are usually employed, which use the grid nodes exclusively. The shape functions are then linear distributions, whose value is zero outside the corresponding element. This results in a second-order accurate representation of the solution on smooth grids

The finite element method has received much impetus from research community because of its integral formulation and the use of unstructured grids, which are both preferable for flows in or around complex geometries. The method is also particularly suitable for the simulation of non-Newtonian fluids. But. the finite element method has a very rigorous mathematical foundation, particularly for elliptic and parabolic problems. Although it can be proved in certain cases that the FEM is mathematically equivalent to the finite volume method in discretisation way, but the numerical effort is much more, which may explain why the finite volume method became more popular among conventional numerical method(Blazek, 2001; Anderson, 1995).

1.2.1.3 Finite volume method (FVM)

In FVM, the integral from of Navier-stokes/ Euler equations are directly utilized for discretization. Unlike the other numerical methods like finite difference and finite element method, where values are calculated at discrete places on a meshed geometry, FVM uses a finite small volume near the mesh node. In finite volume method discretization, the physical space is divided into a number of arbitrary polyhedral control volumes. The accuracy of the spatial discretisation rely upon the particular scheme with which the fluxes are estimated.

The main advantage of the FVM is that the spatial discretisation is carried out directly in the physical space. Thus, there are no problems with any transformation between coordinate systems, like in the case of the finite difference method. Compared to the finite differences, one further advantage of the finite volume method is that it is very flexible - it can be rather easily implemented on structured as well as on unstructured grids. This renders the finite volume method particularly suitable for the treatment of flows in complex geometries (Blazek, 2001; Anderson, 1995).

1.2.2 Mesoscopic methods

In mesoscopic methods, the group/population of molecules/discrete particles are considered. There two methods which makes in mesoscopic numerical tool, namely, lattice gas automata (LGA) and lattice Boltzmann method (LBM).

1.2.2.1 Lattice Gas Automata (LGA)

The fundamental idea of lattice gas automata was introduced by Von Neumann in 1940's. The basic idea of LGA was to divide the physical domain into discrete space and time (Sukop and Throne, 2005). In particular, the Frisch-Hasslacher-Pomeau (FHP) model of (Frisch et al., 1986) presented popular LGA model. In LGA model, a cellular automata or an algorithmic entity is considered, which occupies a position on a lattice point in space. That is why it also called as lattice gas cellular automata. At a particular time, a cellular automata analyze its own state along with its neighbors. Thus, collision rules along with initial and boundary conditions yield the evolution of system in time (Sukop and Throne, 2005; Miller, 1995; Chen and Doolen, 1998). The one dimensional cellular automata, which is simplest LGA model considers its own and neighboring lattice states. There are 256 possible ways to update, if automation have two possible states (Frisch et al., 1986; Miller, 1995; Chen and Doolen, 1998; Sukop and Throne, 2005). The advantages of lattice gas automata, are exact computing (no round off error), ease in parallel simulation, etc. But it has more drawbacks associated with it than advantages. For example, Galilean In-variance, statistical noise, difficulty in 3D simulation, Boolean mathematics, etc (Chen et al., 1992; Chen and Doolen, 1998; Sukop and Throne, 2005).

1.2.2.2 Lattice Boltzmann method (LBM)

In recent years, scientific and researchers community are widely using, an alternative approach to solve Navier-Stokes field equations. This approach is called as the lattice Boltzmann method (LBM) or lattice Boltzmann equation method (LBE). The lattice

Boltzmann method is mesoscopic method as it utilizes a kinetic Boltzmann equation. The concept of LBM has been derived from lattice gas cellular automata (LGA or LGCA). The LBM solves a fully discrete kinetic equation for populations $f(x,t)$, called particle distributions functions (PDF) designed to reproduce the Navier-Stokes equations within hydrodynamic limit. The particle distribution functions corresponding to the discrete velocity (e_k) fitting into the regular spacial domain with nodes $\mathbf{x}$, which enables the very efficient *stream* and *colloid* steps of lattice Boltzmann algorithm (Chikatamarla and Karlin, 2009).

1.2.3 Microscopic methods

The Monte Carlo simulation falls under the category of microscopic methods. The description of which is given below.

1.2.3.1 Monte Carlo simulation

The development of this method started back in 1950's. The fundamental idea of this method is to select points/nodes in the region enclosed by the boundary and then take the weighted data as the estimated value of the integral. A Monte Carlo method is a methodology that involves using random numbers and probability to solve problems. In this method, for iteratively evaluating a deterministic model using sets of random numbers as inputs. This method is often used when the model is complex, nonlinear, or involves more than just a couple uncertain parameters. A simulation can typically involve over 10,000 evaluations of the model, a task which in the past was only practical using super computers (Metropolis and Ulam, 1949; Hoffman, 1998; Wittwer, 2004).

1.3 Problems considered

The convection heat transfer phenomenon get complicated by the fact that it involves fluid motion as well as heat conduction. The fluid motion increases heat transfer, since it brings hotter and cooler lumps of fluid into contact, initiating higher rates of conduction at a greater number of locations in a fluid. Therefore, the rate of heat transfer through a fluid is higher by convection than it is by conduction. In fact, the higher the fluid velocity, higher the heat transfer rate (Cengel and Afshin, 2011).

After exploring the various numerical tools for computational fluid dynamics (CFD), now the fundamental of the physical problems considered for present doctoral work have been discussed herein. The lattice Boltzmann method (LBM) is used for simulating the two basic problems diversely found in the industrial as well as domestic activities, as given below:

1. Convective flow and heat transfer in enclosure.
2. Convective flow and heat transfer from channel built-in rectangular cylinder.

The fundamentals of these problems are discussed herein.

1.3.1 Natural convection heat transfer in enclosures

Natural convection in enclosures has received huge impetus of investigators as the transport process in a fluid where the fluid motion is derived by the interaction of a difference in density with a gravitational field, which is quite common in several engineering, scientific and environmental problems (Davis, 1968; Calcagni et al., 2005). It is quite clear that the effectiveness and efficiency of industrial and domestic equipment can often be improved by investing their thermal behavior/performance. The use of natural convective heat transfer for attaining enhanced, uniform heating in enclosed spaces (viz., high viscosity oil tanks, ovens, furnaces, or for cooling electronic components and refrigerator

condensers), eliminates the necessity for recirculating pumps or fans which are maintenance (Ekundayo, 1994). This problem is used as a benchmark problem for validation of numerical algorithms due to its simple configuration, still possessing a rich variety of heat transfer and fluid flow characteristics. Figure 1.3 represents the idealized flow of fluid

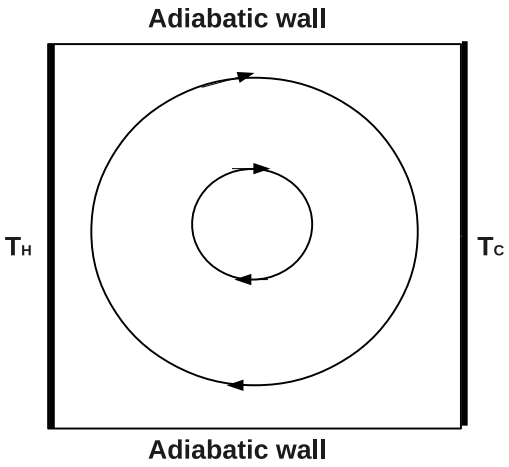

FIGURE 1.3: Cavity with differentially heated walls.

inside the cavity with differentially heated walls. It is simplest problem thus used for initial validations. The physical insight of cavity represented by circular motion is idealized one. The circulation takes place in clockwise direction between hot and cold walls due to difference density. The natural convection in a square enclosure is considered as very good model and vehicle for both experimental and theoretical investigations (Calcagni et al., 2005).

1.3.2 Heat transfer from built-in square/rectangular cylinder

In fluid mechanics, the bodies are differentiated into two types, a streamlined and bluff body. The streamlined bodies are one which do not alter or disturb the streamline distribution or simply saying streamlines follow smoothly over the surface of body (e.g., airfoil). In contrast, the body which alerts or breaks the streamline distribution along with the change in velocity, direction, etc. is called as bluff body (Bharti, 2006). Examples of generally observed bluff bodies are flat plates, triangular, square, rectangular, circular,

elliptical, polygonal cylinders, etc. The point of separation is usually fixed at the sharp edge for bluff bodies with sharp edges (triangular, square, rectangular, etc.).

The fundamental factor which differentiates the streamlined body with bluff one is size of wake formation. In case of streamlined bodies, losses are generally occur inside the boundary layer region resulting in small/thin wake size. On the other hand, in bluff body case, the separation of boundary layer take place, due to high pressure gradient, resulting in large wake containing energetic eddies dissipating large amount of mechanical energy, hence, increasing drag (Bharti, 2006).

Over the century, the flow past a bluff bodies has posed a challenging fluid mechanics problem involving the interaction of a boundary layer, a separating free shear layer, and a wake, each with varying or coupled processes of developing instabilities as the Reynolds number is increased. Such kind of fluid flows constitute an important class of engineering applications. The nature of the flow regulate the device performance affecting force, vibration, or heat transfer rates for many engineering applications (Sharma and Eswaran, 2004). Contrary to the circular cylinder, the separation points of the square cylinder are fixed at its leading/trailing edges. Additionally, the width of the wake immediately behind the cylinder is at least one diameter, whereas it is less than half a diameter for circular cylinder. Consequently, the Karman vortex street is significantly longer and broader for the square cylinder than for the circular cylinder. Thus, the square cylinder is a more bluff body than circular cylinder. From an engineering standpoint, the flow around structures that typically have rectangular or near-rectangular cross sections-i.e., buildings, electronic equipment, etc., are more equivalent to the flow around square cylinders than circular ones. Thus, the flow past a square cylinder is an important and fundamental problem of engineering/scientific point of interest (Sharma and Eswaran, 2004).

1.4 Outline of thesis

This dissertation has been divided into 12 chapters, which are arranged as follows. Chapter 2 provides the critical review of literature related to the problems of heat transfer in enclosures (differential heated, open ended, partially heated, magneto-hydrodynamic) and channel confined heated rectangular cylinder. It expedite the objectives of present work. It is followed by, the general assumptions along with governing field equations and physical flow governing parameters in Chapter 3. The detailed description of the lattice Boltzmann method (LBM), its recovery to mass, momentum and energy equations, kinetic boundary conditions, flow and thermal field algorithm, advantages and disadvantages of the numerical scheme are explored in Chapter 4. The validation of present in-house developed LBM code is ascertained by solving the benchmark problems of lid driven cavity, channel flow (for flow field) and differential heated cavity (for thermal field). The numerical validation is elucidated in Chapter 5.

Extensive results obtained from the numerical simulation of present work for flow and heat transfer in enclosures and from heated square/rectangular cylinders are presented in discussed in Chapters 6-10. The problem description along with boundary conditions, grid independence, validation and then the details analysis of the results are illustrated in these chapters. The detailed physical insights of heat and flow characteristics are illustrated by presenting the evaluation of isotherms and streamline, vorticity patterns, respectively, for the ranges of the conditions considered herein.

In case of heat transfer in enclosures, the investigation of heated cavity is carried out for laminar range of Rayleigh and Prandtl numbers (Chapter 6). The influence of one vertical wall exposed to both hot and cold conditions and other wall at cold condition is explored for laminar Rayleigh number range (Chapter 7). The influence of magnetic field and cooler size (placed at middle of one vertical wall) on laminar natural convection heat transfer characteristics (Chapter 8). In the problem of natural convection in partially heated open ended enclosure, the influence of heating location, heater size, Rayleigh number and Prandtl number on heat transfer rate have been explored (Chapter 9).

Moreover, the effect of Prandtl number on natural convection heat transfer in square cavity with cold vertical walls and adiabatic horizontal wall containing built-in heated square block at center is explored in Chapter 10 for laminar range of Rayleigh number.

In numerical simulations of forced convection from heated built-in square/rectangular cylinder, the influence of wall confinement (blockage ratio, β), aspect ratio of cylinder (a_r) and Reynolds number (Re) on fluid flow nature and heat transfer rate have been explored for laminar range of Reynolds number (Chapter 11). Finally, the simple empirical correlations have been developed for possible utilization in engineering/scientific applications for all problem considered herein. In particular, the Thesis explores the results of the following cases by using thermal lattice Boltzmann method (TLBM).

1. Natural convection analysis of differentially heated square cavity: Effect of Prandtl and Rayleigh numbers.

$$\overline{Nu} = f(Ra, Pr) \tag{1.1}$$

2. Natural convection analysis of partially-differentially-simultaneously heated square cavity: Effect of Rayleigh numbers.

$$\overline{Nu} = f(Ra) \tag{1.2}$$

3. Magneto-hydrodynamic natural convection in partially-differentially heated square cavity: Effect of cooler length, magnetic field direction and Hartmann number.

$$\overline{Nu} = f(L_c, Ra, Ha, \theta_M) \tag{1.3}$$

4. Natural convection heat transfer in an open ended square enclosure with partially heated wall: Effect of heater size and location.

$$\overline{Nu} = f(Ra, L_h) \tag{1.4}$$

5. Natural convection heat transfer in an open ended square enclosure with partially heated wall: Effect of Prandtl number.

$$\overline{Nu} = f(Ra, Pr) \tag{1.5}$$

6. Natural convection heat transfer square cavity containing heated square block: Effect of Prandtl number.

$$\overline{Nu} = f(Ra, Pr) \tag{1.6}$$

7. Forced convection heat transfer from built-in heated rectangular cylinder: Effect of blockage ratio, aspect ratio of cylinder and Reynolds number.

$$\overline{Nu} = f(Re, a, \beta) \tag{1.7}$$

Finally, Chapter 12 the major findings of this thesis is discussed, followed by recommendations for future work.

Chapter 2

LITERATURE REVIEW

In recent decades, the advances in the computational fluid dynamics (CFD) have enabled the analysis of detailed physical insight of the system at much better level and lower cost. In particular, the exploration of the fluid flow and heat transfer characteristics of system has received much impetus from global research community. The problem of the natural convection in cavity (differential heated, open ended, etc) and flow past a cylinder represents the idealization of domestic as well as industrial activities. These flow and heat transfer problems are also widely used to benchmark the numerical algorithms and/or solvers.

The study of heat transfer in heated enclosures is considered as an important problem owing to its wide theoretical and pragmatic relevance. Among others, the investigation of natural convection heat transfer in closed, as well as open, ended cavities is considered as an important research field due to the wide ranges of the industrially important applications including chemical vapor deposition (Spall, 1996), cooling devices in electronic equipment (Bilgen and Muftuoglu, 2008; Hsu and Wang, 2000; Du et al., 1998), polymer and material processing (Hsiao, 2007; Habib et al., 2005), solar collectors (Hobbi and Siddiqui, 2009), electronic card arrays (Manca and Nardini, 2010), domestic refrigerators and oven (Skok et al., 1990) etc. The cavities can be differentiated on the basic of its heating of walls, for instance, cavity with differentially heated vertical walls, top heating

and bottom cooling (Rayleigh-Benard convection), heated cavity with open end (open ended cavity).

Similarly, flow past a cylinder is also considered to be as very important owing to its overwhelming theoretical and practical relevance (hot wire anemometry, tubular and pin heat exchangers, sensors and probes, filtration screens and aerosol filters, RTM process of manufacturing fiber reinforced composites, etc. (Bharti, 2006)). The flow of fluids, especially Newtonian fluid, over bluff bodies of different shapes (circular, square, elliptic, triangular, spheres and spheroids, for instance, has been explored well over century (Dhiman et al., 2006a,b, 2007; Sahu et al., 2009; Koteswara Rao et al., 2011; Sharma et al., 2012). The study of flow past a square cylinder is very important to gain the knowledge of engineering parameters such as drag coefficient, Nusselt number, wake size, etc., which are often used to design of cooling towers, antennas, chimneys, antennas, support structures, high rise building, etc (Chatterjee et al., 2009; Sharma et al., 2012). Though, a reasonable amount of information is available for flow past shapes other than circular cylinder (Bharti, 2006), it neither extensive nor comprehensible. The subsequent sections presents the detailed review of convective flow and heat transfer in enclosures and of a square/rectangular cylinder.

2.1 Heat Transfer in Enclosures

The study of convective heat transfer mechanism is important owing to its diverse applications in domestic as well as industrial fields (Davis, 1968; de Vahl Davis, 1983; Lin and Nansteel, 1987). Heat transfer in enclosure is considered as benchmark problem for testing new numerical algorithms (de Vahl Davis, 1983). Heat transfer in differentially heated cavity is considered as one of the simplestproblem. Numerous studies exploring the heat transfer characteristics of cavity with differential heated walls are available by various approaches (Lin and Nansteel, 1987; Hiller et al., 1989; Djebali et al., 2009). Many industrial as well as theoretical problems, among others, can be represented by the various configuration of heat transfer in enclosures (Figure 2.6). The following sections explore

the relevent literature of these heat transfer cases. Figure 2.1 represent the these listed enclosures in schematic form.

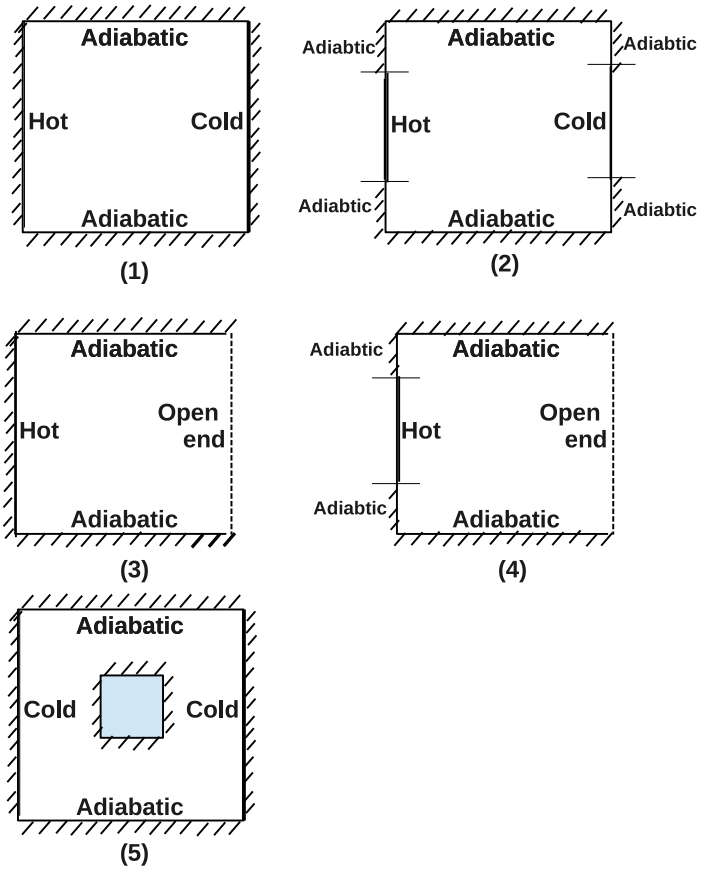

FIGURE 2.1: Schematic representation of various configuration of heat transfer in enclosures: (1) differentially heated, (2) partially-differentially heated, (3) open ended, (4) open ended with partial heating and (5) cavity with heated built-in square block.

2.1.1 Differentially Heated Cavity

Natural convection heat transfer characteristics in a differentially heated cavity is considered as one of the benchmark problem (Davis, 1968; Cormack et al., 1974a,b; Imberger, 1974a; Bejan and Tien, 1978; Patterson and Imberger, 1980; de Vahl Davis, 1983; Markatos and Pericleous, 1984; Phillips, 1984; Lin and Nansteel, 1987; Hiller et al., 1989; Basak et al., 2006; Djebali et al., 2009; Teamah et al., 2011), which is used to test new algorithms and numerical methods. A tremendous amount of literature delineating heat transfer characteristics in differentially heated cavity have been explored over the century. For instance,

a comprehensive review of natural convection in enclosures is given by Ostrach (1972). Imberger (1974b) carried out experimental investigation of the natural convection in a shallow cavity with differentially heated walls. In their study, the depth to length ratios of cavity were chosen as 10^{-2} and 1.9×10^{-2} to present the experimental results of the core flow of cavity. Later, Mcdonough and Catton (1982) elucidated the effect of Prandtl number ($0.71 \leq Pr \leq 650$) on Rayleigh-Benard convection in thin horizontal fluid layers by using mean field approximation obtained from Boussinesq approximation. For the wide range of Rayleigh numbers ($2000 \leq Ra \leq 25000$), they noted that the physical significance of Prandtl number in Benard convection is primarily setting the preferred wave-number, i.e., size of the convection cell. Subsequently, Hart (1983) numerically analyzed the natural convection in the differentially heated rectangular cavity for low Prandtl number fluids ($Pr = 0.01, 0.03, 1$) and for a range of Rayleigh number ($10^3 \leq Ra \leq 10^5$). They concluded that a parallel flow core will exist with approximately unit non-dimensional amplitude (=1) up to $Gr \approx 8000$ for smaller Prandtl number (< 0.1) and aspect ratio ($AR < 1$). Similarly, Janssen et al. (1993) explored the heat transfer characteristics of the steady and time-periodic flow of air in a differentially heated cubical cavity by using finite volume method (FVM). They observed that in the periodic flow regime, the calculated frequency was almost the same as for the two-dimensional square cavity, implying the same instability mechanism is in both cases responsible for the bifurcation. Henkes and Hoogendoorn (1993) reported the scaling of the natural convection in a differentially heated enclosure for two fluids (air and water) at high Rayleigh numbers. They presented scaling of Navier-Stokes equation for various regions of cavity such as vertical boundary layer, core, corner and horizontal layer. Afterwards, Janssen and Armfield (1996) delineated the stability of vertical boundary layers in differentially heated enclosures. They reported the convective instability sets in for Rayleigh numbers much smaller than those at which the absolute instability occurs, which are in excellent agreement with those for the boundary layer along a plate (Bejan, 2003).

Quere and Behnia (1998) investigated the onset of unsteadiness, the route to chaos and the dynamics of fully chaotic natural convection in a square differentially heated enclosure containing air ($Pr = 0.71$) and having top and bottom adiabatic walls for Rayleigh number up to $Ra \leq 10^{10}$. They noted that the internal gravity waves have significant role in the time-dependent dynamics of the solutions, both at the onset of unsteadiness and in the fully chaotic regime. Subsequently, the low-order modeling for the flow in a differentially heated cavity was reported by Podvin and Quere (2001) by using the proper orthogonal decomposition (P.O.D.) for cavity with aspect ratio of 4 containing air ($Pr = 0.71$). They observed two situations of moderate complexity. Later, low Prandtl number (Pr=0.0321) natural convection in volumetrically heated rectangular enclosure, i.e., slander cavity $AR = 4.0$ (Piazza and Ciofalo, 2000), square cavity, $AR = 1.0$ (Arcidiacono et al., 2001) and shallow cavity, $AR = 0.25$ (Arcidiacono and Ciofalo, 2001) has been investigated by using implicit finite volume method for wide range of the Grashof number ($10^4 \leq Gr \leq 10^{11}$). These studies have demarcated the different flow regimes, such as steady, time-periodic and chaotic, etc. Subsequently, Ahlers and Xu (2001) experimentally measured the dependence of Prandtl number ($4 \leq Pr \leq 34.1$) on heat transfer characteristics in turbulent Rayleigh-Benard convection in the cylindrical cells with aspect ratio of $AR = 0.5$ and 1.0 for wide range of the Rayleigh number ($3 \times 10^7 \leq Ra \leq 10^{11}$). They found smaller ($\approx 2\%$) dependence of Prandtl number (Pr) on the Nusselt number (Nu) for the fixed value of the Rayleigh number (Ra), which is in agreement of the theory of low Reynolds number, (Re). Roy and Basak (2005) have used the penalty finite element method with bi-quadratic rectangular elements to compute the natural convection in a square enclosure with non-uniformly heated walls for broad range of Rayleigh number ($10^3 \leq Ra \leq 10^6$) and Prandtl number ($0.2 \leq Pr \leq 100$). Similarly, Sathiyamoorthy et al. (2007) investigated steady natural convection flow in a square cavity with linearly heated side walls for the wide range of governing parameters ($0.71 \leq Pr \leq 10$ and $10^3 \leq Ra \leq 10^6$). They used penalty based Galerkin finite element method to solve the non-linear coupled partial differential equations, governing the flow and thermal fields. Subsequently, the effects of Prandtl number ($0.01 \leq Pr \leq 15$) on natural convection in

triangular cavity (aspect ratio, $AR = 1.0$) having the localized heating for range of dimensionless heating location ($0.15 \leq L_{hc} \leq 0.95$) from bottom have been elucidated (Koca et al., 2007) by using the stream function vorticity based finite difference method. They found that the momentum and heat transfer characteristics are greatly influenced with the change in Prandtl number. Jami et al. (2007a) have carried out numerical investigation of natural convection in a square enclosure with cylindrical heat conducting body by thermal lattice Boltzmann method for fixed value of Prandtl number, ($Pr = 0.71$) and Rayleigh number in the range as $10^3 \leq Ra \leq 10^6$ and for wide range of temperature difference ($\Delta T = 0 - 50$). The average Nusselt number (Nu) at both hot and cold walls found to vary linearly with temperature difference (ΔT) under otherwise identical conditions. Kao and Yang (2007) investigated the oscillatory flows in Rayleigh-Benard convection in a square enclosure using passive scalar thermal approach based on lattice Boltzmann method. In the range of Prandtl number of $0.71 \leq Pr \leq 70$ and for Rayleigh number of $Ra \leq 10^5$, they noted the bifurcation to secondary instability takes place at a specific Prandtl numbers (Pr), particularly, at $Ra = 48000$ for $Pr = 6.0$ and at $Ra = 76000$ for $Pr = 25$. Subsequently, Varol et al. (2009b) used finite difference method to investigate the natural convection heat transfer in a square enclosure filled with a porous medium with partition. For fixed value of the Prandtl number ($Pr = 0.71$), the effect of partition on the rate of heat transfer resulted in low heat transfer when partition angle is 45^o than that of 135^o. The investigation of Prandtl number (Pr) dependence on natural convection have been studied in two different systems viz.,triangular enclosure (Yu et al., 2010a) with coaxial cylindrical obstacle and cylindrical enclosure in a coaxial triangular obstacle (Yu et al., 2010b). They observed that for low Prandtl number ($Pr \leq 0.1$) heat and flow characteristics are of same order, and are nearly independent of Prandtl number for $Pr \geq 0.71$. Cheng (2011) has numerically investigated the mixed convection heat transfer characteristics in lid driven square cavity for wide ranges of flow governing parameters ($0.01 \leq Pr \leq 50$, $0.01 \leq Ri \leq 100$, $100 \leq Gr \leq 4.84 \times 10^6$ and $10 \leq Re \leq 2200$). Lai and Yang (2011) used lattice Boltzmann method (LBM) to investigate natural convection in square cavity filled with Al_2O_3/water They found that the Nusselt number increased with increasing value of the Rayleigh number (Ra) and the concentration of

the nanoparticles. Subsequently, Kefayati et al. (2012a) investigated the effect of Prandtl number ($0.025 \leq Pr \leq 6.2$), Rayleigh number ($10^4 \leq Ra \leq 10^6$) and Hartmann number ($0 \leq Ha \leq 150$) on natural convection magneto-hydrodynamics (MHD) in an open cavity by using lattice Boltzmann approximation. Their results (Nusselt number) found to decrease with increasing value of the Hartmann number (Ha). Recently, Park et al. (2012) studied natural convection heat transfer in a square enclosure consisting of hot and cold cylinders. They utilized finite volume method in conjunction with immersed boundary condition to investigate the effects of Rayleigh number ($10^3 \leq Ra \leq 10^6$) on the momentum and heat transfer characteristic on the vertical center-line of an enclosure at constant Prandtl number ($Pr = 0.71$). In addition to the literature discussed herein this section, Table 2.1 summarizes the physical parameters used in various studies.

TABLE 2.1: A summary of the physical parameters accounted in the literature on natural convection in square enclosure.

Source	*Pr*	*Ra*	Numerical method
Lin and Nansteel (1987)	7.0	$10^3 - 10^6$	$\psi - \xi$ formulation with central difference
Hiller et al. (1989)	$5.8 - 6 \times 10^3$	$10^4 - 2 \times 10^7$	Experimental
Peng et al. (2003b)	0.71	$10^3 - 10^5$	Nonuniform grid LBGK (3D)
Roy and Basak (2005)	$0.2 - 10.0$	$10^3 - 10^6$	Galerkin FEM
Basak et al. (2006)	$0.7 - 10.0$	$10^3 - 10^6$	Penalty FEM
Dixit and Babu (2006)	0.71	$10^3 - 10^{10}$	Interpolation based LBGK
Kuznik et al. (2007)	0.71	$10^3 - 10^8$	Taylor series least square DDF TLBM
Kao and Yang (2007) #	$0.71 - 70.0$	$10^3 - 10^6$	LBGK-DDF passive scalar
Djebali et al. (2009)	$0.025 - 6$	$10^3 - 10^6$	LBGK-DDF passive scalar
Mezrhab et al. (2010)	0.71	$10^3 - 10^6$	Double MRT-LBM
Mondal and Li (2010)	0.71	$10^3 - 10^6$	Nonuniform grid LBGK
Teamah et al. (2011) *	$0.01, 100$	$10^3 - 10^6$	FVM

** Double diffusive convection, # Rayleigh Benard convection*

2.1.2 Partially-differentially heated cavity

The cavity with one wall heated whereas other exposed to ambient represents the idealized model. However, there are many applications where cavity is exposed to the non-linear thermal conditions. Such cases can be well represented by partially differentially heated cavity. Few studies have delineated the influence of partial heating and cooling on the

natural convection in cavity (Yucel and Turkoglu, 1994; Aydin and Yang, 2000; Li et al., 2006; Cheikh et al., 2007; Oztop, 2007; Nithyadevi et al., 2007; Deng, 2008; Kandaswamy et al., 2008; Ben-Cheikh et al., 2011; Yesiloz and Aydin, 2011; Cianfrini et al., 2013). Among others, Oztop and Abu-Nada (2008) presented the numerical analysis of natural convection heat transfer characteristics of a partially heated rectangular cavity filled with nanofluids for the wide range of Rayleigh number ($10^3 \leq Ra \leq 5 \times 10^5$), length of heater ($0.25 \leq L_h \leq 0.75$), aspect ratio ($0.5 \leq AR \leq 2$) and volume fraction of nanoparticles ($0 - 0.2$). The major finding of the study was the heat transfer enhancement, using nanofluids, is more significant at low aspect ratio. The investigation of natural convection heat transfer in square cavities due to discrete source-sink pairs is explored by Deng (2008). Their study elucidated the influence of the location and size of heating source on heat transfer characteristics in cavity with the sizes of sources and sinks were, H/4 for two sources-sinks pairs and H/6 for three sources-sinks pairs, respectively at Rayleigh number of $10^2 \leq Ra \leq 10^6$ and Prandtl number of $Pr = 0.71$. They reported rise in heat transfer rate with number of eddies formed in the cavity. Likely, Varol et al. (2009b) studied the natural convection inside the right angle trapezoidal enclosure filled with a fluid-saturated porous medium having the left heated vertical wall of the cavity and the inclined wall is partially cooled. For numerical experimentation they studied three cases with cooler located (a) adjacent to the top wall, (b) in the middle inclined wall and (c) adjacent to the bottom wall for range of Rayleigh numbers ($100 \leq Ra \leq 1000$) and aspect ratio ($AR = 0.25, 0.5, 0.75$). Their case (a) yielded higher heat transfer. Subsequently, Ben-Cheikh et al. (2010) presented 3D analysis of momentum and thermal characteristics in cavity with partially heated from below and entirely cooled from above. They investigated the influence of partially heated walls on heat transfer behavior of cavity for two fluids (air, Pr=0.71 and di-electric liquids, Pr=25) for laminar range of Rayleigh numbers ($10^3 \leq Ra \leq 10^6$). The higher heat transfer rate is observed for dielectric liquids. The experimental as well as numerical investigation of natural convection heat transfer in an inclined quadrangle cavity heated and cooled on side by side walls is carried out by Yesiloz and Aydin (2011). For visualization of the fluid motion in the enclosure, the particle tracing method (PTM) is utilized in their work and numerical simulation

are obtained by using commercial CFD package FLUENT. The influence of Rayleigh number ($10^5 \leq Ra \leq 10^7$) and inclination angle ($0^o \leq \phi \leq 360^o$) on heat transfer rate has been elucidated by using distilled water as a working fluid (Yesiloz and Aydin, 2011). Later, Sheikhzadeh et al. (2011a) delineated the influence of partially heated wall with different heating and cooling positions on natural convection in a square cavity for Rayleigh number of $10^3 \leq Ra \leq 10^6$. They numerically studied the effect of location (middle, top and bottom) on both vertical walls on rate of heat transfer. and observed maximum heat transfer rate for cavity with middle-middle postion. Subsequently, the influence of isothermal as well as non-isothermal heating on natural convection in tilted (at 30^o) square cavity is reported by Singh et al. (2012) by using Galerkin finite element method for broad range of Rayleigh number ($10^3 \leq Ra \leq 10^5$) and Prandtl number ($Pr = 0.025, 998.24$). They observed that the overall heat transfer rate is larger for the uniform heating case as compared to that of a nonuniform heating case irrespective of Prandtl number. A summary of physical domain, physical parameters and numerical methods used in the discussed literature are summarized in Table 2.2.

2.1.3 Magneto-hydrodynamic natural convection in enclosure

The study of influence of magnetic field on natural convection heat transfer and fluid flow characteristics is primarily important in the field of science and technology (Qiana and Bau, 2009; Benos et al., 2014). A magneto-hydrodynamic is a suitable method to accelerate to shoot plasma into fusion devices or to yield the high energy wind tunnels for simulating hyper-sonic flight. Such problems found applications in electronic packages, microelectronic devices during their actions. Although the application of the magnetic field does not limit to these applications and it was utilized at various industries such as crystal growth in liquids, cooling of nuclear reactors, and so on (Qiana and Bau, 2009; Rahman et al., 2011b; Kefayati, 2013b; Benos et al., 2014). Moreover, the magnetic field used to supress the convective flow and thus help to control crustal growth and has similar

TABLE 2.2: A summary of related literature on natural convection in differentially cavity with partially heated walls.

S.N.	Source	Cavity type	Parameters	Numerical method	Remarks
1.	Yucel and Turkoglu (1994)	Square	$Ra = 2 \times 10^4, 10^5, 5 \times 10^5$ Pr=0.71, size of cooler=1/4,2/4,3/4,4/4	FVM-SIMPLE	Effect of cooler size on heat transfer rate
2.	Aydin and Yang (2000)	Rectangular	$10^3 \leq Ra \leq 10^6$ Heater size=1/5,2/5,3/5, 4/5	ADIM,SOR	$\overline{Nu} \propto Ra$
3.	Cheikh et al. (2007)	Square	$10^3 \leq Ra \leq 10^7$ Heater size=0.2H-0.5H, Pr=0.71	FVM-QUICK	maximum temperature at the heated surface does not change significantly for the diffusion dominated cases
4.	Chen and Chen (2007)	Square	$10^2 \leq Ra \leq 10^7$ Different heater lenght and strength	FVM-QUICK	Heat source length $\propto \overline{Nu}$
5.	Varol et al. (2010)	Differentially heated partition	$10^3 \leq Gr \leq 10^5, Pr = 0.71, 7$	FDM-SUR	Inclination angle $0^o \leq \phi \leq 360^o$
6.	Oztop (2007)	inclined porous rectangular	$10 \leq Ra \leq 1000$ center of heating location $(0.1 - 0.9)$ cooler size $(0.25 - 0.75)$ inclination angle $(0^o - 90^o)$	SAINTS-SIMPLE-TDMA	$\overline{Nu} \propto Ra$ $\overline{Nu} \propto Ra$
7.	Nithyadevi et al. (2007)	Rectangular	$10^3 \leq Gr \leq 10^5, Pr = 0.71$ $0.5 \leq AR \leq 5$	FVM-SUR	Effect of Heating location rate of heat transfer
8.	Ben-Cheikh et al. (2011)	Parallelepiped	$10^3 \leq Ra \leq 10^7, Pr = 0.71, 6.8$ Heater size=H/3	FVM-Multigrid	$\overline{Nu} \propto Ra, Pr$
9.	Sivasankaran and Bhuvaneswar (2011)	Rectangular	$10^3 \leq Gr \leq 10^6, Ha = 10, 25, 100$ Heater size=H/2, Pr=0.054 inclination angle $(0^o, 45^o, 90^o)$	FVM-Implicit	$\overline{Nu} \frac{1}{\propto} Ha$ $\overline{Nu} \propto Gr$, Aspect ratio
10.	Cianfrini et al. (2013)	Rectangular	$10^3 \leq Ra \leq 10^6, 0.25 \leq H/L \leq 4$ Heater size=0.2H-0.8H	FVM-SIMPLE	$\overline{Nu} \propto Ra$, Heater size

ADIM: Alternate direction implicit method, FEM: Finite element method, SUR: Successive Under Relaxation, SAINTS: Software for arbitrary integration of NavierStokes equation with Turbulence and Porous Media Simulator, SIMPLE: Semi implicit method for pressure linked equation QUICK: Quadratic Upstream Interpolation for Convective Kinematics

application in solidification process (Kakarantzas et al., 2009; Yu et al., 2013). The pioneering work delineating the fundamentals of magneto-hydrodynamics phenomenon can be found elsewhere (Elsasser, 1954; Poots, 1961; Sparrow and Cess, 1961; Siscoe, 1983; Cowling, 1962; Roberts and Soward, 1972). A very limited amount of literature is available for elucidating the influence of magnetic field on natural convection heat transfer and fluid flow characteristics in an enclosure. For instance, applicability of lattice Boltzmann method (LBM) for simulation of magneto-hydrodynamic problem is reported by Chen et al. (1991a). The influence of magnetic field on non-linear natural convection heat transfer in cavity is explored by Kandaswamy and Kumar (1999). They solved the field equations by using finite difference scheme consisting of ADI (Alternating Direction Implicit) and SOR (Successive Over Relaxation) methods. The physical insights were determined for flow governing parameters, such as, Hartmann number ($0 \leq Ha \leq 100$), hot wall temperature ($4^oC \leq T_h \leq 12^oC$) with cold wall temperature ($T_c = 0^oC$). The increase in magnetic field causes shift in heat transfer mechanism from convection to conduction. A two and three dimensional applicability of the lattice Boltzmann method for magneto-hydrodynamic (including Lorentz force due to the magnetic field) problem is reported by Dellar (2002). For numerical experimentation, they used with Hartmann flow, the OrszagTang vortex and the doubly periodic coalescence instability. For representation of magnetic field, they used a separate vector-valued magnetic distribution function which obeys a vector Boltzmann-BGK equation. Subsequently, Breyiannis and Valougeorgis (2006) provided three dimensional lattice Boltzmann method application to MHD problems based on the BGK modeling of the collision term, which is rather simpler approach than the conventional approach, one tensor-valued distribution function to present both the fluids variables (density and momentum) and the magnetic field. Furthermore, their LBM algorithm correctly recovers the field equations. Similarly, the lattice Boltzmann method for magneto-hydrodynamic approach relevant to the fusion problems was delineated by Pattison et al. (2008) by using multiple relaxation time (MRT) LBM. The evolution of the magnetic induction is expressed by introducing a vector distribution function and solving a suitable lattice kinetic equation for this function. The solution of both distribution functions are obtained through stream-and-collide algorithm. They

reported the enhancement of numerical stability by using MRT collision term over that of a single relaxation time approach. For numerical experimentation, they used 3-D MHD lid driven cavity flow, high Hartmann number flows and turbulent MHD flows, with excellent agreement with previous literature. A three dimensional (3D) analysis of free-decaying MHD turbulence by using lattice Boltzmann method (LBM) on a spatial grid of $8000 \times 8000 \times 8000$ is reported for low and high magnetic Prandtl number. They reported numerical instabilities for $Re_m \to \infty$, where Re_m is magnetic Reynolds number. Later, the influence of low Prandtl number magneto-convection around an adiabatic body inside a square enclosure is presented numerically by Sheikhzadeh et al. (2011b). The body is placed at the center of cavity. The field equations are solved by using finite volume method with SIMPLER algorithm for range of Rayleigh number ($10^3 \leq Ra \leq 10^6$), Hartmann number ($0 \leq Ha \leq 100$) and Prandtl number ($0.005 \leq Pr \leq 0.1$). The ratio of the buoyancy force to the Lorentz force (Ra/Ha^2) is introduced as an index to compare the contribution of natural convective heat transfer and magnetic field strength on rate of heat transfer. Their results indicated insignificant effect of Prandtl number on rate of heat transfer at low Ra. Also the rate of heat transfer has linear dependence on Prandtl number. Mixed convection heat transfer analysis in an open channel with triangular cavity is reported by Rahman et al. (2012). The field equations representing the flow and thermal field under magnetic field and Joule effect are numerically solved by using Galerkin weighted residual finite element technique. The flow governing parameters used in their work are Reynolds number ($100 \leq Re \leq 2000$), Hartmann number ($10 \leq Ha \leq 100$), Rayleigh number ($10^3 \leq Ra \leq 10^5$), Joule parameter ($0 \leq J \leq 5$) and Prandtl number ($1 \leq Pr \leq 10$). The heat transfer rate was found to vary in inverse proportion with Hartmann number. Further, the extension of lattice Boltzmann method for simulation of *Braginskii magneto-hydrodynamics* (single-fluid elucidation of large-scale motions in a strongly magnetized plasma, one in which the ion gyro-radius is much smaller than the mean free path between collisions in an nonmagnetic plasma of the same density and temperature) is reported by Dellar (2011). They introduced an anisotropic collision operator for the hydrodynamic distribution functions for simulation of Braginskii magneto-hydrodynamics, which has a different relaxation time to the component of stress

directed parallel to the magnetic field. Subsequently, Taghikhani and Najafkhani (2013) delineated the influence of magnetic field on natural convection flow and heat transfer in a cavity with internal heat generation by using fast stream-function and vorticity method ($\psi-\Omega$). They solved stream function equation by using fast Poisson's equation solver on a rectangular grid (POICALC function in MATLAB), vorticity and temperature equations are solved using red-black Gauss-Seidel and bi-conjugate gradient stabilized (BiCGSTAB) methods, respectively. In order to compare the contribution of natural convection and magnetic field strength on heat transfer rate, they introduced a parameter, which is ratio of Lorenz force to buoyancy force $\frac{Ha^2}{Ra}$. They observed a thermally driven natural convection for $\frac{Ha^2}{Ra} < 0.005$, electromagnetically driven flows occur when $\frac{Ha^2}{Ra} > 0.1$, while, combined effect of thermally as well as electromagnetically driven flows is observed for $0.05 \leq \frac{Ha^2}{Ra} \leq 0.1$.

Recently, Chatterjee and Halder (2014) presented the MHD mixed convection heat transfer characteristics in square enclosure containing two rotating circular cylinders by using finite volume method for range of flow governing parameters such as Reynolds number ($Re = 100$), Rayleigh number ($10^3 \leq Ra \leq 10^5$), Hartmann number ($0 \leq Ha \leq 50$). Their study indicated a decrease in the bulk average fluid temperature with Rayleigh and Hartmann number, whereas, the rotation caused reduction in the average fluid temperature when there is no magnetic field. Similarly, Luo et al. (2014) delineated the thermal radiation effects on MHD natural convection in a square enclosure by utilizing the Chebyshev-Collocation spectral method for Grashof number $Gr = 2\times10^5$ and 2×10^6; and Prandtl number ($Pr = 0.733$), for the fixed value of emmisivity (i.e., 0.6). They observed the magnetic force can suppress both fluid flow and heat transfer. The numerical study of mixed convection in lid driven cavity containing nanofluid is studied by Muthtamilselvan and Doh (2014) by using by the SIMPLE approach. They reported linear increase in average Nusselt number with the solid volume fraction at constant Reynolds number. Other studies encompassing the MHD convection effect in cavity are summarized in Table 2.3.

TABLE 2.3: A summary of related literature on MHD natural convection in heated cavity.

S.N.	Source	Physical parameters	Numerical method	Remarks
1.	Kahveci and Oztuna (2009)	$Ha = 0 - 100;\quad 10^3 \leq Ra \leq 10^7$ $Pr = 1$	PDQ	Cavity with partition, $\overline{Nu}$decreases up to 80% if partition is placed at the mid-point
2.	Pirmohammadi and Ghassemi (2009)	$Ha = 0 - 70;\quad 10^3 \leq Ra \leq 10^5$ $Pr = 0.02; 0^o \leq \theta_M \leq 135^o$	FVM-SIMPLER	Tilted enclosure, $\overline{Nu} \propto \theta_M;\quad$ for $\quad \theta_M \leq 45^o$
3.	Grosan et al. (2009)	$0 \leq Ha \leq 50;\quad 10 \leq Ra \leq 10^5$ $0.01 \leq AR \leq 1$ $0 \leq \theta_M \leq \frac{\pi}{2}$	FDM	Internal heat generation, $\overline{Nu}\frac{1}{\propto}\theta_M$
4.	Rahman et al. (2011a)	$0 \leq Ha \leq 20;\quad 10^3 \leq Ra \leq 10^5$ $100 \leq Re \leq 500$	Galerkin-FEM	Mixed convection, $\overline{Nu} \propto Re, Ra, \frac{1}{Ha}$
5.	Rahman et al. (2011b)	$10 \leq Ha \leq 50;\quad 10^3 \leq Ra \leq 10^5$ $100 \leq Re \leq 500; 0 \leq J \leq 3$ $0.5 \leq Br \leq 5; 2 \leq Le \leq 10$	Galerkin-FEM	Mixed convection, effect of joule heating and MHD $\overline{Nu}\frac{1}{\propto}Ha, J, Br$ $\overline{Nu} \propto Le$
6.	Kefayati et al. (2012a)	$10 \leq Ha \leq 150;\quad 10^3 \leq Ra \leq 10^5$ $0.025 \leq Pr \leq 6.2$	LBM	$\overline{Nu} \propto 1/Ha, Pr$ $\overline{Nu}\frac{1}{\propto}\theta_M \quad$ for $\quad \theta_M > 45^o$
6.	Hossain and Alim (2013)	$Ha = 50;\quad 10^3 \leq Ra \leq 10^5$ $0.026 \leq Pr \leq 1000$ $0^o \leq \theta_M \leq 45^o$	Galerkin-FEM	Trapezoidal cavity, heatline concept, uniformly and non-uniformly heated bottom wall $\overline{Nu}\frac{1}{\propto}\theta_M$
7.	Kefayati (2013c)	$Ha = 0 - 90;\quad 10^3 \leq Ra \leq 10^6$ $0 \leq \phi \leq 0.06$	LBM	WaterAl_2O_3 nanofluid $\overline{Nu} \propto \frac{1}{Ha}$
8.	Kefayati (2013c)	$Ha = 0 - 90;\quad 10^3 \leq Ra \leq 10^6$ $0 \leq \phi \leq 0.06$	LBM	WaterAl_2O_3 nanofluid $\overline{Nu} \propto \frac{1}{Ha}$
9.	Kefayati (2013b)	$Ha = 0 - 90;\quad 10^3 \leq Ra \leq 10^5$ $0 \leq \phi \leq 6\%; 0.5 \leq AR \leq 2$	LBM	Open ended cavity, $\overline{Nu} \propto \frac{1}{Ha}, Ra, AR$
10.	Sheikholeslami and Ganji (2014)	$Ha = 0 - 40;\quad 10^3 \leq Ra \leq 10^6$ $0 \leq \phi \leq 0.06;\quad 1.5 \leq AR \leq 4.5$	LBM	Enhancement ratio $\propto (\frac{1}{Ra}, Ha)$
11.	Mahmoudi et al. (2014)	$Ha = 0 - 60;\quad 10^3 \leq Ra \leq 10^6$ $0 \leq \phi \leq 6\%; 0^o \leq \theta_M \leq 180^o$	LBM	WaterAl_2O_3 nanofluid $\overline{Nu} \propto Ra, \frac{1}{Ha}$

PDQ: polynomial differential quadrature, FEM: Finite element method, SUR: Successive Under Relaxation, J: Joule heating, Le: Lewis number, Br: buoyancy ratio

2.1.4 Open Ended Enclosure

Open ended enclosures are also widely incountered in applications of industrial importance (Spall, 1996; Bilgen and Muftuoglu, 2008; Hsu and Wang, 2000; Du et al., 1998; Hsiao, 2007; Hobbi and Siddiqui, 2009). A limited amount of information of the open ended cavity flow with non-linearly heated wall is documented in the literature. For instance, Shin and Economou (1990) explored the characteristics of natural and forced convection mass transfer in an open ended enclosure by using finite element method (FEM) for Rayleigh numbers of $Ra \leq 10^5$. They observed enhancement in the mass transfer in cavity with aspect ratio (depth:width) of 2:1 by order of one due to both forced and natural convections. Vafai and Ettefagh (1990a) investigated the fluid flow and thermal instabilities for Rayleigh numbers of $10^3 \leq Ra \leq 6 \times 10^5$ at a constant Prandtl numbers ($Pr = 0.71$). They observed one to one relationship between the frequency of the periodic oscillations in the Nusselt number and the central vortex oscillations and location inside the cavity for at higher Rayleigh numbers. Similarly, Vafai and Ettefagh (1990b) studied the influence of sharp corners and the far field boundary conditions on vorticity generation and flow instabilities. They reported the significance of the far field boundary treatments and interaction between physical flow governing parameters.

Yucel and Turkoglu (1994) numerically analyzed the natural convection heat transfer in an enclosure with partial heating/cooling by using the finite volume method (FVM) for the three values of Rayleigh numbers ($Ra = 2 \times 10^4, 10^5$ and 5×10^5) corresponding to laminar flow condition and for the varying heater and cooler sizes (i.e., 0.25, 0.5, 0.75 and 1.0) placed at west-bottom and east-top positions, respectively. They observed that, for a particular cooler size, average Nusselt number decreased with an increase in heater size. On the other hand, for the given heater size, average Nusselt number increased proportionally with the cooler size. Subsequently, Mohamad (1995) investigated the natural convection heat transfer in air ($Pr = 0.71$) from an open ended cavity for the various flow governing parameters such as inclination angle ($10^o \leq \phi \leq 90^o$), aspect ratio (AR = 0.5, 1.0 and 2.0) and the Rayleigh number ($10^3 \leq Ra \leq 10^7$) by using the control

volume-finite difference method. They observed slight change in the heat transfer rate with the change in inclination angle, however, flow instability is noted at high Rayleigh numbers and low inclination angles. The unsteady flow for the moderate to high Grashof numbers is also observed by Angirasa et al. (1995) in their analysis of natural convection in air ($10^3 \leq Ra \leq 10^7$ and $Pr = 0.71$) from an isothermal open ended cavity by using the stream function-vorticity method. Similarly, Khanafer and Vafai (2000, 2002) have presented an accurate representation of flow and thermal boundary conditions of two- and three-dimensional enclosures at an open end based on their numerically investigation of the thermal and hydrodynamic features of an open ended cavity.

The numerical investigation of laminar natural convection in shallow cavity (Polat and Bilgen, 2002) reported that the rate of heat transfer is significantly influenced by the inclination angle of heated plate in the following ranges of Rayleigh number ($10^3 \leq Ra \leq 10^6$) and aspect ratio ($1 \leq AR \leq 0.125$). Subsequently, Manca et al. (2003) numerically explored the mixed convective heat transfer characteristic in channel with an open ended cavity for three heating locations (the heated wall is on the inflow side and the heated wall is on the outflow side;the heated wall is the horizontal surface of the cavity). The physical flow governing parameters used for numerical experimentation were Richardson number ($Ri = 0.1, 100$) and Reynolds number ($Re = 100, 1000$). They observed better thermal performance in terms of both maximum temperature and average Nusselt number for an opposing forced flow configurations. The effects of the Rayleigh number ($10^4 \leq Ra \leq 10^7$) and inclination angle ($0^o \leq \phi \leq 180^o$) on the natural convection heat transfer and surface thermal radiation in a tilted square cavity with an open end were elucidated numerically by Hinojosa et al. (2005). The convective and radiative Nusselt numbers were reported to have substantial and negligible dependencies, respectively, on the inclination angle (ϕ). The natural convection in partially open square cavity (adiabatic walls and a partial opening) is numerically investigated by Bilgen and Oztop (2005) for the broad range of the Rayleigh number ($10^3 \leq Ra \leq 10^6$), aperture opening size ($0.25-0.75$) and inclination angle ($0^o \leq \phi \leq 120^o$). Their study reported the variation of the volumetric flow rate and Nusselt number in the direct proportion with the Rayleigh number, inclination angle and

the aperture size. Subsequently, Nasr et al. (2006) explored the natural convection heat transfer mechanism in an enclosure exposed to heating from the lower corner and cooling from the ceiling for the wide range of Rayleigh numbers ($10^3 \leq Ra \leq 10^6$) and for the constant heater and cooler sizes. The optimum positions of discrete heaters by maximizing the conductance in open ended cavity under the natural convection is determined by Muftuoglu and Bilgen (2008) for the varying heater size ($0.05 \leq L_h \leq 0.2$), number of heaters ($1 \leq n_h \leq 3$) and the Rayleigh number ($10^3 \leq Ra \leq 10^7$). They (Muftuoglu and Bilgen, 2008) further studied the heat transfer and volume flow rate with discrete heaters at their optimum positions. They found that the global conductance and Nusselt number to be an increasing function of the Rayleigh number, the heater size and the number of heaters. Best thermal performance is obtained (Muftuoglu and Bilgen, 2008) by positioning the discrete heaters closer to the bottom and closer to each other at the beginning of fluid flow. Mohamad et al. (2009) explored the natural convection ($10^4 \leq Ra \leq 10^6$) in an open ended rectangular ($0.5 \leq AR \leq 10$) cavity by using passive scalar thermal lattice Boltzmann method (TLBM). The rate of heat transfer was found to vary inversely with aspect ratio (AR) by using the $D2Q9$ (two-dimensional and nine velocity link) and $D2Q4$ (two-dimensional and four velocity link) lattice models to solve for the flow and thermal fields, respectively. Varol et al. (2009a) studied the natural convection in an inclined enclosure having heater placed at corner using the stream function-vorticity approximation approach and finite difference method for the wide ranges of the flow governing parameters ($10^3 \leq Ra \leq 10^6$, $0^o \leq \phi \leq 270^o$ and $0.07 \leq Pr \leq 70$) and length of heater ($0.25 \leq L_h \leq 0.75$) in both $x-$ and $y-$ directions. They noted the stronger dependence of the rate of the heat transfer on the inclination angle (ϕ) and the length of corner heater/cooler. Subsequently, Haghshenas et al. (2010a) used least square based Lattice Boltzmann method (LBM) to investigate the natural convection in an open ended cavity filled with porous medium (Darcy number, $Da = 0.01$) for the wide range of the Rayleigh number ($10^3 \leq Ra \leq 10^6$) and fixed value of the Prandtl number ($Pr = 1.0$). The rate of heat transfer was found to increase with both Rayleigh number and porosity ($0.4 \leq \epsilon \leq 0.9$) of the medium. Later, Kaluri and Basak (2010) studied the heat-line analysis of thermal mixing due to natural convection in discretely heated porous

enclosures containing different fluids. They have used Galerkin finite element method for solving governing equations of the problem. They investigated the heat and fluid flow characteristics of system for physical parameters such as Darcy number ($10^{-6} \leq Da \leq 10^{-3}$), Prandtl number ($0.015 \leq Pr \leq 1000$) and Rayleigh number ($10^3 \leq Ra \leq 10^6$). They noticed weak buoyancy driven flow at low Darcy number (10^{-6}) and also higher convection effect at $Da = 10^{-3}$ due to weak hydraulic resistance of porous medium. Similarly, Andreozzi and Manca (2010) delineated the natural convection heat transfer characteristics in a horizontal open-ended cavity with a heated upper wall for Rayleigh number of $Ra = 10^3$ and 10^6 and aspect ratio of 1 and 10. They observed the streamline patterns showed a convective loop outside of the cavity at $Ra = 10^3$.

Sajjadi et al. (2010) investigated the effects of the inclination angle ($-45^o \leq \phi \leq 45^o$) and Rayleigh number ($10^3 \leq Ra \leq 10^6$) on the thermal hydrodynamic nature of natural convection in cavity by using LBM. Later, the entropy generation Marangoni convection flow of heated fluid in an open ended cavity have been explored by Saleem et al. (2011) by using alternate direct implicit (ADI) method with successive over relaxation (SOR) approach. They observed active spot of maximum entropy generation strongly depends on the magnitudes of Grashof and Prandtl numbers. Recently, Prakash et al. (2012) studied the natural convection losses from the three-dimensional open ended cavity of three different geometrical shapes (i.e., spherical, cubical and hemispherical). The hemispherical open cavity yielded the highest natural convection loss over the wide ranges of the conditions as follow: inclination angle ($0^o \leq \phi \leq 90^o$), opening ratio ($1, 0.5, 0.25$) and Rayleigh number ($4 \times 10^4 \leq Ra \leq 2.5 \times 10^9$). The influence of Prandtl number on magneto hydrodynamics (MHD) on natural convective heat transfer in an open ended cavity is delineated by Kefayati et al. (2012a) by using lattice Boltzmann method (LBM). The elucidated the influence of Prandtl number ($Pr = 0.025, 0.71$ and 6.2), Hartmann number ($0 \leq Ha \leq 150$) and Rayleigh number ($Ra = 10^3, 10^4, 10^5$) on flow and thermal fields. The effect of magnetic field was found to be minimum on heat transfer rate for Pr=0.025. Sheikholeslami et al. (2013b) used lattice Boltzmann method (LBM) for investigating the natural convection phenomenon in a enclosure having curved boundaries and filled with

Cu-water nanofluid. They observed that the inclination angle has significant effect on thermal and hydrodynamic characteristics of cavity. Recently, the influence of magnetic field on the natural convection in an open ended cavity filled with nanofluid using lattice Boltzmann method (LBM) is investigated by Kefayati (2013a) encompassing the broad range of the flow governing parameters such as Rayleigh number ($10^4 \leq Ra \leq 10^6$), Hartmann number ($0 \leq Ha \leq 90$) and the volume fraction of nanoparticles (0 to 0.06). The rate of heat transfer decreased with the increase in Hartmann number for a particular value of the Rayleigh number. More Recently, (Hussein et al., 2014) presented the lattice Boltzmann computation of natural convection in an open cavity filled with Cu-water nanofluid under magnetic field effect. The influence of pertinent parameters such as Hartmann number, nanoparticle volume fraction, Rayleigh number and the inclination of magnetic field. The results indicated that the solid volume fraction has a significant effect on stream-line patterns and heat transfer, depending on the value of Hartmann and Rayleigh numbers. Moreover, the three dimensional analysis of cubical open cavity is explored by Zamora and Kaiser (2014) for laminar, transitional and turbulent characteristics of fluid. For simulation of transitional and turbulent flow, they utilized low Raynolds, $k - \omega$ model.

Recently, few studies have experimentally delineated the physical insight of open ended cavity (Park et al., 2013; Tuhkala et al., 2014; Montiel-Gonzaleza et al., 2014; Lee et al., 2014). Moreover, Table 2.4 and Table 2.5 classifies the convection in open, differentially heated as well as lid driven cavity with completely and partially heated wall, respectively, along with the physical flow governing parameters.

TABLE 2.4: A summary of related literature on natural convection in open ended/differentially cavity with fully heated vertical walls.

S.N.	Source	Cavity type	Range of parameters		Numerical method	Remarks
			Ra/Gr	Pr		
1.	Chan and Tien (1985)	Shallow open	$10^3 \leq Ra \leq 10^6$	1,7	FVM-SIMPLER	AR=0.143,1
2.	Khanafer and Vafai (2002)	Open	$10^3 \leq Ra \leq 10^5$	$0.71 \leq Pr \leq 4.92$	FEM-GWS	AR=1,0.25,0.5
3.	Mohamad et al. (2009)	Rectangular, open	$10^3 \leq Ra \leq 10^6$	0.71	LBM	AR=1,2,4
4.	Varol et al. (2010)	Differentially heated partition	$10^3 \leq Gr \leq 10^5$	0.71, 7	FDM-SUR	Inclination angle $0^o \leq \phi \leq 360^o$
5.	Mohamad et al. (2010)	Square open	$10^4 \leq Ra \leq 10^6$	0.71	LBM	Double diffusive, Lewis number = 2, 4, 8
6.	Haghshenas et al. (2010b)	Square, porous open	$10^3 \leq Ra \leq 10^6$	1	LBM	
7.	Kefayati et al. (2012b)	Rectangular	$10^4 \leq Ra \leq 10^6$	-	LBM	AR=0.5-2,Volumn fraction of nanoparticles (0-0.05)
8.	Kefayati et al. (2012a)	Square open	$10^4 \leq Ra \leq 10^6$	0.025, 0.71, 6.2	LBM	MHD $0 \leq Ha \leq 150$
9.	Sheikholeslami et al. (2013b)	Square cavity with curved boundary	$10^4 \leq Ra \leq 10^6$	–	LBM	Cavity with nanofluids

GWS: Galerkin weighted residuals, FEM: Finite element method, SUR: Successive Under Relaxation, QUICK: Quadratic Upstream Interpolation for Convective Kinematics, MHD: Magneto-hydrodynamics

TABLE 2.5: A summary of literature on natural convection in open ended/differentially cavity with partially heated walls.

S.N	Source	Cavity type	Range of parameters		Numerical method	Remarks
			Ra/Gr	Pr		
1.	Varol et al. (2008)	Triangular	$10^4 \leq Ra \leq 10^6$	0.71	FDM-SUR	ANFIS
2.	Kaluri and Basak (2010)	Square, porous	$10^3 \leq Ra \leq 10^6$	$0.015 \leq Pr \leq 1000$	Galerkin FEM	Discrete heating
3.	Sivakumar et al. (2010)	Square, lid driven	$10^2 \leq Gr \leq 10^6$ $100 \leq Re \leq 1000$	0.71	FVM-QUICK	Discrete heating
4.	Aghajani Delavar et al. (2011)	Square, differentially heated	$10^3 \leq Ra \leq 10^6$	0.71	LBM	Effect of discrete heater
5.	Sankar et al. (2011)	Square, porous, differentially heated,	$10^3 \leq Gr \leq 10^6$	0.71	LBM	Partially heated hot and cold walls $\epsilon = 0.3 - 0.7$
6.	Bhuvaneswari et al. (2011)	Rectangular, differentially heated, porous	$10^3 \leq Gr \leq 10^6$	0.71	FVM	Partially heated hot and cold walls, $\epsilon = 0.3, 0.7$, $0.5 \leq AR \leq 10$, $10^{-5} \leq Da \leq 10^{-2}$
7.	Nikbakhti and B. (2012)*	Rectangular, differentially heated	$10^4 \leq Ra \leq 10^6$		FDM-SUR	Double diffusive convection
8.	Jmai et al. (2013)	Square, differentially heated	$10^4 \leq Ra \leq 10^7$		FVM	Nanoparticles with Volumn fraction (0-0.2)

∗: Mixed convection, ANFIS: Adaptive-network-based Fuzzy Inference System, Da: Darcy number, ϵ: porosity parameter

2.2 Natural convection in square cavity with built-in obstacle

In many engineering applications, the enclosures are often more complex than simple heated enclosures. For instance, the enclosures containing heated/cooled/adiabatic/square/-circular blocks can be considered as the ideal form of partitions and baffles. Thus study of such structures are very important to understand the heat transfer behaviors. Natural convective flow and heat transfer between a cylinder and its surrounding medium has been a problem of theoretical as well as pragmatic significance due to its wide ranges of applications such as, energy storage devices, crop dryers, crude oil storage tanks, heat exchangers, spent fuel storage of nuclear power plants, etc (De and Dalal, 2006). Among others, Adlam (1986) studied the two-dimensional time dependent natural convection in a cavity containing internal bodies by using explicit finite-difference equations in terms of temperature, vorticity and stream function. They investigated three cases, namely, 2D thermosyphon in a region bounded by two concentric squares, two internal blocks heated to a constant temperature with the walls of the containing cavity exposed to ambient. The physical flow governing parameters used in there work are Prandtl number ($Pr = 5.39$) and Rayleigh number ($1 \times 10^6, 2 \times 10^7$). They reported formation of the asymmetric convective cells, which move outwards from the center. House et al. (1990) investigated the influence of the centered, square, heat conducting object on natural convection in a vertical enclosure. They reported the enhancement or reduction of heat transfer across the cavity by a body with a thermal conductivity ratio smaller or greater than unity. Subsequently, fluid flow and natural convection heat transfer characteristics in an enclosure containing heat generating conducting body is reported by Oh et al. (1997) for range of Rayleigh number ($10^3 \leq Ra \leq 10^4$), temperature difference ($\Delta = 0^oC - 50^C$), Prandtl number ($Pr = 0.71$), area ratio ($A_r = 0.25$) and conductivity ratio ($K_r = 1$). They observed the ratio of hot to cold wall average Nusselt number in between 1 to -1. Similarly, the numerical study of transient natural convection heat transfer in an enclosure containing heat generating conducting body is studied by Ha et al. (1999) for three

different fluids (sodium, air, and water). They investigated the physical insights of the system for wide range of Rayleigh numbers ($Ra = 10^3, 10^4$), temperature-difference ratios ($2.5 \leq \Delta T \leq 50$), Prandtl numbers ($Pr = 0.0112, 0.707, 5.83$), and thermal conductivity ratios ($k = 1.71, 5630, 240$). They observed fluid flow circulation in the enclosure increases with increasing Ra, increasing the convective heat transfer rate between active walls. The study of interaction between multiple discrete heat sources in horizontal natural convection cavities is elucidated by Qi-Hong Deng et al. (2002) for range of Rayleigh number ($10^2 \leq Ra \leq 10^5$) and constant Prandtl number ($Pr = 0.71$), relative conductivity ($k^* = 1$) and aspect ratio ($A_r = H/L = 0.5$). Their study concluded that according to the contribution ratios of discrete heat source, the flow structures can be divided into two regimes, i.e. the conduction and the convection regimes. Similar study is reported by Bhoite et al. (2005). Subsequently, the numerical study of natural convection heat transfer in an enclosure containing conducting bodies with thermal conductivity of 0.1, 1 and 50 and range of Rayleigh number ($10^3 \leq Ra \leq 10^7$) by using Chebyshev spectral methodology with multi-domain technique. They observed the patterns of flow and isotherm and the corresponding surface and time averaged Nusselt number are similar to those of neutral isothermal body for dimensionless thermal conductivity is 50. The influence of combined effect of natural convection and radiation heat transfer in an enclosure containing square block at its center is reported by Mezrhab et al. (2006) by using finite volume method with SIMPLER algorithm. They carried out parametric study of surface emissivity ($0 \leq \epsilon \leq 1$), the Rayleigh number ($10^3 \leq Ra \leq 10^8$), and the thermal conductivity ratio ($0 \leq k_r \leq 1$). They reported that the radiation exchange homogenizes the temperature inside the cavity and raises heat transfer rate, particularly when k_r and Ra are high, also, the average Nusselt number varies linearly with surface emissivity, especially at high Rayleigh numbers. The natural convection in a enclosure with built-in tilted heated square block is investigated by De and Dalal (2006) by using finite difference method with stream-function-vorticity formulation for laminar range of Rayleigh number ($10^3 \leq Ra \leq 10^6$). They investigated the effects of the enclosure geometry by using three different aspect ratio (AR) placing the square cylinder at different heights from the bottom wall. They also introduced a concept of heat-function to trace the heat transport. Later,

the lattice Boltzmann simulation of laminar natural convection in an enclosure with a heat-generating cylinder conducting body is delineated by Jami et al. (2007b) for laminar range of Rayleigh number ($10^3 \leq Ra \leq 10^6$) and temperature difference of $0 \leq \Delta T \leq 50$ for air as a working fluid. For given Rayleigh number, the heat transfer rate show linear variation with ΔT. Thereafter, Kim et al. (2008) presented the natural convection heat transfer in an enclosure with cold wall temperature containing hot square block for laminar range of Rayleigh number ($10^3 \leq Ra \leq 10^6$) by using immersed boundary-finite volume method (IB-FVM). They reported remarkable influence of Rayleigh number and the position of the inner circular cylinder on the size and location of convection cell. Numerical investigation of rectangular built-in block in a square cavity on natural convection flow and heat transfer characteristics was carried out by Lu et al. (2009) by using thermal lattice Boltzmann method (TLBM) for heat intensity parameter, i.e., Rayleigh number of $10^3 \leq Ra \leq 10^7$ and air as a working fluid. The results indicated the width of rectangular block and Rayleigh number has remarkable influence on flow structure which can be viewed from different zones appeared in cavity, i.e., steady, periodical, and chaos. Similarly, the influence of location of circular cylinder placed in a square cavity on natural convection heat transfer behavior is studied by Lee et al. (2010). In particular, the location of cylinder at horizontal and diagonal position is investigated for Rayleigh number range of $10^3 - 10^6$. They observed the occurrence of local peaks of the Nusselt number along the surfaces of the cylinder and the enclosure is determined by the gap and the thermal plume governed by the conduction and the convection, respectively. The study of 2D mixed convection from a heated built-in square solid block located at the center of a vented cavity filled with air ($Pr = 0.71$) is carried out by Chamkha et al. (2011). They explored the influence of the outlet positions, Richardson numbers ($0 \leq Ri \leq 10$), Reynolds numbers ($50 \leq Re \leq 200$), locations ($0.25 \leq L_x \leq 0.75$ and $0.5 \leq L_y \leq 0.75$), and aspect ratio ($0.1 \leq AR \leq 0.4$) of inner square cylinder on the natural convection flow and heat transfer by using finite difference method (FDM). The results indicated the rise in average Nusselt number values with Reynolds and Richardson numbers. Subsequently, the combined effects of magnetic field and Joule heating on mixed convection heat transfer characteristics in a lid driven cavity containing a heat-conducting square

block is delineated by Rahman et al. (2011c). The walls of square cavity is maintained by different temperatures. They solved field equations by using a Galerkin weighted residual finite element method with a Newton-Raphson iterative algorithm. They reported that flow and thermal fields strongly depend on magnetic parameter, joule heating parameter, and the size of the inner block at the pure mixed convection zone.

Recently, numerical simulation of natural convection between a circular enclosure and a sinusoidal cylinder is delineated by Sheikholeslami et al. (2013a). They used control volume based finite element method for solving field equation for the broad range of flow governing parameters, such as, Rayleigh number ($10^3 \leq Ra \leq 10^6$), and the number of undulations of the inner cylinder ($N = 2, 3, 5, 6$) and amplitude values ($A = 0.1, 0.3, 0.5$). They reported strong influence of physical parameters on size and formation of the cells inside the enclosure.

2.3 Flow across a heated square obstacle

A considerable amount of research work has been conducted well over the past decades to investigate the flow past heated obstacles of varying shapes (viz., circular, square, triangular) owing to its wide range of applications in industrial and domestic fields. Additionally, this problem is considered as classical flow problem in the the field of transport phenomenon, as it exhibit variety of fluid flow characteristics. The bulk of literature referring to cylinder of circular cross section followed by square, elliptical and rectangular is available. Some pioneering work delineating the role of built-in square cylinder in a channel flow on the hydrodynamic features is reported by (Hasimoto, 1959; Lee, 1975; Matida et al., 1975; Rockwell, 1977; Robertson et al., 1978; Gerrard, 1978; Obasaju, 1979; Petty, 1979; Kareem and Cermak, 1984; Roshko, 1993). An extensive review on the flow past a circular cylinder is now available, (Zdravkovich, 1997a,b; Chhabra, 1996, 1999). Huge amount of literature now available for flow past a square cylinder for laminar as well as turbulent condition and blockage ratios. However, very few studies have been illustrated the heat transfer characteristics of steady cross flow past a square cylinder for combined

effect of Reynolds number and blockage ratio. Further, flow past a square cylinder in unconfined condition have been studied much extensively than confined one (Minewitsch et al., 1994; Paliwal et al., 2003; Bin et al., 2003; Sharma and Eswaran, 2004; Dhiman et al., 2006a,b; Sahu et al., 2009; Agrawal et al., 2006; Dhiman et al., 2007; Dhiman, 2009a; Sharma and Eswaran, 2010; Chatterjee and Biswas, 2011; Chatterjee and Mondal, 2011; Etminan-Farooji et al., 2012). In contrast, there is very limited information available exploring the effect of wall confinement (higher blockage ratio) on forced convection heat transfer characteristics. For instance, Biswas et al. (1990) have explored the mixed convection heat transfer characteristics from heated built-in square cylinder for range of flow governing parameters such as, Reynolds number ($80 \leq Re \leq 500$), Grashof number ($0 \leq Gr \leq 25600$) and constant Prandtl number ($Pr = 0.7$). They reported the enhancement of fluid temperature in channel for particular Reynolds number in mixed convection for range of Grashof number. In their study, at lower Reynolds number, periodicity and asymmetry were initiated for mixed convection. Subsequently, Turki et al. (2003b,a) elucidated the influence of blockage ratio ($\beta = 1/4, 1/8$) on fluid flow and heat transfer characteristics by using the control volume finite element method (CVFEM) for the range of flow governing parameters such as Reynolds number ($60 \leq Re \leq 200$), Richardson number ($0 \leq Ri \leq 0.1$) at $Pr = 0.71$. They observed flow instability at $Ri = 0.13$. Afterwards, Gupta et al. (2003) studied the forced convection heat transfer characteristics in a steady, laminar flow past confined square cylinder for physical parameters such as, Reynolds number ($5 \leq Re \leq 40$), Peclet number ($5 \leq Pe \leq 400$), non Newtonian power law index ($0.2 \leq n \leq 1.5$) and at constant blockage ($\beta = 1/8$). They observed small size as well as delay in wake formation for shear shining fluids. For shear thickening, a opposite behavior is observed. Similarly, Dhiman et al. (2005) investigated the combined effect of blockage ratio ($\beta = 1/2, 1/4, 1/8$), Reynolds number ($5 \leq Re \leq 40$), Prandtl number ($0.71 \leq Pr \leq 4000$) on the heat transfer and fluid flow characteristics of channel flow built in square cylinder. They observed linear increase in average Nusselt number with Reynolds and Prandtl numbers. Consequently, Sharma and Eswaran (2005) elucidated the influence of wall confinement on thermal and hydrodynamic nature of channel

built-in square cylinder for range of flow governing physical parameters such as blockage ratio ($0.1 \leq \beta \leq 0.5$), Reynolds number ($Re = 50, 100, 150$) and Prandtl number of $Pr = 0.71$. In their study, different engineering parameters (Strouhal number, Drag coefficient, Nusselt number) shown proportional increase with blockage ratio. The vortex structures of flow past a square cylinder placed in the vicinity of channel wall is studied by Bhattacharyya and Maiti (2006) for higher Reynolds number ($Re \geq 500$) and the gap between the plane wall to the cylinder to be $L_g = 0.25b$ by using SIMPLER. approach. The shear layer emerging from the bottom face of the cylinder reattaches to the cylinder itself at $L_g > 0.2$.

Dhiman et al. (2008a) elucidated combined influence of power law index ($0.5 \leq n \leq 2.0$) and blockage ratio ($\beta = 1/4, 1/6, 1/8$) on the steady flow hydrodynamics in channel flow with built-in square cylinder for range of Reynolds number ($1 \leq Re \leq 45$). In their study, size of wake region and drag coefficient values are more influenced by blockage ratio and Reynolds number than power law index. Subsequently, the numerical investigation of laminar, steady, mixed convection is carried out by Dhiman et al. (2008b) by using finite volume method. They presented numerical results for wide range of parameters such as, Reynolds number ($1 \leq Re \leq 30$), Richardson number ($0 \leq Ri \leq 1$), Prandtl number ($0.71 \leq Pr \leq 100$) at constant blockage of $\beta = 0.125$. It is observed that lift coefficient have more predominant effect of Richardson number (Ri) than drag coefficient. The effect of wall confinement on wake transition in channel with built-in square cylinder is examined by Patil and Tiwari (2008). In their study, the influence of the critical Reynolds number (Re_{cr}) and blockage ratio ($0.125 \leq \beta \leq 0.7$) on the onset of planer vortex shedding have been investigated. They observed the delay in onset of planer vortex shedding for $0.125 \leq \beta \leq 0.38$ and decrease in Re_{cr} for $\beta > 0.38$. Similarly, Sahu et al. (2010) investigated the influence of blockage ratio ($\beta = 1/2, 1/4, 1/6$), Reynolds number ($60 \leq Re \leq 160$) and power law index ($0.5 \leq n \leq 1.8$) on hydrodynamics of channel built-in square cylinder. The increase in blockage ratio caused delay in onset of vortex shedding to higher Reynolds number for range of power law index. Rao et al. (2010) numerically analyzed the fluid flow and forced convection heat transfer characteristics

by using commercial CFD package $FLUENT$. They explored the effects of Reynolds number effect ($0.1 \leq Re \leq 40$) on the onset of flow separation and the limits of the steady flow regime for non-Newtonian power law fluids ($0.2 \leq n \leq 1.4$) and Prandtl numbers ($0.71 \leq Pr \leq 100$). They observed linear dependence of average Nusselt number ($\overline{Nu}$) on the Reynolds and Prandtl numbers. Three dimensional analysis of aerodynamic coefficients and wake region past a inclined square cylinder is reported by Yoon et al. (2012). They delineated the influence on the wake structure for range of Reynolds number (Re=150, 200, 250 and 300) and angle of inclination ($0^o \leq \theta 25^o$). They concluded that wake region and aerodynamic coefficients are sensitive to inclination of the square cylinder, and the Reynolds number effects are insignificant except for mean lift coefficient.

Recently, Reyes et al. (2013) experimentally investigated the three dimensional analysis of flow past a square cylinder at high blockage ratio ($\beta = 1/2.5$) for range of Reynolds number ($100 \leq Re \leq 256$) and channel aspect ratio (1/1). They reported the delay in onset of vortex shedding at $Re \approx 170$ which for unconfined case is in the range of $50 \leq Re \leq 60$ and slow transition of steady closed circulation bubble region to vortex shedding region. Furthermore, the influence of inserted square obstacle on wall heat transfer rate in channel flows under laminar and unsteady flow condition is reported by Park (2013). The physical parameters used in their study are Reynolds number ($Re = 50, 150$), gap distance ratio ($0.1 - 1$) and blockage ratio ($\beta = 0.1, 0.125, 0.2$) on rate of heat transfer. The results of their study shown linear increase in average Nusselt number ($\overline{Nu}$) with disappearance in the re-circulation length.

More recently, Rashidi et al. (2014) reported the numerical analysis of forced convective heat transfer from a heated square-diamond shaped porous cylinder for range of governing parameters, such as Reynolds number ($1 \leq Re \leq 45$), Darcy number ($10^{-6} \leq Da \leq 10^{-2}$) and porosity ($\epsilon = 0.5$). They reported the decrease in drag coefficient and delay in flow separation with Darcy number for range of Reynolds number. They also observed the shrink in thermal plume with decrease in Darcy number.

2.3.1 LBM studies on flow past square/rectangular cylinder

The lattice Boltzmann method (LBM) have also been used for investigating heat transfer and fluid flow characteristics of channel built-in square cylinder. For instance, Breuer et al. (2000) used lattice Boltzmann method as well as finite volume method for investigating flow hydrodynamics of channel flow with built-in square cylinder for range of Reynolds number ($1 \leq Re \leq 300$) at a constant blockage ratio ($\beta = 1/8$). Both numerical methods provide the local maximum of Strouhal number at $Re = 150$. Subsequently, Agrawal et al. (2006) presented the LBM investigation of low Reynolds number fluid flow characteristics around two square cylinders placed side-by-side. They elucidated the influence of the gap ratio (s/d is the separation between the cylinders and d is the characteristic dimension) on momentum characteristics at Re=73. The major finding of their study was the vortex-shedding from the cylinder occurs either in phase or anti-phase in the synchronized zone. Cheng et al. (2007) determined flow characteristics in linear shear flow past a square cylinder. Numerical experimentation were carried out for wide ranges of flow governing conditions such as Reynolds number ($50 \leq Re \leq 200$) and shear rate ($0 - 0.5$). They found strong influence of Reynolds number and shear rate on vortex shedding and wake formation behind the square cylinder. On the other hand, Han et al. (2007) presented the interpolation-supplemented and Taylor-series expansion-based lattice Boltzmann method and its application to flow past a square cylinder. The physical insights and re-circulation length is obtained at Reynolds number of Re=1 and 15. The aim of their study was to propose the non-uniform mesh structure for the lattice Boltzmann models. Subsequently, Rowghani et al. (2010) carried out lattice Boltzmann simulation of flow past a square cylinder to investigate the influence of wide range of Reynolds number ($0.5 \leq Re \leq 300$) for constant blockage ratio of ($\beta = 1/8$) on fluid flow characteristics (stream lines and vorticity) and engineering parameters (drag coefficient, Strouhal number). For computed drag results, local minima was observed at $Re = 150$ in their study. Later, Moussaoui et al. (2011) presented the lattice Boltzmann computation of flow and heat transfer past three heated square cylinders in a V shape arrangement by using double multiple relaxation time (MRT) approach. The physical parameters used for numerical experimentation are

Reynolds number ($10 \leq Re \leq 100$), gap to diameter ratio (S=1,2) and air ($Pr = 0.71$) as working fluid. They observed by varying S, the nusselt number get insignificantly affected. Perumal et al. (2012) elucidated the effect of Reynolds number ($10 \leq Re \leq 40$) at constant blockage ratio of $\beta = 1/8$ on laminar fluid flow characteristics (stream lines, vorticity, drag and lift coefficients, etc.) of a square cylinder. The critical Reynolds number was found to be $Re = 52$ at $\beta = 1/8$. At this Reynolds number, they studied the influence of cylinder location. At low blockage ratio and $Re = 52$, vortex shedding was found to be strongly dependent. Recently, Premnath et al. (2013) used a multi-block LBM with dynamic sub-grid scale for investigation of transitional flow past a circular cylinder at Reynolds number ($Re = 3900$). They used multiple relaxation time and five different blocks encompassing different grids structure by for numerical computation. In their study, Smagorinsky eddy-viscosity model is used for representing the sub-grid scales effect. The LBM simulation of flow past a side by side placed square cylinders is reported by Burattini and Agrawal (2013). They investigated the wake interaction between square cylinders at constant Reynolds number of Re=73. by varying the lateral separation between cylinders in the range of 0.5-6. They reported nearly constant value of Strouhal number (≈ 0.16). The results of their study indicated the amplitude of the modulation follows a systematic pattern in time that can be obtained by a system of coupled Landau equations. More recently, the lattice Boltzmann simulation of power-law fluid flow and heat transfer characteristics in a channel with a built-in porous square cylinder is reported by Nazari et al. (2014). They investigated the influence of the different arrangements of obstacles, Reynolds number ($Re = 100, 200, 300$), power index ($n = 0.8, 1, 1.2$), blockage ratio ($\beta = 1/2, 1/4, 1/8$) and porosity ($0.75 \leq \epsilon \leq 1$) on the heat transfer characteristics. They observed increase in heat transfer rate with blockage ratio. Table 2.6 represents the summery of literature encompassing the convection heat transfer from built in square cylinder by numerical methods other than the lattice Boltzmann method (LBM). The literature based on use of LBM for study of flow past a square cylinder is expressed in Table 2.7.

TABLE 2.6: A summary of literature on convection heat transfer from confined square cylinder by numerical methods other than LBM.

Source	Physical Parameters	Numerical method	Study Remarks
	Mixed convection		
Biswas et al. (1990)	$80 \leq Re \leq 500; 0 \leq Gr \leq 25600; Pr = 1$	FDM	At lower Reynolds number, periodicity and asymmetry were initiated for mixed convection
Turki et al. (2003b,a)	$\beta = 1/4, 1/8; 0 \leq Ri \leq 0.1; Pr = 0.71$	CVFEM	Flow instability at $Ri = 0.13$
Dhiman et al. (2008b)	$1 \leq Re \leq 30; 0 \leq Ri \leq 1; 0.71 \leq Pr \leq 100; \beta = 0.125$	FVM	Lift coefficient have more predominant effect of Richardson number (Ri) than drag coefficient
	Forced convection		
Gupta et al. (2003)	$5 \leq Re \leq 40; 5 \leq Pe \leq 400; 0.2 \leq n \leq 1.5; \beta = 1/8$	SMAC implicit	Small size as well as delay in wake formation for shear shining fluids. For shear thickening, a opposite behavior is observed
Dhiman et al. (2005)	$\beta = 1/2, 1/4, 1/8; 0.71 \leq Pr \leq 4000; 5 \leq Re \leq 40$	FVM	Linear increase in average Nusselt number with Reynolds number and Prandtl number
Sharma and Eswaran (2005)	$0.1 \leq \beta \leq 0.5; Re = 50, 100, 150; Pr = 0.71$	FVM	Different engineering parameters shown proportional increase with blockage ratio
Dhiman et al. (2008a)	$0.5 \leq n \leq 2.0; \beta = 1/4, 1/6, 1/8; 1 \leq Re \leq 45$	FVM	Size of wake region and drag coefficient values are more influenced by blockage ratio and Reynolds number than power law index
Patil and Tiwari (2008)	$0.125 \leq \beta \leq 0.7$	FDM	delay in onset of planer vortex shedding in $(0.125 \leq \beta \leq 0.38)$ and decrease in Re_{cr} for $\beta > 0.38$
Sahu et al. (2010)	$\beta = 1/2, 1/4, 1/6; 60 \leq Re \leq 160; 0.5 \leq n \leq 1.8$	FVM	The increase in blockage ratio causes delay in onset of vortex shedding to higher Reynolds number for range of power law index was observed
Reyes et al. (2013)	$100 \leq Re \leq 256; \beta = 1/2.5;$	FDM	Delay in onset of vortex shedding is observed at ≈ 170

2.4 Flow past a rectangular obstacle

The momentum and thermal characteristics of flow past a rectangular cylinder is studied less extensively than circular and square cylinders. Few studies have illustrated the fluid flow and heat transfer characteristics of steady cross flow past a rectangular cylinder for combined effect of aspect ratio of cylinder and blockage ratio.

For instance, Okajima (1982) experimentally investigated the vortex-shedding frequencies of various rectangular cylinders in a wind tunnel and in a water tank. The aspect ratio of rectangular cylinder in their study was a=2 and 3 for range of Reynolds number ($70 \leq Re \leq 2 \times 10^4$). The critical Reynolds number shown strong dependence upon the aspect ratio of the cylinder in their study. Similarly, Davis and Moore (1982) and Davis et al. (1983) numerically analyzed the vortex shedding from rectangular cylinder in unconfined and confined channel domain, respectively. The flow governing parameters used in their study was Reynolds number ($100 \leq Re \leq 280$), blockage ratio ($1/4, 1/6$), aspect ratio ($1 \leq a_r \leq 4$) and ($0.6 \leq a_r \leq 1.7$) and upstream velocity profile. They observed increase in drag and Strouhal number with increase in channel confinement (decrease in blockage ratio). Subsequently, Norberg (1993) presented the experimental study of flow around rectangular cylinders to investigate the pressure forces and wake frequencies for range of flow governing parameters (aspect ratio:$1 \leq a_r \leq 3$, Reynolds number: $4 \leq Re \leq 3 \times 10^4$, angle of attack of cylinder: $0^o - 90^o$). They observed multiple wake frequencies at small angles of attack for certain range of Reynolds number and with aspect ratio ($a_r = 2 - 3$). Later, the numerical investigation of unsteady flow-Reynolds number (≤ 200) flow around rectangular cylinder with aspect ratio ($1 \leq a_r \leq 4$) at angle of incidence ($0^o - 90^o$) is reported by Sohankar et al. (1997). The flow separation at downstream corners is observed for cases with one side opposing flow at Re=100. Yang and Fu (2001) reported the fluid flow and heat transfer characteristics from a oscillating rectangular cylinder for wide range physical parameters such as, Reynolds number ($Re = 250, 500$), oscillating speed (0.333,0.5 and 1), oscillating amplitude (0.125,0.333,0.5 and 0.75), aspect ratio ($a_r = 1, 2$)

TABLE 2.7: A summary of literature on convection heat transfer from confined square cylinder by LBM.

Source	Physical Parameters	Study Remarks
Breuer et al. (2000)	$1 \leq Re \leq 300$	Local maximum of Strouhal number at $Re = 150$
Cheng et al. (2007)	$50 \leq Re \leq 200$; Shear rate=0-0.5	Strong dependence of shear rate on vortex shedding and wake formation behind the square cylinder
Rowghani et al. (2010)	$0.5 \leq Re \leq 300; \beta = 1/8$	For computed drag results, local minima was observed at $Re = 150$
Perumal et al. (2012)	$10 \leq Re \leq 40; \beta = 1/8$	The critical Reynolds number was found to be $Re = 52$ at $\beta = 1/8$.
Premnath et al. (2013)	$Re = 3900; \beta = 1/8$	Multiple relaxation time and five different blocks encompassing different grids structure by for numerical computation
Nazari et al. (2014)	$Re = 100, 200, 300; n = 0.8, 1, 1.2; \beta = 1/8$ $\beta = 1/2, 1/4, 1/8; 0.75 \leq \epsilon \leq 1$	Increase in heat transfer rate with blockage ratio

and blockage ratio ($\beta = 0.1, 0.2$). They observed heat transfer enhancement with aspect ratio of rectangular cylinder.

Nitin and Chhabra (2005) elucidated the combined effect of non-Newtonian power law index ($0.5 \leq n \leq 1.4$), Reynolds number ($5 \leq Re \leq 40$), Peclet number ($5 \leq Pe \leq 400$) and blockage ratio ($\beta = 1/8$) on momentum and heat transfer characteristics from heated built-in rectangular cylinder of aspect ratio (width/height) of 2. They observed that increasing power law index caused decrease in both drag and Nusselt number values. Furthermore, Zhi-Qiang and Jie (2005) presented the numerical simulation of flow past a confined rectangular cylinder, which is oscillating. They considered the momentum characteristics as a dynamic and moving boundary problem. They used Galerkin finite element formulation with moving meshes as a numerical tool. They reported significant variation of vortex structures of square cylinder than circular one.

A Three dimensional numerical study of turbulent, separated and reattached flow around rectangular cylinder is reported by Bruno et al. (2010). Subsequently, the lattice Boltzmann simulation of flow past a rectangular cylinder with different aspect ratio have been reported by Islam et al. (2012). The aspect ratio of rectangular cylinder used in their study are $0.15 \leq a_r \leq 4$ for Reynolds number of $Re = 100, 150, 200, 250$ and a constant blockage ratio of $\beta = 1/12$. They observed discontinuity in the range of $1.25 \leq a_r \leq 1.6$, obtained from multiple peaks by Fourier spectrum analysis of the lift force.

2.5 Summary of literature reviews

Based on the aforementioned discussion of the available literature, following remarks can be drawn:

1. Among other CFD methods, Lattice Boltzmann method (LBM) have been successfully utilized over the decades to investigate the convective heat transfer characteristics.

2. Most of studies have reported the flow and thermal characterstics of a single fluid (i.e., fixed value of Prandtl number) in differentially heated square cavity and/or range of Prandtl number for non-differential heated square cavity. To the best of our knowledge, none of the studies, have explored the combined effect of Prandtl number ($0.71 \leq Pr \leq 100$) and Rayleigh number ($10^4 \leq Ra \leq 10^6$) on the natural convection heat transfer in differentially heated square cavity by using LBM.

3. Very limited information is available about the heat transfer characteristics of partially heated enclosures. In particular, the scant results is available exploring combined influence of cooler size and magneto-hydrodynamics (MHD) natural convection in differentially heated cavity.

4. Natural convection in open ended cavity has been well explored over the last few decades, but most of the studies have delineated the heat transfer characteristics of completely heated wall of cavity. Much less is known about combined influence of Prandtl number and partial heating (effect of heating location and size) on heat and fluid flow behavior of open ended cavity.

5. For problem of natural convection in square cavity containing built-in square block, most of the studies have explored the physical insights for constant working fluid (mostly, air). Thus, study of such systems at range of Prandtl numbers is desirable.

6. Forced convection from built-in square cylinder has been studied much extensively. Most of the studies have delineated the influence of Reynolds number at low blockage ratios ($\beta \leq 1/8$). None of the studies, as much known to author, have explored combined effect of aspect ratio of rectangular cylinder, blockage ratio (high) and Reynolds number.

2.6 Objectives

Based on the review of available literature, the following objectives are set up for the present research.

1. Development of the thermal lattice Boltzmann method (TLBM) solver (in C++ programming language) and its utilization for the analysis of following problems.
2. Natural convection heat transfer in differentially heated square cavity: Effect of Prandtl and Rayleigh number.
3. Natural convection in partially-differentially-simultaneously heated/cooled square cavity: Effect of Rayleigh number.
4. Magneto-hydrodynamic natural convection in partially heated square cavity: Effect of cooler size and Hartmann number.
5. Natural convection in partially heated square open ended enclosures: Effect of size and location of partial heater.
6. Natural convection in cavity containing heated square body: Effect of Prandtl number.
7. Steady forced convection heat transfer from heated built-in rectangular cylinder: Effect of wall confinement, aspect ratio of cylinder and Reynolds number.

The next chapter discusses the general assumptions and the governing equations to fulfill the objectives setup in this work.

Chapter 3

GOVERNING EQUATIONS AND DIMENSIONLESS PARAMETERS

This chapter presents the general assumptions, governing field equations along with the dimensionless physical flow governing parameters used in this study. Additionally, the engineering parameters (stream-function, nusselt number, drag force, etc.) are also have been defined and discussed. The problems considered in present work are listed below:

1. Natural convection in differentially heated square cavity.
2. Natural convection in partially-differentially-simultaneously heated/cooled square cavity.
3. Magneto-hydrodynamic natural convection in partially heated square cavity.
4. Natural convection in partially heated square open ended enclosures.
5. Natural convection in cavity containing heated square body.
6. Steady forced convection heat transfer from heated built-in rectangular cylinder.

Thus, the field equations of natural, magneto hydrodynamic (MHD) natural and forced convection heat transfer are presented herein with the general assumptions.

3.1 General assumptions

The following general assumptions are considered herein this work.

1. Two dimensional flow
2. Incompressible fluid
3. Steady state flow
4. Laminar flow
5. Temperature difference ($\Delta T = T_h - T_c$) is small.
6. In case of forced convection, the thermo-physical (namely, density, viscosity, thermal conductivity and heat capacity) are considered to be independent of temperature.
7. In case of natural convection, the thermo-physical properties of the fluid are considered to be a independent of the temperature except the density of the fluid appearing in the body force term in momentum equation.
8. *Boussinesq approximation* (for natural convection problems): For small to moderate variation in the density with the temperature, it is sufficient as well as common to use the well-known Boussinesq approximation to express its dependence on the temperature as $\rho = \overline{\rho}[1 - \beta_t(T - \overline{T})]$, where β_t is coefficient of volumetric expansion at constant pressure and average fluid density ($\overline{\rho}$) at a reference temperature $\overline{T} = \left(\frac{T_H + T_C}{2}\right)$ (Kuznik et al., 2007; Peng et al., 2003a). This approximation is customarily invoked to maintain the level of complexity at a traceable level in most of the studies related to natural/mixed convection (Srinivas et al., 2009). The Boussinesq approximation evidently couples the Navier-Stokes equations with the thermal energy equation, therefore simultaneous solution of these governing equation is required.

9. Further, in this work, viscous heat dissipation, radiation heat transfer and compression work done by pressure are neglected. This approximation restrict the applicability of the present results to the situations where the temperature difference (ΔT) is not too large and/or for moderate viscosity so that the viscous dissipation effects are negligible. Keeping in mind the limitations of the Boussinesq approximation, the temperature difference (ΔT) is maintained to be small such that it justifies the unaccountably of the variation of the fluid viscosity with temperature.

3.2 Governing equations

The convective flow and heat transfer is governed by the equations of continuity, momentum and thermal energy. Under the general assumption, these field equations can be written as follows:

- Continuity equation (mass):

$$\frac{\partial u_x}{\partial x} + \frac{\partial u_y}{\partial y} = 0 \tag{3.1}$$

- x-component of momentum equation:

$$\rho\left(u_x\frac{\partial u_x}{\partial x} + u_y\frac{\partial u_x}{\partial y}\right) = -\frac{\partial p}{\partial x} + \mu\left(\frac{\partial^2 u_x}{\partial x^2} + \frac{\partial^2 u_x}{\partial y^2}\right) + F_x \tag{3.2}$$

- y-component of momentum equation:

$$\rho\left(u_x\frac{\partial u_y}{\partial x} + u_y\frac{\partial u_y}{\partial y}\right) = -\frac{\partial p}{\partial y} + \mu\left(\frac{\partial^2 u_y}{\partial x^2} + \frac{\partial^2 u_y}{\partial y^2}\right) + F_y \tag{3.3}$$

- Thermal energy equation:

$$\left(u_x\frac{\partial T}{\partial x} + u_y\frac{\partial T}{\partial y}\right) = \alpha\left(\frac{\partial^2 T}{\partial x^2} + \frac{\partial^2 T}{\partial y^2}\right) \quad (\text{where} \quad \alpha = \frac{k}{\rho c_p}) \tag{3.4}$$

where, (x, y), (u_x, u_y), p, ρ, α, μ, T and (F_x, F_y) are coordinates along horizontal and vertical directions respectively, velocity components, pressure, density of fluid, fluid thermal diffusivity, kinematic viscosity, temperature, force terms, respectively. The above field equations can be classified into natural, magneto-hydrodynamic (MHD) natural and forced convection field equations by suitably defining the force terms (F_x and F_y) as follows:

- For natural convection,

$$F_x = 0 \quad \text{and} \quad F_y = g_y \rho \beta (T - \overline{T}) \tag{3.5}$$

- For MHD natural convection,

$$\begin{aligned} F_x = & \quad \sigma \mathbf{B}^2 \left[u_y sin\theta_M cos\theta_M - u_x sin^2\theta_M \right] \\ F_y = & \quad \rho g_y \beta (T - \overline{T}) + \sigma \mathbf{B}^2 \left[u_x sin\theta_M cos\theta_M - u_y cos^2\theta_M \right] \end{aligned} \tag{3.6}$$

- For forced convection,

$$F_x = 0 \quad \text{and} \quad F_y = 0 \tag{3.7}$$

The dimensionless form of the above noted field equations can be expressed as follows:

$$\frac{\partial U_x}{\partial X} + \frac{\partial U_y}{\partial Y} = 0 \tag{3.8}$$

$$\left(U_x \frac{\partial U_x}{\partial X} + U_y \frac{\partial U_x}{\partial Y} \right) = -\frac{\partial P}{\partial X} + \frac{1}{\Gamma_m} \left(\frac{\partial^2 U_x}{\partial X^2} + \frac{\partial^2 U_x}{\partial Y^2} \right) + \overline{F_x} \tag{3.9}$$

$$\left(U_x \frac{\partial U_y}{\partial X} + U_y \frac{\partial U_y}{\partial Y} \right) = -\frac{\partial P}{\partial Y} + \frac{1}{\Gamma_m} \left(\frac{\partial^2 U_y}{\partial X^2} + \frac{\partial^2 U_y}{\partial Y^2} \right) + \overline{F_y} \tag{3.10}$$

$$\left(U_x \frac{\partial \theta}{\partial X} + U_x \frac{\partial \theta}{\partial Y} \right) = \frac{1}{\Gamma_e} \left(\frac{\partial^2 \theta}{\partial X^2} + \frac{\partial^2 \theta}{\partial Y^2} \right) \tag{3.11}$$

In Eqs. (3.8) to (3.11), reference length (H), reference velocity (V) and reference pressure (ρV^2) are used to scale the length, velocities and pressure, respectively. The dimensionless temperature is defined as $\theta = (T - T_c)/(T_h - T_c)$. The dimensional force terms ($\overline{F_x}$ and $\overline{F_y}$) are written as:

- Natural convection,

$$\overline{F_x} = 0 \quad \text{and} \quad \overline{F_y} = (Ra \times Pr)\ \theta \tag{3.12}$$

- MHD Natural convection,

$$\begin{aligned} \overline{F_x} = & \quad PrHa^2 \left[U_y sin\theta_M cos\theta_M - U_x sin^2\theta_M\right] \\ \overline{F_y} = & \quad (Ra \times Pr)\ \theta + PrHa^2 \left[U_x sin\theta_M cos\theta_M - U_y cos^2\theta_M\right] \end{aligned} \tag{3.13}$$

- Forced convection,

$$\overline{F_x} = 0 \quad \text{and} \quad \overline{F_y} = 0 \tag{3.14}$$

$$\tag{3.15}$$

The momentum and energy diffusion coefficients (Γ_m and Γ_e) are given as follows:

- For natural convection,

$$\Gamma_m = Pr \quad \text{and} \quad \Gamma_e = \sqrt{Ra \times Pr} \tag{3.16}$$

- For forced convection,

$$\Gamma_m = Re \quad \text{and} \quad \Gamma_e = Pr = Re \times Pr \tag{3.17}$$

The above governing equations may be subjected to the following boundary conditions, depending on the nature of problem.

- No-slip condition,

$$u_x = u_y = 0 \qquad \text{or} U_x = U_y = 0$$

- Open end condition,

$$\frac{\partial u_x}{\partial x} = \frac{\partial u_y}{\partial x} = 0 \qquad \text{or} \frac{\partial U_x}{\partial X} = \frac{\partial U_y}{\partial X} = 0$$

- In-flow fully developed condition,

$$u_x = u_{max}\left[1 - \left(1 - \frac{2y}{H}\right)^2\right] \qquad \text{or} U_x = U_{max}\left[1 - (1 - 2Y)^2\right]$$

- Outflow condition,

$$\frac{\partial u_x}{\partial x} = \frac{\partial u_y}{\partial x} = 0 \qquad \text{or} \frac{\partial U_x}{\partial X} = \frac{\partial U_y}{\partial X} = 0$$

- Isothermal condition,

$$T = T_H/T_C \qquad \text{or} \theta = \theta_H/\theta_C$$

- Adiabatic condition

$$\frac{\partial T}{\partial x(/y)} = 0 \qquad \text{or} \frac{\partial \theta}{\partial X(/Y)} = 0$$

3.2.1 Dimensionless parameters

The various flow governing physical, dimensionless parameters along with its physical meaning used in present work are presented in tabular form as follows (Table 3.1).

Moreover some physical parameters used in this study are expressed below.

TABLE 3.1: A list of the physical parameters considered in present work.

Sr. No.	Parameter	Significance
1.	Grashof number, $Gr = \frac{g\beta\Delta T H^3}{\alpha^2}$	$\frac{\text{Buoyancy force}}{\text{viscous force}}$
2.	Peclet number, $Pe = \frac{LV}{\kappa}$	$\frac{\text{Heat convection}}{\text{Heat conduction}}$
3.	Prandtl number, $Pr = \frac{C_p\mu}{\kappa}$	$\frac{\text{Momentum diffusion}}{\text{Heat diffusion}}$
4.	Reynolds number, $Re = \frac{DV\rho}{\mu}$	$\frac{\text{Inertial force}}{\text{Viscous force}}$
5.	Rayleigh number, $Ra = \frac{g\beta\Delta T H^3}{\nu\mu}$	$\frac{\text{Inertial force}}{\text{Diffusion force}}$
6.	Hartmann number, $Ha = BH\sqrt{\frac{\sigma}{\mu}}$	$\frac{\text{Electromagnetic force}}{\text{Viscous force}}$

κ: Thermal conductivity, B: Magnetic field, σ: Electrical conductivity

- Characteristic velocity (V): Since the characteristic velocity used in the scaling of natural convection problem is not known, thus it's estimation is an important step. In case of natural convection, the reference velocity (V) is approximated (Mohamad et al., 2009; Kuznik et al., 2007; Fattahi et al., 2010, 2012) and also expressed as a function of dimensional groups as follow.

$$V = \sqrt{g\beta\Delta T H} \quad \text{or} \quad V = \frac{\nu}{H}\sqrt{Gr} \quad \text{or} \quad V = \frac{\nu}{H}\sqrt{\frac{Ra}{Pr}} \tag{3.18}$$

- Estimation of pressure: The one of the advantage of LBM lies in the fact that unlike conventional CFD tools, estimation of the pressure field is very easy. For uniform lattice size it is given as below (Chen and Doolen, 1998),

$$P = c_s^2\rho = \frac{1}{3}\rho; \qquad \text{where}\left(c_s = \frac{1}{\sqrt{3}}\right) \tag{3.19}$$

- Surface pressure coefficient (C_P) is defined as ratio of static pressure on the surface of square cylinder to that of free stream pressure (Sivakumar et al., 2007). It is

expressed as follows:

$$C_P = 2\left(\frac{P_s - P_\infty}{\rho U_{avg}^2}\right) \tag{3.20}$$

where, P_s is pressure at the surface of square cylinder and P_∞ corresponds to free stream pressure.

- Similarly, the skin friction coefficient (C_F) along horizontal wall of cylinder can be expressed as,

$$C_f = \frac{2}{Re}\left(\frac{\partial U_x}{\partial Y}\right) \tag{3.21}$$

and for vertical surface of cylinder,

$$C_f = \frac{2}{Re}\left(\frac{\partial U_y}{\partial X}\right) \tag{3.22}$$

- The drag coefficient in non-dimensional form (Paliwal et al., 2003; Dhiman et al., 2006a) is represented as below:

$$C_D = \frac{F_D}{0.5\rho U_{avg}^2 b} = C_{DP} + C_{DF} \tag{3.23}$$

where, F_D is drag force exerted on square cylinder per unit length. C_D is normal force component (in z direction). While, x and y components are friction drag (C_{DF}) and pressure drag (C_{DP}), respectively. The pressure or form drag component is estimated by integrating pressure on two vertical faces of square cylinder. It is expressed as,

- Pressure drag coefficient

$$C_{DP} = \int_s C_P ds \tag{3.24}$$

- In similar manner, the friction drag coefficient along top and bottom walls of square cylinder can be evaluated as,

$$C_{DF} = \int_s C_F ds \tag{3.25}$$

- Re-circulation or wake length (L_r) is estimated from the rear face of square cylinder to the point of reattachment for closed streamlines ($U_x = U_y = 0$) on the symmetry line in downstream flow direction (Sivakumar et al., 2007).

$$L_r = \frac{L_r^*}{b} \tag{3.26}$$

- Stream-function is calculated from the converged velocity field. It is expressed as,

$$\psi = \int U_x dY \tag{3.27}$$

- Similarly, vorticity is calculated as,

$$\xi = \frac{\partial U_y}{\partial X} - \frac{\partial U_x}{\partial Y} \tag{3.28}$$

- Nusselt number: For elucidating the effect of convective heat transfer, Nusselt number (Nu) is considered as one of the important dimensionless parameter. The local and average Nusselt numbers (Chan and Tien, 1985) can be obtained as,

$$Nu = -\frac{\partial T}{\partial n} \tag{3.29}$$

$$\overline{Nu} = \int_s Nu\, ds \tag{3.30}$$

For problem of flow past a rectangular cylinder, the local and average Nusselt number are estimated (Chen and Tian, 2010) along face of cylinder as follow,

$$\overline{Nu}_{front} = \int_A^B Nu\, dX; \qquad \overline{Nu}_{rear} = \int_C^D Nu\, dX \tag{3.31}$$

$$\overline{Nu}_{bottom} = \int_B^C Nu\, dY; \qquad \overline{Nu}_{top} = \int_D^A Nu\, dY \tag{3.32}$$

The mean average Nusselt number along the square cylinder is estimated as follows:

$$\overline{Nu}_{mean} = \frac{\overline{Nu}_{front} + \overline{Nu}_{rear} + \overline{Nu}_{top} + \overline{Nu}_{bottom}}{4} \tag{3.33}$$

The governing equations of the problems considered herein are solved by using the lattice Boltzmann method to obtain the local and global characteristics. The next chapter discusses the basics of LBM along with numerical/computational algorithm.

Chapter 4

LATTICE BOLTZMANN METHOD

The chapter starts with the basics of lattice Boltzmann method (LBM), followed by governing equations of LBM, the recovery of mass, momentum and energy equations, the implementation of boundary condition and the computational algorithm.

4.1 Lattice Boltzmann Method

Mc Namara and Zanetti (1988) presented a lattice Boltzmann method by solving Boltzmann equation and eliminated the statistical noise present in the lattice gas automata (LGA). Further efforts of Higuera et al. (1989) simplified the complex nature of collision term present in Boltzmann equation. They used lattice Boltzmann equation along with the Bhatnagar-Gross-Krook (BGK) model called as lattice Bhatnagar-Gross-Krook (LBGK). Since then the lattice Boltzmann method (LBM) has been established as an alternative powerful computational method for solving fluid dynamics and heat transfer problems (Miller, 1995; Mohamad, 2011; Chen and Doolen, 1998). Though, lattice Boltzmann method has found its roots in lattice gas cellular automata, it can be derived from kinetic Boltzmann equation (He and Luo, 1997).

Conventional computational fluid dynamics (CFD) methods such as finite difference method (FDM), finite element method (FEM) and finite volume method (FVM) are based on dicretizations of macroscopic continuum equations whereas lattice Boltzmann method (LBM) is based on microscopic models and mesoscopic kinetic equation (Boltzmann equation). The fundamental idea of LBM is to construct simplified kinetic models. These simplified models include the essential physics of microscopic or mesoscopic processes in such a way that the microscopic averaged properties are suitable representation of the desired macroscopic equations. These models are simply the discrete distribution functions or population $f(\mathbf{x}, t) = f(\mathbf{x}, \mathbf{e}, t)$ which represents the probability of finding a particle moving with lattice speed *'e'* at position *'x'* and at time *'t'*. Advantages of kinetic nature of LBM over conventional CFD methods are simplicity in algorithm, implementation of boundary conditions at leisure, ease of parallel computing and handling of complex geometries. In conventional CFD methods, estimation of pressure field is normally time consuming as one has to solve Poisson like equation derived from incompressible Navier-Stokes equation, whereas pressure field calculation is extremely simple in LBM as it is done by simply using equation of state. Furthermore, the convection operator is linear, and microscopic distribution functions can be transferred to macroscopic physical quantities by simple arithmetic calculations (Succi and Higuera, 1991; Chen and Doolen, 1998; Mohamad, 2011).

4.1.1 Boltzmann Equation

An Austrian physicist named Ludwig Edward Boltzmann (1844-1906) made astonishing contribution towards the understanding of statistical mechanics. His work elucidated the properties of matter such as the viscosity, thermal conductivity, and diffusion coefficient by predicting the microscopic properties (atom and molecules)(Chen and Doolen, 1998; Sukop and Throne, 2005; Mohamad, 2011). In statistical mechanics, a system is represented by particle distribution function, $f(x, e, t)$. The term $f(x, e, t)$ constitutes the number of particles may be present at a position 'x' at time 't'. A general Boltzmann

equation without the external force term can be represented as follows (He and Luo, 1997; Mohamad, 2011):

$$\frac{\partial f}{\partial t} + \mathbf{e} \cdot \nabla f = \Gamma \tag{4.1}$$

where, f represents the probability distribution function, $\mathbf{e}$ and ∇f are vectors. Γ represents the collision term and is equal to the rate of change between final and initial state of the particle distribution function (PDF). The solution of Boltzmann equation is quite difficult and, hence, it was needed to approximate the collision operator with simple operator without significantly affecting the outcome of the solution. A simplified model for collision operator was introduced by Bhatnagar-Groos-Krook (BGK). The Boltzmann equation along with the BGK collision parameter is described (He and Luo, 1997; Chen and Doolen, 1998; Mohamad, 2011) as follows:

$$\frac{\partial f}{\partial t} + \mathbf{e} \cdot \nabla f = \frac{1}{\tau}\left[f - f^{eq}\right] \tag{4.2}$$

The time and space discretizations of Boltzmann equation (Eq. 4.2) yields the basic lattice Boltzmann equation. It is represented as follows:

$$f_k\left(\mathbf{x} + \mathbf{e_k}\Delta t, t + \Delta t\right) - f_k\left(\mathbf{x}, t\right) = -\frac{1}{\tau}\left[f_k\left(\mathbf{x}, t\right) - f_k^{eq}\left(\mathbf{x}, t\right)\right] \tag{4.3}$$

where, x, k, Δx, Δt, f_k, f_k^{eq}, e_k and τ are coordinates, lattice link direction, lattice step size, time step, particle distribution function, equilibrium distribution function and relaxation time, respectively. The parameters which differentiates the type of problem to be solved are, the relaxation parameter, local equilibrium distribution function and external force term.

In lattice Boltzmann method, the physical domain of chosen system need to be divided into lattices. At each lattice node, the factitious particles (i.e., distribution function) reside. Some of these particles colloids at a lattice node to relax to the equilibrium and some particles stream along respective lattice link directions to the neighboring nodes.

Thus, the evolution of the lattice Boltzmann method takes via two steps.

- Collision

$$\overline{f}\left(\mathbf{x}, t+\Delta t\right) = f_k\left(\mathbf{x}, t\right) - \frac{1}{\tau_\nu}\left[f_k\left(\mathbf{x}, t\right) - f_k^{eq}\left(\mathbf{x}, t\right)\right] \tag{4.4}$$

- Streaming

$$f_k\left(\mathbf{x} + \mathbf{e_k}\Delta t, t+\Delta t\right) = \overline{f}\left(\mathbf{x}, t+\Delta t\right) \tag{4.5}$$

Figure 4.1 illustrate the collision and streaming processes. These features of collision and streaming has been borrowed from the kinetic theory of gases (Chen and Doolen, 1998). The particles move in random direction, during which they colloid with each other and relax to the equilibrium and alter the velocity direction in accordance with scattering rules. The lattice Boltzmann method uses different lattice structures/arrangements for simulation. These are illustrated in subsequent section.

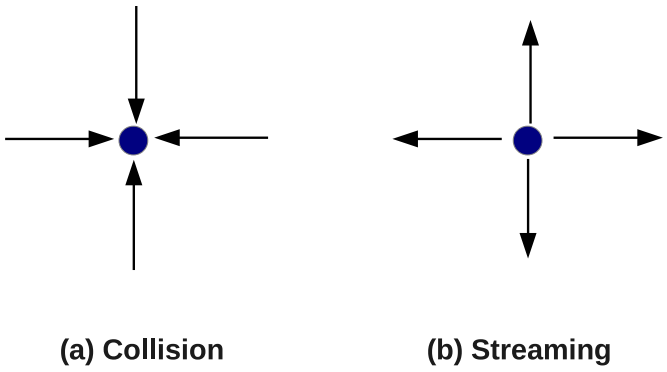

FIGURE 4.1: Evolution of lattice Boltzmann equation via (a) collision and (b) streaming.

4.1.2 Equilibrium distribution function

In lattice Boltzmann method, the concept of equilibrium distribution function is borrowed from kinetic theory of gases. It is very important parameter in LBM simulation as it decides the physics of problem, needed to be solved. The Maxwell-Boltzmann equilibrium

function (f^{eq}) in general form can be expressed as (Mc Namara and Zanetti, 1988; Qian, 1990; Qian et al., 1992, 1993; Chen and Doolen, 1998; Mohamad, 2011),

$$f^{eq} = \frac{\rho}{(2\pi/3)^{D/2}} e^{x_1} \quad \text{where} \quad x_1 = -\frac{3}{2}(\mathbf{e} - \mathbf{u})^2 \tag{4.6}$$

where, D is spatial dimension. It can be simplified as,

$$f^{eq} = \frac{\rho}{(2\pi/3)^{D/2}} e^{x_2} \quad \text{where} \quad x_2 = -\frac{3}{2}(c^2)\mathbf{e}\frac{(\mathbf{e}\cdot\mathbf{u} - u^2)}{2} \tag{4.7}$$

The Maxwell-Boltzmann equilibrium function (f^{eq}) after Taylor series expansion, takes the following general form (Chen et al., 1992),

$$f^{eq} = \Upsilon w_k \left[a + b(\mathbf{e_k}\cdot\mathbf{u}) + c(\mathbf{e_k}\cdot\mathbf{u})^2 + du^2\right] \tag{4.8}$$

where, 'a', 'b', 'c' and 'd' are the constants that need to be estimated depending on the conservation of mass and momentum law. $\mathbf{u}$ is the velocity vector. The term Υ represents the scalar macroscopic parameter, such as density (ρ), temperature, etc (Chen and Doolen, 1998; Mohamad, 2011). These macroscopic quantities can be calculated by the summation of local equilibrium distribution functions, such as,

$$\Upsilon = \sum f_k^{eq} \tag{4.9}$$

The equilibrium distribution function varies from process to process (diffusion, fluid flow, etc.). For a instance, in diffusion process as there is no macroscopic velocity required, the equilibrium distribution function can be approximated as,

$$f^{eq} = \Upsilon w_k \tag{4.10}$$

In fluid flow problems, as higher order terms are involved, the equilibrium distribution function (f^{eq}) takes the following form.

$$f_k^{eq} = \Upsilon w_k \left[1 + \frac{\mathbf{e_k} \cdot \mathbf{u}}{c_s^2} + \frac{(\mathbf{e_k} \cdot \mathbf{u})^2}{c_s^2} - 0.5\frac{\mathbf{u}^2}{c_s^2}\right] \tag{4.11}$$

where, c_s is speed of light and it is expressed as,

$$c_s = \frac{e_k}{\sqrt{3}} \tag{4.12}$$

4.1.3 Lattice patterns

In lattice Boltzmann method the lattice terminology developed by (Qian, 1990; Qian et al., 1992, 1993) is widely adopted. It is expressed by '$DxQy$', where 'x' and 'y' represents the dimension of considered physical domain (1D, 2D, 3D) and link directions, respectively. Figure 4.2 represents the different one and two dimensional lattice models generally used. For a instance, $D1Q2$ (Fig. 4.2, a) model represents the one dimensional problem and two velocity links. In $D1Q3$ lattice model, One stagnant particle or with zero velocity resides on the central node with other two particles stream to the neighboring lattice nodes. The

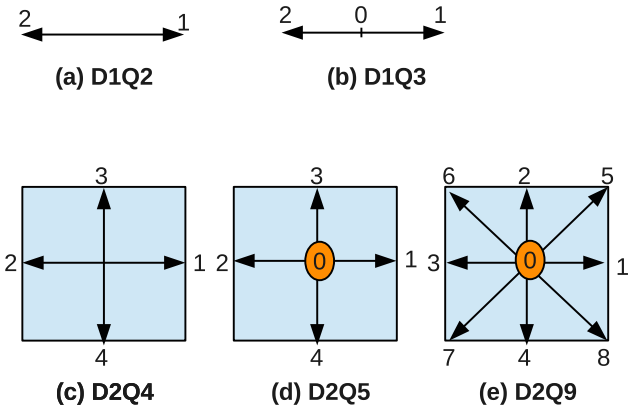

FIGURE 4.2: Different lattice models (for 1D and 2D).

weighting factors of equilibrium distribution function for few chosen lattice arrangements are represented as follows;

- $D1Q2$

$$w_k = \begin{cases} \frac{1}{2} & k = 1, 2 \end{cases} \tag{4.13}$$

- $D1Q3$

$$w_k = \begin{cases} \frac{4}{9} & k = 0 \\ \frac{1}{9} & k = 1, 2 \end{cases} \tag{4.14}$$

- $D2Q4$

$$w_k = \begin{cases} \frac{1}{4} & k = 1, 2, 3, 4 \end{cases} \tag{4.15}$$

- $D2Q5$

$$w_k = \begin{cases} \frac{2}{6} & k = 0 \\ \frac{1}{6} & k = 1, 2, 3, 4 \end{cases} \tag{4.16}$$

- $D2Q9$

$$w_k = \begin{cases} \frac{4}{9} & k = 0 \\ \frac{1}{9} & k = 1, 2, 3, 4 \\ \frac{1}{36} & k = 5, 6, 7, 8 \end{cases} \tag{4.17}$$

The two dimensional and nine velocity link lattice model is widely used for solving fluid flow and heat transfer problems, as it has optimum velocity vectors which is sufficient enough to resolve the hydrodynamics.

4.2 Lattice Boltzmann method for flow field

The fluid flow problem are governed by the Navier-Stokes equation (conservation of mass and momentum equations) in continuum approach. The Navier-Stokes equations for an incompressible, two dimensional without external force term can be expressed as,

- Continuity equation:

$$\frac{\partial u_x}{\partial x} + \frac{\partial u_y}{\partial y} = 0 \tag{4.18}$$

- x-component of momentum equation:

$$\rho\left(\frac{\partial u_x}{\partial t}\right) + \rho\left(u_x\frac{\partial u_x}{\partial x} + u_y\frac{\partial u_x}{\partial y}\right) = -\frac{\partial p}{\partial x} + \mu\left(\frac{\partial^2 u_x}{\partial x^2} + \frac{\partial^2 u_x}{\partial y^2}\right) \tag{4.19}$$

- y-component of momentum equation:

$$\rho\left(\frac{\partial u_y}{\partial t}\right) + \rho\left(u_x\frac{\partial u_y}{\partial x} + u_y\frac{\partial u_y}{\partial y}\right) = -\frac{\partial p}{\partial y} + \mu\left(\frac{\partial^2 u_y}{\partial x^2} + \frac{\partial^2 u_y}{\partial y^2}\right) \tag{4.20}$$

The LHS of momentum equations represents the advection term. The RHS side of Eqs.(4.19 and 4.20) are the pressure gradient term and the shear force due to viscous effect (Srinivas et al., 2009; Bharti et al., 2006; Sivakumar et al., 2006; Mohamad, 2011). The generalized lattice Boltzmann equation (LBE) for flow field with external force term is written as follows:

$$f_k\left(\mathbf{x} + \mathbf{e_k}\Delta t, t + \Delta t\right) - f_k\left(\mathbf{x}, t\right) = -\frac{1}{\tau_\nu}\left[f_k\left(\mathbf{x}, t\right) - f_k^{eq}\left(\mathbf{x}, t\right)\right] + \Delta t\mathbf{F} \tag{4.21}$$

where, $\mathbf{F}$ is force term. The equilibrium distribution function (f_k^{eq}) for two dimensional model (D2Q9 lattice arrangement) is expressed as,

$$f_k^{eq}(\mathbf{x}, t) = \rho w_k\left[1 + \frac{3(\mathbf{u}\cdot\mathbf{e_k})}{c^2} + \frac{9(\mathbf{u}\cdot\mathbf{e_k})^2}{2c^4} + \frac{3\left(\mathbf{u}\cdot\mathbf{u}\right)}{2c^2}\right] \tag{4.22}$$

and the discrete velocity vectors ($\mathbf{e_k}$) for $D2Q9$ lattice model are represented as (Qian, 1990; Qian et al., 1992),

$$\left.\begin{array}{lll} \mathbf{e_6} = (-1,1), & \mathbf{e_2} = (0,1), & \mathbf{e_5} = (1,1) \\ \mathbf{e_3} = (-1,0), & \mathbf{e_0} = (0,0), & \mathbf{e_1} = (1,0) \\ \mathbf{e_7} = (-1,-1), & \mathbf{e_4} = (0,-1), & \mathbf{e_8} = (1,-1) \end{array}\right\} \tag{4.23}$$

The macroscopic variables such as density and velocity can be obtained by simple summation of the equilibrium distribution functions, such as,

$$\rho(\mathbf{x},t) = \sum_k f_k \tag{4.24}$$

$$\mathbf{u}(\mathbf{x},t) = \frac{\sum_k \mathbf{e_k} f_k}{\rho(\mathbf{x},t)} \tag{4.25}$$

The application of lattice Boltzmann method for thermal field is presented in subsequent section.

4.3 Thermal lattice Boltzmann method (TLBM)

After the successful application of the lattice Boltzmann method for solution of various fluid flow phenomenon, Alexander et al. (1993) illustrated the suitability of the lattice Boltzmann method to obtain the thermal field. In their approach, the solution of thermal field is obtained by simply extending the local equilibrium distribution function to the third order. This thermal approach is called as multi-speed approach. This approach retained the simplicity of LBM, but failed to receive much impetus from researchers as it has some serious drawbacks such as, Galilean invariance, numerical instability (as higher order terms are involved), fixed values of Prandtl, etc.

He et al. (1998) proposed double distribution function (DDF) or internal energy distribution function approach, which utilize the two different distribution functions, one each, for

the estimation of flow and thermal fields, due to this, it is also called as double distribution function model (DDF). This approach is proven to be much better in terms of numerical stability and efficiency for the wider range of temperature and Prandtl numbers (Guo et al., 2007; Kuznik et al., 2007; Chen and Tian, 2010). It is, however, disadvantageous as the simplicity of LBM is lost due to the involvement of compression work done by pressure and viscous heat dissipation (Kuznik et al., 2007). The details of the mathematical expressions for the estimation of flow and thermal field are expressed as follows:

- The lattice Boltzmann equation for flow and thermal fields (He et al., 1998),

$$f_k\left(\mathbf{x}+\mathbf{e_k}\Delta t, t+\Delta t\right)-f_k\left(\mathbf{x},t\right)=-\frac{\Delta t}{\tau_\nu+0.5\Delta t}\left[f_k\left(\mathbf{x},t\right)-f_k^{eq}\left(\mathbf{x},t\right)\right]+\frac{\Delta t\tau_\nu}{\tau_\nu+0.5\Delta t}F_k \tag{4.26}$$

$$g_k\left(\mathbf{x}+\mathbf{e_k}\Delta t, t+\Delta t\right)-g_k\left(\mathbf{x},t\right)=-\frac{\Delta t}{\tau_g}\left[g_k\left(\mathbf{x},t\right)-g_k^{eq}\left(\mathbf{x},t\right)\right] \tag{4.27}$$

  where, τ_ν and τ_g are the relaxation parameters for flow and thermal field, respectively.

- The equilibrium internal energy function can be expressed as (Kuznik et al., 2007),

$$\begin{aligned} g_k^{eq} &= -\frac{2}{3}\rho e\left[\frac{\mathbf{u^2}}{c^2}\right] && k=0 \\ g_k^{eq} &= \frac{\rho e}{9}\rho e\left[1.5+1.5\frac{\mathbf{e_k}\cdot\mathbf{u}}{c^2}+4.5\frac{(e_k\cdot u)^2}{c^4}-1.5\frac{\mathbf{u^2}}{c^2}\right] && k=1,2,3,4 \\ g_k^{eq} &= \frac{\rho e}{36}\rho e\left[3+6\frac{\mathbf{e_k}\cdot\mathbf{u}}{c^2}+4.5\frac{(e_k\cdot u)^2}{c^4}-1.5\frac{\mathbf{u^2}}{c^2}\right] && k=5,6,7,8 \end{aligned} \tag{4.28}$$

Guo et al. (2002) proposed a lattice -BGK model for simulation of Boussinesq flow problem. In their study, the thermal field equilibrium distribution function was simplified. The temperature yield is passively advected by the fluid flow and obeys a simpler passive-scalar equation, if the viscous heat dissipation and compression work done are negligible.

The passive scalar equation is expressed as follows:

$$\frac{\partial \theta}{\partial t} + \nabla \cdot (\mathbf{u}\theta) = \phi \nabla^2 \theta \tag{4.29}$$

where, θ and ϕ are the temperature and diffusivity, respectively. The equilibrium distribution function for the thermal field (g_k^{eq}) and $D2Q9$ lattice model is expressed as follows:

$$g_k^{eq} = w_k T \left[1 + 3\frac{\mathbf{e_k} \cdot \mathbf{u}}{c}\right] \tag{4.30}$$

Further, Peng et al. (2003b) presented a passive scalar approach which is simplified version of the double distribution function (DDF) model (He et al., 1998). In this approach, temperature is assumed to be passive scalar and is advected by the flow field. They considered the fact that he viscous heat dissipation term in the energy equation can be neglected for the incompressible flow. The macroscopic temperature equation is similar to a passive scalar evolution equation, if the viscous heat dissipation and compression work done by pressure are negligible. The simplified thermal lattice Boltzmann method of Peng et al. (2003b) has following mathematical form,

$$f_k\left(\mathbf{x} + \mathbf{e_k}\Delta t, t + \Delta t\right) - f_k\left(\mathbf{x}, t\right) = -\frac{1}{\tau_\nu}\left[f_k\left(\mathbf{x}, t\right) - f_k^{eq}\left(\mathbf{x}, t\right)\right] + \Delta t F_k \tag{4.31}$$

$$g_k\left(\mathbf{x} + \mathbf{e_k}\Delta t, t + \Delta t\right) - g_k\left(\mathbf{x}, t\right) = -\frac{1}{\tau_g}\left[g_k\left(\mathbf{x}, t\right) - g_k^{eq}\left(\mathbf{x}, t\right)\right] \tag{4.32}$$

The equilibrium distribution functions for both flow and thermal fields will remain same as given in Eqs. 4.22 and 4.28 for flow and thermal field, respectively. This approach possesses better numerical stability, over other two approaches, in yielding the efficient solution over the broad range of Prandtl number and the simplicity of LBM is also retained (Guo et al., 2007; Chen and Tian, 2010; Kuznik et al., 2007). Further, several studies of thermal lattice Boltzmann method (TLBM) have been carried out in last couple of decades (He et al., 1998; Vahala et al., 1998; Peng et al., 2003a; Zhang and Chen, 2003; Lallemand and Luo, 2003; Watari and Tsutahara, 2004; Tang et al., 2005; Peng, 2005;

Prasianakis and Karlin, 2007; Kuznik et al., 2007; Li et al., 2004; Chen and Tian, 2010; Shim and Gatignol, 2011).

4.3.1 Champman-Enskog multiscale expansion

The objective of the Chapman-Enskog multiscale expansion is to solve Boltzmann equation by successive approximations (Chen and Doolen, 1998; Mohamad, 2011). The detailed procedure of Champman-Enskog multi-scale expansion can be found elsewhere (Hou et al., 1995; Chen and Doolen, 1998; He et al., 1998; Peng et al., 2003b; Mohamad, 2011). The probability distribution function is expanded in the parameter called Knudsen number (ϵ) as follows:

$$f_k(\mathbf{x},t) = f_k^0 + \epsilon f_k^1 + \epsilon^2 f_k^2 + ... = \sum_{k=0}^{\infty} \epsilon^n f_k^n \tag{4.33}$$

In Champman-Enskog expansion method, the Knudsen number (ϵ) parameter is used to the track the order of the terms in the series expansion. From generalized Boltzmann equation (Eqs. 4.2), we get following equation in equilibrium form,

$$\frac{\partial f_k^{eq}}{\partial t_1} + \mathbf{e_k} \cdot \nabla_1 f_k^{eq} = \frac{-1}{\tau} f_k^{(1)} \qquad \text{upto order } \epsilon^0 \tag{4.34}$$

$$\frac{\partial f_k^{(1)}}{\partial t_2} + \frac{\partial f_k^{eq}}{\partial t_2} + \mathbf{e_k} \cdot \nabla f_k^{(1)} + \frac{1}{2} : \nabla\nabla f_k^{eq} + \mathbf{e_k}\nabla \cdot \frac{\partial f_k^{eq}}{\partial t_1} + \frac{1}{2}\frac{\partial^2 f_k^{eq}}{\partial t_1^2} = \tau^{-1} f_k^2 \qquad \text{upto order } \epsilon^1 \tag{4.35}$$

By using Eqs. (4.34) and mathematical rearrangements, the first order equation can be written as follows:

$$\frac{\partial f_k^{(1)}}{\partial t_2} + \left(1 - \frac{2}{\tau}\right)\left[\frac{\partial f_k^{(1)}}{\partial t_1} + \mathbf{e_k} \cdot \nabla_1 f_k^{(1)}\right] = -\frac{f_k^{(2)}}{\tau} \tag{4.36}$$

From equations 4.34 and 4.36, the mass and momentum equations can be obtained as (Chen and Doolen, 1998),

$$\frac{\partial \rho}{\partial t} + \nabla \cdot \rho \mathbf{u} = 0 \tag{4.37}$$

$$\frac{\partial \rho \mathbf{u}}{\partial t} + \nabla \cdot \Pi = 0 \tag{4.38}$$

where, Π is momentum flux tensor. It can be expressed as follows:

$$\Pi_{\alpha\beta} = \sum_k (e_k)_\alpha (e_k)_\beta \left(f_k^{eq} + \left(1 - \frac{1}{2\tau}\right) f_k^{(1)} \right) \tag{4.39}$$

where, $f_k^{(1)}$ and α, β are non equilibrium part of particle distribution function and coordinate directions, respectively. Thus it can be seen that, the lattice Boltzmann equation (Eq. 4.3) is second order accurate in ϵ (Qian et al., 1992; Chen et al., 1992; Chen and Doolen, 1998; Dong et al., 2010; Mohamad, 2011). For flow field and $D2Q9$ lattice model, Eq. (4.39) reduces to the following form.

$$\Pi_{\alpha\beta}^{(0)} = \sum_k (e_k)_\alpha (e_k)_\beta f_k^{eq} = p\delta_{\alpha\beta} + \rho u_\alpha u_\beta \tag{4.40}$$

$$\Pi_{\alpha\beta}^{(1)} = (1 - (2\tau)^{-1}) \sum_k (e_k)_\alpha (e_k)_\beta f_k^1 = \nu(\Delta_\alpha(\rho \mathbf{u}_\beta) + \Delta_\beta \mathbf{u}_\alpha)) \tag{4.41}$$

where 'p' is pressure and it is expressed as,

$$p = c_s^2 \rho \tag{4.42}$$

$$p = \frac{\rho}{3} \quad \text{as} \quad c_s = \frac{1}{\sqrt{3}} \tag{4.43}$$

Also, 'ν' is kinematic viscosity and it is related to the relaxation parameter (τ) as follows:

$$\nu = c_s^2 \left(1 - \frac{1}{2\tau}\right) \quad \text{or} \quad \nu = \left(\frac{2\tau - 1}{6}\right) \tag{4.44}$$

It gives the momentum equation similar to traditional Navier-Stokes equations in low density variation or low Mach number (Ma) limit as follows (Qian, 1990; Qian et al., 1993; Chen and Doolen, 1998):

$$\rho \left(\frac{\partial \mathbf{u}_\alpha}{\partial t} + \Delta_\beta \cdot \mathbf{u}_\alpha \mathbf{u}_\beta\right) = -\Delta_\alpha p + \nu \Delta_\beta \cdot (\Delta_\alpha \rho \mathbf{u}_\beta + \Delta_\beta \rho \mathbf{u}_\alpha) \tag{4.45}$$

Further, the application of the lattice Boltzmann method to flow field and recovery of the mass and momentum equations have been explored. in the subsequent section.

4.3.1.1 Recovery of the Energy equation

The energy equation can be recovered from the evolution equation of thermal energy particle distribution function (g) by using Champman-Enskog multiscale expansion. The details of energy equation from thermal lattice Boltzmann method can be found elsewhere (He et al., 1998; Peng et al., 2003a; Guo et al., 2002). The thermal lattice Boltzmann equation can be expressed as follows:

$$g_k \left(\mathbf{x} + \mathbf{e_k}\Delta t, t + \Delta t\right) - g_k \left(\mathbf{x}, t\right) = -\frac{\Delta t}{\tau_g} \left[g_k \left(\mathbf{x}, t\right) - g_k^{eq} \left(\mathbf{x}, t\right)\right] \tag{4.46}$$

The Taylor series expansion of above equation upto second order $O(\delta^2)$ yields,

$$\delta(\partial_t + \mathbf{e_k} \cdot \mathbf{\Delta}) g_k + \frac{\delta^2}{2} [\partial_t + \mathbf{e_k} \cdot \mathbf{\Delta}]^2 g_k + O(\delta^2) = -\frac{g_k - g_k^0}{\tau_g} \tag{4.47}$$

where, $g_k^0 = g_k^{eq}$. Expansion of g_k about g_k^0, we get the following equation similar to Eq.4.33.

$$g_k(\mathbf{x}, t) = g_k^{(0)} + \epsilon g_k^{(1)} + \epsilon^2 g_k^{(2)} + ... = \sum_{k=0}^{\infty} \epsilon^n g_k^{(n)} \tag{4.48}$$

The expansion of g_k upto second order gives,

$$g_k(\mathbf{x},t) = g_k^{(0)} + \epsilon g_k^{(1)} + \epsilon^2 g_k^{(2)} + O(\epsilon^2) \tag{4.49}$$

The first order expansion of Eq. (4.47) gives,

$$(\partial_t + \mathbf{e_k}\cdot\mathbf{\Delta})g_k^{(0)} = -\frac{g_k^{(1)}}{\tau_g} \tag{4.50}$$

The second order expansion of Eq. (4.47),

$$\delta_{t1} g_k^{(0)} + \left(1 - \frac{1}{2\tau_g}\right)(\partial_{t0} + \mathbf{e_k}\cdot\mathbf{\Delta})g_k^{(1)} = -\frac{g_k^{(2)}}{\tau_g} \tag{4.51}$$

After summation of Eqs. (4.50) and (4.51), we get,

$$\delta_{t0}(\rho\varepsilon) + \Delta\cdot(\rho\mathbf{u}\varepsilon) = 0 \tag{4.52}$$

$$\delta_{t1}(\rho\varepsilon) + \left(1 - \frac{1}{2\tau_g}\right)\varsigma^{(1)} = 0 \tag{4.53}$$

where, ς is thermal flux tensor. It is expressed as follows:

$$\varsigma^{(1)} = \sum_k (\partial_{t0} + \mathbf{e}\cdot\Delta)g_k^{(1)} \tag{4.54}$$

After neglecting the $O(u^2\delta T)$, $\quad \varsigma^{(1)} = -\frac{2\tau_g}{3}\Delta^2(\rho\varepsilon)$ (4.55)

The combination of the Eqs. (4.55) gives,

$$\delta_{t1}(\rho\varepsilon) + \Delta\cdot(\rho\mathbf{u}\varepsilon) = \alpha\Delta^2(\rho\varepsilon) \tag{4.56}$$

where, α is thermal diffusivity and it is represented as,

$$\alpha = \frac{2(\tau_g - 0.5)}{3}$$

The simplified thermal lattice Boltzmann approach of Peng et al. (2003b) is adopted herein.

4.4 Force term in LBM

In order to incorporate force (buoyancy, magnetic, etc) term in the LBM model, a generalized force term can be expressed as follows (Fattahi et al., 2012; Kefayati et al., 2012a):

$$F_k = w_k F \frac{c_k}{c_k^2} \tag{4.57}$$

$$c_k = \frac{\Delta x + \Delta y}{\sqrt{3}} \tag{4.58}$$

$$F_k = 3 w_k F \tag{4.59}$$

F_k is then added to the collision term of lattice Boltzmann equation.

4.5 LBM for MHD natural convection problem

The lattice Boltzmann method (LBM) can also be applied to magneto-hydrodynamic (MHD) natural convection problem by just adding following a force term in collision term of lattice Boltzmann equation (LBE).

$$f_{Collision} = f(\mathbf{x}, t) - \frac{1}{\tau}[f(\mathbf{x}, t) - f^{eq}(\mathbf{x}, t)] + \Delta t \mathbb{F} \tag{4.60}$$

The combined effect of magnetic field and natural convection problem can be incorporated in LBM algorithm by adding $\mathbf{F} = F_x + F_y$ into above equation.

$$F_x = 3w_k\rho\left[(\frac{Ha^2\nu}{N_x^2})(vsin(\phi)cos(\phi) - usin^2(\phi))\right] \quad \text{where} \quad Ha = BH\sqrt{\frac{\sigma}{\mu}} \tag{4.61}$$

$$F_y = 3w_k\rho(g\beta(T - \overline{T})) + 3w_k\rho\left[(\frac{Ha^2\nu}{N_x^2})(usin(\phi)cos(\phi) - vcos^2(\phi))\right] \tag{4.62}$$

where, $Ha, B, H, \sigma, \mu, \beta, N_x, \nu$ and ϕ are Hartmann number, magnetic field, characteristic length, electrical conductivity, dynamic viscosity, coefficient of thermal expansion, number of lattice nodes on characteristic length, kinematic viscosity and angle of magnetic field, respectively. It should be noted that $Ha = 0$ corresponds to the pure natural convection.

4.6 Boundary Conditions for Lattice Boltzmann Method

An accurate representation and suitable implementation of boundary conditions is one of crucial as well as important step in the development of the numerical solvers. The boundary conditions implementation for Navier-Stokes equations solvers is somehow straightforward. The conventional CFD tools use macroscopic variables on boundaries. In LBM, however, boundary conditions are specified by unknown distribution functions directing towards the flow field. Therefore, it is very important to choose and solve appropriate equations for estimating the particle distribution functions at the boundaries for a particular boundary condition. A huge amount of literature is now available for exploring the lattice Boltzmann boundary conditions (Ziegler, 1993; Skordos, 1993; Noble et al., 1995; Ginzbourg and d'Humieres, 2003; Zou and He, 1997; Sofone and Sekerka, 2005; Chopard and Dupuis, 2003; Like et al., 2013; Kefayati, 2013a; Yang, 2013; Heubes et al., 2014). The different kind of boundary conditions used in lattice Boltzmann method are, bounce back scheme, periodic, outlet, symmetry and Neumann boundary conditions respectively. These boundary conditions along with its application for flow and thermal fields are illustrated below.

4.6.1 Boundary Conditions for Flow Field

Flow field boundary conditions comprises the popular bounce back scheme, periodic, Von Neumann, open boundary conditions.

4.6.1.1 Bounce Back Boundary Scheme

The lattice Boltzmann method uses the same concept of the lattice gas automata (LGA) particle distribution function bounce back boundary scheme (Wolfram, 1986; Chen and Doolen, 1998; Sukop and Throne, 2005; Mohamad, 2011). The bounce back scheme is very popular because of its simplicity or ease in coding making the lattice Boltzmann method suitable for simulating the complex geometries. As reported by Ziegler (1993) reported that the bounce back scheme is second order accurate if the solid boundary is shifted to half of distance between solid and fluid node. Figure 4.3 illustrates the bounce back boundary

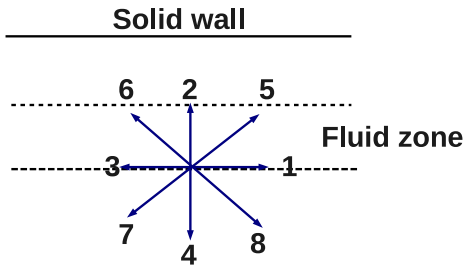

FIGURE 4.3: Halfway bounce back treatment.

condition for solid (no slip) wall. It is assumed that the particle distribution function directing towards the flow field (i.e., f_4, f_7, f_8) are known from streaming step. These distribution function after striking the solid wall, return to the flow domain. Therefore, the bounce back scheme for no slip wall is expressed as below:

$$f_2 = f_4; \quad f_5 = f_7; \quad f_6 = f_8 \tag{4.63}$$

It should be noted that distribution function f_5 at a particular node (i,j) is equal to the f_5 at (i-1,j-1) due to streaming process. Therefore, boundary conditions must be applied after streaming process (Mohamad, 2011; Sukop and Throne, 2005).

4.6.1.2 Periodic Boundaries

These are simplest boundary treatment as physical domain of consideration becomes closed by the edges/boundaries being treated as if these are attached to the opposite edges (Sukop and Throne, 2005). These boundary treatments are necessary and useful in systems to isolate a repeating flow conditions (Mohamad, 2011). Figure 4.4 illustrates

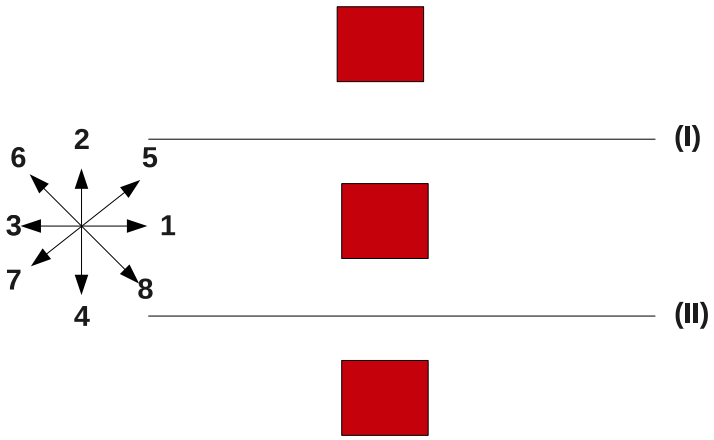

FIGURE 4.4: Periodic boundary treatment (Sukop and Throne, 2005; Mohamad, 2011).

the use of periodic boundary treatments for the flow over square tubes. It can be seen that the fluid flow order above the line I and below the line II are the exactly similar. Therefore, it is adequate to model the area between two lines, i.e., I and II. The particle distribution function leaving the line I are same as that of infiltrating line II (Chen and Doolen, 1998; Mohamad, 2011). Therefore, the boundary treatment for such situations are expressed by using periodic boundary conditions as follows:

$$\begin{aligned} &\text{Along line I} \quad f_{4,I} = \quad f_{4,II}; \quad f_{7,I} = f_{7,II}; \quad f_{8,I} = f_{8,II}; \\ &\text{Along line II} \quad f_{2,II} = \quad f_{2,I}; \quad f_{5,II} = f_{5,I}; \quad f_{6,II} = f_{6,I}; \end{aligned} \tag{4.64}$$

4.6.1.3 Von Neumann Condition

The Von Neumann boundary conditions are used for modeling known velocity at specified wall/boundary. It is very common condition to use known component of velocity at the

boundary, viz., inlet velocity for a channel flow. It is used to calculate the unknown particle distribution functions and thereby to calculate macroscopic density/velocity (Sukop and Throne, 2005; Chen and Doolen, 1998; Mohamad, 2011). The estimation of unknown particle distribution function at wall is given by Zou and He (1997). For a instance, consider a channel flow with uniform velocity along inlet U_∞ as shown in Figure 4.5. Along west wall (x=0), the unknown particle distribution function are f_1, f_5 and f_8. we

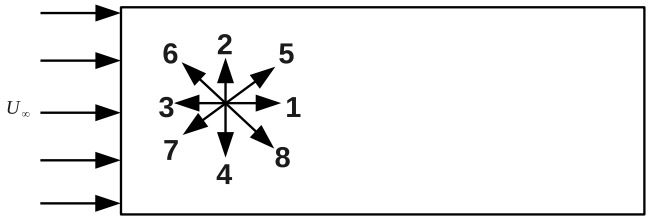

FIGURE 4.5: Channel flow with inlet velocity U_∞.

have three basic equations expressed as follows:

$$\begin{aligned} \rho_0 = \quad & f_0 + f_1 + f_2 + f_3 + f_4 + f_5 + f_6 + f_7 + f_8 \\ \rho_0 u_0 = \quad & (f_1 + f_5 + f_8) - (f_3 - f_6 - f_7) \\ \rho_0 v_0 = \quad & (f_2 + f_5 + f_6) - (f_4 - f_7 - f_8) \end{aligned} \tag{4.65}$$

The equilibrium condition is applied along the normal direction to the boundary, as follows:

$$f_1 - f_1^{eq} = f_3 - f_3^{eq} \tag{4.66}$$

where f_1^{eq} and f_3^{eq} are flow field equilibrium distribution functions. These are expressed as,

$$f_1^{eq} = f_3^{eq} = \frac{\rho_0}{9}\left[1 + 3u_0 + \frac{9}{2}u_0^2 - \frac{3}{2}(u_0^2 + v_0^2)\right] \tag{4.67}$$

The velocity components along the west are $u_0 = U_\infty, v_0 = 0$ with ρ_0 is density along west wall. Therefore, after the mathematical rearrangements of equations (4.65-4.67), the

unknown distribution functions are represented as follows (Zou and He, 1997; Sukop and Throne, 2005; Mohamad, 2011):

$$\begin{aligned} \rho_0 &= \frac{f_0 + f_2 + f_4 + 2(f_3 + f_6 + f_7)}{1 - u_0} \\ f_1 &= f_3 + \frac{2(\rho_0 u_0)}{3} \\ f_5 &= f_7 - \frac{(f_2 - f_4)}{2} + \frac{\rho_0 u_0}{6} + \frac{\rho_0 v_0}{2} \\ f_8 &= f_6 + \frac{(f_2 - f_4)}{2} + \frac{\rho_0 u_0}{6} - \frac{\rho_0 v_0}{2} \end{aligned} \tag{4.68}$$

The unknown distribution functions are specified at the west boundary of Figure 4.5, similar method can be applied for other boundaries.

4.6.1.4 Outlet wall conditions

These boundary treatments are usually applicable when the macroscopic physical parameters (velocity, pressure, temperature, etc.) are unknown. Let us consider the east/outlet wall of Figure 4.5. The unknown particle distribution functions along outlet wall are f_3, f_6 and f_7. These can be calculated by using second order polynomial as follows (Mohamad, 2011):

$$f_{3,nx} = 2f_{3,nx-1} - f_{3,nx-2} \tag{4.69}$$

$$f_{6,nx} = 2f_{6,nx-1} - f_{6,nx-2} \tag{4.70}$$

$$f_{7,nx} = 2f_{7,nx-1} - f_{7,nx-2} \tag{4.71}$$

where, nx represents the lattice nodes along outlet/east wall.

4.6.2 Boundary Conditions for Thermal Field

Excellent review on the boundary conditions of thermal lattice Boltzmann equation are available (DOrazio and Succi, 2003; Like et al., 2013). In order to model the boundary conditions for the thermal field, the fundamental idea of bounce back scheme is used for both Dirichlet and Neumann boundary conditions (Like et al., 2013). The different thermal boundary conditions covered herein are constant wall temperature (CWT), adiabatic, outlet and open boundaries.

4.6.2.1 Constant Wall Temperature (CWT) conditions

Consider a parallel walls through which fluid flows (as shown in Figure 4.6). The upper wall is maintained at some temperature (T_W), which is higher than ambient temperature ($> T_\infty$), while the lower plate is at ambient. In order to estimate the unknown distribution

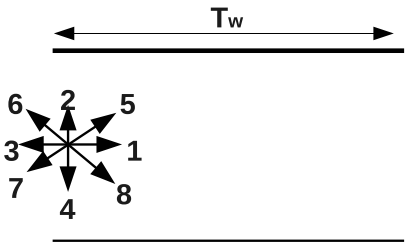

FIGURE 4.6: Flow through parallel plates with top is subjected to heating at T_W and lower wall is at ambient ($> T_\infty$).

function along considered wall/boundary, a flux boundary condition is used. A flux at a particular boundary is represented as follows (Mohamad, 2011):

$$g_k^{eq}(x_w,t) - g_k(x_w,t) + g_{\overline{k}}^{eq}(x_w,t) - g_{\overline{k}}(x_w,t) = 0 \tag{4.72}$$

where, x_w, is boundary wall. k and $\overline{k}$ are opposite link directions as shown in Figure 4.7. The thermal equilibrium distribution function can be obtained from Eqs. (4.28). In order to retain the second order accuracy of the lattice Boltzmann method, a half-way bounce back scheme is utilized (Gallivan et al., 1997). In general form, CWT condition can be

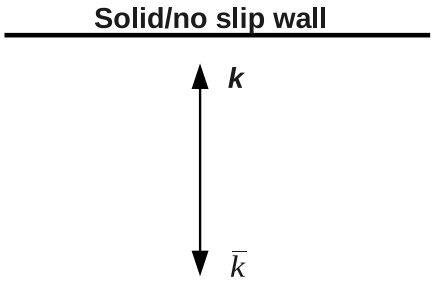

FIGURE 4.7: Lattice link directions towards a no slip wall.

expressed as,

$$g_k = T_w(w_k + w_{\overline{k}}) - g_{\overline{k}} \tag{4.73}$$

where, T_w represents the wall temperature.

4.6.2.2 Adiabatic Boundaries

In adiabatic boundaries, the temperature gradient is zero, which means, same temperature along consecutive lattice nodes in respective direction. The unknown distribution functions can be obtained as (Chen and Doolen, 1998; Mohamad, 2011),

$$\frac{\partial T}{\partial X} = 0 \tag{4.74}$$

$$\text{It implies} \quad T(nx) = T(nx-1) \tag{4.75}$$

$$\text{in terms of distribution functions, we get} \quad f_k(nx) = f_k(nx-1) \tag{4.76}$$

where, nx represents the boundary lattice nodes.

4.6.2.3 Outflow conditions

The outflow boundary condition can be represented in similar fashion as flow field (as given in previous section (4.6.1.4)). These can be calculated by using second order polynomial

as follows (Mohamad, 2011):

$$g_{3,nx} = 2g_{3,nx-1} - g_{3,nx-2} \tag{4.77}$$

$$g_{6,nx} = 2g_{6,nx-1} - g_{6,nx-2} \tag{4.78}$$

$$g_{7,nx} = 2g_{7,nx-1} - g_{7,nx-2} \tag{4.79}$$

where, nx represents the lattice nodes along outlet/east wall.

4.7 Lattice Boltzmann algorithm

Figure 4.8 represents the general lattice Boltzmann method algorithm for fluid flow problems (Mc Namara and Zanetti, 1988; Chen and Doolen, 1998; Sukop and Throne, 2005; Mohamad, 2011). The LBM algorithm is composed of *collision, streaming, implementation of boundary conditions* and *estimation of macroscopic*.

1. The initialization of flow variables is done by using zero velocity $\mathbf{u} = 0$ and non-zero density $\rho > 0$, followed by estimation of equilibrium distribution function f_k^{eq}. For initial time step ($t = 0$), the particle distribution function (f_k) will be similar as that of equilibrium distribution function. Hence, $f_k = f_k^{eq}$, which completes the first/initialization step.

2. The second of the LBM algorithm is collision step, which begins the iteration loop. The right hand side of the lattice Boltzmann equation represents the collision equation (Eq. 4.4).

3. Particles are streamed along neighboring lattice in respective lattice link direction, which is called as streaming step (Eq. 4.5).

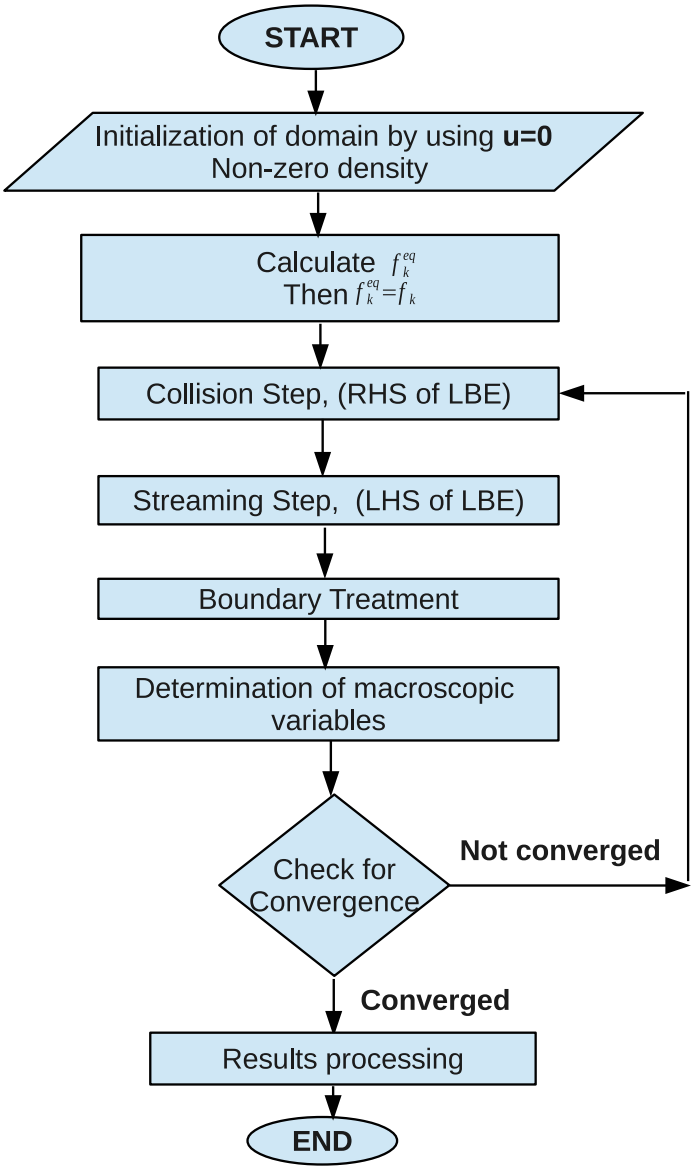

FIGURE 4.8: Lattice Boltzmann algorithm for fluid flow problems

4. The estimation of unknown particle distribution function along the boundary of system/wall is carried out by using various LBM boundary treatments (as discussed in section 4.6).

5. The macroscopic variables such as density (ρ), velocity ($\mathbf{u}$), etc are determined.

6. Check for the convergence criterion (Eq. 4.80). If its not satisfied then repeat steps (2) to (5). Otherwise, proceed to next steps.

7. Estimation of engineering parameters, such as, drag coefficient, Nusselt number, stream-function, vorticity

8. Output of desired fields (velocity, pressure, etc) is obtained.

The absolute error (ϵ, Eq. 4.80) criterion for checking the convergence of numerical solution is expressed as follows:

$$\epsilon_{\max} = \max |\phi_i^{new} - \phi_i^{old}|_{i=1}^{N} \leq 10^{-9} \tag{4.80}$$

where, ϕ represents physical flow variables (i.e., velocity components u_x, u_y, and temperature T) checked for convergence and N is the number of lattice nodes in the computational domain. The superscripts 'new' and 'old' represent for the flow variables calculated at the present and previous time/iterative calculation steps.

4.7.1 Thermal Lattice Boltzmann Algorithm

The algorithm of thermal lattice Boltzmann method depends on the approach which are utilizing for solution of thermal field. In widely used double distribution function (DDF) thermal model, the determination of thermal field is carried out separately after flow field. A generalized thermal lattice Boltzmann method algorithm is shown in Figure 4.9. The algorithm consists of following steps.

1. Initialization of the density ($\rho > 0$), velocity ($u_x = 0, u_y = 0$), and temperature ($T = T_c$).

2. Determination of equilibrium distribution functions (f_k^{eq} and g_k^{eq}) by using the values initialized in step (1).

3. To start with, distribution functions and equilibrium distribution functions are set equal to their part, i.e., $f_k = f_k^{eq}$ and $g_k = g_k^{eq}$.

4. Sequential determination of flow field followed by the thermal field

   (a) Collision step.

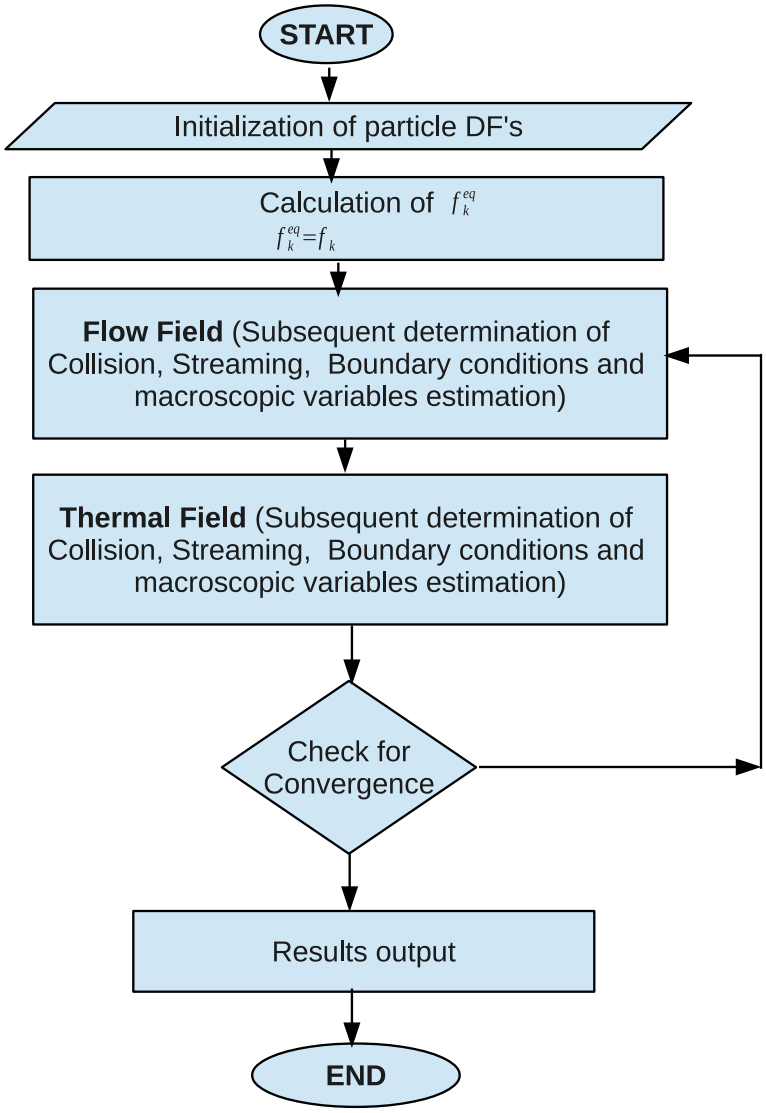

FIGURE 4.9: Lattice Boltzmann algorithm for non-isothermal problems

(b) Streaming step.

(c) Updating of boundary conditions.

(d) Estimation of macroscopic quantities.

5. Check for the convergence criterion (Eq. 4.80)

(a) If satisfied, go to step (6).

(b) Else, repeat steps (4) to (5).

6. Process the flow and thermal fields to estimate the local and global characteristic.

4.8 Advantages of LBM

1. LBM is easy to understand, implement and simple for programming.
2. The lattice Boltzmann equation is a linear partial differential equation (Mohamad, 2011)
3. It requires nearly ten times low memory than the finite element method simulation, by using coarse grid/lattice size for achieving same level of accuracy (Kandhai et al., 1998).
4. It has the inherent spatial locality of the updating rules, i.e., the collision and streaming steps are completely local, which makes it ideal for parallel computing. .
5. Easy implementation of boundary conditions, which are kinetic in nature and thus making it suitable for handling complex structures/geometries.
6. Lattice Boltzmann method is explicit.
7. Conventional CFD methods for solving incompressible flows, such as finite-difference, finite-element and finite-volume require solution of a Poisson/Poisson like equation for the pressure field estimation, which is induced by the mass-continuity equation and the momentum-conservation equation. In LBM, this time consuming step is removed due to the incompressibility requirement has been relaxed and the effects of pressure changes are controlled by an equation of state rather than a Poisson/Poisson like equation.
8. LBM has very efficient explicit time stepping scheme, for example, high cell Reynolds-number.

4.9 Disadvantages of LBM

1. Difficulty in extending the uniform lattice structure to non-uniform one (He and Luo, 1996).

2. LBM is weakly compressible scheme (no Poisson equation is solved for the pressure). Thus, low Mach number ($Ma < 0.3$) restriction must be followed to avoid compressibility in lattice Boltzmann method.

3. Computational time required by the LBM for fine grid simulation shows a momentous rise compared to the coarse grid simulation (Kandhai et al., 1998).

4. LBM has inherently transient scheme.

5. It can be observed from the Champman-Enskog expansion, the whole procedure is dependent on the relaxation parameter (τ). All errors are dependent on τ.

4.10 Applications of LBM

The lattice Boltzmann method can be applied for simulation of wide range of problems as given follows (Chen and Doolen, 1998; Sukop and Throne, 2005):

1. Incompressible flows

2. Multicomponent and multiphase flows

3. Fully compressible and thermal flows

4. Particulate Suspensions

5. Non Newtonian rheology

6. Microfluidics

7. Turbulent Flows

8. Anisotropic Dispersion

The computational algorithm of LBM discussed in this chapter has been used to developed an in-house solver based on passive scalar (or modified double distribution function) thermal lattice Boltzmann method (TLBM) in C++ programming language. The solver has

been validated on the standard benchmark problems before utilizing for the investigation of convective flow characteristics to fulfill the objectives of this thesis.

Chapter 5

VALIDATION OF LBM CODE

This chapter presents the validation of the in-house solver based on thermal lattice Boltzmann method with standard benchmark problems.

5.1 Lid Driven Enclosure

The classical problem of lid driven cavity is considered as a benchmark problem for studying and understanding various fluid dynamics fundamentals such as vortex structures, stability, etc (Ghia et al., 1982a; Shankar and Deshpande, 2000). The problem represents a classical topic of internal or bounded flows. It is used for testing/verifying the numerical algorithm accuracy and stability. The physical domain of lid driven cavity is shown in Figure 5.1. The top wall of square cavity is subjected to a uniform velocity of U in horizontal direction. The other three walls of cavity are solida no-slip walls. The numerical simulation is carried out for Reynolds number of $Re = 100, 400$ and 1000. The validation of present in-house LBM solver is ascertained by comparison velocity variation along the geometric center of cavity with benchmark results of Ghia et al. (1982a). Figure 5.2 shows comparison between the velocity components profiles plotted along geometric center of cavity with that of the benchmark results of (Ghia et al., 1982a). It can be observed

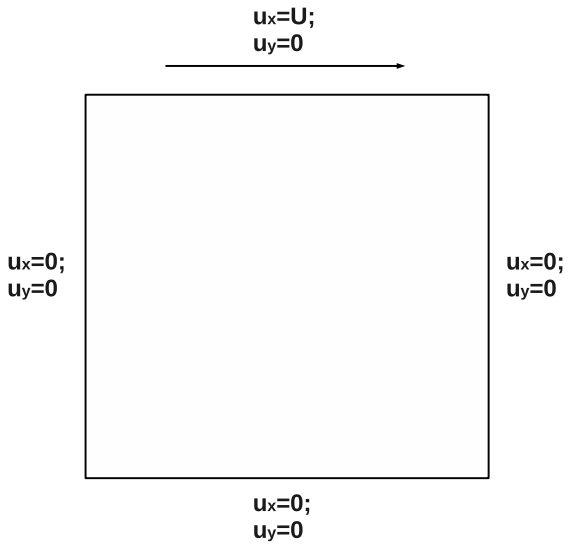

FIGURE 5.1: The physical domain of lid driven cavity along with boundary conditions.

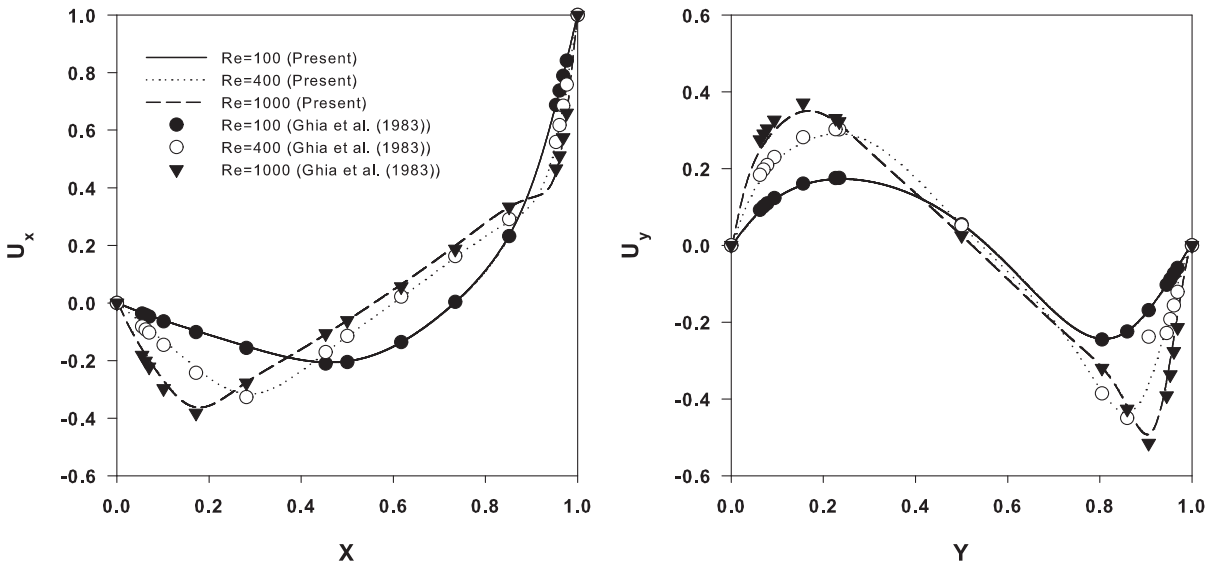

FIGURE 5.2: The variation of velocity components along geometric center of cavity at different Reynolds number.

that the comparison shows excellent agreement and thus confirms the accuracy of present LBM code (developed in C++ programming language).

Further, in order to check the robustness of LBM scheme, a comparison of CPU time as well as number of iterations required for getting converged solution has been conducted between conventional CFD solver (Fluent 6.2.36) and in-house developed LBM solver with same initial guess for Reynolds number of Re=100, 400 and convergence criterion of $10^{-4}, 10^{-5}$. It is observed that LBM gets solution at much faster rate than FLuent. Following table shows CPU time as well as number of iterations required for getting converged solution.

Re	Convergence criterion	CPU Time (Second)		Number of Iterations	
		CFD solver (Fluent)	LBM solver	CFD solver (Fluent)	LBM solver
100	10^{-4}	45	5	1296	384
	10^{-5}	100	11	2160	3024
400	10^{-4}	50	8	1479	1110
	10^{-5}	120	32	2039	7725

5.2 Flow between parallel walls

Consider a two dimensional, laminar, steady and developing flow of fluid (incompressible, Newtonian) with uniform velocity U_∞ in a plane confined channel of height H and length L (as shown in Figure 5.3). The flow conditions for above physical domain is given as,

$$\begin{aligned} &u_x = U_\infty, \quad && u_y = 0; && x = 0, 0 \leq y \leq H \\ &\frac{\partial u_x}{\partial x} = 0, \quad && \frac{\partial u_y}{\partial x} = 0; && x = L, 0 \leq y \leq H \\ &u_x = 0, \quad && u_y = 0; && 0 \leq x \leq L, y = 0 \text{ and } H \end{aligned} \tag{5.1}$$

For Newtonian fluids, it is know that velocity profile becomes fully developed at non-dimensional distance of $\approx 0.05Re$ (Bharti, 2006). The length of channel is taken to be

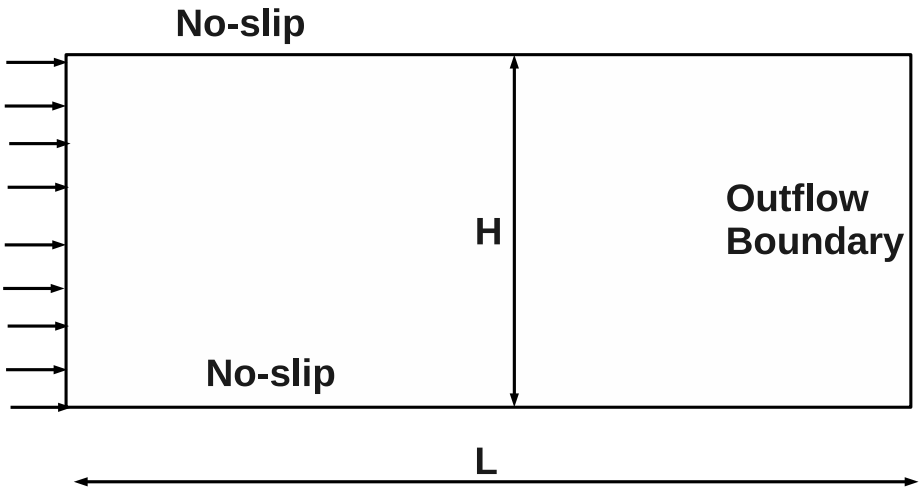

FIGURE 5.3: The schematic representation of developing flow in channel.

sufficient so that velocity profile becomes fully developed, which can be accomplished from the velocities at the exit of channel.

The lattice Boltzmann computations are carried out for flow field at Reynolds number of Re=10 with L=25H. A uniform lattice size of $(N_x \times N_y)1000 \times 40$, where N_x and N_y are the lattice nodes along length and height, respectively. The fully developed velocity profile can be estimated analytically by following equation (Chhabra, 1996; Bharti, 2006; Dhiman, 2006; Bharti et al., 2007),

$$U_x(y) = U_{max}\left[1 - \left(\left|1 - \frac{2y}{H}\right|\right)^2\right] \tag{5.2}$$

where, U_{max} is maximum velocity of fully developed flow in the channel and it is related to average velocity U_{avg} as,

$$U_{max} = \frac{3U_{avg}}{2} \tag{5.3}$$

The U_x is estimated at X=2 and 4 at $0 \leq y \leq H$ and Re=10. It can be seen from Figure 5.4, the simulation results shows excellent likeness with analytical results (Eq. 5.2). Keeping in mind the above mentioned inadvertent factors influencing the numerical

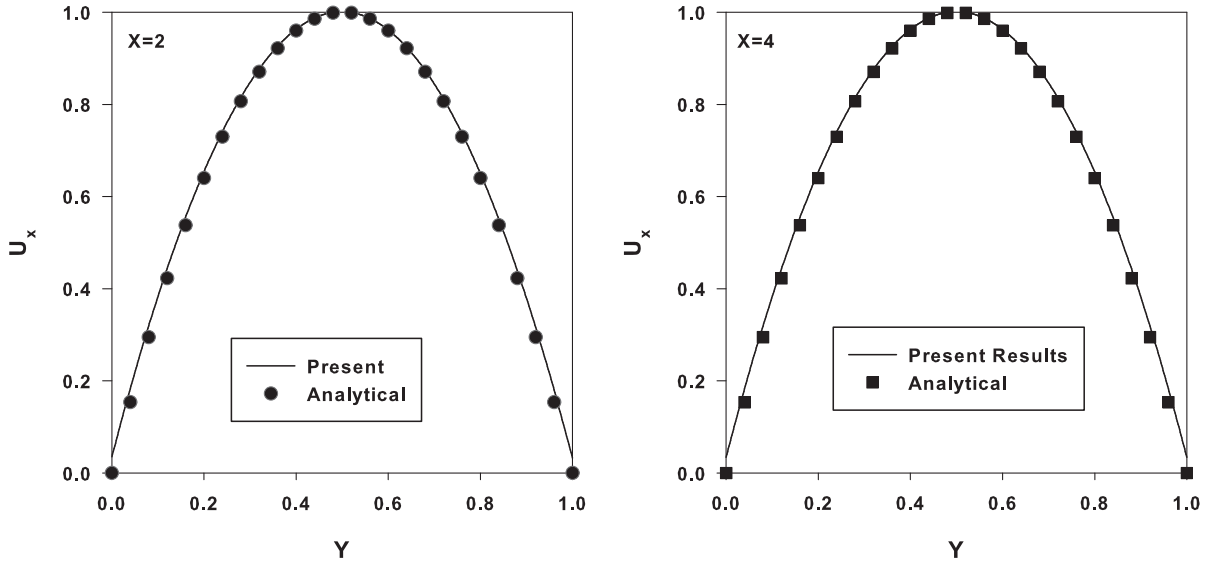

FIGURE 5.4: The variation of U_x along geometric center of channel at Re=10 at X=2, 4.

results, the above comparison ascertains the confidence in the accuracy and reliability of the present in-house thermal lattice Boltzmann method (TLBM) solver.

Having gained the confidence in the present computational solution algorithm of TLBM solver, the ensuing chapters presents the influence of flow governing parameters on the detailed natural convection flow phenomenon of heated cavities of varying configurations as well as forced convection flow and heat transfer from channel built-in rectangular cylinder.

Chapter 6

NATURAL CONVECTION IN DIFFERENTIALLY HEATED CAVITY

6.1 Introduction

A thermal lattice Boltzmann method is utilized for the numerical simulation of the natural convection heat transfer phenomena inside a differentially heated square cavity. Numerical simulations are performed to elucidate the combined effects of Prandtl number ($0.71 \leq Pr \leq 100$) and Rayleigh number ($10^4 \leq Ra \leq 10^6$) on heat transfer and fluid flow characteristics inside the cavity. The detailed insights are gained by the evaluation of isotherms, stream functions and vorticity profiles.

6.2 Problem Description

Consider the steady, laminar, natural convection heat transfer in an incompressible fluid from an infinitely long square cavity ($AR = L/H = 1.0$, where L and H are cross-sectional length and height of the cavity), as shown in Figure 6.1. The west wall of cavity is maintained at temperature (T_h) whereas east wall temperature is maintained at temperature of $T_c (< T_h)$. The governing equations (in dimensional and dimensionless

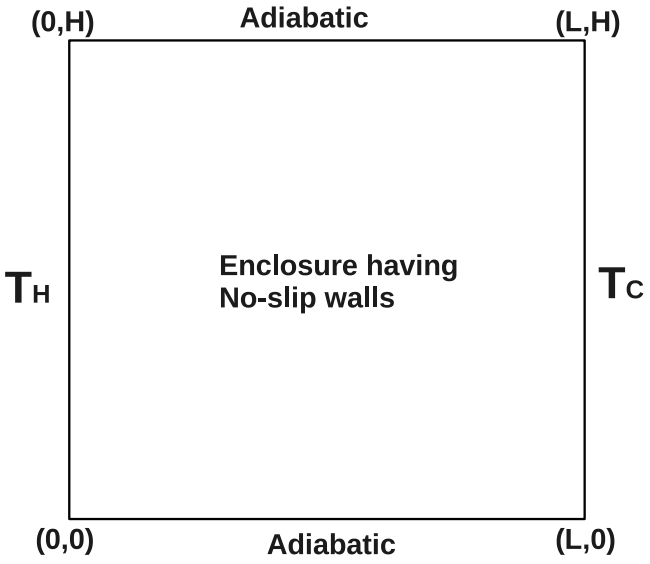

FIGURE 6.1: Schematic representation of the computational domain (i.e., cavity) and boundary conditions.

forms) along with general simplifications are expressed in Chapter 3. The boundary conditions for the cavity with differentially heated walls are expressed as below,

- West (hot) wall ($x = 0$) is considered as no-slip and maintained isothermally i.e.,

$$u_x = 0, u_y = 0, T = T_H; \tag{6.1}$$

- East (cold) wall ($x = L$) is considered as no-slip wall and maintained isothermally, i.e.,

$$u_x = 0, u_y = 0, T = T_C; \tag{6.2}$$

- Top ($y = H$) and bottom ($y = 0$) walls considered as no-slip wall and maintained at adibatic condition, i.e.,

$$u_x = 0, u_y = 0, \frac{\partial T}{\partial y} = 0; \tag{6.3}$$

In non-dimensional form, the boundary conditions are expressed as,

- West (hot) wall ($X = 0$)

$$U_x = 0, U_y = 0, \theta = 1; \tag{6.4}$$

- East (cold) wall ($X = 1$)

$$U_x = 0, U_y = 0, \theta = 0; \tag{6.5}$$

- Bottom ($Y = 0$)and top ($Y = 1$) walls,

$$U_x = 0, U_y = 0, \frac{\partial \theta}{\partial Y} = 0 \tag{6.6}$$

6.3 Results and discussions

Extensive results have been obtained and presented herein this section for the following ranges of conditions.

1. The Prandtl number ($0.71 \leq Pr \leq 100$) is varied as $0.71, 1, 5, 10, 15, 20, 30$, 50, 60, 70, 80, 90 and 100.
2. The Rayleigh number ($10^4 \leq Ra \leq 10^6$) varied in the logarithmic manner.

For the above mentioned broad ranges of flow governing parameters, the local and global convective flow characteristics such as the evolution of stream functions, isotherms and

vorticity; variation of velocity components and temperature on horizontal and vertical center lines; and the Nusselt number are obtained and discussed herein.

6.3.1 Grid independence study

Prior to the presenting the new results obtained in this work, a systematic analysis of grid (lattice size) independence has been carried out for extreme values of Prandtl number (Pr=0.71 and 100) and Rayleigh number (Ra=10^4 and 10^6) by using the four grid structures having the uniform lattice spacing. Table 6.1 presents the grid (or lattice size)

TABLE 6.1: The influence of the grid size on average Nusselt number ($\overline{Nu}$) at hot wall (X=0).

	$Ra = 10^4$		$Ra = 10^6$	
Grid size	$Pr = 0.71$	$Pr = 100$	$Pr = 0.71$	$Pr = 100$
$G1(81 \times 81)$	2.267	28.87	8.785	46.27
$G2(101 \times 101)$	2.235	30.49	8.801	47.85
$G3(121 \times 121)$	2.218	30.70	8.821	48.12
$G4(141 \times 141)$	2.218	31.45	8.812	48.44

effects on average Nusselt number (Nu) estimated at hot wall ($X = 0$). It is seen that the refinement in grid from $G1$ to $G2$, $G2$ to $G3$, and $G3$ to $G4$ results in reduction in average variation in the mean Nusselt number ($\overline{Nu}$) which are $2.4\%, 0.5\%$ and 0.9%, respectively. The small changes in the results are accredited with the 2-3 folds of the computational time. Therefore, keeping in mind the greater accuracy (or less truncation errors) in the numerical solution procedure, grid G3 (101×101) is, however, found to be sufficiently refined to resolve the hydrodynamics of natural convection flows considered in this work.

6.3.2 Validation of results

Further, the reliability and accuracy of new results is established by comparing the present results with available results in the literature. It is evident from the literature that none of the existing studies have explored the influences of Prandtl number (Pr) for the physical

TABLE 6.2: Comparison of present numerical values of average Nusselt number ($\overline{Nu}$) at hot wall ($X = 0$) with those available in literature at Prandtl number of Pr=0.71.

		Mesh sizes		
Ra	Source	41×41	81×81	101×101
10^4	Present study	2.267	2.235	2.218
	de Vahl Davis (1983)	-	2.243	-
	Kao et al. (2006)	2.207	2.231	-
	Kao and Yang (2007)	2.251	2.491	-
10^6	Present study	8.808	8.785	8.801
	de Vahl Davis (1983)	8.798	8.928	-
	Kao et al. (2006)	8.406	8.696	-
	Kao and Yang (2007)	8.519	8.734	8.776
	Fattahi et al. (2012)	8.623	8.883	8.891

problem considered in this work. The limited results are available for a fixed value of Prandtl number ($Pr = 0.71$) and extreme values of Rayleigh number ($Ra = 10^4$ and 10^6), which are used for the validation of present results as given in Table 6.2. An analysis of Table 6.2 suggests that the present results are confined within $2 - 3\%$ of the previous results. These inherent uncertainties seen in Table 6.2 are very common in such studies due to modeling error, dicretization (or linearization) error, numerical errors (due to iteration, round up and programming) as well as accuracy of numerical scheme, etc (Bharti et al., 2007). Keeping in mind all these factors, the present results reported herein are believed to be reliable and accurate to within $\pm 2 - 3\%$. This ascertains and inspires the confidence in accuracy and reliability of present in-house developed LBM solver.

6.3.3 Characteristic Velocity (V)

In case of natural convection problems, the determination of characteristic velocity (Eq. 3.18) is crucial and important step (Kao et al., 2006; Kao and Yang, 2007; Fattahi et al., 2012). The characteristic velocity (V) is being used to quantify the limits of incompressibility for the LBM solver (Dellar, 2003). It is done on the basis of Mach number ($Ma = V/c_s; \quad c_s = c/\sqrt{3}$) calculations (Qian et al., 1992; Dellar, 2003). To ensure the working of LBM solver in near incompressible regime, the mach number should be limited

TABLE 6.3: Variation of characteristic velocity (Eq. 3.18) and Mach number with Prandtl and Rayleigh numbers

.

	Prandtl number, Pr				
Ra	0.71	1	10	50	100
Characteristic velocity, V					
10^4	0.158	0.133	0.040	0.018	0.013
10^5	0.125	0.100	0.030	0.014	0.010
10^6	0.160	0.140	0.0843	0.020	0.014
Mach number, Ma					
10^4	0.274	0.231	0.069	0.031	0.023
10^5	0.217	0.173	0.051	0.024	0.017
10^6	0.277	0.242	0.045	0.034	0.024

to less than 0.3, ($Ma < 0.3$). Table 6.3 shows estimated values of characteristic velocity for the ranges of the Prandtl (Pr) and Rayleigh numbers (Ra). All values of characteristic velocities are found to be in near incompressible limit as the Mach number (Ma) values reported in Table 6.3 are well within the specified range (i.e., $Ma < 0.3$). Therefore, the present LBM solver is working well within the limits of incompressibility regime for the ranges of parameters considered in this work, and, hence, can be further used to obtain new results.

6.3.4 Flow field

The physical insights of the natural convection in differentially heated cavity are obtained by detailed analysis of flow field. In particular, the stream-function, isotherms and vorticity patterns and local variation of Nusselt number at hot and cold walls are examined in this section. It is evident that the kinematic viscosity (ν) and thermal diffusivity (α) are two significant governing parameters which are responsible for the development of hydrodynamics and thermal boundary layers, respectively. The development of the boundary layers, in turn, influence the hydrodynamics and heat transfer characteristics. These influence are examined by systematic variation of Prandtl number (Pr), which is directly related to the development of thickness of boundary layers. In order to investigate the effect of Prandtl number, normalized stream-function and voriticty are used.

The normalized stream-function (ψ^*) and vorticity (ξ^*) are defined as follows:

$$\psi^* = \frac{\psi - \psi_{min}}{\psi_{max} - \psi_{min}} \qquad \text{and} \qquad \xi^* = \frac{\xi - \xi_{min}}{\xi_{max} - \xi_{min}} \tag{6.7}$$

Figure 6.2-6.4 depict the representative variation of streamline, vorticity and center line velocity for the range of conditions covered herein. All the contours are equi-spaced at a value of 0.05. The streamline profiles (Figure 6.2) shows that the natural convection heat transfer mechanism starts dominating at lowest value of Rayleigh number ($Ra = 10^4$) and for all values of Prandtl numbers ($0.71 \leq Pr \leq 100$). The predominance of the natural convection enhances with the increasing values of both the Rayleigh and Prandtl numbers. The degree of predominance is very clearly seen in Figure 6.2 over the ranges of conditions considered herein. For example, the circular and symmetric flow patterns seen at Pr=0.71 remains symmetric (but not circular) about heated and cooled walls at $Ra = 10^4$. It clearly explains the establishment of natural convection phenomenon. At increasing Rayleigh number and/or Prandtl number (Pr) disturbs the flow symmetry and flow patterns are more confined to the hot wall because of the stronger movement of fluid between the hot and cold walls (Guo et al., 2007; Kuznik et al., 2007; Mezrhab et al., 2010; Kao and Yang, 2007; Ghazanfarian and Abbassi, 2010; Lee et al., 2010). Over the range of Rayleigh number (Ra), the flow pattern (Figures 6.2 and 6.3) also shows stronger dependence on the Prandtl number.

At low Prandtl numbers, convective heat transport is reinforced by inertia force rather than viscous force. For $Pr \leq 1.0$, it can be observed that fluid from heated wall of cavity moves upwards, encounters top adiabatic wall then displaces towards cold wall and moving down to cold adiabatic wall and, hence, completing clockwise circulation (Jami et al., 2007a). This circulation in clockwise direction creates a quasi motionless zone in the center of cavity. After Pr=10, streamlines circulation breaks in center of cavity, and symmetric streamlines along vertical walls are observed. Due to dominant viscous effect than inertial after Prandtl numbers of 1, the bifurcation of stream-functions near active walls is observed. As Prandtl number (Pr) increases, streamlines become more

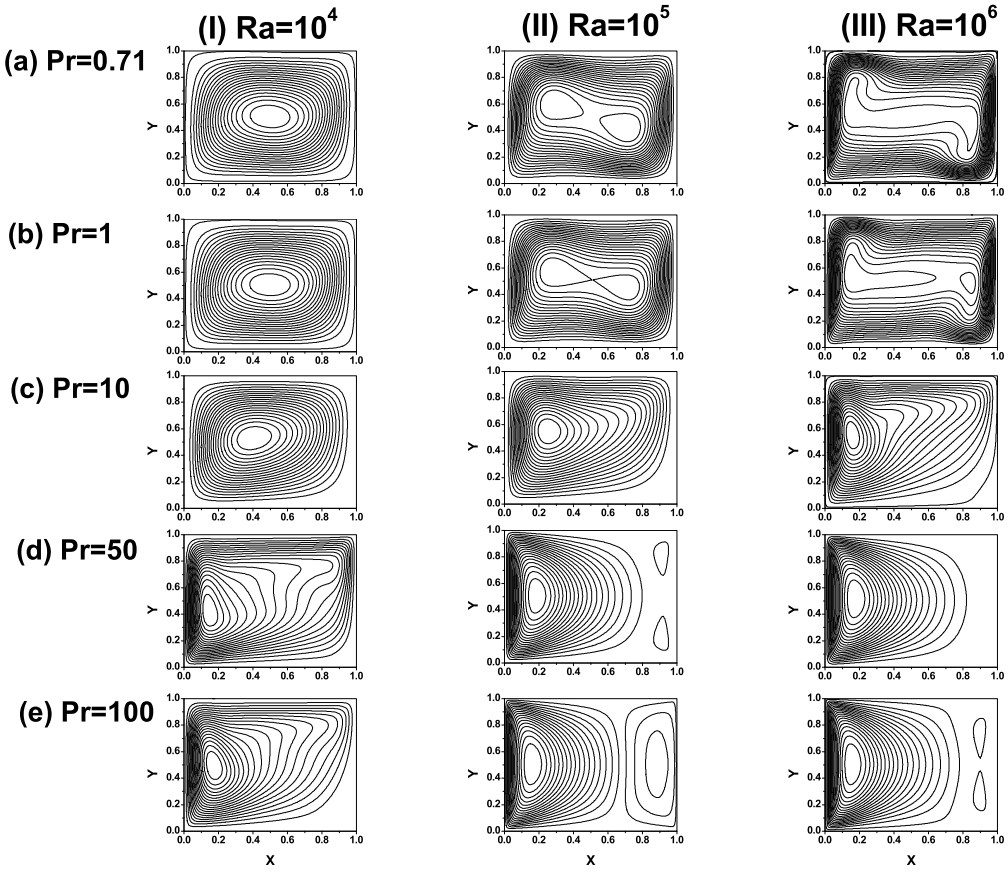

FIGURE 6.2: Influence of Prandtl number (Pr) and Rayleigh number (Ra) on streamline patterns in a square cavity for three values of Rayleigh number (i) $Ra = 10^4$, (ii) $Ra = 10^5$ and (iii) $Ra = 10^6$ for range of Prandtl number (a) Pr=0.71, (b) Pr=1, (c) Pr=10, (d) Pr=50 and (e) Pr=100.

concentrated towards heated isothermal walls. The formation of quasi-motionless zone along vertical axis in center of cavity takes place. This zone increases with the increase in Prandtl number from $Pr = 10$ to 100. With the increase in Prandtl number (Pr), fluid viscosity increases, it causes lower diffusion of heat as compared to velocity. With the increase in Rayleigh number to $Ra = 10^5$ and 10^6, fluid velocity inside cavity increases due to increased thermal expansion, it causes stronger circulation between active isothermal walls or simply convective heat transfer mechanism increases. At lower Prandtl numbers ($Pr \leq 1$), clockwise circulation of streamlines of lowest considered Rayleigh number with central single vortex separates and become two vortices in elongated streamline in the center of cavity at $Ra = 10^5$ (Mezrhab et al., 2010). With the increase in Prandtl number,

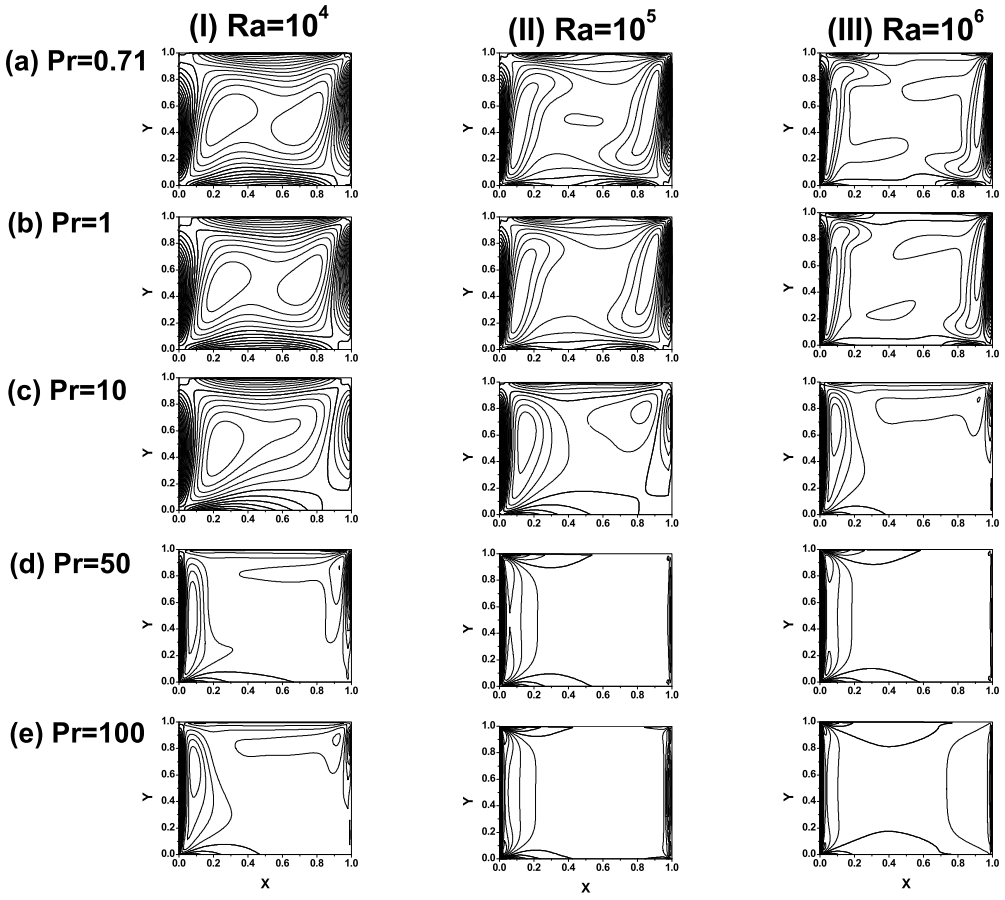

FIGURE 6.3: Influence of Prandtl number (Pr) and Rayleigh number (Ra) on vorticity patterns in a square cavity for three values of Rayleigh number (i) $Ra = 10^4$, (ii) $Ra = 10^5$ and (iii) $Ra = 10^6$ for range of Prandtl number (a) Pr=0.71, (b) Pr=1, (c) Pr=10, (d) Pr=50 and (e) Pr=100.

the circulation along active walls decreases. At $Pr = 10$, streamlines are similar to that of $Pr = 0.71$ and $Ra = 10^4$, except the change in position of single vortex which is observed to be shifted slightly towards hot wall than center of cavity. This is due to the fact that from this Prandtl number earlier conduction dominant heat transfer mechanism gets converted into convection dominant. As Prandtl number increases further, single vortex starts shifting more towards hot wall and its size increases indicating increase in momentum boundary layer thickness. At $Ra = 10^6$, for low Prandtl numbers ($Pr \leq 1$) two vortices, formed in the center of cavity, starts shifting towards isothermal active walls, making third vortex to be formd at the center of cavity. Figure 6.3 elucidates vorticity distribution in cavity. At small Rayleigh number ($Ra = 10^4$), inclined vortices

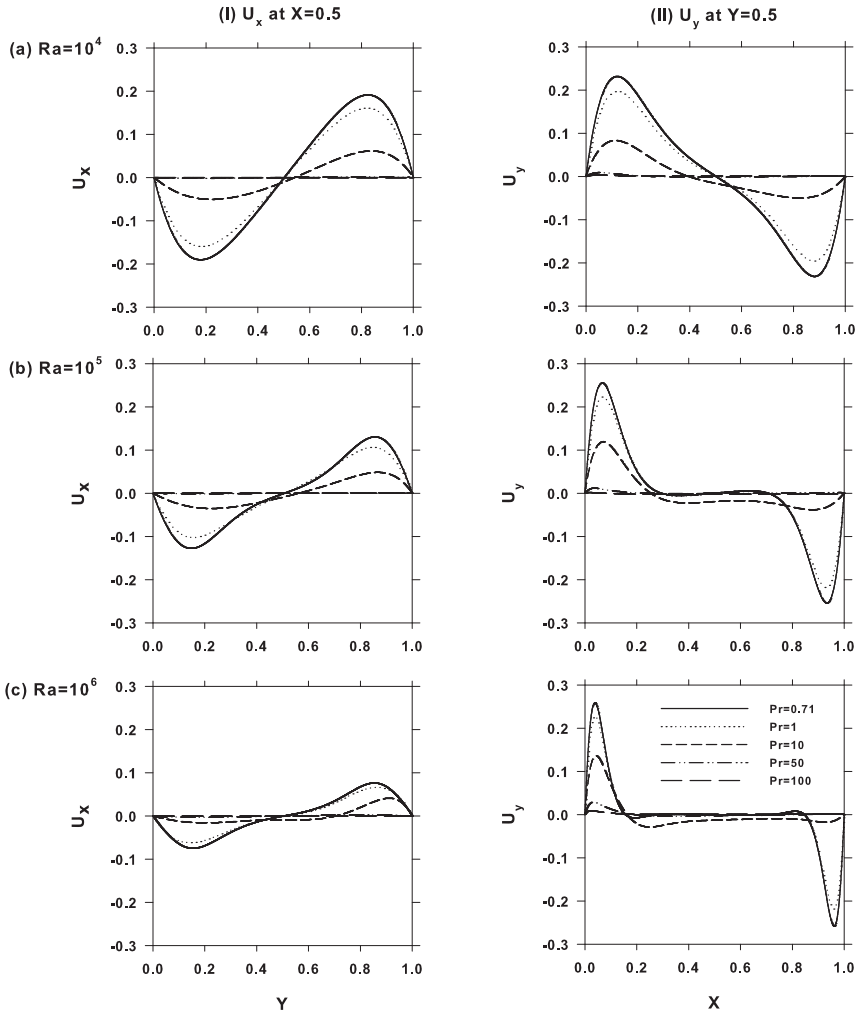

FIGURE 6.4: Representative variations of velocity components along (i) horizontal and (ii) vertical centerlines for whole range of Prandtl number (Pr) and Rayleigh number (Ra), (a) $Ra = 10^4$, (b) $Ra = 10^5$ and (c) $Ra = 10^6$.

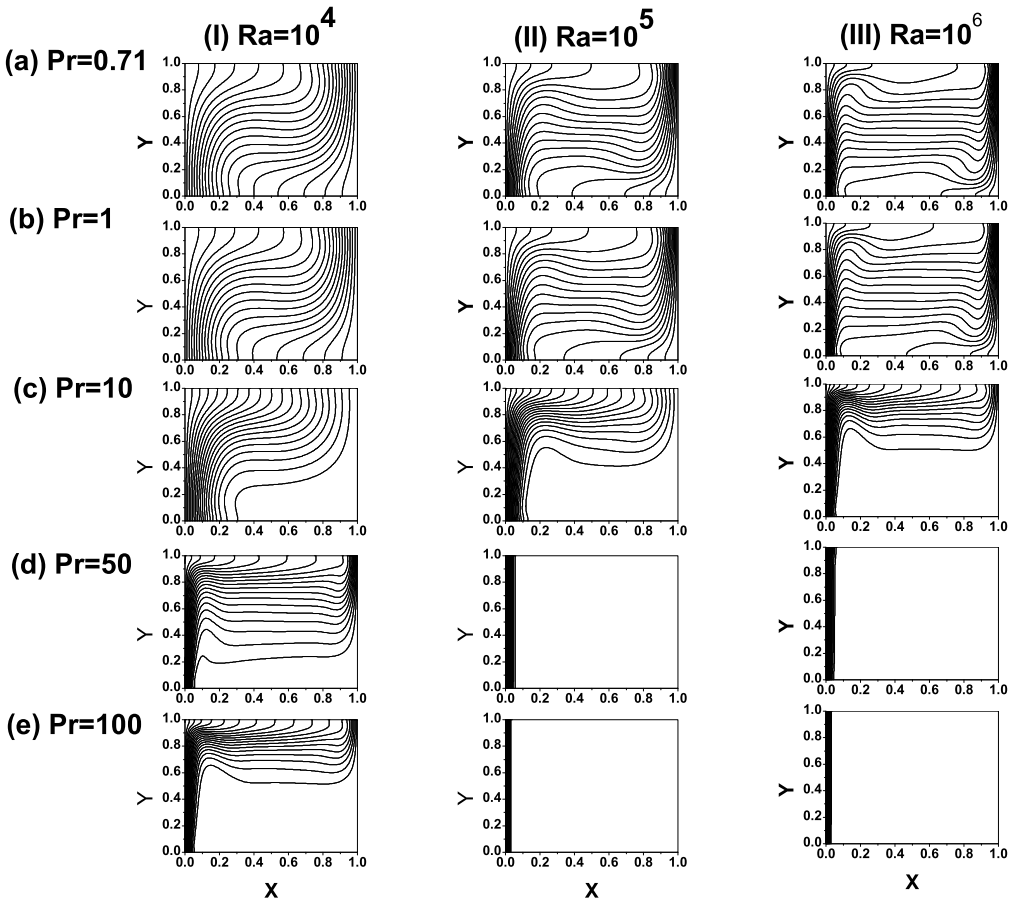

FIGURE 6.5: Influences of Prandtl (Pr) and Rayleigh (Ra) numbers on the isotherms patterns in a square cavity for three values of Rayleigh number (i) $Ra = 10^4$, (ii) $Ra = 10^5$ and (iii) $Ra = 10^6$ for range of Prandtl number (a) Pr=0.71, (b) Pr=1, (c) Pr=10, (d) Pr=50 and (e) Pr=100.

in the center of cavity are observed indicating the beginning of convection effect for small Prandtl numbers, but for higher Prandtl numbers ($Pr \geq 10$) due to increased viscous effect, vorticity values are smaller, it results in less vortex formation. The impact of increased Rayleigh number, i.e., convection effect on strength of vorticity is observed by larger vortex formation in the center of cavity and concentrated vorticity lines near active walls for smaller Prandtl numbers. For better understanding of the stream-function and vorticity behavior with the increasing values of the Rayleigh and Prandtl numbers, the minimum and maximum values of the stream-function (ψ_{min}, ψ_{max}) and vorticity (ξ_{min}, ξ_{max}) with their location of occurrence (x, y) within the cavity are presented in Table 6.4 for the ranges of flow governing parameters. An analysis of Table 6.4 suggests

TABLE 6.4: Variation of maximum and minimum values of the streamfunction (ψ_{max} and ψ_{min}) and vorticity (ξ_{max} and ξ_{min}) with Rayleigh and Prandtl numbers. The bracketed numbers show their location (x,y) of occurance within the cavity.

		Prandtl number, Pr				
Variable	*Ra*	0.71	1.0	10	50.0	100.0
ψ_{max}	10^4	0.0019	0.002	4.65×10^{-5}	0.0014	2.2×10^{-4}
		(0.72,1.0)	(0.72,1.0)	(0.33,1.0)	(0.14,1.0)	(0.17,1.0)
	10^5	7.7×10^{-4}	3.8×10^{-4}	7.1×10^{-5}	2.53×10^{-5}	3.54×10^{-5}
		(0.75, 1)	(0.75,1)	(0.96, 0.08)	(0.91,0.19)	(0.86,0.32 to 0.33)
	10^6	0.0016	8.4×10^{-4}	2.8×10^{-4}	7.1×10^{-5}	4.8×10^{-5}
		(0.85,1.0)	(0.85,1.0)	(0.95,0.11)	(0.92,0.16)	(0.90,0.25)
ψ_{min}	10^4	-0.947	-0.676	-0.078	-0.070	-0.056
		(0.5,0.51)	(0.5,0.51)	(0.4,0.53)	(0.14,0.42)	(0.18,0.49)
	10^5	-0.448	-0.332	-0.0567	-1.38×10^{-3}	-2.2×10^{-4}
		(0.61,0.29)	(0.58,0.28)	(0.55,0.25)	(0.51,0.18)	(0.51,0.16)
	10^6	-0.468	-0.355	-0.078	-0.0065	-0.0011
		(0.15,0.55)	(0.15,0.54)	(0.16,0.55)	(0.17,0.51)	(0.16,0.5)
ξ_{max}	10^4	0.0072	0.0051	7.1×10^{-4}	0.0043	0.0027
		(0.0,0.39)	(0.0,0.39)	(0.0,0.43)	(0.0,0.37)	(0.0,0.54)
	10^5	0.0102	0.0074	0.0012	9.6×10^{-5}	1.6×10^{-6}
		(0.0,0.37)	(0.0,0.36)	(0.0,0.5)	(0.0,0.52)	(0.0,0.86)
	10^6	0.017	8.4×10^{-4}	0.0022	2.8×10^{-4}	4.8×10^{-5}
		(0.0,0.33)	(0.0,0.32)	(0.0,0.53)	(0.0,0.48)	(0.0,0.95)
ξ_{min}	10^4	-0.0024	-0.0017	-2.4×10^{-4}	-0.0012	-7.6×10^{-5}
		(0.73,0.47)	(0.1,0.26)	(0.12,0.44)	(0.07,0.42)	(0.09,0.67)
	10^5	-0.0028	-0.0021	-3.5×10^{-4}	-2.2×10^{-5}	-6.0×10^{-6}
		(0.11,0.39)	(0.1,0.26)	(0.12,0.44)	(0.05, 0.9)	(0.03, 0.94)
	10^6	-0.0047	-0.0034	-6.0×10^{-4}	-6.4×10^{-5}	-2.0×10^{-5}
		(0.06,0.37)	(0.06,0.43 to0.45)	(0.08,0.7)	(0.04, 0.92)	(0.01,0.99)

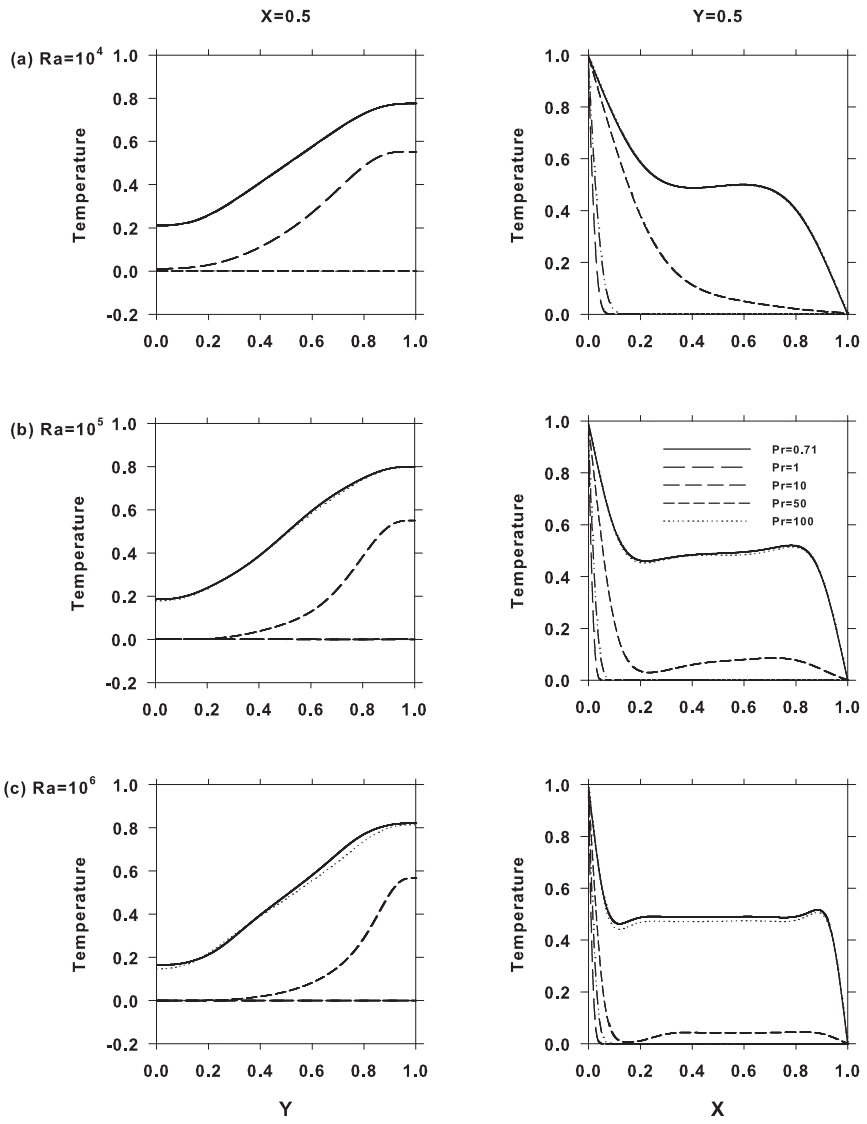

FIGURE 6.6: Temperature distribution along (i) horizontal and (ii) vertical centerlines for range of Prandtl and Rayleigh numbers.

that the magnitude of both the minima and maxima of the stream-function (ψ_{min}, ψ_{max}) increases with increasing values of Rayleigh number for all values of Prandtl number. However, the influence of Rayleigh number (Ra, or natural convection) on the ψ_{max} is seen to be of similar order for all values of Pr. Whereas ϕ_{min} seems to have stronger effect at larger values of Pr. In case of ϕ_{min}, the stronger effect at lower Pr further enhances with increasing values of Pr, thereby suggesting that the natural convection and conduction plays stronger role on the flow characteristics. The qualitatively similar patterns are also observed (Table 6.4) for the minimum and maximum values of the vorticity (ξ_{min}, ξ_{max}). Further insights of the flow characteristics are explored by analyzing the behavior of the

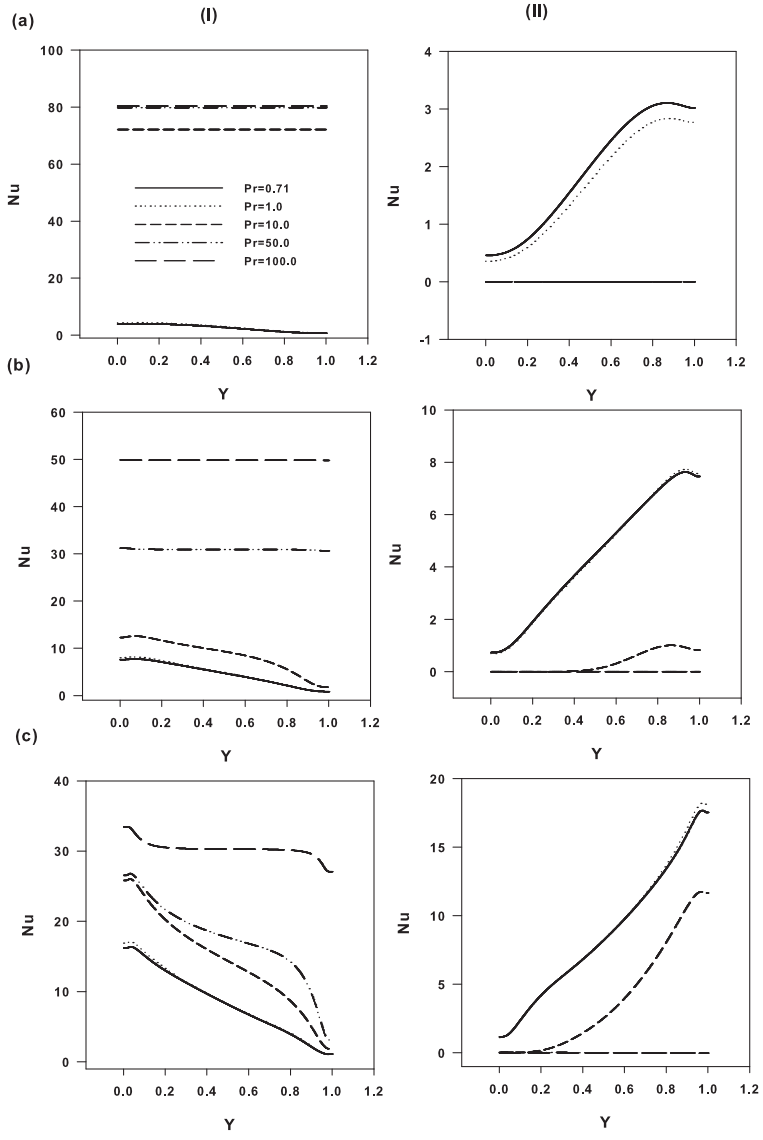

FIGURE 6.7: Local Nusselt number distribution plotted along (I) hot wall ($X = 0$) and (II) cold wall ($X = 1$) at $(a)Ra = 10^4, (b)Ra = 10^5$ and $(c)Ra = 10^6$.

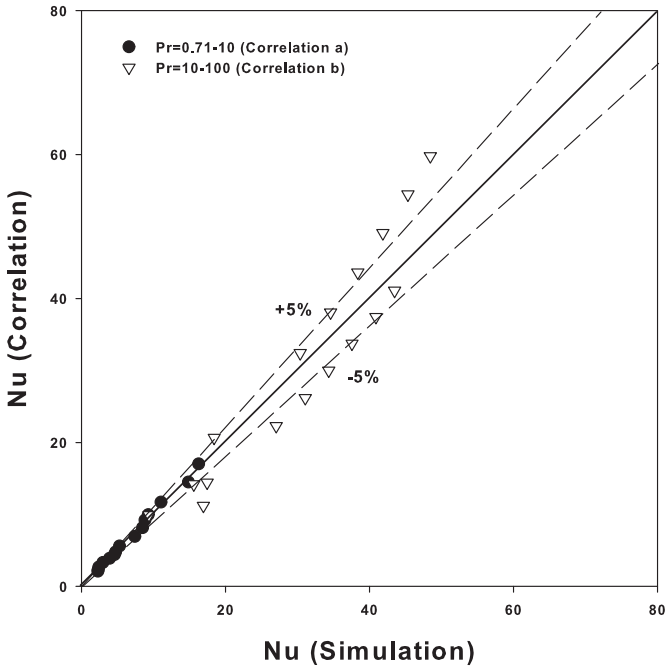

FIGURE 6.8: Comparison between simulated and predicted values (Eq. 6.8) of the average Nusselt number on the hot wall.

velocity components on the center lines of the cavity.

Figure 6.4 shows representative variations in the velocity components along the horizontal and vertical center lines of the cavity. The x-component of velocity (i.e., u) is plotted at vertical center line ($X = 0.5$) and y-component of velocity (v) is plotted along horizontal center line ($Y = 0.5$) of cavity. The scaling of velocity is done by using characteristic velocity as given in Table 6.3. It can be observed that due to symmetric Boussinesq effect and lower viscous force, for smaller Prandtl numbers ($Pr \leq 1$) velocity profiles are symmetric along geometric center of cavity. As viscous force increases, due to lesser effect of Boussinesq effect, symmetry of velocity is lost, for highest value of $Pr = 100$, velocity profiles are parallel to wall. The smooth and symmetric patterns seen at smaller values of Rayleigh number ($Ra = 10^4$) becomes of narrow amptitude on increasing the value of the Rayleigh number. It also shows the stronger as well as complex effect of Prandtl number at large values of Ra. The stronger and complex dependence of flow characteristics on the dimensionless flow governing parameters shall also influence the heat transfer phenomena. These are presented and discussed in the ensuing sections.

6.3.5 Heat transfer

The natural convection heat transfer in a differentially heated square cavity is explored and discussed in terms of the isotherm patterns, center-line temperature behavior, local and average Nusselt numbers in this section.

6.3.5.1 Isotherm patterns

Figure 6.5 represents temperature distribution in a square cavity for the ranges of conditions covered herein. The temperature distribution (or isotherms patterns) represents the various zones of heat transfer. Figure 6.5 shows the shifting of isotherms in geometrically symmetric manner from hot wall to the cold wall, which suggests that both walls are equally participative in the heat transfer, and, thereby indicating the convective heat transfer mechanism for lower Prandtl numbers ($Pr \leq 1$) over the ranges of Rayleigh number (Ra). For $Pr \geq 10$ and ($Ra = 10^4$) the isotherm patterns are parallel to the vertical walls. The isotherms patterns are also seen to be concentrated towards the hot wall. The clustering of isotherm lines near the hot wall suggests that the major convection occurs in the close vicinity of hot wall. The size of clustering zone (i.e., width of clustering) reduces with the increasing values of Pr. It also suggests that heat transfer mode is still dominated by the conduction for higher values of the Prandtl number ($Pr \geq 10$). The clustering of the isotherms represents the larger temperature gradients, thereby, resulting in the larger heat transfer rates. An increase in the value of Rayleigh number to 10^5 and for small values of the Prandtl numbers ($Pr \leq 1$) results in isotherms to be more inclined towards cold wall as well as becomes parallel to horizontal axis with formation of thin boundary layer near both active walls. For $Pr = 10$, due to combined effect of buoyancy force and higher viscosity, convective heat transfer mechanism is found to be predominant in upper half of domain and temperature in lower half of cavity is found to be very low. For large Prandtl numbers ($Pr > 10$), effects of Ra is found to be negligible and heat transfer is again governed by convection mode having very high heat transfer rates. For $Ra = 10^6$, isotherms become parallel to horizontal wall in most of area of cavity for lower

Prandtl numbers ($Pr \leq 1$). For Pr=10, fluid circulation between active walls covers most of the part of cavity, only area close to bottom wall is excluded with the formation of boundary layer near hot wall. It can be observed that effect of Pr on natural convection at $Ra \geq 10^5$, is found to be negligible.

The heat transfer behavior is further explored by analyzing the center-line variation of the temperature. Figure 6.6 represents the variations of temperature along the horizontal (Y=0.5, right column) and vertical (X=0.5, left column) center-lines over ranges of Ra and Pr. The temperature at vertical center-line of cavity ($X = 0.5$) is seen to be increasing along the length for all considered Rayleigh numbers (Ra) and $Pr \leq 10$. For higher Prandtl numbers ($Pr > 10$), the temperature variation is observed to be in the close vicinity of the hot wall. It is also visible through the isotherms patterns which are confined towards hot wall and almost negligible variation of temperature away from the hot wall towards the cold wall. On the other hand, the temperature distribution plotted along horizontal center-line of cavity ($Y = 0.5$) shows the decrease in temperature along with the length, which is almost parallel to horizontal axis in the middle portion of cavity. For higher Prandtl numbers ($Pr \geq 50$), shows a sudden drop in the temperature from higher value ($\theta = 1$) to low value ($\theta = 0$) in upper portion of cavity. The temperature profiles in the middle portion of cavity becomes parallel to horizontal axis which is in accordance with previous discussion on isotherm patterns.

6.3.5.2 Local Nusselt number

The Nusselt number (Nu, Eqs. 3.29 and 3.30) is used to represent the dimensionless heat transfer coefficient in the heat transfer studies. Therefore, it is the parameter which signifies the heat transfer rates. The local Nusselt number (Nu, Eq. 3.29) variations along hot and cold walls of the cavity are shown in Figure 6.7 to elucidate the effect of flow governing parameters (Ra and Pr). Over the range of Rayleigh numbers as expected, the higher values of Nusselt number (Nu) are obtained for the larger values of the Prandtl number (Pr). For fixed Prandtl number (Pr), the local Nusselt (Nu) number on both hot

and cold walls increases with the increasing value of Rayleigh number (Ra). Irrespective of the values of Ra and Pr, the large value of Local Nu at the bottom of hot wall decreases along the wall untill top of wall. The decrease in local Nusselt number value is, however, depends on both Rayleigh and Prandtl number in a complex manner. The stronger influence is seen at smaller values of Prandtl number, which diminishes with its increasing value for all values of Ra.

6.3.5.3 Average Nusselt number

The local Nusselt number (Nu, Figure 6.7) is integrated over the hot and cold wall to determine the overall heat transfer rate, i.e., average Nusselt number ($\overline{Nu}$, Eq. 3.30). Table 6.5 represents the variation of average Nusselt number with the Prandtl and Rayleigh numbers. As discussed in detailed flow field phenomenon, the increasing values of Rayleigh number narrow down the range of Prandtl number where the natural convection is dominating mode of heat transfer. It is clearly seen in Table 6.5 where the average Nusselt number values suddenly change to very high value with the marginal increase in the values of Prandtl number (Pr).

TABLE 6.5: The dependence of average Nusselt number ($\overline{Nu}$) of hot wall on Prandtl and Rayleigh numbers.

	$(\overline{Nu}_{x=0})$		
Pr	$Ra = 10^4$	$Ra = 10^5$	$Ra = 10^6$
0.71	2.257	4.570	8.816
1	2.288	4.724	9.267
5	2.970	7.402	14.837
10	3.890	8.471	16.260
15	4.316	8.917	16.920
20	4.771	9.355	17.452
30	6.862	15.587	18.417
50	16.899	27.029	30.262
60	20.196	31.074	34.577
70	22.886	34.330	38.362
80	25.807	37.583	41.849
90	27.270	40.882	44.342
100	30.491	43.503	48.430

6.3.6 Empirical correlation

For the scientific and engineering applications, it is worth to develop a simple closure relationship presenting the functional dependence of the heat transfer rates (in case of heat transfer studies) on the dimensionless flow governing parameters. Such equations can be used for interpolating the present results for the intermediate values of Rayleigh numbers for their utilization in design and engineering analysis. A huge amount of literature is available for empirical correlations of heat transfer rate with physical parameters such as, Rayleigh number, Grashof number, Prandtl number, etc in natural convection in differentially heated cavity (Howard, 1963; Heslot et al., 1987; Grossmann and Lohse, 2000; Stevens et al., 2013). Table 6.6 summerizes the empirical correlation developed in previous studies of natural convection in cavity. In this work, an empirical correlation

TABLE 6.6: Empirical correlations reported in literature.

Source	Empirical correlation	Range
Basak et al. (2006)	$\overline{Nu} = 1.622Ra^{0.145}$	$Ra \geq 5000, Pr = 0.71$
	$\overline{Nu} = 1.224Ra^{0.177}$	$Ra \geq 5000, Pr = 10$
Kao and Yang (2007)#	$\overline{Nu} \propto Ra^r, 0.2 \leq r \leq 0.286$	$10^6 \leq Ra \leq 10^{11}$
Grossmann and Lohse (2000)	$\overline{Nu} = 0.22Ra^{0.289}$	$10^6 \leq Ra \leq 10^{11}$
Howard (1963)	$\overline{Nu} \propto Ra^{1/3}$	$10^6 \leq Ra \leq 10^{11}$
Markatos and Pericleous (1984)	$\overline{Nu} = 0.1436Ra^{0.299}$	$10^3 \leq Ra \leq 10^6$
	$\overline{Nu} = 0.06Ra^{1/3}$	$10^7 \leq Ra \leq 10^{16}$
Niemela et al. (2000)	$\overline{Nu} = 0.124Ra^{0.309\pm0.0043}$	$10^6 \leq Ra \leq 10^{17}$
	$\overline{Nu} \propto Pr^{0.14}$	$Pr = 0.1, Ra = 5 \times 10^5$
Yu et al. (2011)	$\overline{Nu} = 0.1659Ra^{0.2823}$	$10^4 \leq Ra \leq 10^6$

(# Rayleigh-Benard convection)

encompassing the functionality of average Nusselt number ($\overline{Nu}$) at hot (or isothermal) wall with Prandtl number (Pr) and Rayleigh number (Ra) is developed. An standard closure relationship for present simulation results for heat transfer is given in the following form:

$$\overline{Nu} = APr^B Ra^C + D \tag{6.8}$$

Three different correlations along with R^2 values and minimum (δ_{min}) and maximum

TABLE 6.7: The empirical correlations for entire range of data with R^2, minimum ($\%\delta_{min}$), maximum ($\%\delta_{max}$) relative deviations and $\%\delta_N$ values for Rayleigh number of $10^4 \leq Ra \leq 10^6$.

Sr. No.	Prandtl number	A	B	C	D	R^2	δ_{min}	δ_{max}	δ_N
1.	$0.71 \leq Pr \leq 10$	0.1198	0.3183	0.2326	0.0	0.98	0.25	6.6	4.550
	$10 \leq Pr \leq 100$	0.1081	0.1628	0.8829	0.0	0.923	5.6	30.9	15.20
2.	$0.71 \leq Pr \leq 30$	0.1499	0.2977	0.2528	0.0	0.97	0.2	15.0	5.596
	$30 \leq Pr \leq 100$	0.3940	0.1110	0.7255	0.0	0.95	0.1	21.1	8.850
3.	$0.71 \leq Pr \leq 100$	0.1965	0.1203	0.8339	3.3205	0.94	1.1	31.0	13.92

(δ_{max}) deviations are obtained by dividing data sets as shown in Table 6.7. It can be observed that the empirical correlations (2) for data range of $0.71 \leq Pr \leq 30; 30 \leq Pr \leq 100$ give best fit among three developed correlations.

It can be observed that the R^2 values of correlations given in Table 6.7 are close to each other. For deciding about the best possible correlation, the normalized percentage standard deviation ($\%\delta_N$) between simulation and correlation values has been obtained for all three cases by using following equation as given by Singh et al. (2008) as given below:

$$\%\delta_N = 100\sqrt{\frac{\sum\left[\frac{Nu_{simu}-Nu_{pred}}{Nu_{simu}}\right]^2}{N}} \tag{6.9}$$

where, Nu_{simu} and Nu_{pred} represents the average Nusselt number values obtained from simulation and predicted by empirical correlations (Table 6.7). N represents the number of data points (in present study, total number of data points N=39). It can be observed that the normalized percentage standard deviation is minimum for second correlation $\%\delta_N = 5.596$ and 8.850, and R^2 values are also relatively high. So correlations (2a) and (2b) represent the present data with better accuracy. Figure 6.8 represents the comparison between numerical values of average Nusselt number ($\overline{Nu}$) with that of predicted values by correlations (2a) and (2b) given in Table 6.7 for $Pr \leq 30$ and $Pr \geq 30$, respectively. The average error between simulated results and one obtained from empirical correlation is about 1.1% and 3.7% for correlations of range $Pr \leq 30$ and $Pr \geq 30$, respectively.

Therefore, the closure relationship presented herein can be used to predict the values of the average Nusselt number with the bound of $\pm 4 - 5\%$.

6.4 Concluding Remarks

The applicability of thermal lattice Boltzmann method (TLBM) is utilized for the investigation of the natural convection heat transfer in an square cavity. In particular, the numerical simulations are performed to investigate the effects of Prandtl numbers ($0.71 \leq Pr \leq 100$) on natural convective heat transfer mechanism for three different Rayleigh numbers viz., $Ra = 10^4, 10^5$ and 10^6. The numerical results are obtained and presented in terms of the streamline and vorticity patterns, the center-line variations of the velocity and temperature, and local and average Nusselt numbers. The following conclusions can be drawn from the results:

1. Natural convection effect increases with the increase in Prandtl number (Pr) for all values of the Rayleigh number (Ra) due to the increased viscous force effect in comparison to inertial force. As thermal diffusion is inversely proportional to Prandtl number, velocity is more diffused than thermal energy. For $Ra = 10^4$, dominant heat transfer mechanism is conductive for $Pr \geq 10$.

2. For higher Prandtl numbers, temperature distribution weakens and isotherms are more stratified towards the hot wall indicating predominant momentum boundary layer.

3. The average Nusselt number (dimensionless heat transfer coefficient) of isothermal wall ($x = 0$) is seen to increase with the Prandtl and Rayleigh numbers.

4. The numerical data are presented as a empirical correlation relating the average Nusselt number ($\overline{Nu}$) with Prandtl number (Pr) and Rayleigh number (Ra).

Chapter 7

NATURAL CONVECTION IN PARTIALLY-SIMULTANEOUSLY HEATED-COOLED SQUARE CAVITY

7.1 Problem description

Consider the steady, laminar, natural convection heat transfer in an incompressible fluid from an infinitely long square cavity ($AR = L/H = 1.0$, where L and H are cross-sectional length and height of the cavity), as shown in Figure 7.1. The west wall ($x = 0$) of cavity is subjected to equal length of hot and cold conditions, i.e., lower half ($0 \leq y \leq H/2$) of cavity is at ambient ($T_C < T_H$), whereas the upper half ($H/2 \leq y \leq H$) is exposed to hot condition (T_H). The east wall ($x = L$) is kept at ambient ($T_C < T_H$). The top ($y = 0$) and bottom ($y = H$) walls are thermally insulated. The aim of the study is to explore physical insights of cavity exposed to contrast thermal conditions for different heat

intensity (i.e., Rayleigh number). The study is carried out for Rayleigh number ($10^4 \leq Ra \leq 10^6$) and Prandtl number ($Pr = 0.71$). The governing equations (in dimensional

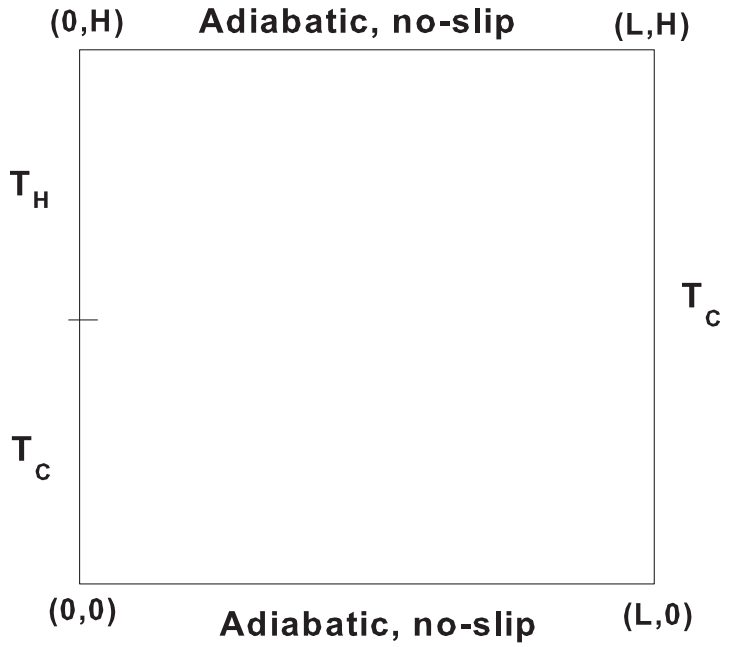

FIGURE 7.1: Schematic representation of the partially-differentially heated square cavity and boundary conditions.

and dimensionless forms) along with general simplifications are expressed in Chapter 3. The physical realistic boundary conditions (in non-dimensional form) for problem under consideration are expressed as below,

- West wall ($X = 0$)

$$U_x = 0, U_y = 0, \theta = 0 \quad \text{for} \quad 0 \leq Y \leq 1/2; \tag{7.1}$$

$$U_x = 0, U_y = 0, \theta = 1 \quad \text{for} \quad 1/2 \leq Y \leq 1; \tag{7.2}$$

- East (cold) wall ($X = 1$)

$$U_x = 0, U_y = 0, \theta = 0; \tag{7.3}$$

- Bottom ($Y = 0$)and top ($Y = 1$) walls,

$$U_x = 0, U_y = 0, \frac{\partial \theta}{\partial Y} = 0 \tag{7.4}$$

Extensive results have been obtained and presented herein for the following ranges of conditions. The Rayleigh number ($10^3 \leq Ra \leq 10^6$) varied in the logarithmic manner at a constant Prandtl number ($Pr = 0.71$). For these broad ranges of flow governing parameters, the local and global convective flow characteristics such as the evolution of stream functions and isotherms; variation of velocity components and temperature on horizontal and vertical center lines; and the Nusselt number are obtained and discussed herein the preceding sections. Before presenting new results obtained from this numerical simulation, the ensuing section studies the grid independence and validaity of the solver for the present problem.

7.1.1 Grid independence study and validation of results

In order to ensure the accuracy and reliability of present solver, grid independence study has been carried out based on average Nusselt number ($\overline{Nu}$) estimated at wall exposed to both hot and cold conditions ($x = 0$). The adequacy of five uniform lattice (grid) sizes G1(41×41), G2(61×61), G3(81×81), G4(101×101) and G5(121×121) have been examined in Figure 7.2. It can be observed that change in $\overline{Nu}$ value after lattice size of 81×81 is negligible with enormous increase in computational time. Therefore, for present work, a lattice size of 81×81 is chosen which is found to be optimum with respect to computational time and also restrict LBM in low Mach number limit. This lattice size (81×81) is believed to be sufficiently refine enough to resolve thermal and hydrodynamic features within interested range of conditions.

Further, the reliability and accuracy of new results is established by comparing the present results with available results in the literature. It is, however, evident from the literature that none of the existing studies have explored the study of cavity with one wall subjected

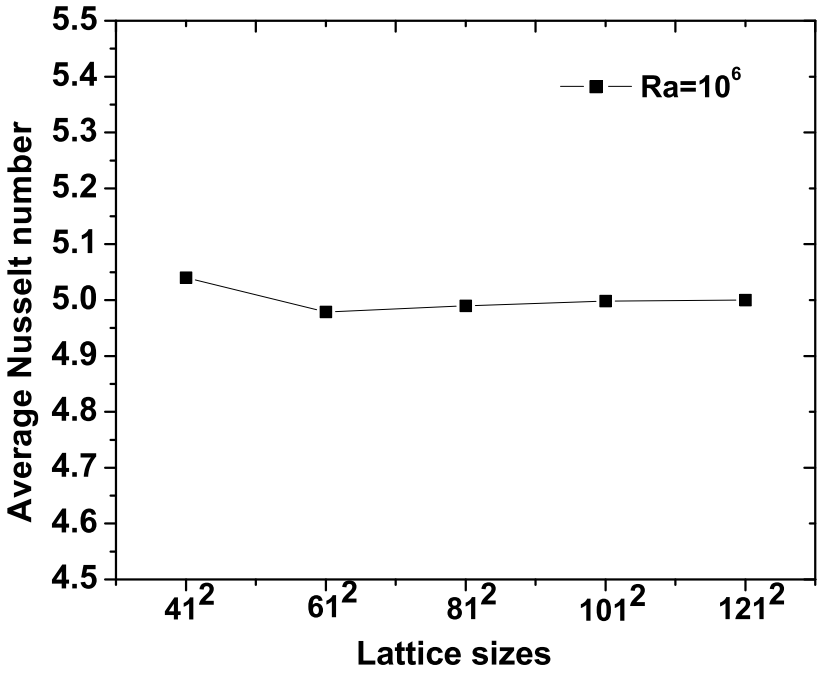

FIGURE 7.2: Grid independence study.

to both hot and cold conditions. The detailed validation of present solver for the differentially heated cavity has already been presented elsewhere (Chapter 6), and, thus, not repeated herein.

7.2 Results and Discussions

Extensive results have been obtained and presented herein this section for the following ranges of conditions. The Rayleigh number ($10^3 \leq Ra \leq 10^6$) varied in the logarithmic manner at a constant Prandtl number ($Pr = 0.71$). For these broad ranges of flow governing parameters, the local and global convective flow characteristics such as the evolution of stream functions and isotherms; variation of velocity components and temperature on horizontal and vertical center lines; and the Nusselt number are obtained and discussed herein the preceding sections.

7.2.1 Fluid flow results

Figure 7.3 represents the dependence of streamline and isotherm patterns on the dimensionless flow governing parameters. Fluid near the vicinity of cold portion of west wall ($x = 0$) of cavity approaches the heated upper part of cavity. As fluid come in the vicinity of hot part of cavity, rise in fluid temperature is observed and move towards the top adiabatic wall. Then fluid flows in right direction towards east (cold, $X = 1$) wall with the gradual decrease in fluid temperature and strikes the cold east wall and then approaches the bottom wall and thus completing a clockwise circulation. At lowest considered Rayleigh number (i.e., $Ra = 10^3$) the streamline patterns are circular with formation of quasi-motionless portion at upper middle part of cavity. At $Ra = 10^3$, the mode of heat transfer is conduction dominant due to weak buoyancy driven flow. Increase in Rayleigh number causes rise in the fluid circulation between thermally active walls which make formation of very low temperature region called convection cell near lower left corner of cavity. The size of the convection cell is found to vary proportionally with Rayleigh number (Ra). The isotherm behavior illustrated in figure (7.3,II) is in accordance with the streamline patterns. Due to conduction dominant heat transfer isotherm distribution towards hot surface are weak. For higher Rayleigh number ($Ra \geq 10^4$), isotherm pattern become more and more stratified towards the hot surface and become parallel to horizontal axis. Further insights of flow behavior in cavity are explored by analyzing the center line variations of temperature and velocity components in cavity. Figure 7.4 illustrates the temperature variation along horizontal and vertical center lines of the cavity. The temperature distribution at along vertical center line (Figure 7.4, I) of cavity ($X = 0.5$) represents the linear increase in temperature. This is because low temperature fluid from lower cold part of cavity moves towards the heated surface with the gradual increase in the temperature. (Figure 7.4, II) illustrates the temperature variation along horizontal center line of cavity. The temperature distribution becomes more and more parallel to the horizontal axis with the increase in Rayleigh numbers due to clockwise circulation of fluid in the cavity.

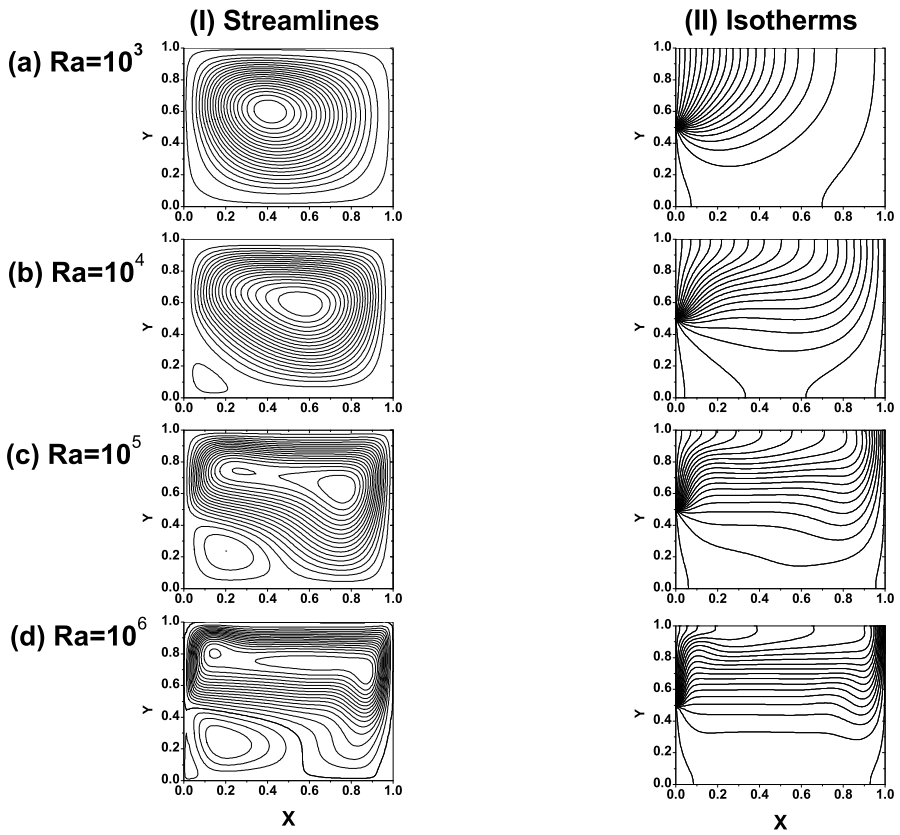

FIGURE 7.3: Influence of Rayleigh number on the streamline and isotherm pattern.

Figure 7.5 represents the velocity components variation along vertical and horizontal center line of cavity. The x-component of velocity (U_x) is plotted at vertical center line ($X = 0.5$) and y-component of velocity (U_y) is plotted along horizontal center line ($Y = 0.5$) of cavity, respectively. The velocity profiles clearly insights the clockwise circulation of fluid. At low Rayleigh number ($Ra = 10^3$), circulation is weak and increase in Rayleigh number increases the circulation strength in the cavity. This behavior is in accordance with previous discussion.

7.2.2 Heat transfer rate

The rate of heat transfer in cavity is illustrated by analyzing the local and average Nusselt number ($\overline{Nu}$) as represented in Figures 7.6 and 7.7 respectively. The effect of contrast

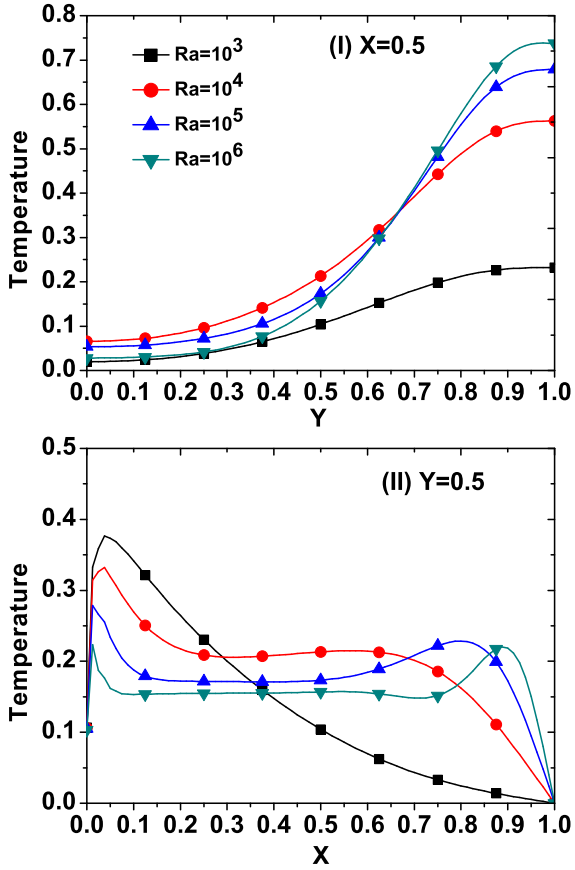

FIGURE 7.4: Temperature distribution along (i) horizontal and (ii) vertical centerlines for the range of Rayleigh numbers.

thermal heating along west wall ($X = 0$) can be clearly seen from Nusselt number behavior. The first half shows very low temperature with sudden rise in Nu value from Y=0.5 and then gradual decrease in Nu values. This is due to flow of fluid from heated region towards cold region with gradual decrease in temperature (Figure 7.6, I). The variation of local Nusselt number along cold wall (Figure 7.6, II) shows linear increase in the Nusselt number values implies higher fluid temperature as compared to the lower half of cold wall. This is due to heated fluid from hot surface approaches cold wall with the decrease in temperature but still higher temperature than fluid in the vicinity of lower region of cold wall. Average Nusselt number ($\overline{Nu}$) is obtained by integrating local Nusselt number values along considered wall. Figure 7.7 represents the average Nusselt number values estimated for both vertical walls for range of Rayleigh numbers. For both considered walls, as expected, average Nusselt number ($\overline{Nu}$) shows increase with Rayleigh number.

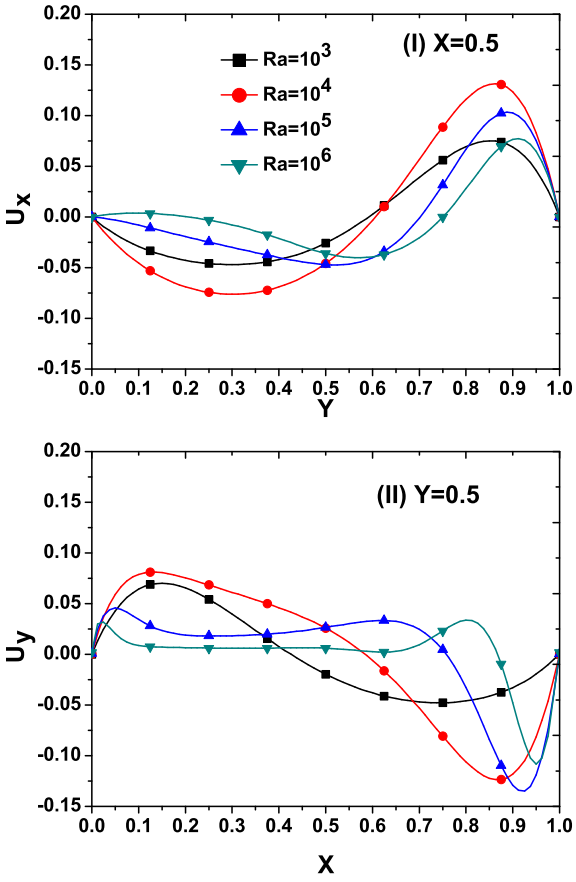

FIGURE 7.5: Velocity profiles along (i) horizontal and (ii) vertical center-lines for the range of Rayleigh numbers.

In case of mixed heated wall ($X = 0$), relatively small increase (16.3%) in $\overline{Nu}$ value is observed for Rayleigh number of $Ra \leq 10^4$ indicating conduction dominant heat transfer. A steep rise in the average Nusselt number ($\overline{Nu}$) value is observed for $Ra \geq 10^5$. For cold wall ($X = 1$), a linear rise in $\overline{Nu}$ with Rayleigh number is observed. The average Nusselt number values at Rayleigh number of $Ra = 10^5$ are nearly equal for both vertical walls indicating equal rate of heat transfer. Further, for better analysis of heat transfer in system, overall Nusselt number ($\widehat{Nu}$) is estimated by using following relations:

$$\widehat{Nu} = \frac{\overline{Nu}_{X=0} + \overline{Nu}_{X=1}}{2} \tag{7.5}$$

Simmilar trend as that of mixed heated and cold wall is observed for overall Nusselt number ($\widehat{Nu}$) with Rayleigh numbers.

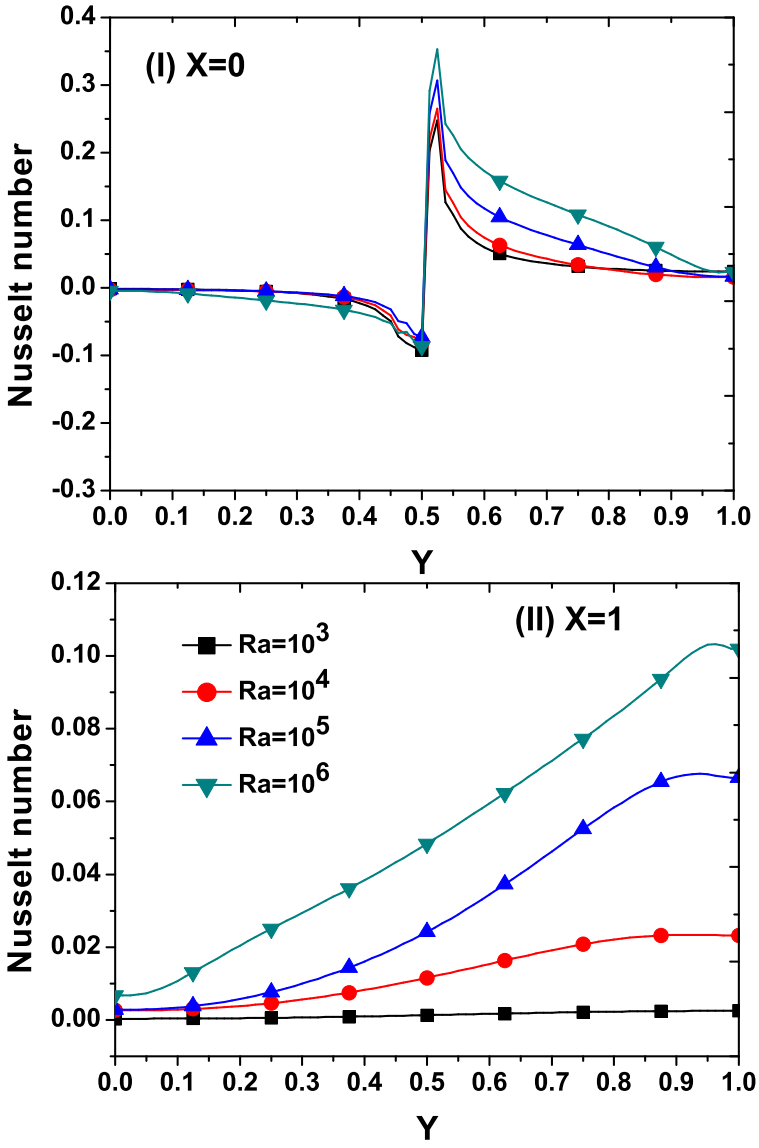

FIGURE 7.6: Local Nusselt number variation along (i) west wall ($X = 0$) and (ii) east wall ($X = 1$) for range of Rayleigh number.

7.2.3 Empirical correlation

For the scientific and engineering applications, it is worth to develop a simple closure relationship presenting the functional dependence of the heat transfer rates (in case of heat transfer studies) on the dimensionless flow governing parameters. Such correlations can be used for the interpolating present results for the intermediate values of Rayleigh numbers (Koteswara Rao et al., 2011) for their utilization in design and engineering analysis. In this

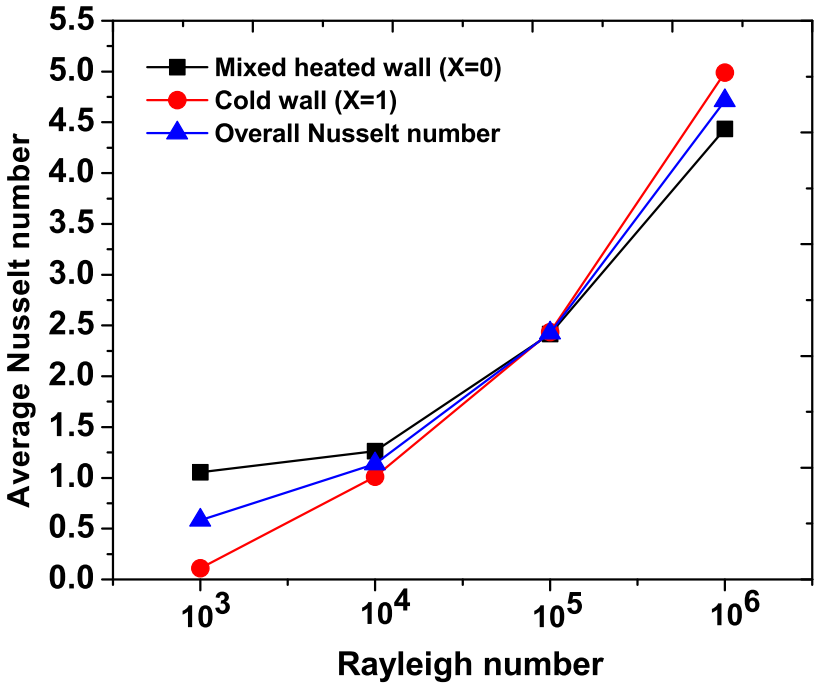

FIGURE 7.7: Average Nusselt number ($\overline{Nu}$) variation along (I) west wall ($X = 0$) and (II) east wall ($X = 1$) for range of Rayleigh number.

work, an empirical correlation encompassing the functionality of overall Nusselt number ($\widehat{Nu}$) with Rayleigh number (Ra) is obtained. The following correlation fit the present data excellently:

$$\widehat{Nu} = 0.07Ra^{0.31} \quad (R^2 = 0.99) \tag{7.6}$$

Figure 7.8 represents the comparison between present numerical simulation values of overall Nusselt number ($\widehat{Nu}$) and predicted values from Eqn. **??**. It can be seen that predicted values are in excellent agreement with the simulation values as indicated by The coefficient of determination (R^2) value, which is $R^2 = 0.99$. The average error between simulated and predicted values is observed to be 2.4%.

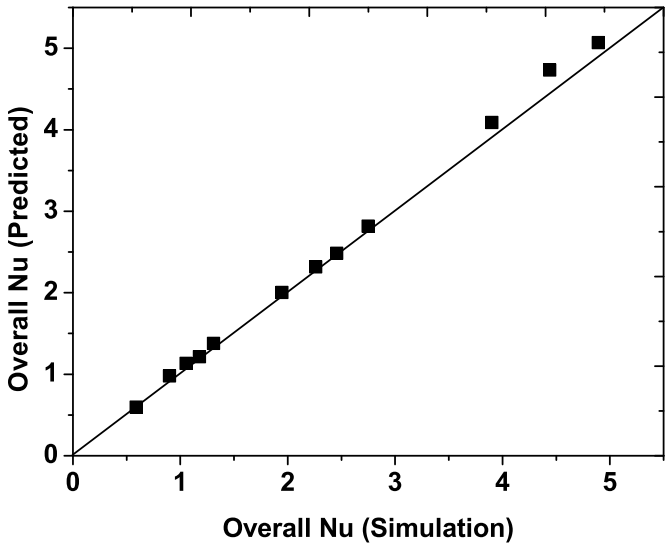

FIGURE 7.8: Comparison between simulated and predicted overall Nusselt number ($\widehat{Nu}$).

7.3 Concluding Remarks

In present numerical investigation, the influence of Rayleigh number ($10^3 \leq Ra \leq 10^6$) on natural convective heat transfer mechanism in a square cavity with one wall subjected to equally both hot and cold thermal conditions, have been elucidated. The upper part ($0.5 \leq Y \leq 1$) of west wall of cavity is subjected to higher temperature (T_H) and lower part ($0 \leq Y \leq 0.5$) is exposed to ambient ($T_C < T_H$). A thermal lattice Boltzmann method with passive scalar and D2Q9 lattice model is used as a numerical tool. The numerical results are obtained and presented in terms of the streamline and isotherm patterns, the center line variations of the velocity and temperature, and local and average Nusselt numbers. Further, the numerical data is presented as a empirical correlation relating the average Nusselt number (Nu) with Rayleigh number (Ra). The following conclusions can be drawn from the results:

1. Formation of convection cell near lower part of mixed heated wall ($X = 0$) of cavity is observed after $Ra \leq 10^4$, as low temperature fluid retained in that region.

2. The size of convection cell increases with the increase in Rayleigh number (Ra).

3. The average Nusselt number ($\overline{Nu}$) and overall Nusselt number ($\widehat{Nu}$) value show linear increase with Rayleigh number.

4. At $Ra = 10^5$, the rate of heat transfer of both vertical walls is almost same, which is indicated by nearly same values of average Nusselt number ($\overline{Nu}$).

5. The present numerical results have been correlated by using a simple empirical correlation thereby enabling the interpolation of the present simulation results for the intermediate values of physical parameters, i.e., Rayleigh number (Ra).

Chapter 8

MAGNETO-HYDRODYNAMIC NATURAL CONVECTION IN DIFFERENTIALLY HEATED CAVITY

8.1 Introduction

This chapter explores the influence of cooler size on magneto-hydrodynamic (MHD) natural convective heat transfer characteristics of partially-differentially heated square enclosure. The combined influence of cooler size (L_c), Hartmann number (Ha), angle of magnetic field direction (θ_M) and Rayleigh number (Ra) on heat transfer characteristics have been studied and presented herein.

8.2 Problem Description

The physical model used in the present work is shown in Figure 8.1. A square partially-differentially heated cavity ($AR = 1$) with one vertical wall ($x = 0$) exposed to partial heating (T_h) in the middle location with other vertical wall exposed to the cooling (T_c) is considered. The partial heater is placed at the middle location ($H/4 \leq y \leq 3H/4$), while other wall is subjected to cooling with variable cooler size (L_c). The cooler is also

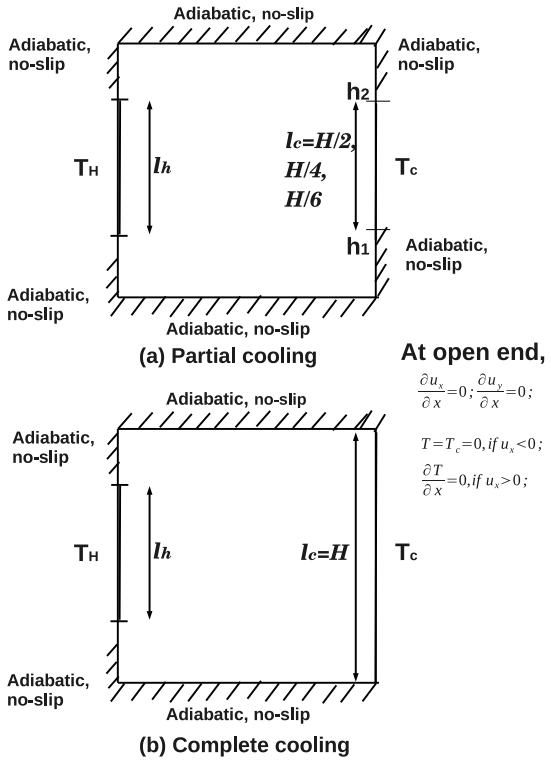

FIGURE 8.1: Schematic representation of the square partially differentially heated/-cooled cavity.

placed at the middle location of one of the vertical wall of cavity. In particular , the influence of four cooler lengths, $L_c = 1, 1/2, 1/4, 1/6$ have been investigated. The top and bottom walls are maintained at adiabatic condition. The working fluid is considered as air ($Pr = 0.71$). The uniform magnetic field ($\mathbf{B} = B_x\mathbf{e_x} + B_y\mathbf{e_y}$) (of constant magnitude $B = \sqrt{B_x + B_y}$) is applied at angle of θ_M with horizontal axis, where $\mathbf{e_x}$ and $\mathbf{e_y}$ are the unit vectors in the Cartesian coordinates. The magnetic field has been applied in three directions $\theta_M = 0^o, 45^o, 90^o$. The governing equations of MHD-natural convection

heat transfer with general assumptions are detailed in Chapter 3. The physical realistic boundary conditions for problem under consideration are expressed as follows:

- West wall ($x = 0$) is considered as no-slip and exposed to partial heating,

$$u_x = 0, u_y = 0, \frac{\partial T}{\partial x} = 0 \quad \text{for} \quad 0 \leq y \leq H/4; \tag{8.1}$$

$$u_x = 0, u_y = 0, T = T_H \quad \text{for} \quad H/4 \leq y \leq 3H/4; \tag{8.2}$$

$$u_x = 0, u_y = 0, \frac{\partial T}{\partial x} = 0 \quad \text{for} \quad 3H/4 \leq y \leq H; \tag{8.3}$$

- East wall ($x = L$) is considered as no-slip wall and exposed to the partial cooling with different cooler sizes, i.e.,

$$u_x = 0, u_y = 0, \frac{\partial T}{\partial x} = 0 \quad \text{for} \quad 0 \leq y \leq h_1; \tag{8.4}$$

$$u_x = 0, u_y = 0, T = T_c \quad \text{for} \quad h_1 \leq y \leq h_2; \tag{8.5}$$

$$u_x = 0, u_y = 0, \frac{\partial T}{\partial x} = 0 \quad \text{for} \quad h_2 \leq y \leq H; \tag{8.6}$$

  where, h_1 and $h_2 = (h_1 + l_c)$ are lengths for the different cases of cooler sizes and middle heating locations are given below. In case of *middle heating*, $h_1 = (1 - l_c)/2$ and $h_2 = (1 + l_c)/2$

- Top and bottom walls are maintained adiabatically, i.e.,

$$u_x = 0, u_y = 0, \frac{\partial T}{\partial y} = 0; \tag{8.7}$$

In non-dimensional form, the boundary treatments can be expressed as below:

- West wall ($X = 0$),

$$U_x = 0, U_y = 0, \frac{\partial \theta}{\partial X} = 0 \quad \text{for} \quad 0 \leq Y \leq 1/4; \tag{8.8}$$

$$U_x = 0, U_y = 0, \theta = 1 \quad \text{for} \quad 1/4 \leq Y \leq 3/4; \tag{8.9}$$

$$U_x = 0, U_y = 0, \frac{\partial \theta}{\partial X} = 0 \quad \text{for} \quad 3/4 \leq Y \leq 1; \tag{8.10}$$

- East wall ($X = 1$),

$$U_x = 0, U_y = 0, \frac{\partial \theta}{\partial X} = 0 \quad \text{for} \quad 0 \leq Y \leq H_1; \tag{8.11}$$

$$U_x = 0, U_y = 0, \theta = 0 \quad \text{for} \quad H_1 \leq y \leq H_2; \tag{8.12}$$

$$U_x = 0, U_y = 0, \frac{\partial \theta}{\partial X} = 0 \quad \text{for} \quad H_2 \leq Y \leq 1; \tag{8.13}$$

  where, $H_1(h_1/H)$ and $H_2(h_2/H) = (H_1 + L_c)$ are lengths for the different cases of cooler sizes is expressed as below: In case of *middle heating*, $H_1 = (1 - L_c)/2$ and $H_2 = (1 + L_c)/2$

- Top and bottom walls are maintained adiabatically, i.e.,

$$U_x = 0, U_y = 0, \frac{\partial \theta}{\partial Y} = 0; \tag{8.14}$$

The objective of present work is to explore fluid flow and heat transfer characteristics of square partially-differentially heated cavity exposed to the magnetic field at three different directions ($\theta_M = 0^o, 45^o, 90^o$), Hartmann number ($Ha = 0, 60, 120$), different cooler sizes ($L_c = 1,\ 1/2,\ 1/4,\ 1/6$) at laminar range of Rayleigh number ($10^3 \leq Ra \leq 10^5$) with air ($Pr = 0.71$) as a working fluid by using in-house developed thermal lattice Boltzmann code. Before presenting new results obtained in this work, the grid independence test and validation of results is presented in next section.

8.3 Grid independence test and validation of results

In this work, the size of the computational domain, i.e., square, is itself fixed by the problem definition. In order to ensure the accuracy and reliability of present code and to determine the optimum lattice size, the grid independence study is carried out by using the five uniform grid lattice size $(N_x \times N_y) : G_1(41\times41), G_2(61\times61), G_3(81\times81), G_4(101\times101)$ and $G_5(121\times121)$. Here, N_x and N_y represents the number of lattice nodes in $x-$ and $y-$ directions, respectively. The adequacy of five uniform grid/lattice sizes have been examined for

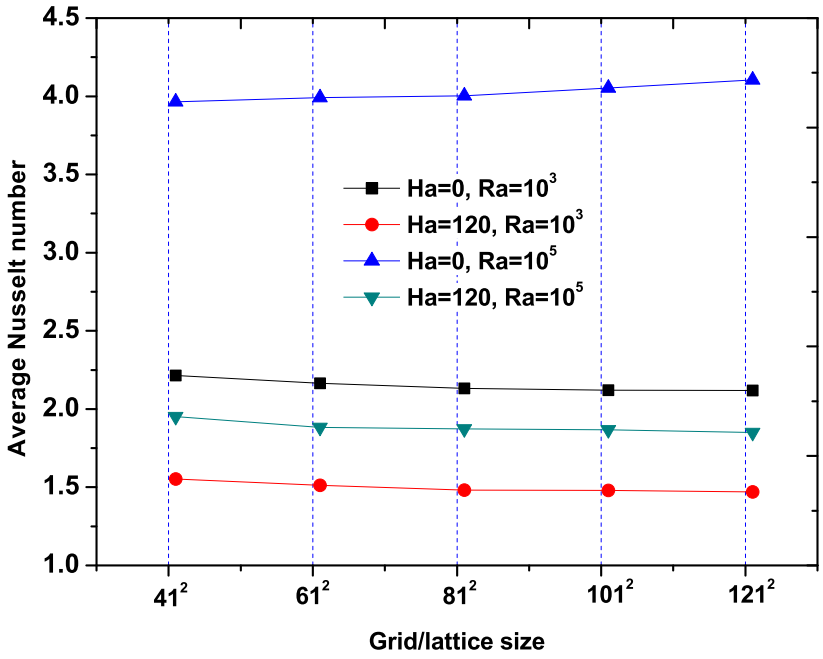

FIGURE 8.2: Influence of grid sizes on average Nusselt number $(\overline{Nu})$ at Ha=0,120, $\theta_M = 0$ and $Ra = 10^3, 10^5$

extreme values of Hartmann number $(Ha = 0, 120)$ and Rayleigh number of $Ra = 10^3, 10^5$ at angle of magnetic field direction $(\theta_M = 0)$. The influence of the grids on average Nusselt number of partially heated wall is studied. Figure 8.2 presents the effect of grid size on average Nusselt number values. The relative percentage deviations between G1 to G2, G2 to G3, G3 to G4, G4 to G5 are $(2.3\%, 1.4\%, 0.5\%, 0.1\%)$; $(2.6\%, 2.0\%, 0.2\%, 0.5\%)$; $(0.6\%, 0.2\%, 1.2\%, 1.3\%)$ and $(3.5\%, 0.5\%, 0.2\%, 0.9\%)$ for (Ha=0, $Ra = 10^3$), (Ha=120, $(Ra = 10^3,)$ (Ha=0, $Ra = 10^5$) and (Ha=120, $Ra = 10^5$), respectively. The small changes in the results are accredited with the 2-3 folds of the computational time. Therefore,

keeping in mind the greater accuracy (or less truncation errors) in the numerical solution procedure, grid G3 (101×101) is, however, found to be sufficiently refined to resolve the hydrodynamics of natural convection flows considered in this work. For chosen grid size of 101^2, the mach values have been estimated for range of physical parameters of problem. It is observed that Ma values are well within the permissible value of 0.3, required for incompressibility.

The analysis of the available literature suggests that none of the results are documented for the problem considered herein. However, considerable results are reported in the literature for the limiting case of the present problem, i.e., natural convection in square cavity with differentially heated vertical walls and thermally isolated top and bottom walls. The simulation for above physical domain is carried out at Hartmann number of Ha=0, which represents pure convection. To ascertain the reliability and accuracy of the present solution approach, therefore, the results obtained herein for the limiting case (Hartmann number, Ha=0) have been compared with the previous studies (de Vahl Davis, 1983; Kao et al., 2006; Kao and Yang, 2007). It can be seen from Table 8.1, the present

TABLE 8.1: Comparison of present numerical values of average Nusselt number ($\overline{Nu}$) at partially heated wall ($X = 0$) with those available in literature at Hartmann number of Ha=0, Rayleigh number of $Ra = 10^4$, and Pr=0.71.

Source	$\overline{Nu}$
Present study	2.228
de Vahl Davis (1983)	2.243
Kao et al. (2006)	2.231
Kao and Yang (2007)	2.251

simulation results show excellent agreement with previous studies (de Vahl Davis, 1983; Kao et al., 2006; Kao and Yang, 2007). The average deviation of the two (present and literature) values is seen to be about 0.7%. Such minor inherent errors tend to arise due to the enormous factors such as numerical methodologies, grid size, convergence criterion, approximations errors (round up and programming), etc .

Keeping in mind the above mentioned inadvertent factors influencing the numerical results, the above comparison ascertains the confidence in the accuracy and reliability of the present in-house TLBM solver. The results presented herein this work are, therefore, believed to be accurate and reliable within $\pm 1 - 2\%$.

Having gained the confidence in the present computational solution algorithm of TLBM solver, the ensuing section presents the new results emphasizing the influence of flow governing parameters (i.e., cooling size, Hartmann number, angle of magnetic field direction and Rayleigh number) on the detailed magneto-hydrodynamic natural convection flow phenomenon of partially-differentially heated cavity in terms of the streamline, isotherms and average Nusselt numbers.

8.4 Results and Discussions

Lattice Boltzmann simulations have been carried out over the broad ranges of conditions: (Hartmann number ($Ha = 0, 60, 120$), angle of magnetic field direction ($\theta_M = 0^o, 45^o, 90^o$), length of cooler ($L_c = 1, 1/2, 1/4, 1/6$) and Rayleigh number ($Ra = 10^3, 10^4, 10^5$) for partially heated west wall ($X = 0$). The partial heater as well as cooler is placed at middle of vertical wall. Extensive results have been obtained and presented herein for the local and global flow characteristics such as the evolution of stream functions, isotherms and average Nusselt numbers.

8.4.1 Streamline patterns

Figures 8.3 to 8.11 elucidate the effect of different cooler sizes on streamline variations for different magnetic field direction, Hartmann number and Rayleigh number. It can be observed that the streamline patterns is nearly same for all cooler sizes at Ha=0, i.e., the cooler size has insignificant effect on streamline variation at Ha=0 (pure convection case). The increase in Hartmann number causes remarkable change in flow pattern, which is

evident from streamline patterns for all considered θ_M and Ra. At Ra=10^3 and Ha=0 for all θ_M (Figure 8.3), the streamlines are pure circular with quasi-motionless region (formed due to circulation of fluid between hot and cold region of cavity) at center of cavity. The streamline structure remain nearly same for all L_c. The physical parameters considered herein have remarkable influence on the fluid flow structure, which is indicated by the size of location of the convection cell (formed due to circulation of fluid between active walls of cavity). The strength of convection increases with Rayleigh number and decreases with augmentation of Hartmann number.

Magnetic field applied in horizontal direction ($\theta_M = 0$), as shown in Figures 8.3-8.11 has capacity to slow down the fluid circulation in cavity. The increase in Ha restricts the fluid circulation in cavity, resulting in the shifting of the convection cell in the vicinity of partially heated wall. The size of the convection cell becomes elongated vertically. The decrease in the cooler size, only affects the strength of fluid circulation. It can be seen from streamlines contours, for horizontal magnetic field ($\theta_M = 0$), the cooler size (L_c) size insignificant effect on the fluid structure in the cavity.

The increase in Rayleigh number ($Ra \geq 10^4$), the fluid circulation between hot and cold parts of cavity increases, or simply convection effect increases (Figures 8.6, 8.7 and 8.8). It results in the increase in the size of convection cell. For Ra=10^4 and 10^5, the increase in Hartmann number, slightly affects the fluid flow circulation in cavity. Due to similar effect induced by both Ra and Ha, small change is observed in the convection cell of cavity. The size nearly remains same for all higher Ha (=60 and 90), only its location is slightly shifts with change in cooler size. It can be observed from Figures 8.9-8.11, i.e., at $Ra = 10^5$ and Ha=0, due to much higher fluid circulation between active walls, the fluid confines towards the hot and cold wall of cavity, with bifurcated central convection cell with the formation of eddies at the corner part of cell. The size of eddies decreases with decrease in cooler size L_c.

The change in magnetic field direction at $\theta_M = 45^o$ (Figures 8.3, 8.7 and 8.10), causes remarkable change in the fluid flow pattern and thermal characteristics of cavity due to

change in Lorentz force (Mahmoudi et al., 2014). At $\theta_M = 45^o$, the influence of magnetic field ($Ha > 0$), causes the fluid flow pattern to be circulated in diagonal shape. The applied magnetic field direction has remarkable influence on the fluid flow pattern at Ha=60 and 120. The deformation of streamlines and isotherms are found to be maximum for $\theta_M = 45^o$, which is indicated by the inclined flow pattern. The flow behavior is stretched from top left corner towards bottom right corner (diagonal shape). At lower Ha, the flow circulation is smooth and circular. The increase in Ha, ceases the flow circulation and streamline patterns become desorted. The increase in Ra ($Ra \geq 10^4$), as discussed earlier, increases flow circulation, and at $\theta_M = 45^o$, the flow circulation occupies full cavity and it is inclined for $Ha > 0$. Moreover, the cooler length has insignificant effect on streamline patterns.

Now, the application of magnetic field in vertical direction ($\theta_M = 90^o$), the flow pattern is found to be similar to $\theta_M = 45^o$, only the direction of fluid flow is opposite, i.e., from bottom left corner to the top right corner. The effect of Ha, is similar to earlier discussions.

Thus, the streamline (fluid flow pattern) has complex dependence on the physical parameters considered herein (Hartmann number, Rayleigh number, angle of magnetic field and cooler size). Such complex dependences are the result of complex thermal patterns, discussed in ensuing section.

8.4.2 Isotherm patterns

The effect of various flow governing parameters of MHD natural convection on temperature field in cavity is depicted herein in terms of isotherm patterns (Figures 8.12-8.20). At $Ra = 10^3$, the heat transfer mode is conduction dominated and the isotherm patterns are slightly parallel to vertical axis. For horizontal magnetic field direction ($\theta_M = 0^o$), the strength of isotherms enhances with increase in Rayleigh number (due to increase in buoyancy effect) for all Hartmann number values studied herein. As discussed before, increase in Ha, reduces the flow circulation in the cavity, which is also evident from isotherms patterns. Increase in Ha, the isotherms become more crowded towards the

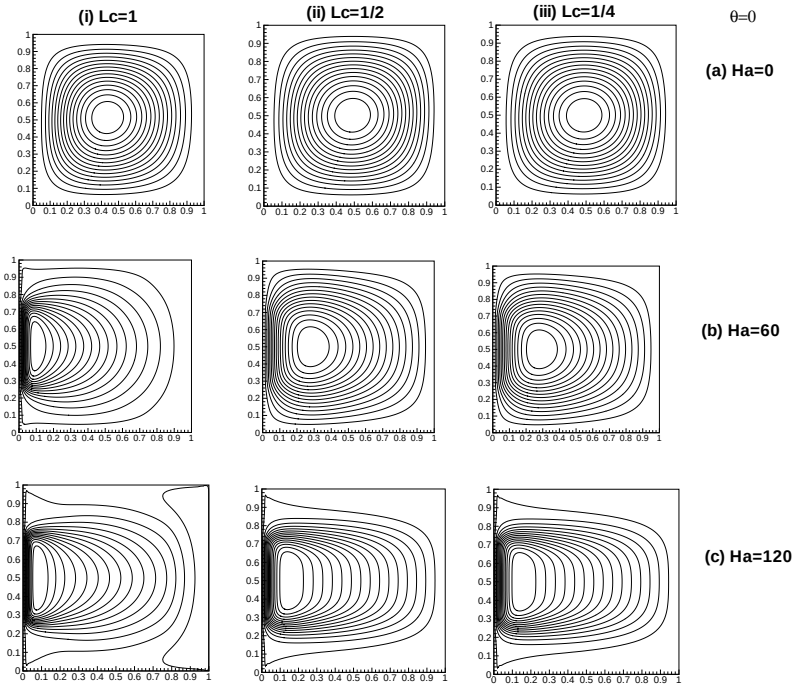

FIGURE 8.3: Influence of Hartmann number ($Ha = 0, 60, 120$) and cooler size ($L_c = 1, 1/2, 1/4$) on streamline patterns at $Ra = 10^3$ and magnetic field direction of $\theta_M = 0^o$.

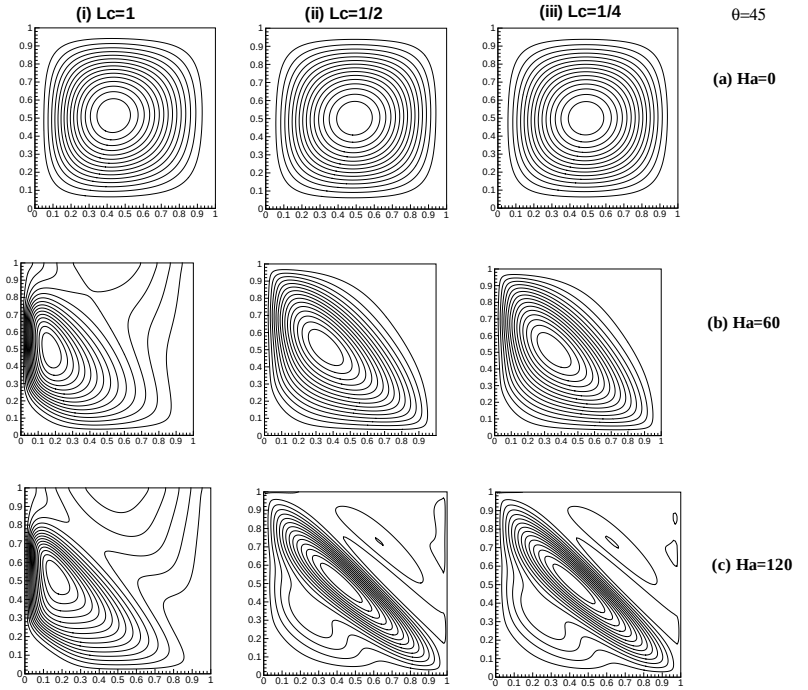

FIGURE 8.4: Influence of Hartmann number ($Ha = 0, 60, 120$) and cooler size ($L_c = 1, 1/2, 1/4$) on streamline patterns at $Ra = 10^3$ and magnetic field direction of $\theta_M = 45^o$.

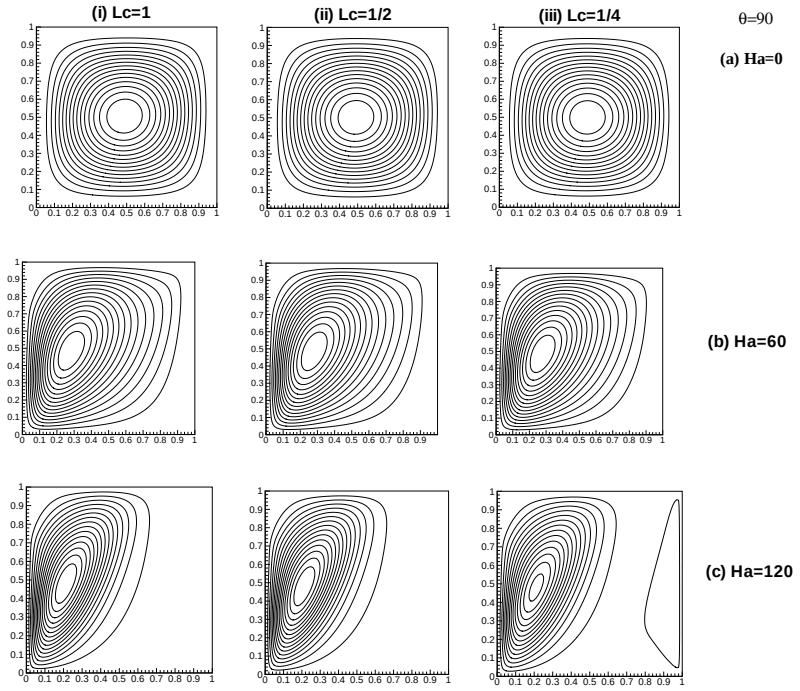

FIGURE 8.5: Influence of Hartmann number ($Ha = 0, 60, 120$) and cooler size ($L_c = 1, 1/2, 1/4$) on streamline patterns at $Ra = 10^3$ and magnetic field direction of $\theta_M = 90^o$.

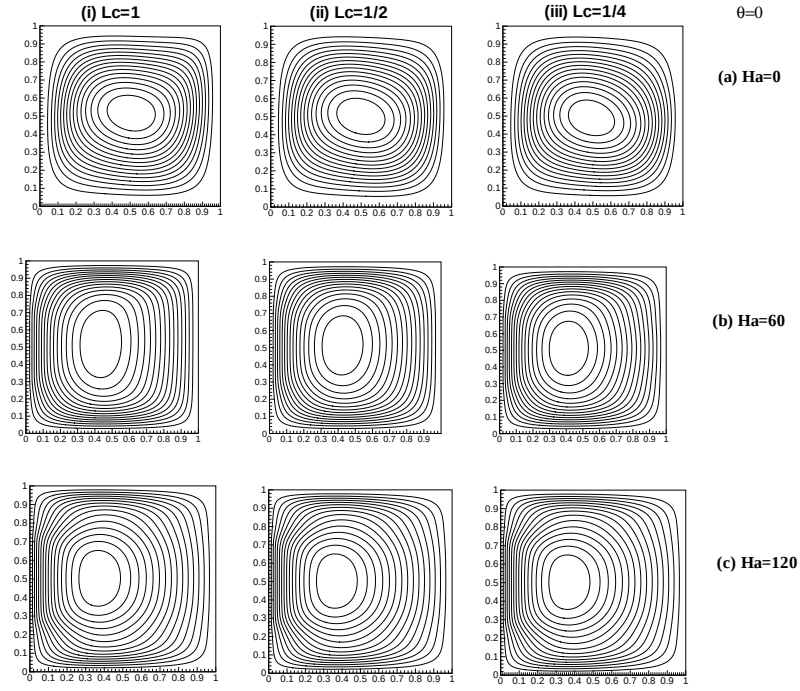

FIGURE 8.6: Influence of Hartmann number ($Ha = 0, 60, 120$) and cooler size ($L_c = 1, 1/2, 1/4$) on streamline patterns at $Ra = 10^4$ and magnetic field direction of $\theta_M = 0^o$.

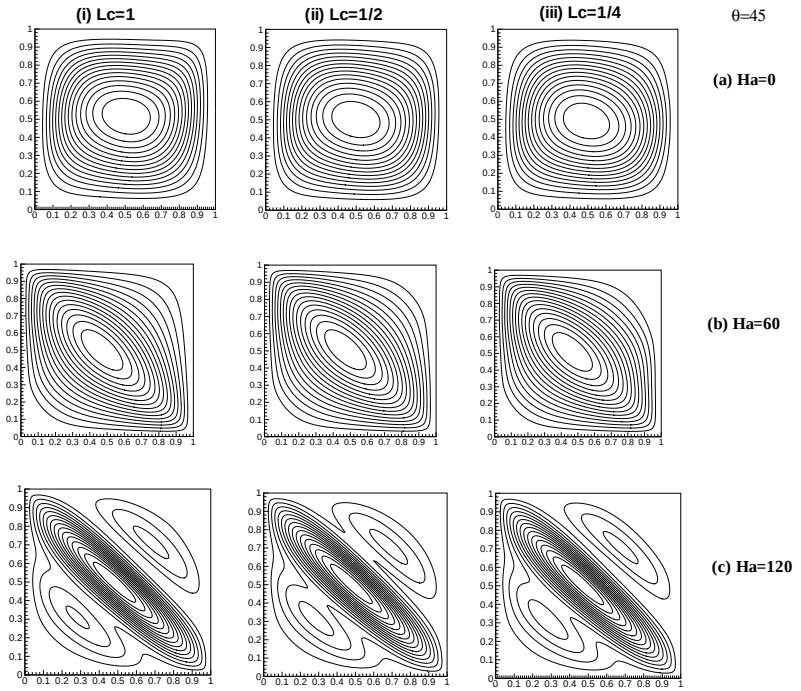

FIGURE 8.7: Influence of Hartmann number ($Ha = 0, 60, 120$) and cooler size ($L_c = 1, 1/2, 1/4$) on streamline patterns at $Ra = 10^4$ and magnetic field direction of $\theta_M = 45^o$.

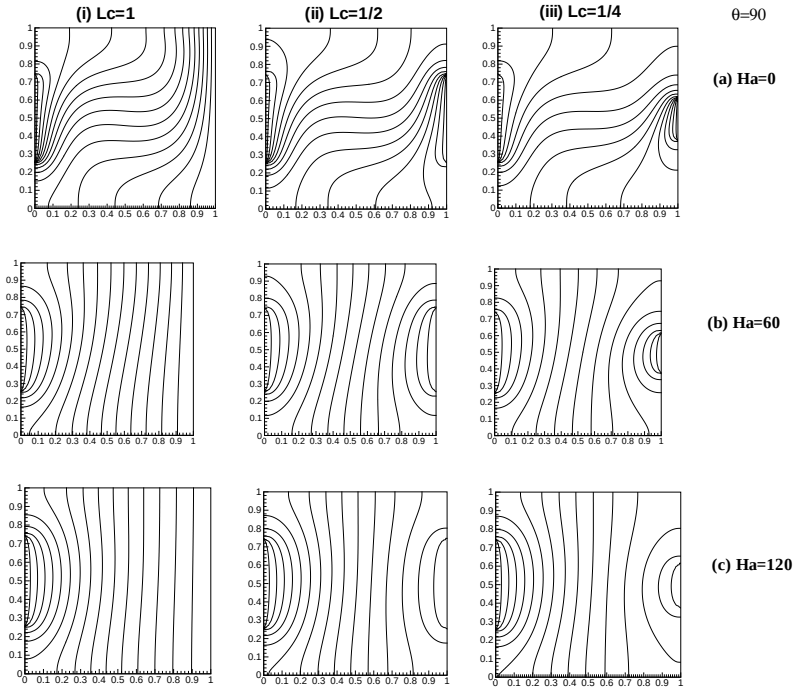

FIGURE 8.8: Influence of Hartmann number ($Ha = 0, 60, 120$) and cooler size ($L_c = 1, 1/2, 1/4$) on streamline patterns at $Ra = 10^4$ and magnetic field direction of $\theta_M = 90^o$.

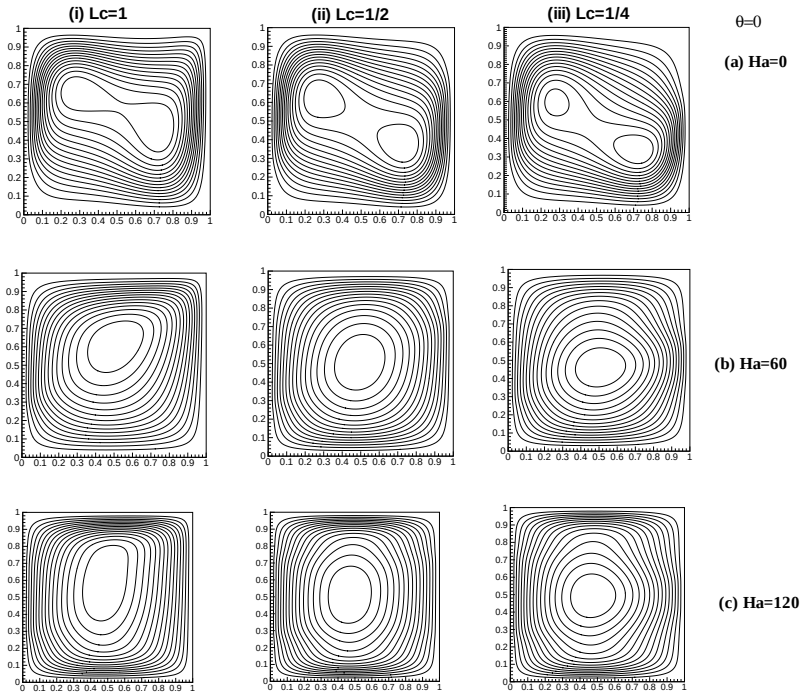

FIGURE 8.9: Influence of Hartmann number ($Ha = 0, 60, 120$) and cooler size ($L_c = 1, 1/2, 1/4$) on streamline patterns at $Ra = 10^5$ and magnetic field direction of $\theta_M = 0^o$.

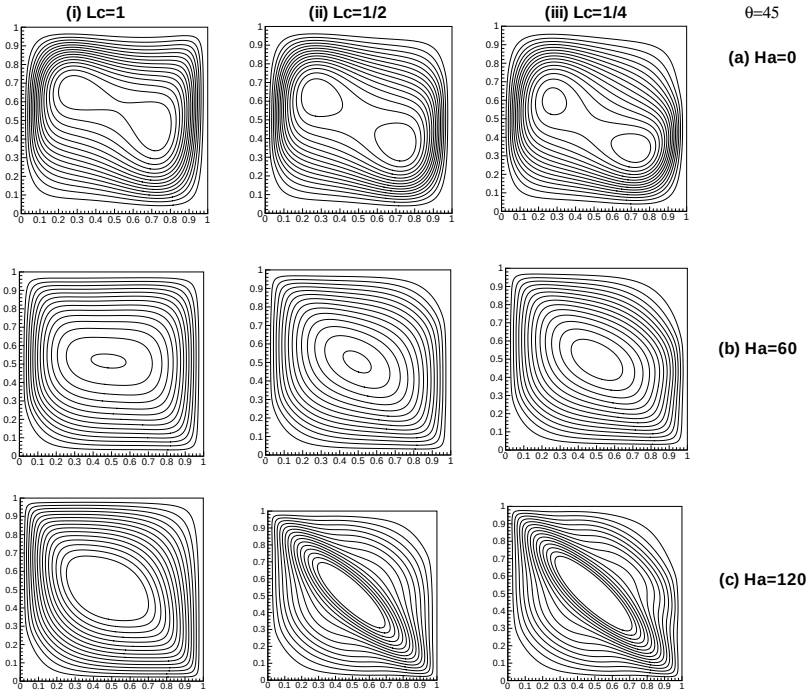

FIGURE 8.10: Influence of Hartmann number ($Ha = 0, 60, 120$) and cooler size ($L_c = 1, 1/2, 1/4$) on streamline patterns at $Ra = 10^5$ and magnetic field direction of $\theta_M = 45^o$.

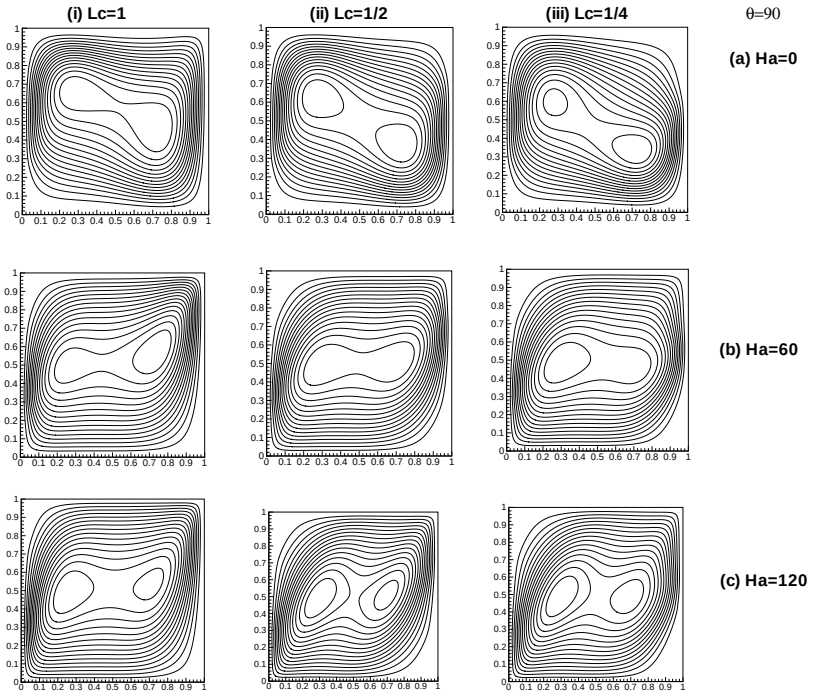

FIGURE 8.11: Influence of Hartmann number ($Ha = 0, 60, 120$) and cooler size ($L_c = 1, 1/2, 1/4$) on streamline patterns at $Ra = 10^5$ and magnetic field direction of $\theta_M = 90^o$.

heated part of cavity with almost half region of cavity is filled with low (zero temperature fluid).

For $Ha > 0$ (Figures 8.12-8.20), the size of cooler length, causes influence on buoyancy force. Decreasing cooler length from $L_c = 1$ to $1/2$ and $1/4$, helps to clear the dense crowding and isotherms pattern spread horizontally. The dense crowding means higher temperature gradient, thus yielding higher heat transfer. Thus, decrease in cooler length, decreases rate of heat transfer (decrease in Nu). For a constant Rayleigh number (Ra), the change of magnetic field direction, from horizontally to vertically, increases the isotherm spreading in the cavity. It causes, the flow pattern in diagonal shape (as discussed in previous section). Similar effect is observed of cooler length (L_c) on isotherm pattern as for $\theta_M = 0^o$.

The increase in Rayleigh number (heat intensity), as known increases the buoyancy force and flow circulation in the cavity. As expected, the isotherms becomes crowded all over cavity region with augmentation in Ra, signifying higher heat transfer rates. Moreover,

the presented isotherm patterns are in accordance with the streamline structure for given range of parameters. The heat transfer characteristics of cavity is depicted in terms of average Nusselt number ($\overline{Nu}$) estimated at the isothermal wall ($X = 0$) at cavity. This is presented in next section.

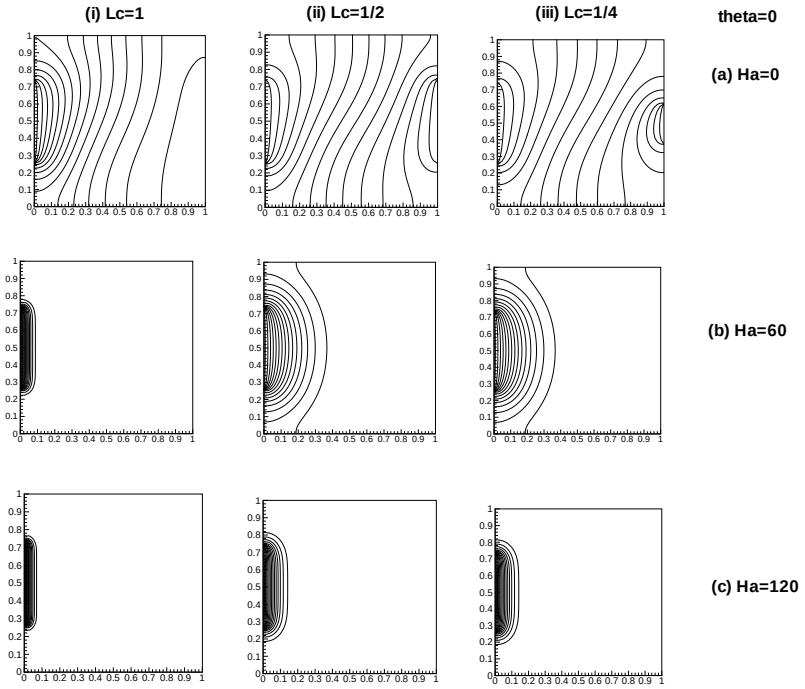

FIGURE 8.12: Influence of Hartmann number ($Ha = 0, 60, 120$) and cooler size ($L_c = 1, 1/2, 1/4$) on isotherm patterns at $Ra = 10^3$ and magnetic field direction of $\theta_M = 0^o$.

8.4.3 Heat transfer characteristics

In this section, the heat transfer characteristics of cavity is elucidated in terms of the average Nusselt number ($\overline{Nu}$). Figure 8.21 presents the ($\overline{Nu}$) variation for different Rayleigh number ($10^3 \leq Ra \leq 10^5$), Hartmann number ($Ha = 0, 60, 120$), angle of magnetic field direction ($\theta_M = 0^o, 45^o, 90^o$) and cooler size ($L_c = 1, 1/2, 1/4$).

The average Nusselt number is plotted as a function of cooler size (L_c) for Hartmann and Rayleigh number for different θ_M as shown in Figure 8.21. It can be seen that, $\overline{Nu}$ value increases with Rayleigh number and decreases with augmentation of Hartmann number, which is clear from previous discussions. The influence of cooler size is maximum for Ra=

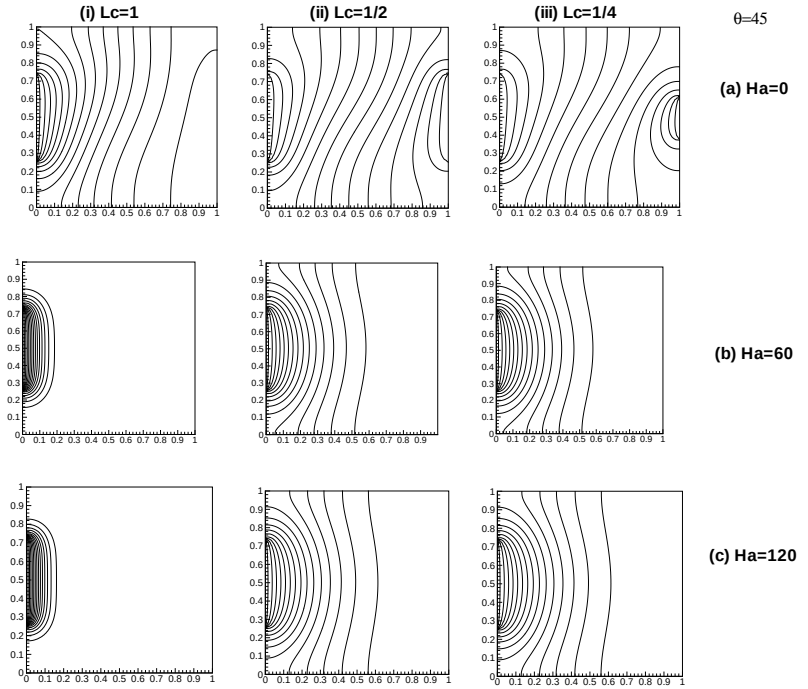

FIGURE 8.13: Influence of Hartmann number ($Ha = 0, 60, 120$) and cooler size ($L_c = 1, 1/2, 1/4$) on isotherm patterns at $Ra = 10^3$ and magnetic field direction of $\theta_M = 45^o$.

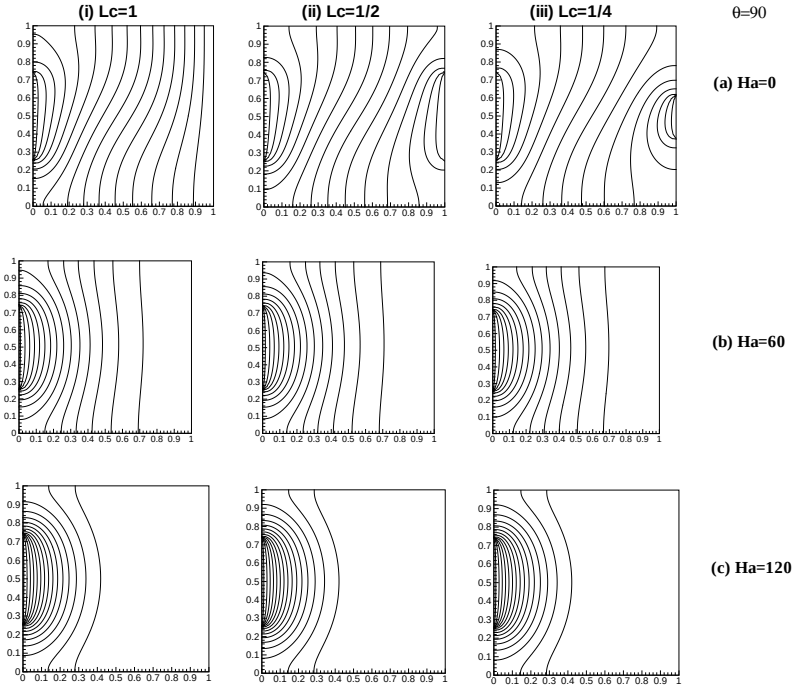

FIGURE 8.14: Influence of Hartmann number ($Ha = 0, 60, 120$) and cooler size ($L_c = 1, 1/2, 1/4$) on isotherm patterns at $Ra = 10^3$ and magnetic field direction of $\theta_M = 90^o$.

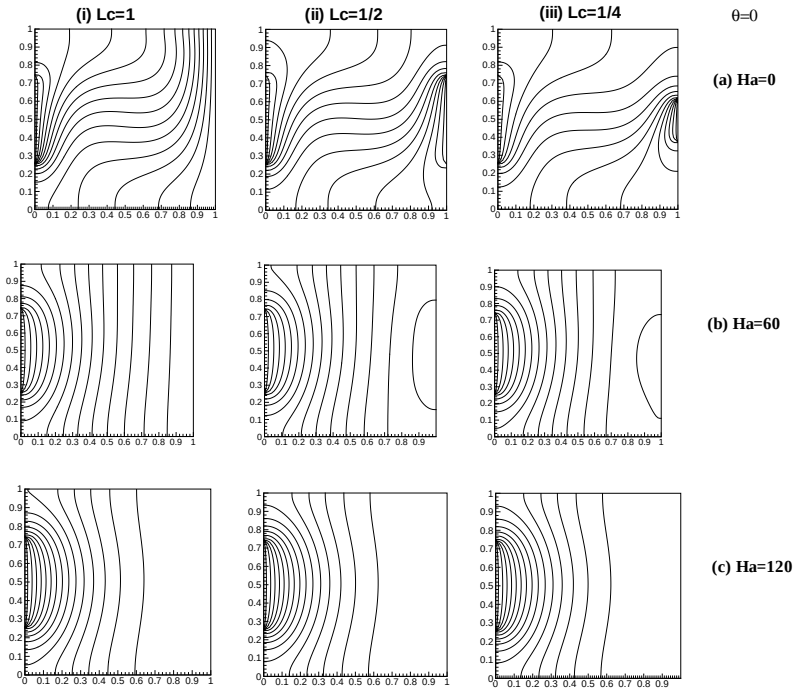

FIGURE 8.15: Influence of Hartmann number ($Ha = 0, 60, 120$) and cooler size ($L_c = 1, 1/2, 1/4$) on isotherm patterns at $Ra = 10^4$ and magnetic field direction of $\theta_M = 0^o$.

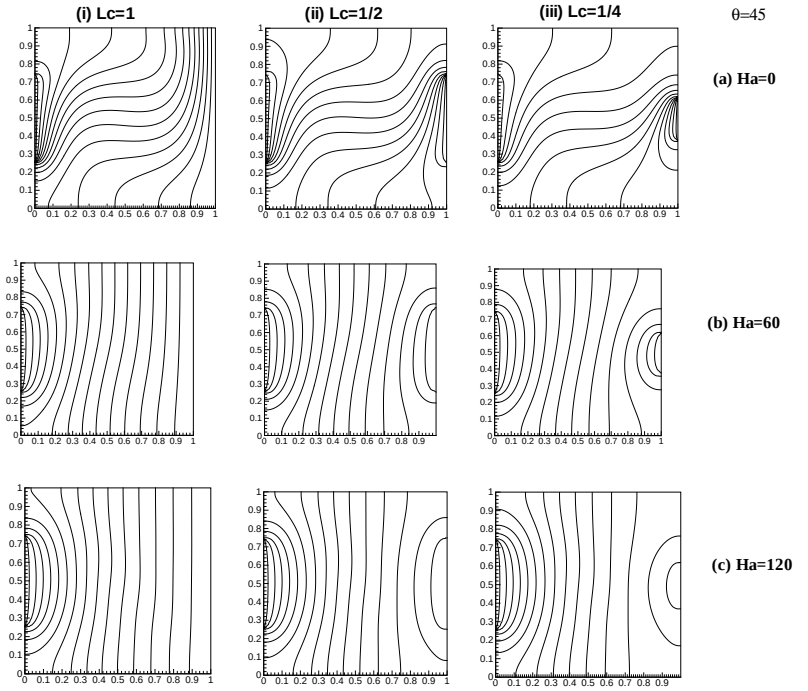

FIGURE 8.16: Influence of Hartmann number ($Ha = 0, 60, 120$) and cooler size ($L_c = 1, 1/2, 1/4$) on isotherm patterns at $Ra = 10^4$ and magnetic field direction of $\theta_M = 45^o$.

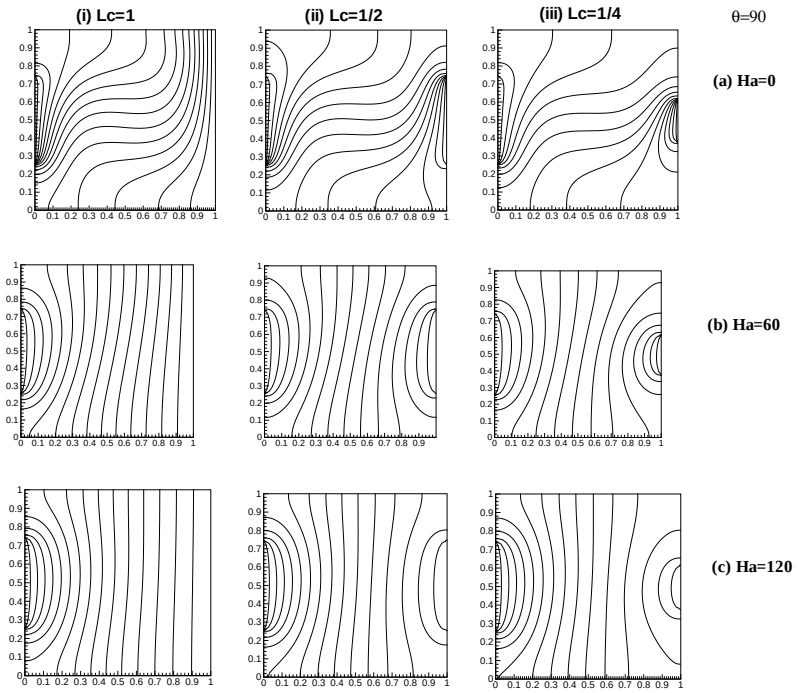

FIGURE 8.17: Influence of Hartmann number ($Ha = 0, 60, 120$) and cooler size ($L_c = 1, 1/2, 1/4$) on isotherm patterns at $Ra = 10^4$ and magnetic field direction of $\theta_M = 90^o$.

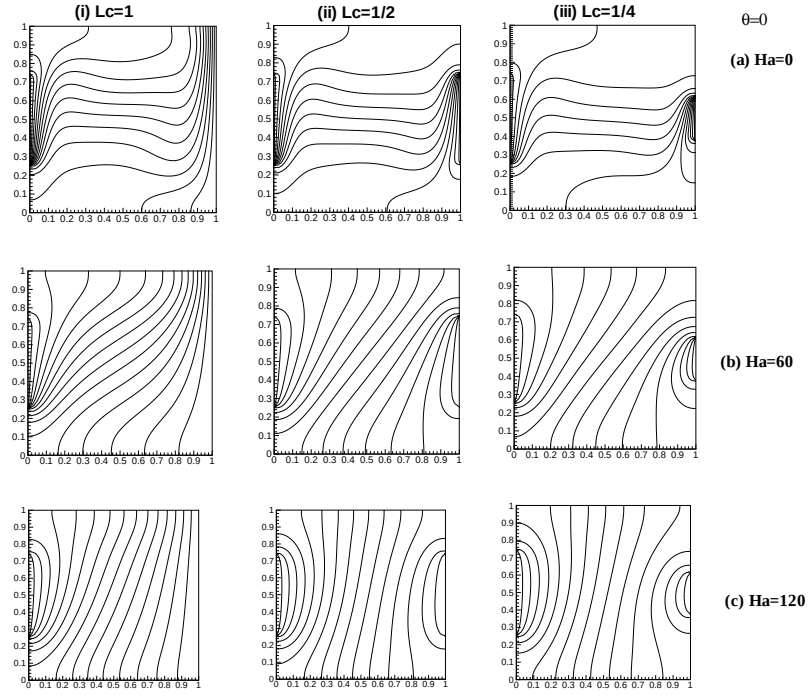

FIGURE 8.18: Influence of Hartmann number ($Ha = 0, 60, 120$) and cooler size ($L_c = 1, 1/2, 1/4$) on isotherm patterns at $Ra = 10^5$ and magnetic field direction of $\theta_M = 0^o$.

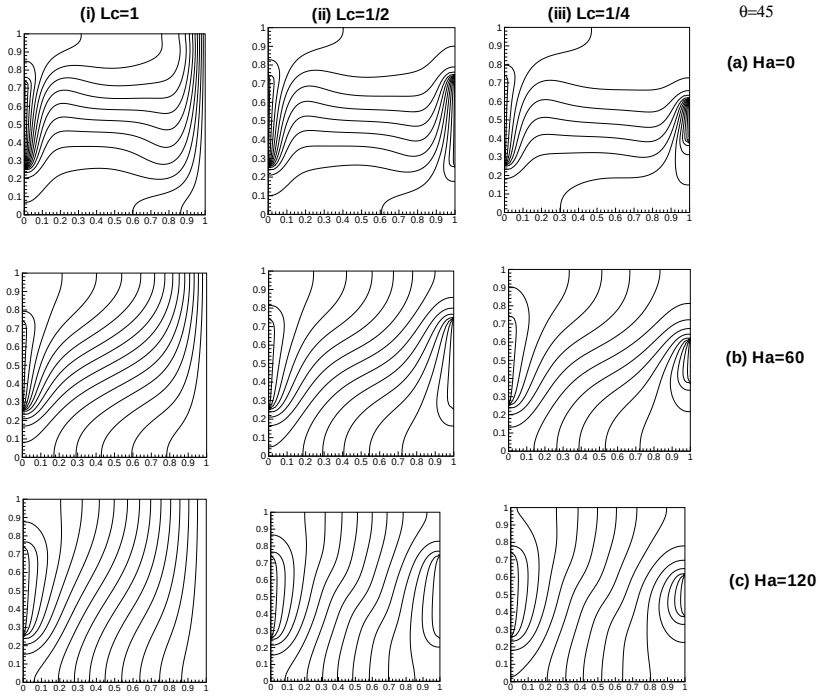

FIGURE 8.19: Influence of Hartmann number ($Ha = 0, 60, 120$) and cooler size ($L_c = 1, 1/2, 1/4$) on isotherm patterns at $Ra = 10^5$ and magnetic field direction of $\theta_M = 45^o$.

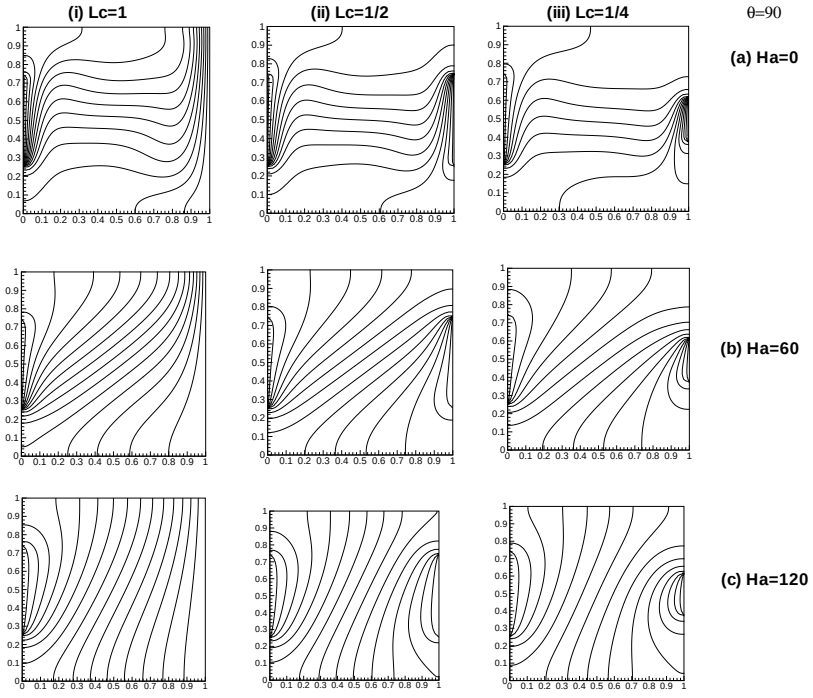

FIGURE 8.20: Influence of Hartmann number ($Ha = 0, 60, 120$) and cooler size ($L_c = 1, 1/2, 1/4$) on isotherm patterns at $Ra = 10^5$ and magnetic field direction of $\theta_M = 90^o$.

10^5. For all cases considered herein, at Ha=0, $\overline{Nu}$ values are highest followed by Ha=60 and Ha=120.The magnetic field direction slightly affects $\overline{Nu}$ only for $Ha > 0$ (except pure convection). Thus, the average Nusselt number is strongly influenced by Rayleigh number, Hartmann number and cooler size. The θ_M has insignificant influence on average Nusselt number value. In general, average Nusselt number has complex dependence on physical flow governing parameters covered in this study.

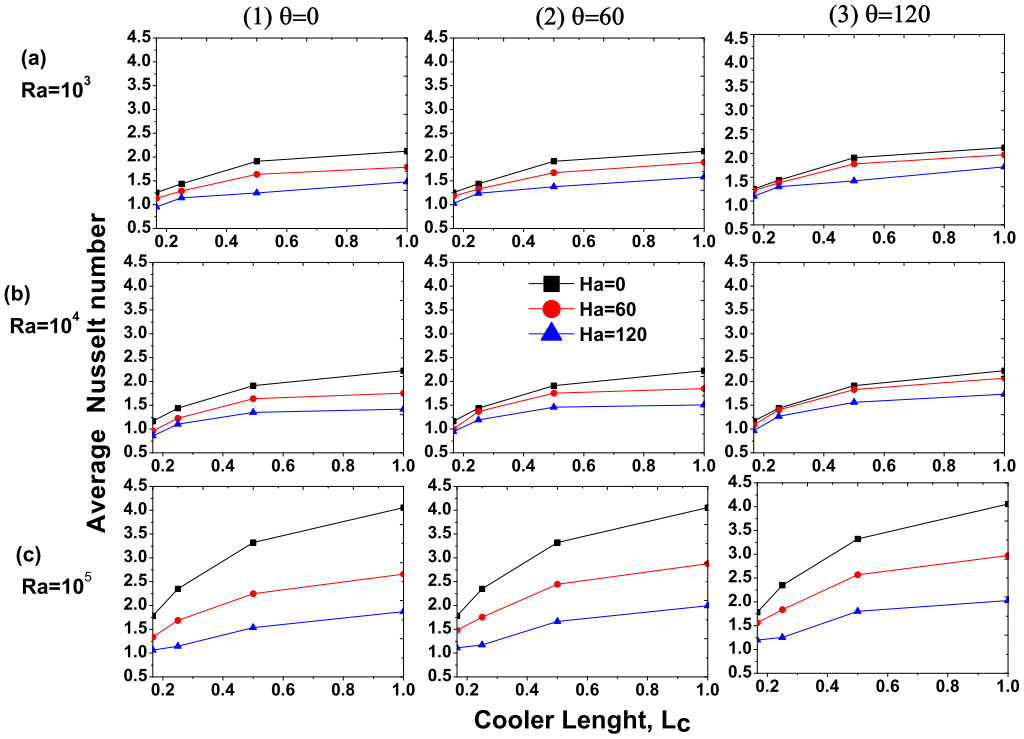

FIGURE 8.21: The average Nusselt number ($\overline{Nu}$) estimated for different Hartmann number ($Ha = 0, 60, 120$), angle of magnetic field direction ($\theta_M = 0^o, 45^o, 90^o$), cooler length ($L_c = 1, 1/2, 1/4, 1/6$) and Rayleigh number $Ra = 10^3, 10^4, 10^5$.

8.4.4 Empirical Correlation

Present simulation results have been summarized by functional dependence of average Nusselt number ($\overline{Nu}$) on lenght of cooler (L_c) and Hartmann number for given Rayleigh number (Ra) and angle of magnetic field direction (θ_M) within range considered herein

$(10^3 \leq Ra \leq 10^5; 0 \leq Ha \leq 120; 1/6 \leq L_c \leq 1; 0^o \leq \theta_M \leq 90^o)$, i.e.,

$$\overline{Nu} = f(L_c, Ra.Ha, \theta_M) \tag{8.15}$$

Table 8.2 presents the Nusselt number correlations developed for range of Rayleigh number and angle of magnetic field direction with corresponding coefficient of determination R^2 values. Then the correlation coefficients (a,b,C,...,etc) of Nusselt number correlation listed in Table 8.2 are presented in Table 8.3. Figure 8.22 show the comparison between the

TABLE 8.2: Nussult number correlations developed ($\overline{Nu} = f(L_c, Ha)$) for given Rayleigh number (Ra) and angle of magnetic field (θ_M).

Ra	θ_M	$\overline{Nu}$	R^2
10^3	0^o	$aL_c^b c\mathrm{Ha}$	0.97
	45^o	$a + \frac{b}{L_c} + \frac{C}{L_c^2} + \frac{d}{L_c^3} + e\mathrm{Ha} + f\mathrm{Ha}^2$	0.91
	90^o	$a + \frac{b}{L_c} + C\mathrm{Ha} + \frac{d}{L_c^2} + e\mathrm{Ha}^2 + f\frac{L_c}{\mathrm{Ha}} + \frac{g}{L_c^3} + h\mathrm{Ha}^3 + i\frac{\mathrm{Ha}^2}{L_c} + j\frac{\mathrm{Ha}}{L_c^3}$	0.95
10^4	0^o	$a + b\ln L_c + c\mathrm{Ha} + d\ln L_c^2 + e\mathrm{Ha}^2 + f\ln L_c\mathrm{Ha}$	0.99
	45^o	$a + b\ln L_c + c\mathrm{Ha} + d\ln L_c^2 + e\mathrm{Ha}^2 + f\ln L_c\mathrm{Ha}$	0.99
	90^o	$a + \frac{b}{L_c} + C\mathrm{Ha} + \frac{d}{L_c^2} + e\mathrm{Ha}^2 + f\frac{L_c}{\mathrm{Ha}}$	0.98
10^5	0^o	$a + \frac{b}{L_c} + C\mathrm{Ha} + \frac{d}{L_c^2} + e\mathrm{Ha}^2 + f\frac{L_c}{\mathrm{Ha}}$	0.99
	45^o	$a + \frac{b}{L_c} + C\mathrm{Ha} + \frac{d}{L_c^2} + e\mathrm{Ha}^2 + f\frac{L_c}{\mathrm{Ha}}$	0.99
	90^o	$a + \frac{b}{L_c} + C\mathrm{Ha} + \frac{d}{L_c^2} + e\mathrm{Ha}^2 + f\frac{L_c}{\mathrm{Ha}}$	0.96

numerical and predicted (Table 8.2) values of the average Nusselt number. It is observed that the proposed predictive closure correlations (Table 8.2) predicts the average Nusselt number ($\overline{Nu}$) values within acceptable level of deviations from the computed values.

8.5 Concluding Remarks

In this study, lattice Boltzmann simulations have been carried out to investigate the influence of cooler size ($L_c = 1, 1/2, 1/4$) on magneto-hydrodynamic (MHD) natural convective heat transfer characteristics in partially-differentially heated square cavity. The west wall (X=0) is partially heated with heater size ($L_h = 1/2$) and east wall is partially cooled with four cooler lengths of $L_c = 1, 1/2, 1/4$. Other parts of cavity are maintained at

TABLE 8.3: Correlation coefficients of Nusselt number correlation presented in Table 8.2.

θ_M	a	b	C	d	e	f
			$Ra = 10^3$			
0^o	2.14	4.66	0.997	-	-	-
45^o	2.03	0.30	-0.233	2.8×10^{-2}	-1.8×10^{-4}	-4.2×10^{-5}
90^o	1.63	0.644	3.1×10^{9}	-0.278	7.7×10^{8}	-6.5×10^{-3}
			$Ra = 10^4$			
0^o	2.2	0.29	-7.8×10^{-3}	-0.7×10^{-2}	-1.1×10^{-5}	-2.4×10^{-3}
45^o	2.2	0.29	-7.8×10^{-3}	-0.21	-3.5×10^{-7}	-2.4×10^{-3}
90^o	2.5	-0.28	-2.7×10^{-3}	-7.9×10^{-3}	-4.3×10^{-5}	-1.2×10^{-3}
			$Ra = 10^5$			
0^o	4.7	-0.74	-2.5×10^{-2}	4.4×10^{-2}	4.4×10^{-5}	-2.4×10^{-3}
45^o	4.9	-0.90	-2.3×10^{-2}	6.5×10^{-2}	3.5×10^{-5}	2.4×10^{-3}
90^o	5.3	-1.3	-3.3×10^{-2}	0.11	8.9×10^{5}	-3.4×10^{-3}

For $\theta = 90^0$ and $Ra = 10^3$: $g = 2.6 \times 10^{-2}$, $h = 4.2 \times 10^{6}$ $i = -4.6 \times 10^{-6}$ and $j = 1.0 \times 10^{-3}$

adiabatic condition. In particular, the effects of Rayleigh number ($Ra = 10^3, 10^4, 10^5$), Hartmann number ($Ha = 0, 60, 120$), angle of magnetic field ($\theta_M = 0^o, 45^o, 90^o$) on streamlines, isotherms and average Nusselt number have been studied and reported in this work. From this study, following conclusions can be drawn:

1. Fluid circulation in cavity creates formation of convection cell in central region of cavity. The size of convection cell varies proportionally with Rayleigh number, while it decreases with augmentation of Hartmann number. At $Ra = 10^5$, convection cell elongates and bifurcates with the formation of two eddies at the corner of cell. The size of these eddies reduces with decrease in cooler length.

2. Increase in Ha controls the flow circulation in cavity.

3. The decrease in cooler size, reduce buoyancy effect, thereby, fluid circulation.

4. The change in the magnetic field direction from horizontal to vertical, slightly increases the flow circulation in cavity for Ha=60, 120.

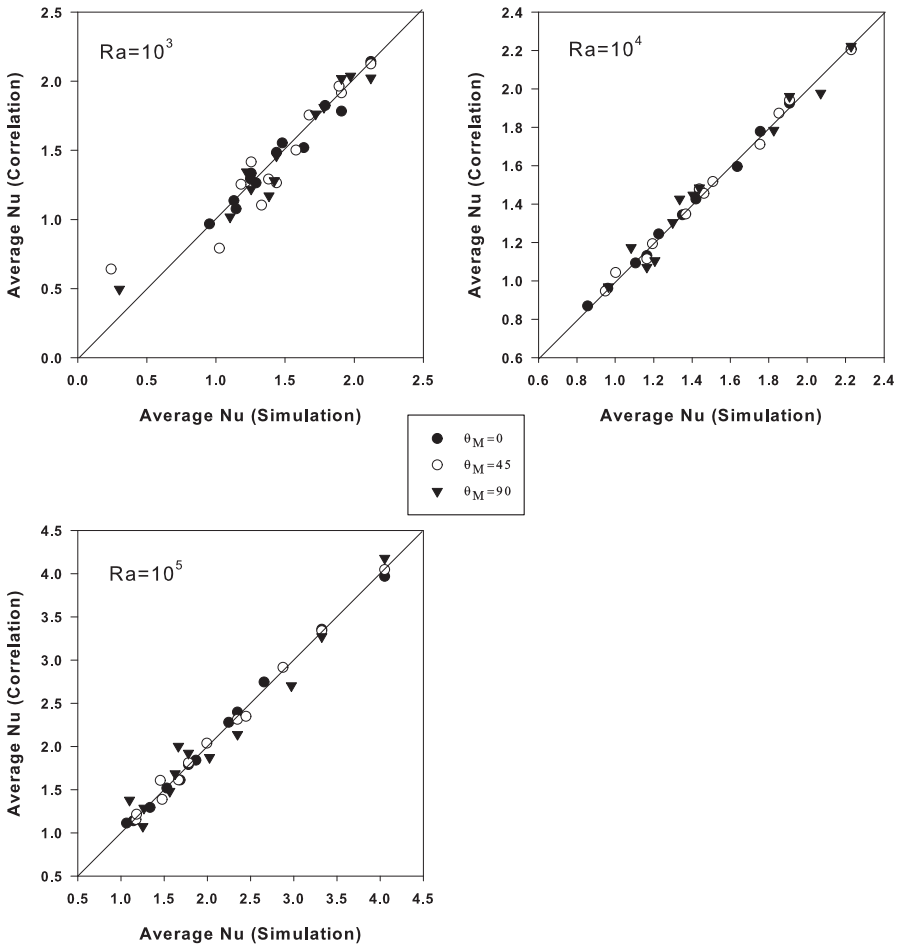

FIGURE 8.22: Comparison between present numerical and predicted (Table 8.2, Table 8.3).

5. The decrease in cooler lenght from $L_c = 1$ to $1/2$ and $1/4$, helps to clear the dense crowding and isotherms pattern spread horizontally in cavity.

6. The average Nusselt number increases with Rayleigh number and decreases with Hartmann number.

7. Nusselt number correlations for different Rayleigh number (Ra) and angle of magnetic field direction have been proposed showing functional dependence of average Nusselt number with length of cooler size (L_c) and Hartmann number Ha.

Chapter 9

NATURAL CONVECTION IN PARTIALLY HEATED OPEN ENDED CAVITY

In this chapter, the natural convection heat transfer in an open ended (east wall) enclosure subjected to the partial heating (of the west wall) is investigated numerically by using the passive scalar thermal lattice Boltzmann method (PS-TLBM) with $D2Q9$ lattice model. In particular, the following objectives have been explored herein:

1. The influences of heater size (L_h), heating location (bottom, middle and top) and heat intensity, i.e., Rayleigh number (Ra) in the laminar range, on the thermal and hydrodynamic features are elucidated for a fixed value of the Prandtl number ($Pr = 0.71$).

2. The influence of Prandtl number ($0.71 \leq Pr \leq 7$) and Rayleigh number ($10^4 \leq Ra \leq 10^6$) on heat transfer rate of partially heated open ended cavity with fixed heater size ($L_h = H/2$) and heating location (middle) on rate of heat transfer.

9.1 Problem description

Consider the two-dimensional, steady, laminar, natural convection in an incompressible Newtonian fluid in the open ended cavity of length L and height H ($AR = L/H = 1$ for square cavity), as shown in Figure 9.1. The open ended cavity is, however, physically represented by the east wall ($x = L$) open to the ambient (temperature T_c). The bottom ($y = 0$) and top ($y = H$) walls of cavity are thermally insulated. The west wall ($x = 0$) is partially heated (heater size, $l_h < H$) isothermally (temperature T_h) at either of the three different locations, viz., (i) top heating, (ii) middle heating and (iii) bottom heating, respectively. The length of partial heated section (l_h) of the west wall ($x = 0$) is varied in the range as $0.25H \leq l_h \leq 0.75H$. The governing equations (in dimensional and dimensionless forms) along with general simplifications are expressed in Chapter 3. The

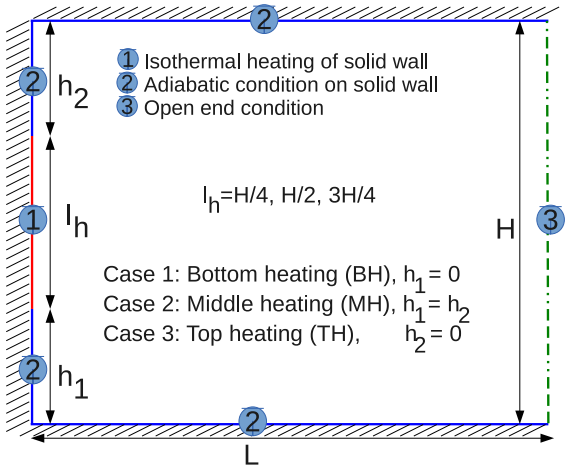

FIGURE 9.1: Schematic representation of the computational domain (i.e., open ended cavity) and boundary conditions.

boundary conditions in non-dimensional form are expressed as follow:

- At the west ($X = 0$) wall,

$$\begin{aligned} &U_x = 0, \quad U_y = 0 \quad \text{for} \quad 0 \leq Y \leq 1 \\ &\theta = \theta_h = 1 \quad \text{for} \quad h_1 \leq Y \leq h_2 \\ &\frac{\partial \theta}{\partial X} = 0 \quad \text{for} \quad h_1^*(\neq 0) \geq Y \geq 0 \quad \text{and} \quad h_2(\neq 1) \leq Y \leq 1 \end{aligned} \tag{9.1}$$

where, h_1 and $h_2 = (h_1 + L_h)$ are dimensionless lengths given as follow for the different cases of heating arrangements. The L_h $(= l_h/H)$ being the dimensionless length of the heating section.

1. In the case of *top heating* (case -I), $h_1 = (1 - L_h)$ and $h_2 = 1$
2. In case of *middle heating* (case -II), $h_1 = (1 - L_h)/2$ and $h_2 = (1 + L_h)/2$
3. In the case of *bottom heating* (case -III), $h_1 = 0$ and $h_2 = L_h$

- At the east $(X = 1)$ wall,

$$\frac{\partial U_x}{\partial X} = 0, \qquad \frac{\partial U_y}{\partial X} = 0 \quad \text{and} \quad \begin{array}{ll} \theta = \theta_c = 0 & \text{for} \quad U_x < 0 \\ \dfrac{\partial \theta}{\partial X} = 0 & \text{for} \quad U_x > 0 \end{array} \tag{9.2}$$

- At the bottom $(Y = 0)$ and top $(Y = 1)$ walls,

$$U_x = 0, \qquad U_y = 0 \qquad \text{and} \qquad \frac{\partial \theta}{\partial Y} = 0 \tag{9.3}$$

9.2 Results and discussions

Computational simulations have been carried out over the broad ranges of conditions $(0.25 \leq L_h \leq 0.75,\ 10^3 \leq Ra \leq 10^6,\ Pr = 0.71)$ for three different heating locations. In particular, extensive results have been obtained and presented herein for the local and global flow characteristics such as the evolution of stream functions and isotherms, variation of velocity and temperature along the horizontal and vertical center lines, and local and average Nusselt numbers. Prior to the presentation of the new results obtained herein this work, however, a systematic analysis of grid independence test, quantification of incompressibility limits and validation of results have been presented in the ensuing section to ascertain the accuracy and efficacy of the in-house PS-TLBM numerical solution procedure. The problem has been divided into two parts.

1. Influence of heater size and location on natural convective heat transfer rate in partially heated open ended cavity.

2. Influence of Prandtl number on on natural convective heat transfer rate in partially heated (middle heating) open ended cavity.

9.2.1 Grid independence test

The reliability and accuracy of the numerical solution procedure is naturally dependent upon a judicious choice of optimal parameters such as sizes of the computational domain and computational grid. In this work, the size of computational domain is itself defined by the problem, therefore, a thorough grid independence study has been carried out using four uniform lattices/grids, i.e., G_1 (61×61); G_2 (81×81); G_3 (101×101) and G_4 (121×121), for three different values of the heater size ($L_h = 0.25$, 0.5 and 0.75) at the Rayleigh number of $Ra = 10^4$. Each heater is individually placed at the mid-section (i.e., middle heating) of the west wall ($x = 0$). The adequacy of grid size is examined by comparing the values of the average Nusselt number ($\overline{Nu}$) at the partially heated west wall ($x = 0$) in Table 9.1.

TABLE 9.1: Grid independence test for three values of heater size ($0.25 \leq L_h \leq 0.75$) by using four different grids (G_1 to G_4) of uniform square lattice size ($N_x \times N_y$) at Rayleigh number ($Ra = 10^4$) and middle heating case. The N_x and N_y represents the number of lattice nodes in $x-$ and $y-$ directions, respectively.

		average Nusselt number ($\overline{Nu}$) at the west wall		
Grid details		$L_h = 0.25$	$L_h = 0.50$	$L_h = 0.75$
G_1	(61×61)	3.319	3.942	4.280
G_2	(81×81)	3.282	3.934	4.226
G_3	(101×101)	3.299	3.947	4.236
G_4	(121×121)	3.283	3.959	4.258

It is observed that the relative changes in the average Nusselt number ($\overline{Nu}$) values with the change in lattice size from coarsest (G_1) to the finest (G_4) are 1.39%, 0.44% and 0.53% for the heater size (L_h) of 0.25, 0.5 and 0.75, respectively. Also, the relative changes in

the average Nusselt number ($\overline{Nu}$) values with the changes in the lattice size ($G_1 \rightarrow G_2$, $G_2 \rightarrow G_3$ and $G_3 \rightarrow G_4$) are seen to be (1.13%, 0.19%, and 1.28%), (0.50%, 0.33%, and 0.25%) and (0.76%, 0.30%, and 0.52%) for the heater size (L_h) of 0.25, 0.5 and 0.75, respectively. The above analysis of Table 9.1 shows insignificant change in the average Nusselt number ($\overline{Nu}$) values on the further refinement of lattice grid size G_3, however, with the immense increase in CPU time to obtain the converged solution. Thus, the lattice grid size G_3 (101×101) is believed to be sufficiently refined enough to resolve the thermal and hydrodynamic features with an acceptable level of accuracy over the range of conditions considered herein. The results presented hereafter are based on the lattice grid size G_3 (101×101).

9.2.1.1 Quantification and validation of incompressibility limits

The quantification of incompressibility limits is one of the necessity of the lattice Boltzmann method (LBM) solver a-prior to its utilization in the flow and thermal computations. Generally, the limits of compressibility/incompressibility are quantified in terms of the Mach number (Ma), defined (He et al., 2011) as

$$Ma = \frac{V}{c_s} \qquad \text{where} \qquad c_s = \frac{c}{\sqrt{3}}$$

In order to keep the flow in the incompressible region, LBM solvers must have the restriction of lower Mach number (Ma). The available literature (Dellar, 2003) suggests that the Mach number value should be within permissible limit (i.e., $Ma \leq 0.3$) to maintain the condition of incompressible flow in the LBM solvers. Table 9.2 shows the values of characteristic velocity (V, Eq. 3.18) and corresponding Mach number (Ma). Over the range of Rayleigh number (Ra) considered herein, it can be observed that estimated values of the Mach number (Ma) are much less than the permissible limit (i.e., $Ma < 0.3$ as incompressible limit). Therefore, present PS-TLBM numerical methodology and computational

algorithm is working well within the incompressible range. Hence, the present methodology is further confidently used to obtain the new results over the ranges of conditions considered herein.

TABLE 9.2: The numerical values of characteristic velocity (V) and Mach number (Ma) over the considered range of the Rayleigh number (Ra).

Ra	V	Ma
10^4	0.03	0.05
10^5	0.10	0.17
10^6	0.17	0.29

9.2.1.2 Validation of results

The review of the available literature suggests that none of the results are documented in the literature for the problem considered herein. Therefore, the reliability and accuracy of the present numerical solution procedure is ascertained by obtaining and comparing the results for the limiting case of the present problem, i.e., natural convection in open ended square cavity of which west wall ($x = 0$) is completely ($L_h = 1$) heated isothermally while the east wall is open to ambient. Table 9.3 compares the present values of the average Nusselt number ($\overline{Nu}$) at the west wall ($x = 0$) with the available literature results (Mohamad, 1995; Mohamad et al., 2009; Bilgen and Oztop, 2005; Sajjadi et al., 2010; Kefayati, 2013a; Chan and Tien, 1985) over the wide range of Rayleigh number ($10^3 \leq Ra \leq 10^6$). It can be observed from Table 9.3 that the maximum error in between the present and literature values of the average Nusselt number ($\overline{Nu}$) is 3.4% whereas all others values are confined within the range of $\pm 1 - 3\%$. Such minor inherent errors tend to arise due to the enormous factors such as numerical methodologies, grid size, convergence criterion, approximations errors (round up and programming), etc (Srinivas et al., 2009; Bharti et al., 2006; Sivakumar et al., 2006; Tian et al., 2014). Keeping in mind the above mentioned inadvertent factors influencing the numerical results, the above comparison ascertains the confidence in the accuracy and reliability of the present in-house

TABLE 9.3: Comparison of the present results (average Nusselt number, $\overline{Nu}$ at west wall) of completely heated ($L_h = 1$) open ended square cavity with the literature values for a range of conditions.

Source	average Nusselt number ($\overline{Nu}$) at the west wall			
	$Ra = 10^3$	$Ra = 10^4$	$Ra = 10^5$	$Ra = 10^6$
Present	1.387	3.386	7.295	14.358
Mohamad (1995)	-	3.264	7.261	14.076
Bilgen and Oztop (2005)	1.310	3.530	7.850	15.200
Mohamad et al. (2009)	-	3.373	7.323	14.380
Kefayati (2013a)	-	3.319	7.391	14.404
Chan and Tien (1985)	1.070	3.410	7.690	15.000

PS-TLBM solver. The results presented herein this work are, therefore, believed to be accurate and reliable within $\pm 1 - 3\%$.

Having gained the confidence in the present computational solution algorithm of PS-TLBM solver, the ensuing section presents the influence of flow governing parameters (i.e., heater size, heating location and Rayleigh number) on the detailed natural convection flow phenomenon of partially heated open cavity in terms of the streamline and isotherm patterns, center line variations of the velocity components and temperature, and local and average Nusselt numbers.

9.2.2 Part I: Effect of heater size and heating location

In this section, the combined influence of heater size (0.25,0.5,0.75), heating locations (bottom, middle and top), Rayleigh number ($Ra = 10^3, 10^4, 10^5, 10^6$) is investigated for constant Prandtl number ($Pr = 0.71$). The variation of streamline, vorticity, isotherms, center-line variation of velocity components as well as temperature and Nusselt number variation have been presented and discussed in preceeding sections.

9.2.2.1 Detailed flow patterns

The detailed physical insights of the natural convection in an partially heated open ended cavity are illustrated by presenting the evaluation of streamline patterns and variations of

velocity components along the center-lines of cavity and their dependencies on the ranges of the conditions considered herein.

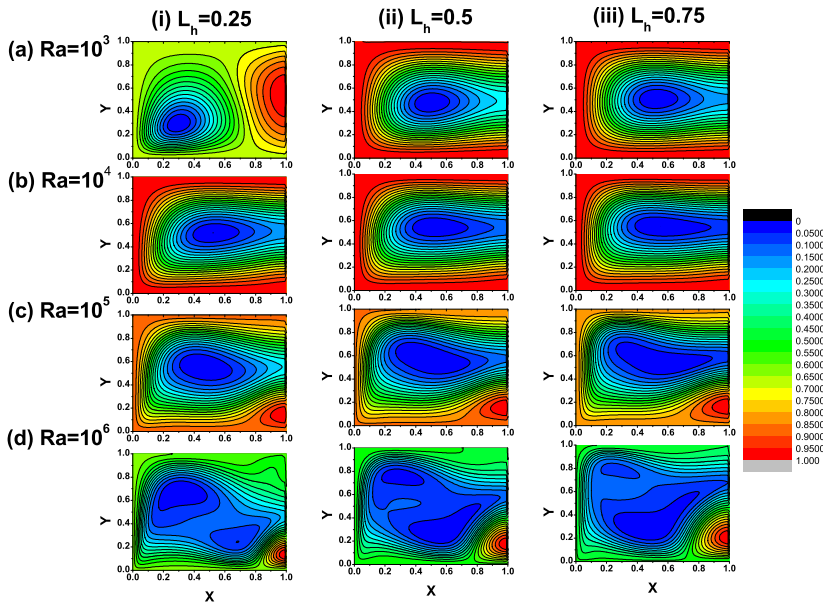

FIGURE 9.2: The dependence of the streamline patterns in the open ended partially heated cavity on the heater size (L_h) and Rayleigh number (Ra) for the bottom heating location.

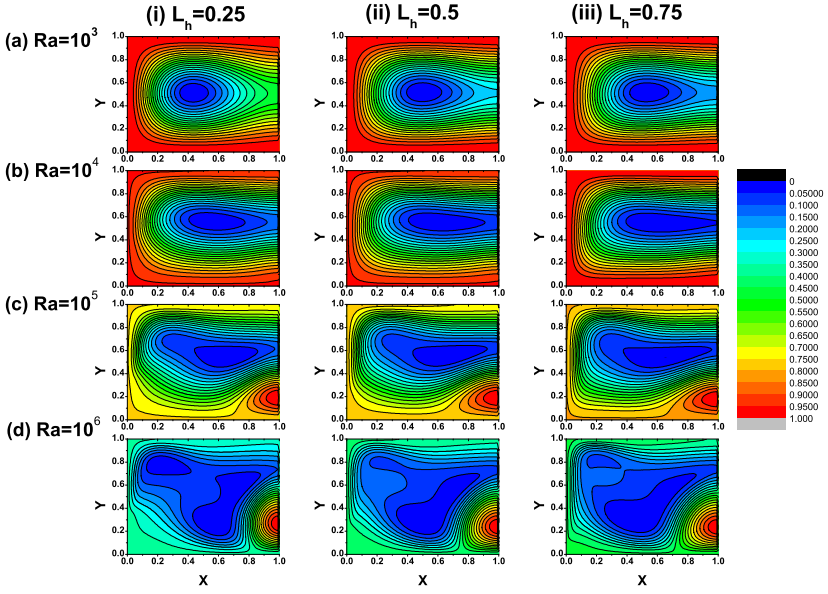

FIGURE 9.3: The dependence of the streamline patterns in the open ended partially heated cavity on the heater size (L_h) and Rayleigh number (Ra) for the middle heating location.

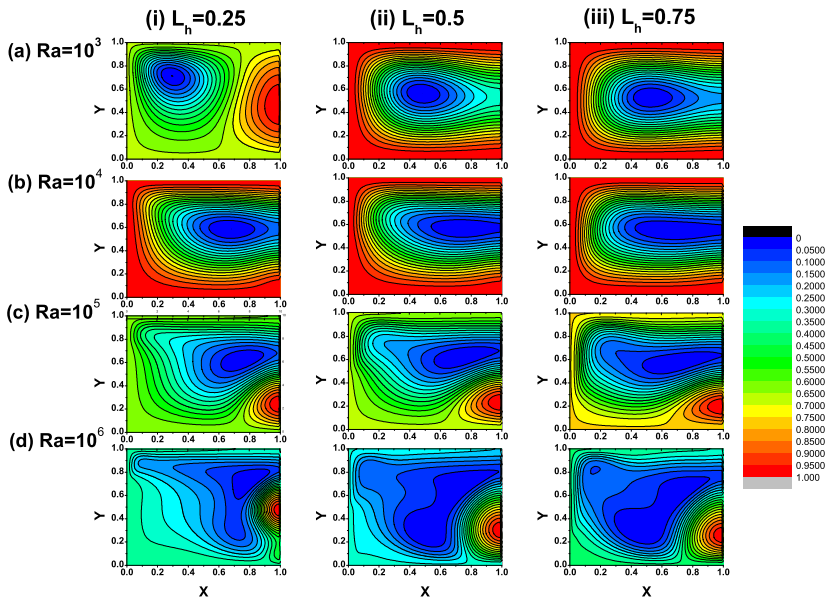

FIGURE 9.4: The dependence of the streamline patterns in the open ended partially heated cavity on the heater size (L_h) and Rayleigh number (Ra) for the top heating location.

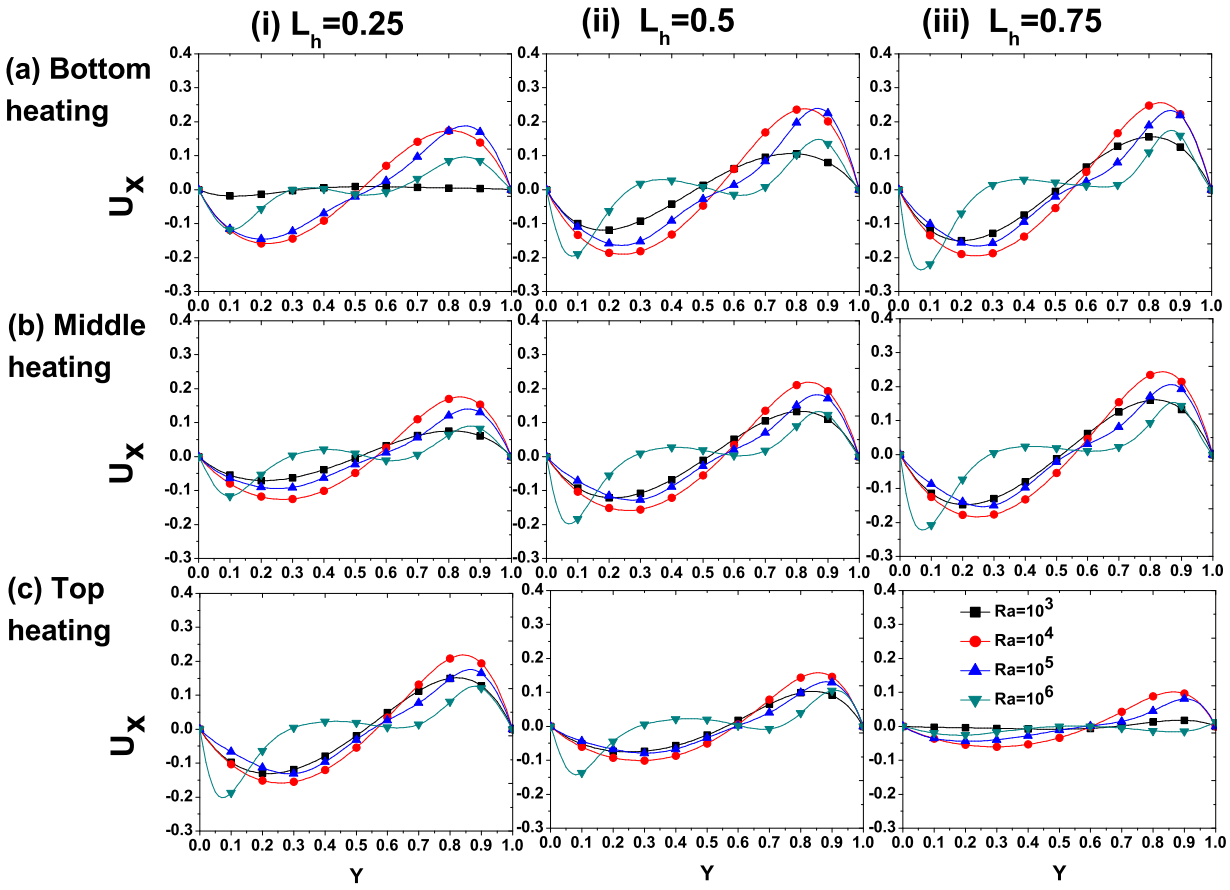

FIGURE 9.5: The variation of the horizontal component of dimensionless velocity (U_x) along the vertical center-line $(0.5, Y)$ of cavity with the heater size (L_h), heating locations (Bottom, middle, top) and the Rayleigh number (Ra).

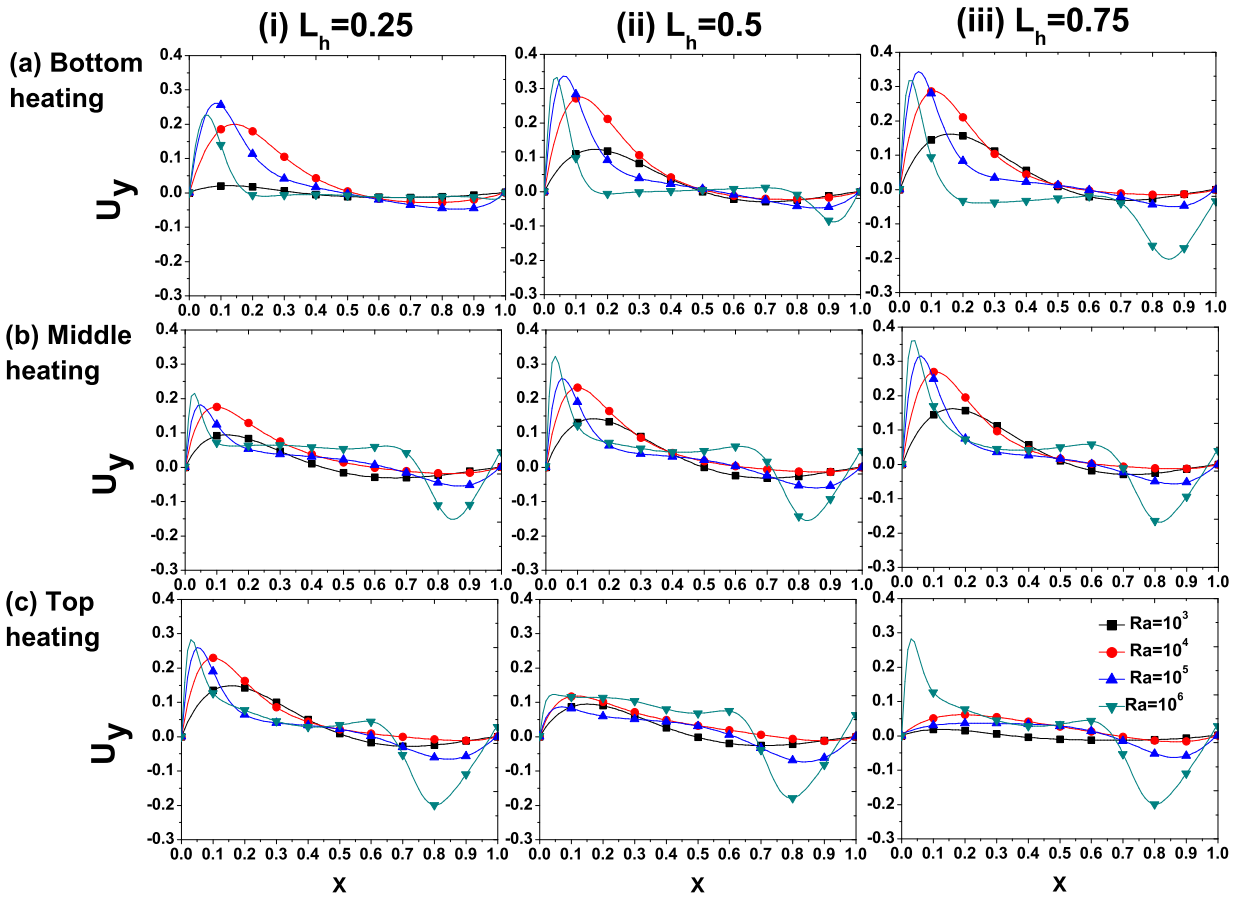

FIGURE 9.6: The variation of the vertical component of dimensionless velocity (U_y) along the horizontal center-line $(X, 0.5)$ of cavity with the heater size (L_h), heating locations (Bottom, middle, top) and the Rayleigh number (Ra).

(A) Streamline patterns: It is evident that kinematic viscosity (ν) and thermal diffusivity (α) are two significant fluid properties which are responsible for the development of hydrodynamic and thermal boundary layers, respectively. The development of the boundary layers, in turn, influences the flow and heat transfer characteristics. Such influences are examined by systematic variation of Rayleigh number (Ra), which is directly related to development of thickness of boundary layers. In order to delineate the influences of the flow governing parameters on the flow field, the stream-function is normalized as follow:

$$\psi^* = \frac{\psi - \psi_{min}}{\psi_{max} - \psi_{min}} \tag{9.4}$$

The representative dependence of the flow influencing parameters on the normalized

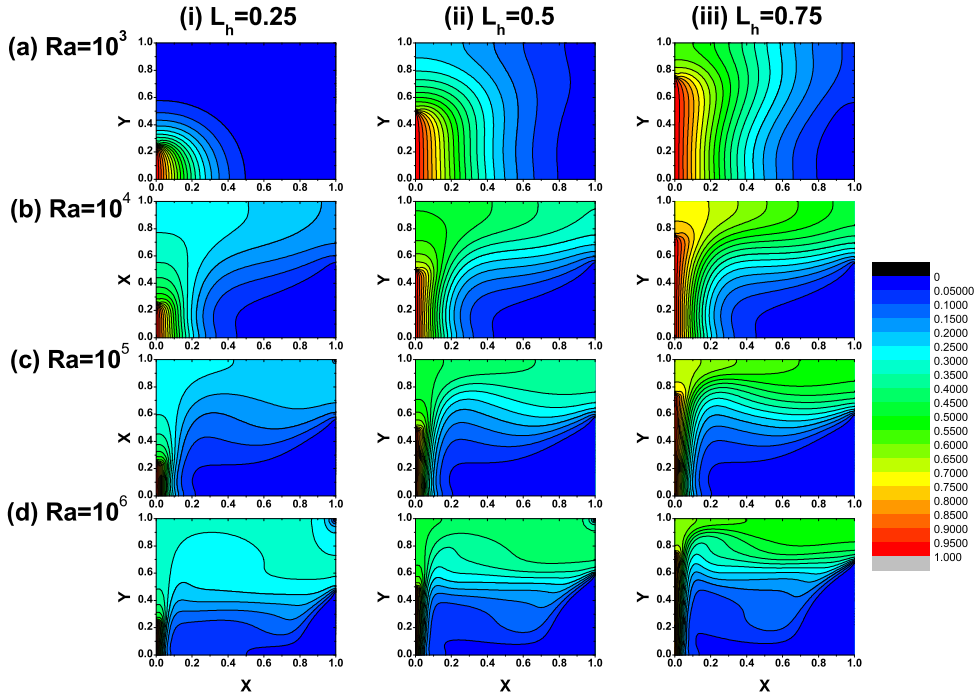

FIGURE 9.7: Representative variations of the isotherm patterns with the heater size (L_h) and Rayleigh number (Ra) for the bottom heating location of the open ended cavity.

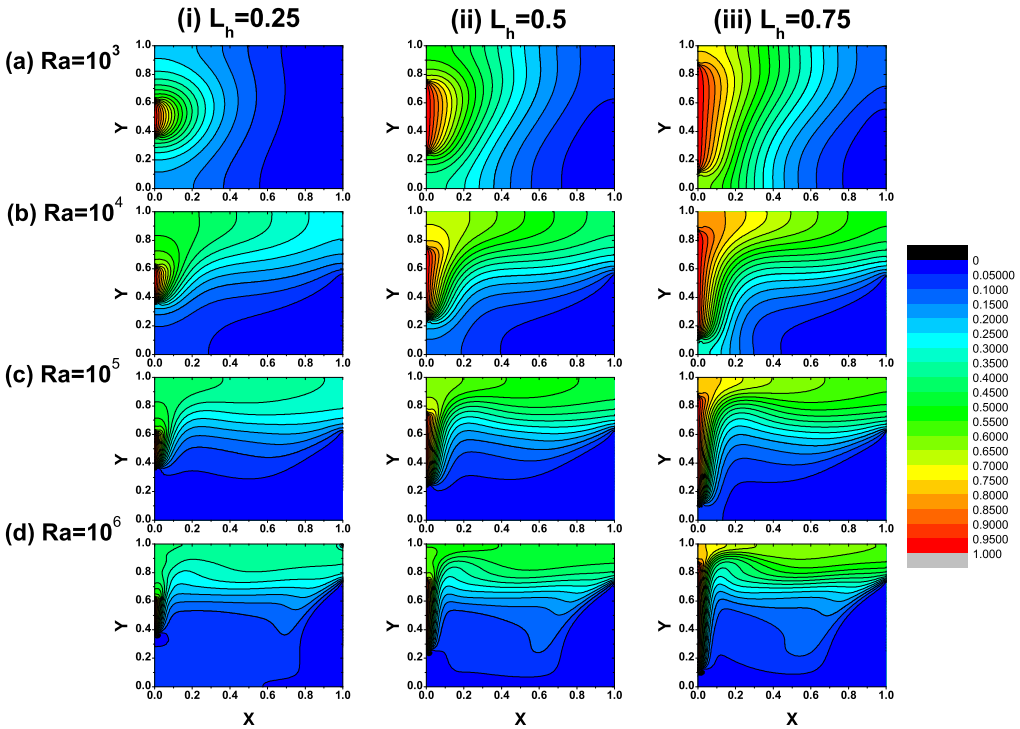

FIGURE 9.8: Representative variations of the isotherm patterns with the heater size (L_h) and Rayleigh number (Ra) for the middle heating location of the open ended cavity.

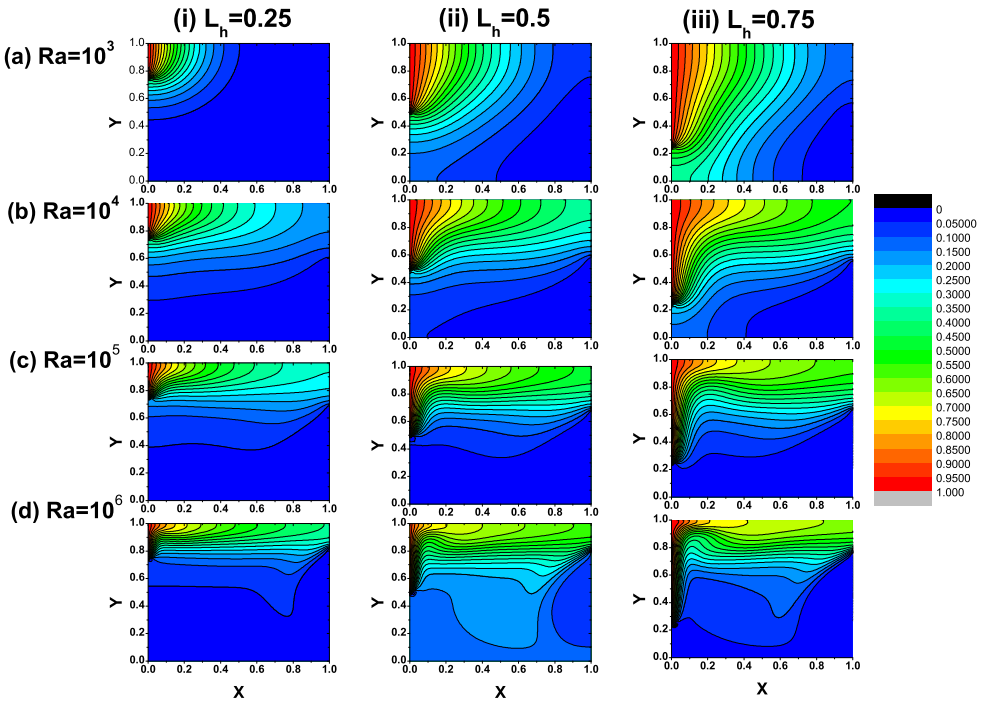

FIGURE 9.9: Representative variations of the isotherm patterns with the heater size (L_h) and Rayleigh number (Ra) for the top heating location of the open ended cavity..

streamline (ψ^*) patterns are shown in Figure 9.2 - 9.4 for three different heating locations (bottom, middle and top) on the west wall, respectively, at four values of Rayleigh numbers ($Ra = 10^3,\ 10^4,\ 10^5$ and 10^6) for the three different heating sizes ($L_h = 0.25,\ 0.5$ and 0.75). Equidistant contours ($\Delta\psi^* = 0.05$) of streamline consisting of $\psi^*_{min} = 0$ and $\psi^*_{max} = 1$ are plotted in each of these figures. An examination of Figure 9.2 - 9.4 shows that the streamline patterns are bifurcated into two parts for the smallest heater size ($L_h = 0.25$) at the lowest value of the Rayleigh number ($Ra = 10^3$). It implies that the conduction dominated heat transfer is possibly due to the weak convection and buoyancy driven flow under the above mentioned conditions ($L_h = 0.25$ and $Ra = 10^3$). The increasing value of the heating size ($L_h \geq 0.5$) reciprocates the buoyancy induced flow in an open ended cavity. Due to the induced buoyancy, the flow originates from the lower end of open part of cavity, and approaches the heated part of wall. It causes the rise in temperature of fluid with the formation of plume. After striking the top adiabatic part of cavity, fluid flows towards open side of cavity with gradual decrease in the temperature. As a result of the varying thermal gradient within the cavity, this fluid re-circulation

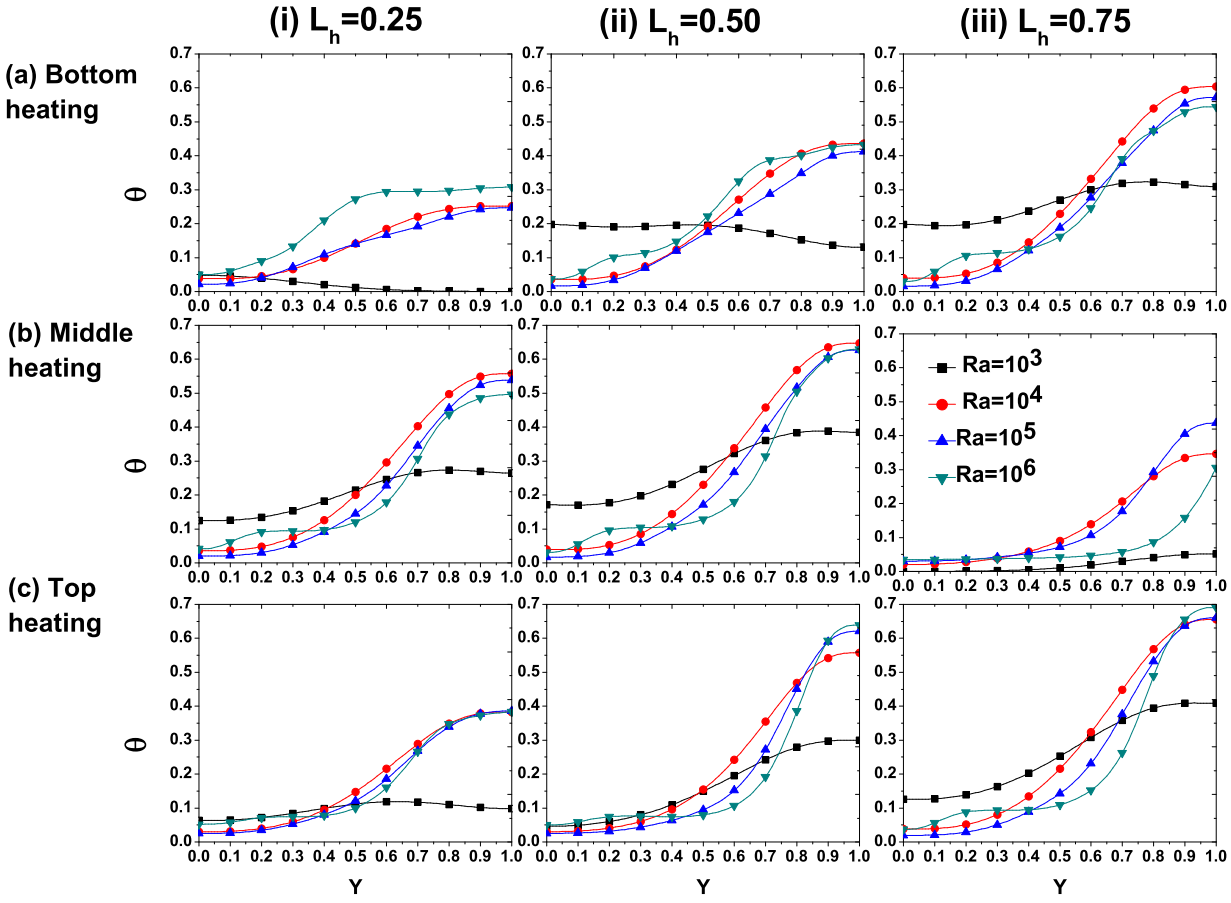

FIGURE 9.10: The influences of heating length (L_h), heater location (bottom, middle, top) and Rayleigh number (Ra) on the distribution of the dimensionless temperature (θ) along the vertical center-line ($0.5, Y = Y$) of the open ended cavity.

causes formation of elliptical quasi-motionless portion in the cavity. Such convection flow behavior is in accordance with the literature (Mohamad, 1995; Mohamad et al., 2009; Haghshenas et al., 2010a).

For a fixed value of the heater size (L_h), an increasing value of the Rayleigh number (Ra) enhances the intensity of the fluid re-circulation between the hot and cold parts of cavity, which in turn causes an increase in the size of quasi-motionless region in the cavity. For the intermediate value of the Rayleigh number ($Ra \geq 10^5$), a formation of convection cell on the lower right (near open end) is observed due to the acceleration of fluid towards hot wall. Similar patterns are also noted in Bilgen and Oztop (2005). For a fixed value of the Rayleigh number (Ra), the increasing value of the heater size (L_h) attributes to the strengthening of the buoyancy induced flow. It, in turn, causes the stretching of elliptical

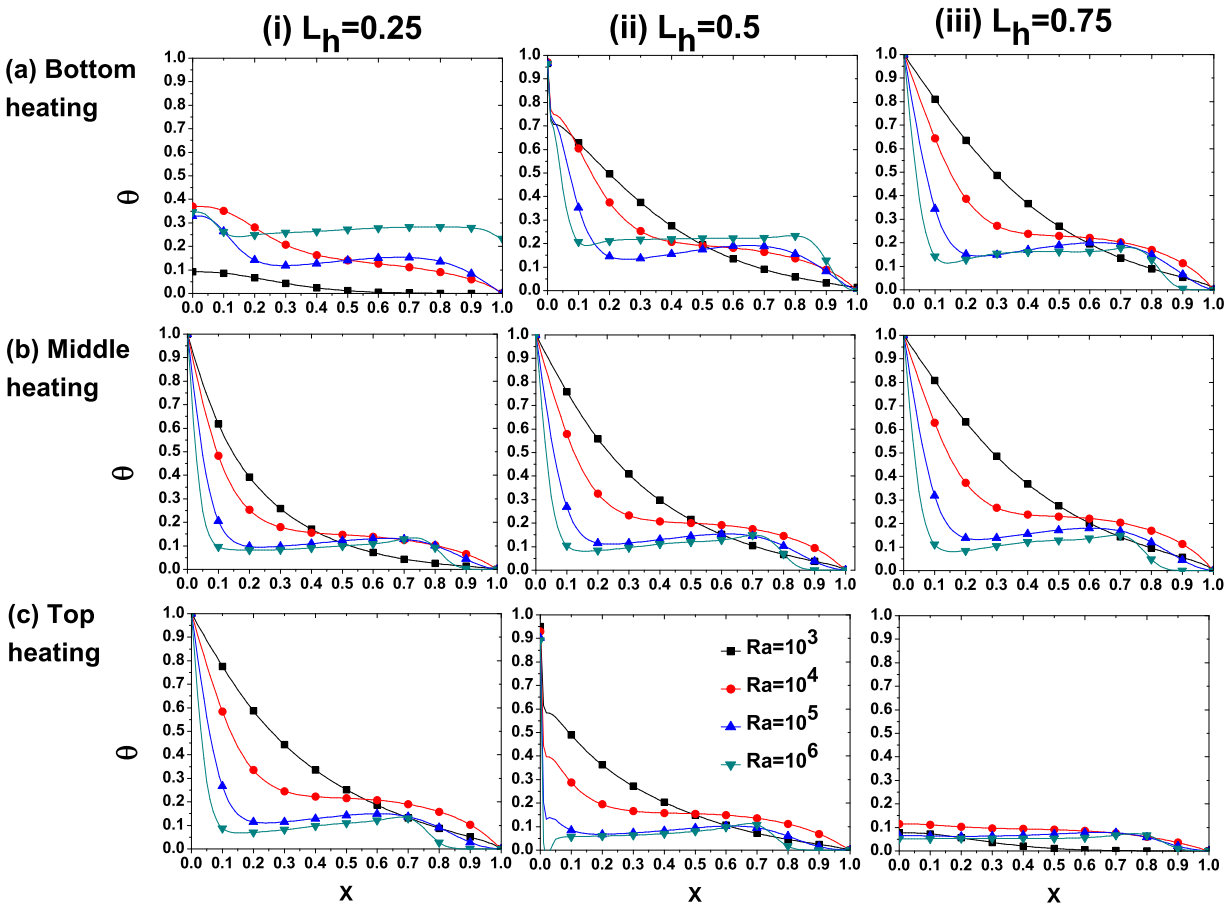

FIGURE 9.11: The influences of heating length (L_h), heater location (bottom, middle, top) and Rayleigh number (Ra) on the distribution of the dimensionless temperature (θ) along the horizontal center-line ($X = X, 0.5$) of the open ended cavity.

quasi-motionless region towards the open end of the cavity. All other flow features are seen to be nearly unchanged with the change in the heater size. For the better understanding of the effects of heater size ($0.25 \leq L_h \leq 0.75$), heating locations (bottom, middle and top) and Rayleigh number ($10^3 \leq Ra \leq 10^6$) on the evolution of streamline patterns, the minimum and maximum values of stream-functions (ψ_{min} and ψ_{max}) with their location of occurrence (x, y) within the cavity are summarized in Table 9.4. It can be observed from the examination of Table 9.4 that the increasing value of the heater size (L_h) causes an increase in the both the minima and maxima of the stream-function (ψ_{min}, ψ_{max}), which in turn suggests an enhancement of the convective flow strength, irrespective of the all other flow governing parameters (heating location and Rayleigh number). On the other hand, for the fixed length of heater (L_h), the middle heating location yields higher values

TABLE 9.4: Influences of the heating size (L_h), heating locations (bottom, middle and top) and Rayleigh number (Ra) on the maximum and minimum values of the stream-functions (ψ_{max}, ψ_{min}) and their location of occurrence (x, y) in the cavity.

	$Ra = 10^3$		$Ra = 10^4$		$Ra = 10^5$		$Ra = 10^6$	
Heater location	ψ_{min} (x,y)	ψ_{max} (x,y)	ψ_{min} (x,y)	ψ_{max} (x,y)	ψ_{min} (x,y)	ψ_{max} (x,y)	ψ_{min} (x,y)	ψ_{max} (x,y)
				$L_h = 0.25$				
Top	-0.015	0.0079	-0.2285	0.0022	-0.607	0.360	-1.983	3.184
	(0.3,0.71)	(0.53,0.62)	(0.68,0.58)	(0.99,0.06)	(0.75,0.62)	(0.99,0.24)	(0.81,0.73)	(0.99,0.46)
Middle	-0.066	7.13e-07	-0.413	6.37e-05	-1.069	0.347	-8.694	15.3946
	(0.43,0.51)	(0.99,0.0)	(0.56,0.56)	(0.99,0.01)	(0.67,0.55)	(0.99,0.19)	(0.58,0.26)	(0.99,0.27)
Bottom	-0.164	0.077	-0.4654	6.95e-06	-1.434	0.2000	-9.309	5.728
	(0.29,0.29)	(0.99,0.55)	(0.52,0.52)	(0.99,0.0)	(0.45,0.56)	(0.99,0.15)	(0.32,0.68)	(0.99,0.13)
				$L_h = 0.50$				
Top	-0.077	2.01e-06	-0.3689	2.23e-04	-1.128	0.5775	-21.84	49.833
	(0.48,0.56)	(0.01,0.69)	(0.75,0.57)	(0.99,0.02)	(0.74,0.62)	(0.99,0.23)	(0.51,0.28)	(0.99,0.3)
Middle	-0.1112	6.02e-07	-0.516	8.02e-06	-1.4783	0.4409	-32.49	45.26
	(0.5,0.52)	(0.99,0.0)	(0.59,0.56)	(0.99,0.0)	(0.67,0.56)	(0.99,0.19)	(0.5,0.28)	(0.99,0.24)
Bottom	-0.099	7.25e-05	-0.592	7.94e-06	-1.695	0.278	-19.8124	16.87
	(0.5,0.48)	(0.29,0.29)	(0.52,0.54)	(0.99,0.0)	(0.49,0.57)	(0.99,0.16)	(0.56,0.26)	(0.99,0.18)
				$L_h = 0.75$				
Top	-0.123	1.91e-06	-0.521	8.02e-06	-1.602	0.519	-47.18	68.60
	(0.53,0.53)	(0.01,0.98)	(0.68,0.55)	(0.99,0.0)	(0.69,0.57)	(0.99,0.2)	(0.46,0.3)	(0.99,0.26)
Middle	-0.135	1.9e-06	-0.584	7.99e-06	-1.722	0.422	-50.00	59.55
	(0.53,0.52)	(0.01,0.02)	(0.59,0.55)	(0.99,0.0)	(0.65,0.54)	(0.99,0.18)	(0.44,0.3)	(0.99,0.24)
Bottom	-0.134	2.63e-06	-0.616	7.96e-06	-1.770	0.348	-39.65	38.57
	(0.51,0.52)	(0.01,0.02)	(0.55,0.55)	(0.99,0.0)	(0.61,0.53)	(0.99,0.17)	(0.45,0.28)	(0.99,0.21)

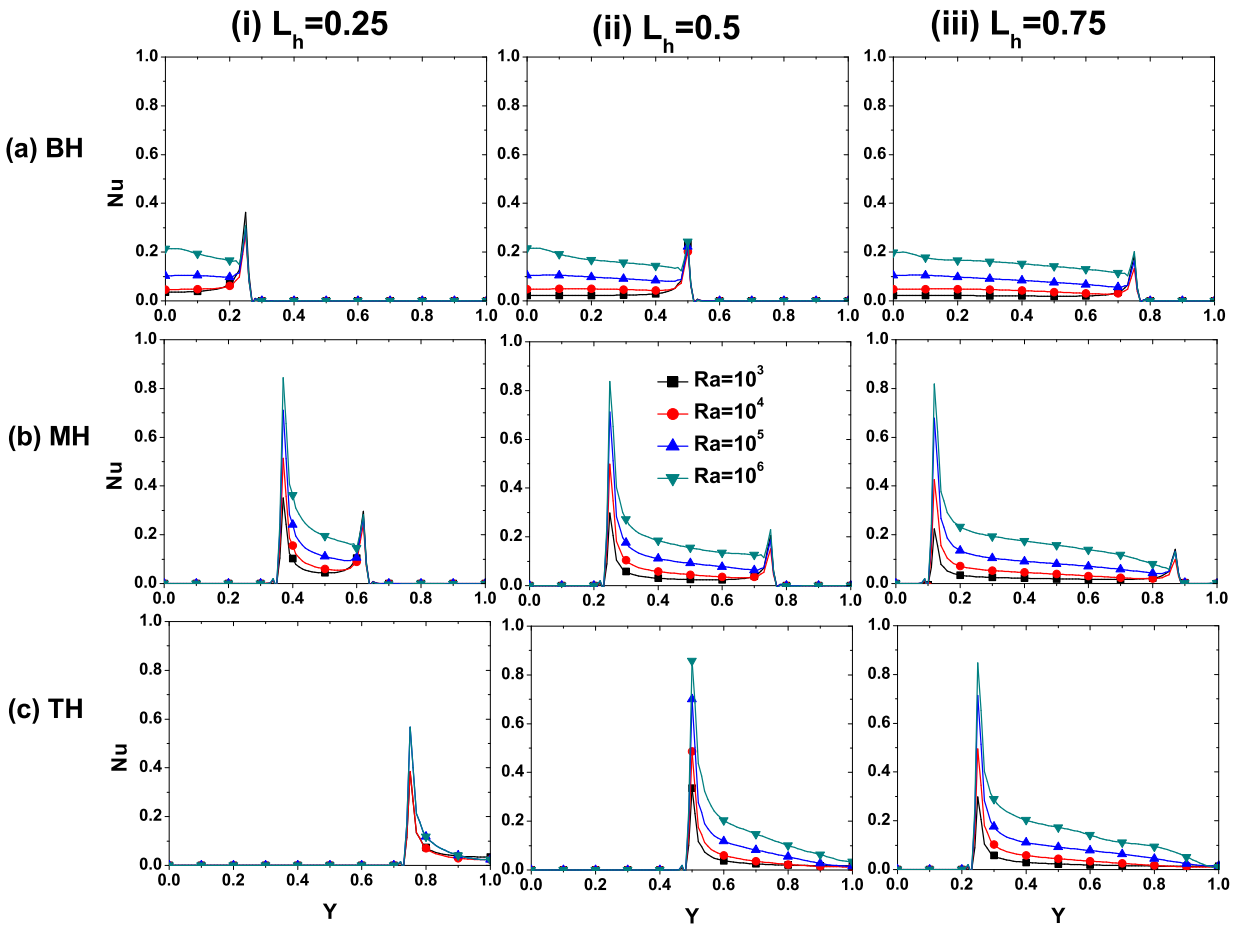

FIGURE 9.12: Variation of the local Nusselt number (Nu) on the partially heated wall with the heating locations (bottom, middle and top), heater size (L_h) and Rayleigh numbers (Ra).

of both the minima and maxima of the stream-function (ψ_{min}, ψ_{max}). It indicates an stronger convection effects in the middle heating followed by the bottom and top heating positions, respectively.

(B) Centerline velocity profiles: Further insights of the flow characteristics are analyzed with the help of center-line velocity profiles. Figures 9.5 and 9.6 depict the variations of the velocity components along the vertical and horizontal center-lines of cavity, respectively, for a range of conditions covered herein. Figure 9.5 illustrates the variation of horizontal component of velocity, $U_x(y)$, plotted along the vertical center-line ($X = 0.5$, Y) of the cavity. The effect of flow circulation can be clearly seen in Figure 9.5, as the velocity profiles $U_x(y)$ have both the negative and positive values in the intermediate zone and the similar values (i.e., zero) at the end points due to the no-slip walls of the cavity. In

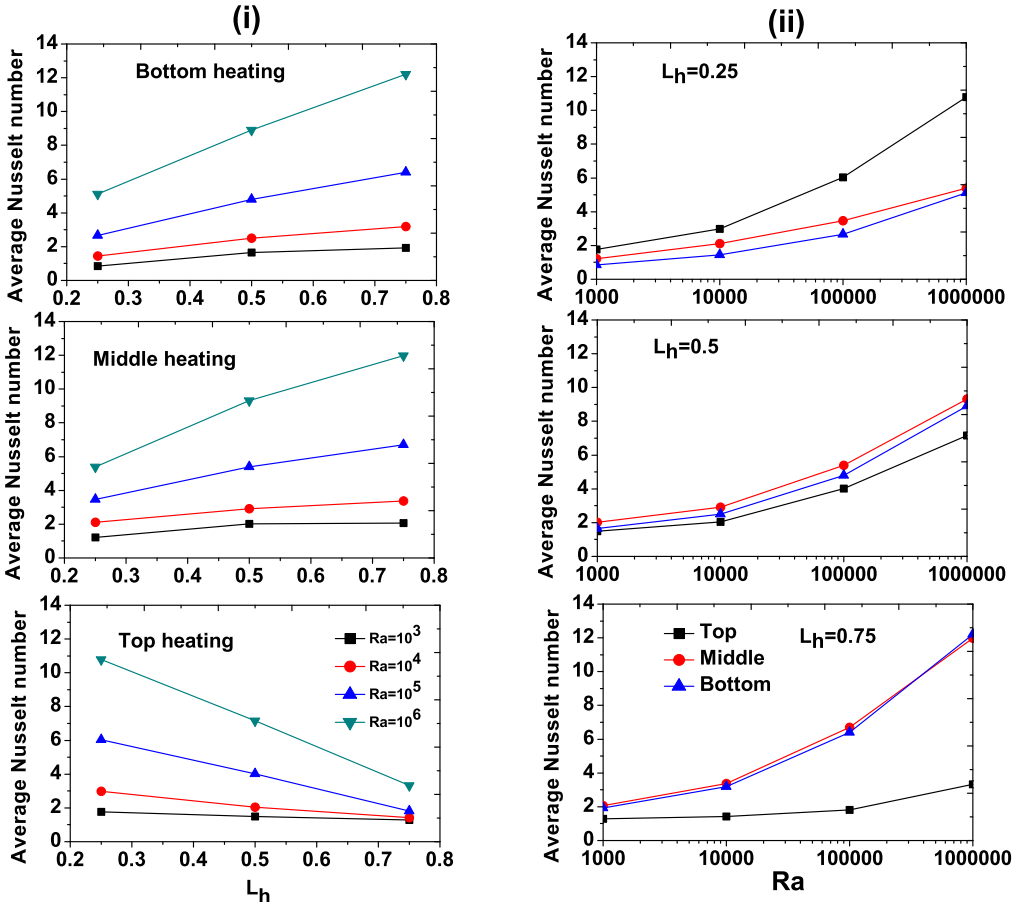

FIGURE 9.13: Dependence of the average Nusselt number ($\overline{Nu}$) of partially heated wall on the Rayleigh numbers (Ra), heating locations (bottom, middle and top) and the heater size (L_h).

general, the horizontal velocity $U_x(y)$ originates from zero and attains its minimum value. It is followed by the gradual increase until it reaches to a maximum value and which further drops down to the zero values, and therefore, representing the flow circulation, irrespective of the flow governing parameters. However, due to the conduction dominating heat transfer at the smallest heater size ($L_h = 0.25$) and Rayleigh number ($Ra = 10^3$), the horizontal velocity $U_x(y)$ values are nearly close to zero. It suggests that the flow circulation is not observed at these conditions, which is also evident from the streamline patterns (Figures 9.2 - 9.4). The bottom heating shows that both the maximum as well as minimum values of the horizontal velocity $U_x(y)$ increase with the increasing value of heater size (L_h) due to the enhancement of the buoyancy induced flow. The center-line horizontal velocity $U_x(y)$ patterns remain nearly similar to that of bottom heating case.

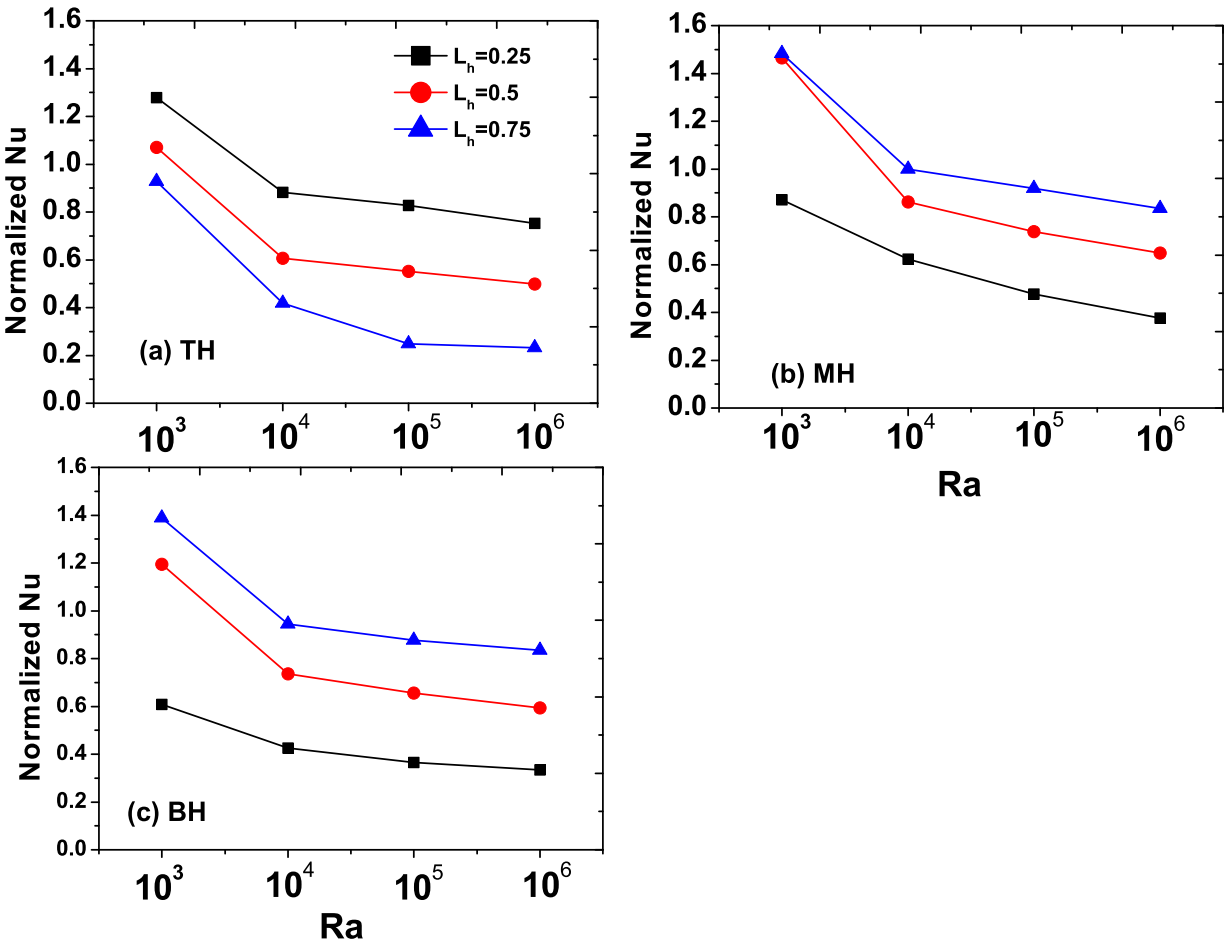

FIGURE 9.14: Variation of normalized Nusselt number (Nu^N) estimated along partially heated wall for a range of Rayleigh numbers ($10^3 \leq Ra \leq 10^6$), and heater size ($0.35 \leq L_h \leq 0.75$) for (a) top, (b) middle and (c) bottom heating locations.

The top heating location, however, shows remarkable difference in the velocity variation in comparison to the other two heating locations. It is presumably due to the presence of cold fluid (lower temperature) in vertically lower part of the cavity.

The variations of the vertical component of velocity (U_y) along the horizontal center-line (X, $Y = 0.5$) of cavity are depicted in Figure 9.6. Similar to the horizontal velocity profiles (U_x), the vertical velocity (U_y) patterns also show a complex dependence on the flow governing parameters. It shows that the zero velocity at the west wall (due to no-slip boundary) increases sharply to its maximum value and then a gradual decrease in the values is observed near the west wall of the cavity. The velocity profiles are seen to be nearly unchanged in the middle portion of the center-line. However, the sharp decrease

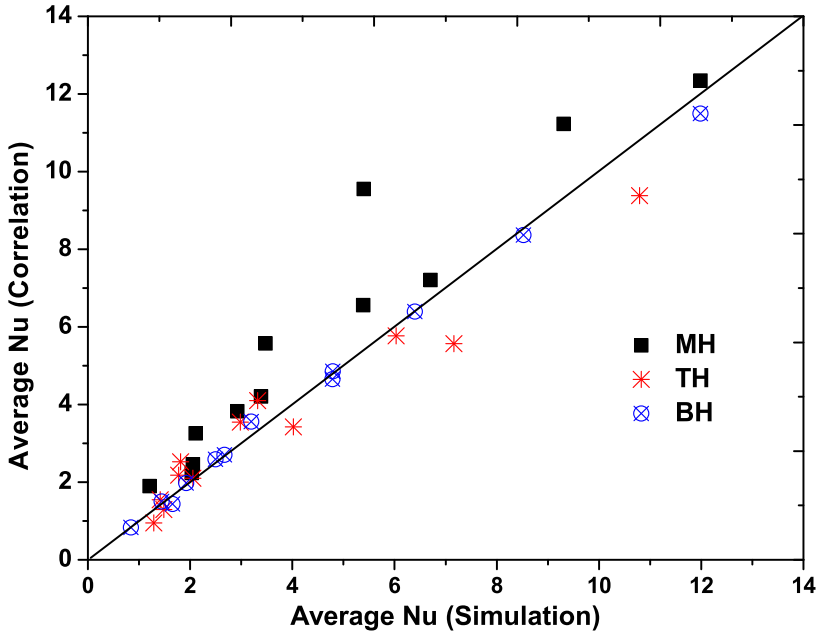

FIGURE 9.15: Comparison between numerical and predicted values (Eq. 9.6) of the average Nusselt number of the partially heated wall.

to the minimum value followed by an increase to zero or positive value is seen in the close vicinity of the east open end wall. The zero velocity at the west (no-slip) wall and non-zero velocity at the east open end wall are also seen in Figure 9.6. The sharp increase followed by a decrease (or vice versa) are the clear representation of quasi-motionless zone formed in that portion of the cavity. For a fixed heater size, the effects of heating locations on the horizontal velocity profiles $U_x(y)$ are observed near the open end of cavity. For the bottom heating case, horizontal velocity $U_x(y)$ value remains nearly zero, but the formation of minima is observed in the increasing order for the middle and top heating, respectively.

The detailed flow patterns, presented and discussed in the preceding section, are the physical consequences of the influences of the natural convection flow governing parameters on the thermal field. Therefore, the dependencies of thermal field on the governing parameters are explored in the ensuing sections.

9.2.2.2 Heat transfer results

The dependence of the isotherm patterns, the local Nusselt number on the heated surface and the average Nusselt number on the heating length (L_H), heating locations (bottom, middle and top) and the Rayleigh number (Ra) is presented and discussed in the ensuing sections. Further, the present numerical results and their dependence on the various flow governing parameters is also presented as a predictive closure relationship.

(A) Isotherm patterns: Figures 9.7-9.9 depict the dependencies of the isotherm (i.e., constant dimensionless temperature θ) contour patterns on the heater size ($0.25 \leq L_h \leq 0.75$), and laminar range of the Rayleigh numbers ($10^3 \leq Ra \leq 10^6$) at a fixed value of the Prandtl number ($Pr = 0.71$) for the three different heating locations (bottom, middle and top), respectively. Equidistant isotherm contours ($\Delta\theta = 0.05$) consisting of $\theta_{min} = 0$ and $\theta_{max} = 1$ are plotted in each of these figures. In general, the compactness (or dense clustering) of the temperature lines indicates the larger temperature gradients (and thus, highest heat transfer rate). For bottom heating location (Figure 9.7), it can be observed that for lowest values of the Rayleigh number ($Ra = 10^3$), the isotherm patterns remain almost parallel to the vertical axis and heat transfer becomes conduction dominated. For the smallest heater ($L_h = 0.25$), isotherms remain clustered in close vicinity of the bottom heated part due to the weak buoyancy induced flow and it develops very low temperature region in the upper part of the cavity. An increasing length of heater ($L_h > 0.25$) though causes an enhancement in the strength of buoyancy induced flow, however, the heat transfer is still mainly governed by the conduction mode. An increase in Rayleigh number (Ra) causes an increased circulation in between the active walls of the cavity due to the increased buoyancy induced flow. The isotherm patterns are also seen to start shifting towards the heated part of cavity. For the cavity of larger heater sizes, isotherms become more dense towards the heating part due to increased convective effect. The boundary layer formation also takes place for Rayleigh number of $Ra = 10^5$ and onward. It can also be observed that with the increase the Rayleigh number, thickness of boundary layer decreases.

The isotherms patterns for the middle and top heating locations are illustrated in Figures 9.8 and 9.9, respectively. The physical insights for these configurations are similar to that observed in the case of bottom heating location. At the lower value of the Rayleigh number ($Ra = 10^3$), the isotherms patterns remain nearly same for all three heating locations. It implies and ascertains that the heat transfer mode is conduction. A convective regime is established for higher values of the Rayleigh number ($Ra \geq 10^4$) due to the higher circulation between hot wall and ambient. For the middle heating location and Rayleigh number of $Ra = 10^6$, due to higher acceleration of fluid towards heater from cold wall, formation of a convection cell takes place, which can be observed from Figure (9.8d).

For top heating position (Figure 9.9) and smallest heater ($L_h = 0.25$), the isotherm contours remain stratified towards heater with the formation of low temperature region at lower part of the cavity for larger values of the Rayleigh number ($Ra \geq 10^4$). For larger heater ($L_h > 0.25$), due to increased circulation between active walls of enclosure, isotherms occupy almost entire cavity region. As the Rayleigh number (Ra) increased to 10^5, isotherms become confined to upper part of the cavity due to the heater location and low temperature fluid contained in lower part of cavity. Similar convection cell effects can be observed at the lower-right end of the enclosure.

Further insights of the thermal behavior inside the cavity are presented in the ensuing section by examining the variation of the dimensionless temperature along the horizontal and vertical center-lines of the cavity.

(B) Center-line temperature profiles: Figures 9.10 and 9.11 depict the distribution of dimensionless temperature (θ) along the horizontal $(X, 0.5)$ and vertical $(0.5, Y)$ center-lines of the cavity, respectively, for the ranges of conditions covered herein. Irrespective of the heating size and heating locations, center-line temperature (θ) along the horizontal center-line $(X, 0.5)$ is seen to vary in a linear manner (Figure 9.10) for all values of the Rayleigh number (Ra), expect for the lowest value of the Rayleigh number ($Ra = 10^3$). The temperature pattern seen at $Ra = 10^3$ is clearly due to conduction dominated heat transfer, as discussed in previous sections. For a fixed heating location, the increase

in heater size shows an increase in the maximum value of temperature (θ) along the horizontal center-line, which is an indication of increasing convection effects, irrespective of the value of the Rayleigh number (Ra). The temperature distribution, however, remains nearly same for all the heating locations.

Similarly, Figure 9.11 illustrates the distribution of temperature (θ) along vertical $(0.5, Y)$ center-line of the cavity. For the bottom heating location and the smallest heating length ($L_h = 0.25$), the temperature is seen to be very low and nearly parallel to horizontal axis. It is clearly due to entrapment of the high temperature fluid in the lower region of cavity. The increasing values of the heater size shows a linear decrease in fluid temperature (θ) along vertical center-line. The temperature distribution is observed to be nearly same for all values of the heating lengths (L_h), except that for bottom heating at the smallest heater ($L_h = 0.25$) and top heating at the largest heater ($L_h = 0.75$). The above seen local variations in the heat transfer characteristic (center-line temperature and isotherms) with the flow governing parameters, in turn, are expected to reflect the influences in the heat transfer rates (i.e., local and average Nusselt numbers). The ensuing subsection presents and examines the local and averaged heat transfer rate and their dependence on the various parameters.

(C) Local and averaged Nusselt numbers: The representative variations of local Nusselt number (Nu, Eq. 3.29) at the heated wall with the heater size (L_h), heating locations and Rayleigh number (Ra) are illustrated in Figure 9.12. The local Nusselt number (Nu) is seen to have a complex dependence over the ranges of the flow governing parameters accounted herein. For instance, for the lower values of the Rayleigh number ($Ra \leq 10^4$), local Nusselt number is seen to be almost independent on the flow governing parameters due to the conduction dominating mode of the heat transfer. Over the range of heater size (L_h), as expected, the local Nusselt number (Nu) seen to increase with increasing value of the Rayleigh number (Ra), irrespective of the placement of the heater. The highest local Nusselt number (Nu) values are, thus, observed for the largest value of the Rayleigh number (Ra). A sharp peak can also be seen in Figure 9.12 at the starting (of the middle and top heating locations) and at the end (of bottom and middle

heating locations), respectively. Such peaks are clear representation of the sharp changes in thermal gradients at those spatial locations due to the sudden change in the temperature from a heating mode to ambient mode and vice-versa. The sharp gradients ultimately leads to the higher heat transfer at such locations. The peaks, if observed, are always higher at the starting point, compared to that at the end point, of the heating location because of the larger (and sudden) temperature variations at this location. The heating length (L_h) has very marginal influence on the local value of the Nusselt numbers, over the ranges of the Rayleigh number (Ra) and heating locations. It can also be seen from Figure 9.12 that the middle heating location shows the highest peak in the curves in comparison to the other heating locations, under otherwise identical conditions. It is very clear indication of the largest value of the local Nusselt number which, in turn, suggests the maximum heat transfer under middle heating location compared to that for some value of the Rayleigh number and heating length in other heating locations.

Furthermore, the average Nusselt number ($\overline{Nu}$, Eq. 3.30) is obtained by integrating the local values of the Nusselt number (Nu, Eq. 3.29 and Figure 9.12) on the active wall. Table 9.5 depicts the influences of the Rayleigh number ($10^3 \leq Ra \leq 10^6$) and heating length ($0.25 \leq L_h \leq 0.75$) on the average Nusselt number ($\overline{Nu}$) of open ended cavity heated partially at either of the three (bottom, middle and top) heating location on the west wall. Also included in Table 9.5 are the values of the average Nusselt number ($\overline{Nu}$) for a completely heated ($L_h = 1$) open ended cavity over the range of Rayleigh number ($10^3 \leq Ra \leq 10^6$). For the better understanding of the influences of the heater size and heating locations on the average heat transfer rate, the average Nusselt number ($\overline{Nu}$) is plotted (Figure 9.13) as a function of the dependent variables (Rayleigh number, heating length and heating location). Figure 9.13(i) shows the variations of the average Nusselt number ($\overline{Nu}$) of an active wall with the Rayleigh number ($10^3 \leq Ra \leq 10^5$) and heating length ($0.25 \leq L_h \leq 0.75$) for a fixed heating location. Similarly, Figure 9.13(ii) depicts the dependence of the average Nusselt number ($\overline{Nu}$) on the Rayleigh number ($10^3 \leq Ra \leq 10^5$) and heating locations (bottom, middle and top) for a length of heating (L_h). In general, the average Nusselt number ($\overline{Nu}$) shows a linear dependence on the

dimensionless parameters (Ra and L_h) and heating locations. As expected, irrespective of the heating location and heating length (L_h), an enhancement in the average Nusselt number ($\overline{Nu}$) is seen with the increasing value of the Rayleigh number (Ra). For the top heating location and all values of the Rayleigh number (Ra), the average Nusselt number decreased with an increasing value of the heating length (L_h). On the other hand, the bottom and middle heating locations show an inverse influence of the heating length (L) on the average Nusselt number ($\overline{Nu}$) in comparison to that for the top heating location. For all the heater sizes (L_h), the middle heating location yielded the highest rate of heat transfer compared to that of other two locations. Further, to elucidate

TABLE 9.5: Dependence of the average Nusselt number ($\overline{Nu}$) of the partially heated cavity on the heating location, heating size (L_h) and Rayleigh number (Ra).

Heater location	average Nusselt number ($\overline{Nu}$) at the west wall			
	$Ra = 10^3$	$Ra = 10^4$	$Ra = 10^5$	$Ra = 10^6$
	(a) $L_h = 0.25$			
(i) Top	1.773	2.984	6.029	10.79
(ii) Middle	1.207	2.110	3.473	5.399
(iii) Bottom	0.842	1.442	2.671	5.124
	(b) $L_h = 0.50$			
(i) Top	1.485	2.053	4.019	7.161
(ii) Middle	2.031	2.921	5.385	9.308
(iii) Bottom	1.655	2.494	4.786	8.895
	(c) $L_h = 0.75$			
(i) Top	1.287	1.418	1.811	3.322
(ii) Middle	2.056	3.385	6.701	11.98
(iii) Bottom	1.925	3.196	6.397	12.20
	(d) $L_h = 1$ (Completely heated west wall)			
–	1.387	3.386	7.295	14.358

the influence of heating size on the heat transfer, the average Nusselt number ($\overline{Nu}$) has further been normalized with the corresponding value for the fully heated open ended cavity under otherwise identical conditions. The normalized average Nusselt number (Nu^N) is expressed as follow:

$$Nu^N = \frac{\overline{Nu}_{\text{partial heating}}}{\overline{Nu}_{\text{complete heating}}} = \frac{\overline{Nu}(Ra, L_h, \text{heating location})}{\overline{Nu}(Ra, L_h = 1, \text{heating location})} \tag{9.5}$$

Figure 9.14 represents the variation of normalized average Nusselt number (Nu^N) with Rayleigh number (Ra) for the different heater sizes and locations. The normalized values

above and lower than unity (i.e., $Nu^N > 1$ and $Nu^N < 1$) suggest the enhancement and deterioration in the heat transfer in comparison to the completely heated open ended cavity. Irrespective of the heating location and heater size, qualitatively similar dependence of Nu^N on Ra is observed over the ranges of conditions considered herein. For instance, for a fixed value of the heating length (L_h), the highest normalized value (at the smallest value of Ra) is seen to decrease with increasing value of the Rayleigh number (Ra) for all the heating locations. A sharp decrease in the normalized average Nusselt number (Nu^N) values with the increase in the Rayleigh number (Ra) from 10^3 to 10^4 can also be seen in the Figure 9.14 over the ranges of parameters considered herein. It clearly indicates the shifting of dominant mode of the heat transfer from a conduction to convection. Similarly, the dependence of the normalized values on the heating length is also seen to qualitatively similar for all the heating locations and Rayleigh numbers. The significance of the natural convection losses is also depicted in Figure 9.14 with the change of the heating location from top to bottom and middle locations. Consequently, for the bottom and middle heating locations, the normalized Nusselt number (Nu^N) is found to be directly proportional to the heater size (L_h); whereas it is seen to have inversely proportional dependence on the heater size (L_h) for the top heating location, under otherwise identical conditions.

The above predictions suggest a complex nature of dependence of the average Nusselt number ($\overline{Nu}$) on the dimensionless flow governing parameters (Ra and L_h) and heating locations (top,middle and bottom), respectively. Such dependencies are presented as an empirical correlation in the ensuing section.

(D) Empirical correlation: The empirical predictive correlations expressing the functional dependence of the numerical/experimental results is highly appreciated by the scientific and engineering communities due to their easy use in the process engineering design and developments. In the present study, the functional dependence of the present numerical values of the average Nusselt number ($\overline{Nu}$) of a partially heated open ended cavity on the flow governing parameters, namely, Rayleigh number (Ra), heater size (L_h)

and heating locations is expressed as follow:

$$\overline{Nu} = aRa^b L_h^c \tag{9.6}$$

Based on the statistical analysis of the present numerical values to obtain the best possible fit, Table 9.6 presents the correlations coefficients (a. b and c) with their maximum (δ_{max}) and minimum (δ_{min}) relative deviations in between the numerical and predicted (Eq. 9.6) values over the ranges of the parameters considered herein. Figure 9.15 show the comparison between the numerical and predicted (Eq. 9.6) values of the average Nusselt number. It is observed that the proposed predictive closure correlation (Eq. 9.6) predicts the average Nusselt number ($\overline{Nu}$) values within acceptable level of deviations from the computed values.

TABLE 9.6: The empirical correlations for three different heating locations with the minimum (δ_{min}) and maximum (δ_{max}) relative deviation from the present numerical data.

Location	$\overline{Nu}$	$\delta_{min}(\%)$	$\delta_{max}(\%)$
(i) Top	$0.1781Ra^{0.2114}L_h^{c\,-0.753}$	0.95	25.67*
(ii) Middle	$0.5237Ra^{0.2336}L_h^{c\,0.5704}$	0.68	12.80
(iii) Bottom	$0.4282Ra^{0.2545}L_h^{c\,0.7857}$	0.80	11.49

*Excluding the value at $L_h = 0.75$ and $Ra = 10^5$. This point deviates by about 35%.

9.2.2.3 Concluding remarks

In this work, numerical experimentation of steady laminar natural convective heat transfer in an open ended square enclosure with partially heated wall is carried out by using in-house developed CFD solver based on the passive scalar thermal lattice Boltzmann method (PS-TLBM). In particular, the effects of heating location (bottom, middle and top) on the partially heated wall and heater size (L_h=0.25, 0.5 and 0.75) on the heat and fluid flow characteristics of an incompressible fluid have been investigated for the wide range of Rayleigh number ($10^3 \leq Ra \leq 10^6$) at a fixed value of the Prandtl number ($Pr = 0.71$). The following conclusions can be drawn from the present study:

1. At lowest value of the Rayleigh number ($Ra = 10^3$), streamlines bifurcate for the bottom and top heating locations due to weak buoyancy driven flow. For middle heating location, such bifurcation is not observed due to comparatively higher buoyancy driven flow. Irrespective of the heating locations and heater sizes, the size of elliptical quasi-motionless region increase with increasing value of the the Rayleigh number (Ra).

2. At highest value of the Rayleigh number ($Ra = 10^6$), the streamlines elongate and bifurcate for all heating location and heater sizes. It shows the clockwise circulation with formation of vortex near lower part of open end of cavity. The maximum size of the vortex is seen for the top heating location case.

3. Linear dependence of the average Nusselt number ($\overline{Nu}$) on the Rayleigh number is observed, irrespective of the heating locations and heater size. However, average Nusselt number ($\overline{Nu}$) shows a proportional dependence for the bottom and middle locations and inversely proportional dependence for the top heating location on the heater size, i.e., an increasing value of L_h enhanced $\overline{Nu}$ for the bottom and middle locations and deteriorated $\overline{Nu}$ for the top heating location.

4. Over the range of Rayleigh number, middle partial heating location shows higher heat transfer rate followed by bottom and top heating locations. The significant convection losses are indicated in the top heating location as $\overline{Nu}$ decreased with increase in the heater size.

5. The normalized average Nusselt number (Nu^N) have shown the enhancement as well deterioration in the heat transfer from a partially heated open cavity compared to that of the fully heated open ended cavity.

6. Finally, the present numerical results are presented in the form of a simple predictive empirical correlation encapsulating the functional dependence of the the average Nusselt number (Nu) on the heater size (L_h) and Rayleigh number (Ra) for the different heating locations. It thereby enables the interpolation of the present results for the intermediate values of governing parameters.

9.2.3 Part II: Effect of Prandtl number

In this part, as shown in Figure 9.16, the is west wall of cavity ($x = 0$) is subjected to partial heating (T_H) with middle heating and the size of the heater is kept constant at half of the characteristic length ($L_h = H/2$). The east wall ($x = L$) is open to the ambient, i.e., maintained at temperature of $T_C (< T_H)$. Numerical simulations are

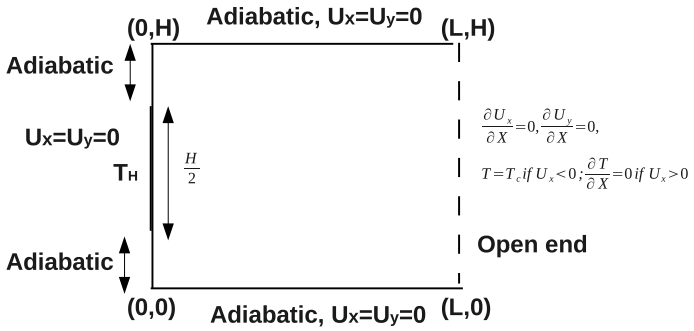

FIGURE 9.16: Physical domain considered for open ended cavity with partially heated wall (middle location).

performed for three different fluids, air ($Pr = 0.71$), R-12 refrigerant ($Pr = 4.5$) and water ($Pr = 7$) for Rayleigh numbers of $Ra = 10^4, 10^5$, and 10^6. For these broad ranges of flow governing parameters, the local and global convective flow characteristics such as the evolution of stream functions, isotherms; variation of velocity components and temperature on horizontal and vertical center-lines; and the Nusselt number are obtained and discussed herein the preceding sections.

9.2.3.1 Isotherms and flow structure

The physical insights of the natural convection in partially heated open ended cavity are obtained by detailed analysis of flow and thermal fields. In particular, the stream-function, isotherms, center-line variation of velocity components and temperature are examined in this section. It is clearly evident that the kinematic viscosity (ν) and thermal diffusivity (α) are two significant fluid parameters which are responsible for the development of hydrodynamic and thermal boundary layers, respectively. The development of the boundary layers, in turn, influences the flow and heat transfer behavior. Such influences are

examined by systematic variation of Rayleigh number (Ra), which is directly related to development of thickness of boundary layers.

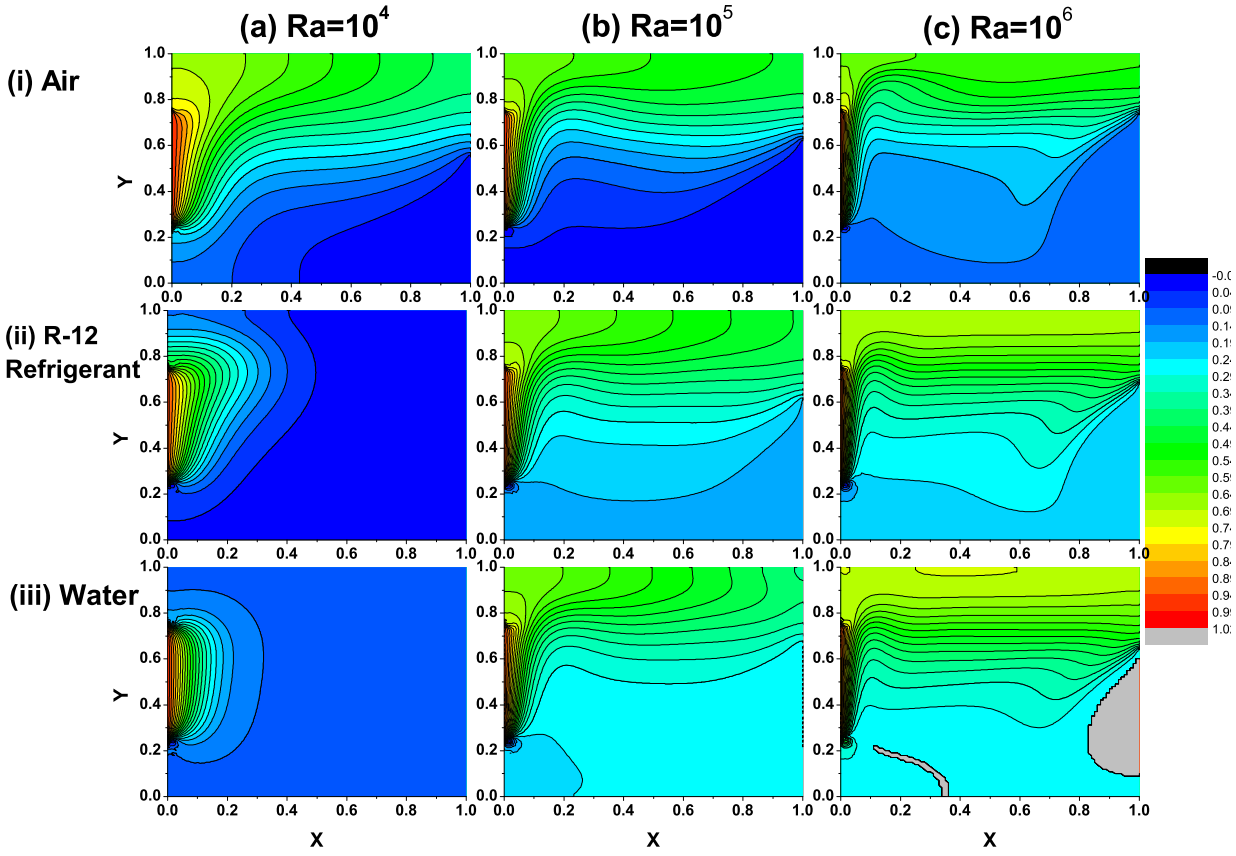

FIGURE 9.17: Streamline patterns obtained for different Rayleigh numbers and fluids.

In an open ended cavity with fully heated wall, the flow enters from the lower half of an open end of cavity, approaches heated wall resulting in rise in temperature which causes fluid to move in upward direction due to buoyancy effect. During this motion of fluid, a gradual rise in temperature is observed till fluid reaches top (adiabatic) part of cavity. Then fluid starts approaching towards open end of cavity with gradual decrease in temperature. This clockwise movement of fluid causes formation of elliptical quasi-motionless portion in center of cavity with face opening towards open end. This zone is created because of density difference between inflow and outflow fluid (Mohamad et al., 2009; Haghshenas et al., 2010a). Isotherms are slightly shifted towards heated part of cavity. For open ended cavity with partial heater, flow and thermal patterns remains nearly same, except the isotherms are observed to be more confined towards partially

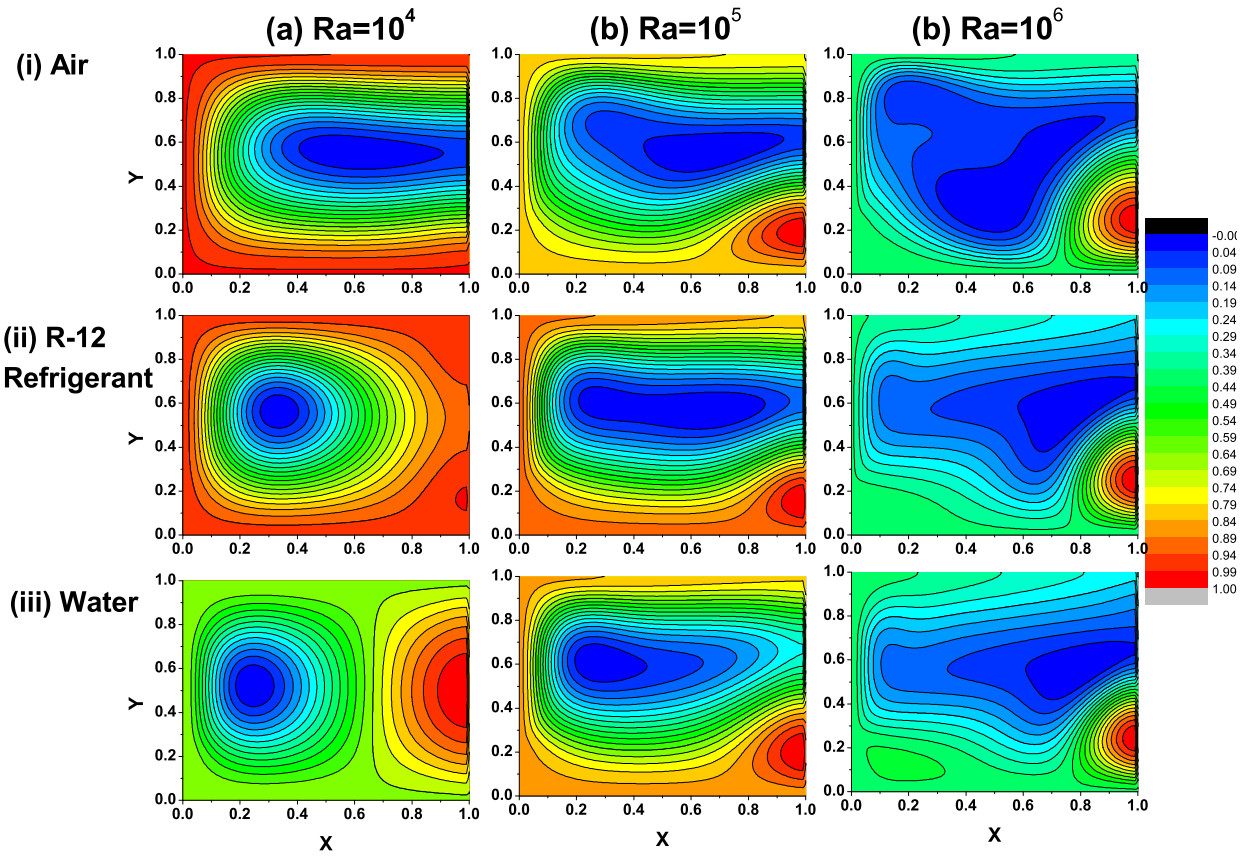

FIGURE 9.18: Isotherm patterns for different Rayleigh numbers and fluids.

heated part due to buoyancy effect.

The influence of Rayleigh number on natural convection in open ended cavity is illustrated in the form of isotherms (temperature contours). Figure 9.17 illustrates the isotherm patterns for range of physical parameters considered herein. It can be observed that with the increase in Prandtl number, isotherms become more confined (dense clustering of isotherm lines) towards heated part of west wall ($X = 0$). This is due to increase in viscosity causes low penetration of heat. The increase in Rayleigh number causes increase in circulation of fluid in the cavity and reduces the thickness of boundary layer. A constant temperature zone is created in the center of cavity, due to quasi-motionless elliptical region for all considered fluids herein. It is suggested by parallel isotherm lines to horizontal axis. For three considered fluids, isotherm patterns are nearly same for $Ra = 10^5$, only change is observed at lower half of cavity. For water, the isotherms distribution is observed to be concentrated along upper half of domain, while lower half of cavity is filled with low temperature fluid. For $Ra = 10^5$, the region of low temperature fluid is found to be

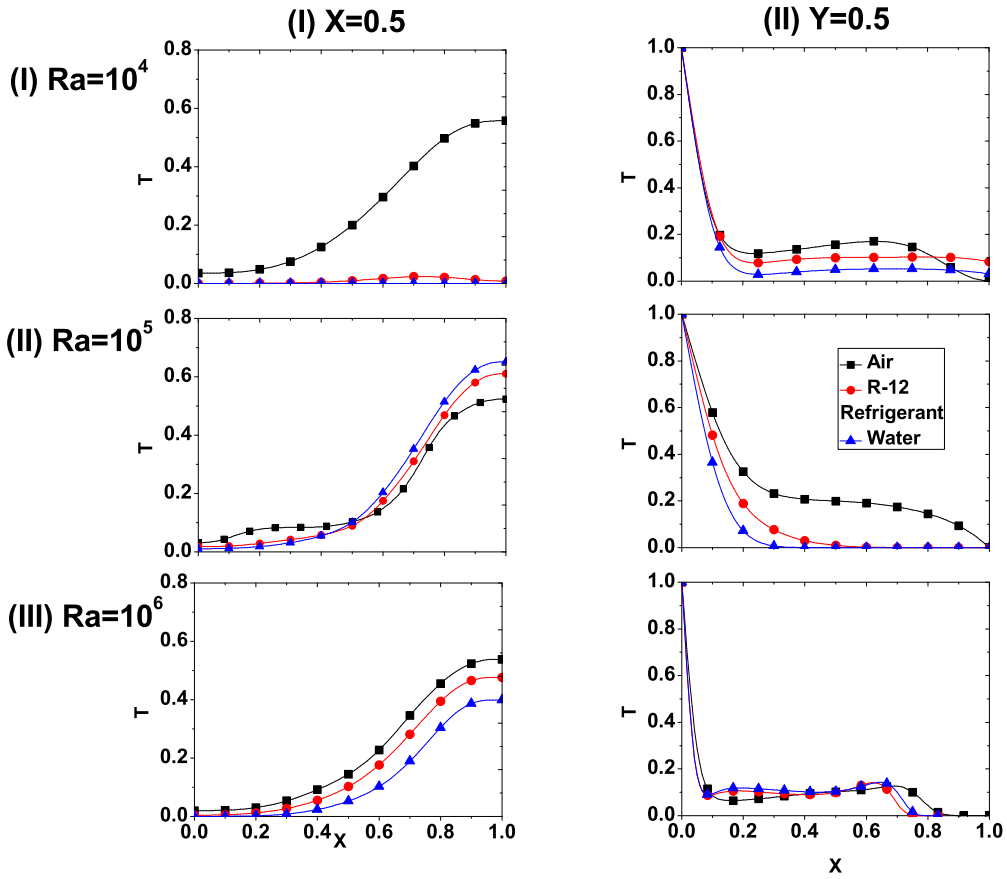

FIGURE 9.19: Temperature distribution plotted at vertical and horizontal center-line of cavity for Rayleigh numbers of $10^4 \leq Ra \leq 10^6$ and different fluids.

minimum for air, followed by R-12 refrigerant. Further the increase in heat intensity (i.e., Rayleigh number), fluid leaving through part of open end i.e., $(X = 1)$ of cavity decreases. This behavior can be illustrated from streamline patterns (Figure 9.18). In order to delineate the influences of the flow governing parameters on the flow field, the stream-function is normalized as follow:

$$\psi^* = \frac{\psi - \psi_{min}}{\psi_{max} - \psi_{min}} \tag{9.7}$$

At lowest considered Rayleigh number ($Ra = 10^4$), elliptical quasi-motionless region is created in the center of cavity, due to clockwise movement of fluid for air as working fluid. For R-12 refrigerant, which has higher momentum diffusivity than thermal diffusivity,

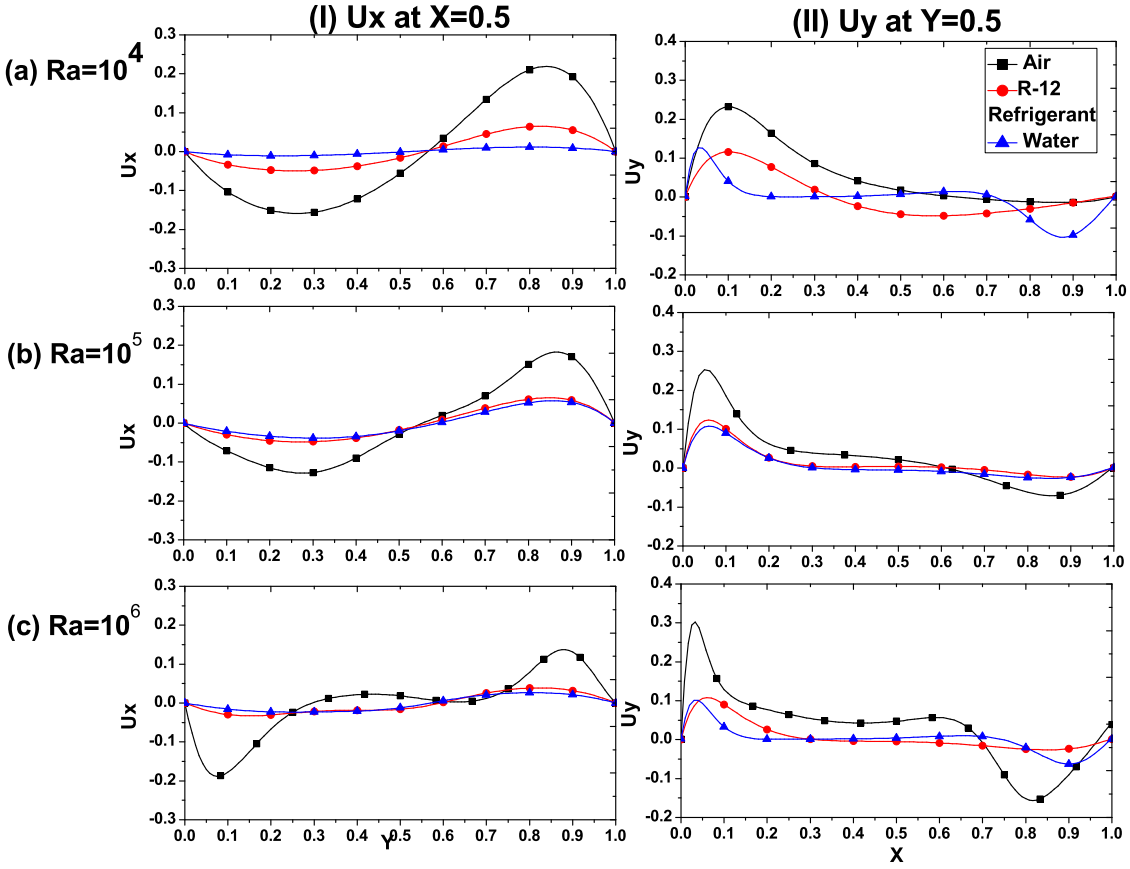

FIGURE 9.20: Velocity components plotted at (U_x) plotted at $X = 0.5$ and vertical component of velocity (U_y) plotted at $Y = 0.5$ for Rayleigh numbers of $10^4 \leq Ra \leq 10^6$ and different fluids.

isotherms become more stratified towards partially heated part of active wall. It creates a low temperature fluid zone at lower and upper part of open end of cavity. Further increasing Prandtl number to 7 (water), due to relatively higher momentum diffusivity, bifurcation of streamlines occurs, due to splitting into low (near open end) and high (heated wall end) temperature fluid region. The increase in Rayleigh number (i.e., heat intensity) causes higher circulation of fluid along active walls, the area of quasi-motionless region elongates towards the open end of cavity for all considered fluids. As fluid accelerates along heated wall of wall, formation of convection cell take place near lower open end of cavity. A larger convection cell is observed for air as a working fluid followed by R-12 refrigerant and water. Further physical insights of the flow characteristics are analyzed with the help of center-line temperature and velocity profiles.

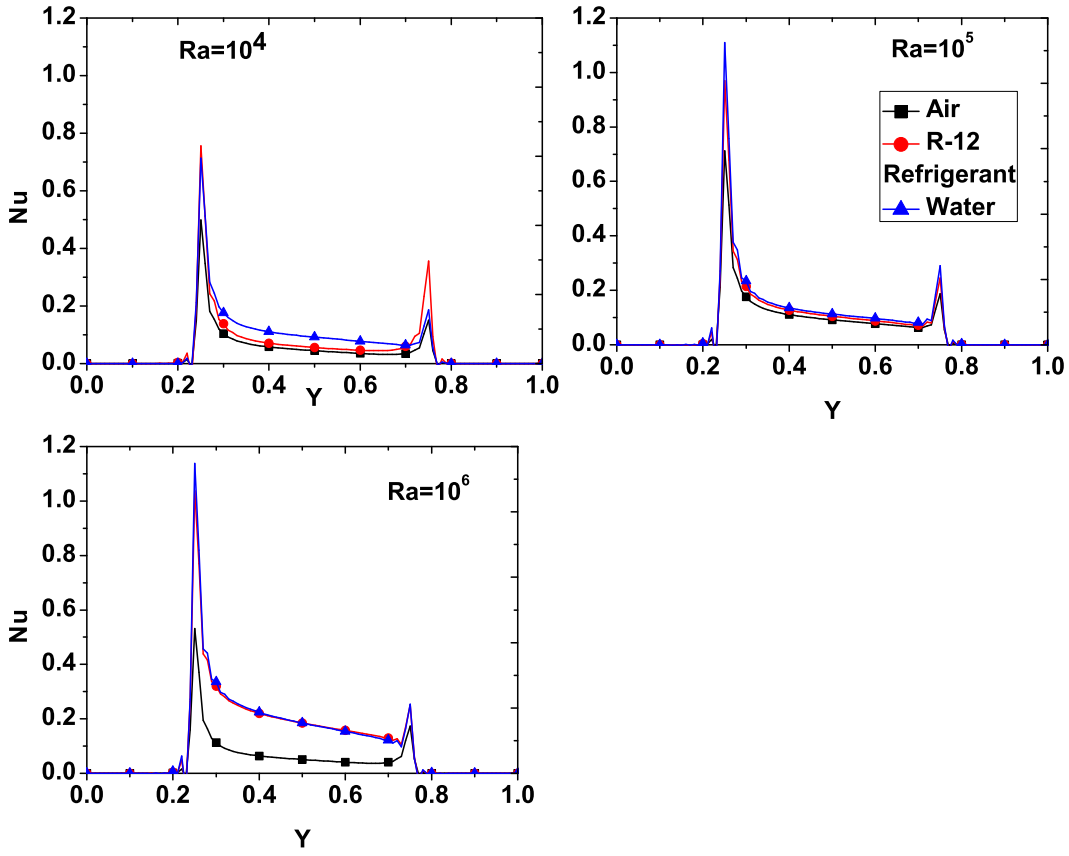

FIGURE 9.21: Local Nusselt number variation along partially heated wall ($X = 0$) for different fluids and Rayleigh numbers.

In order to get clear idea of flow and thermal behavior in the center of cavity, center-line profiles of velocity components and temperature are plotted. Figure **??** represents the temperature profile plotted along vertical (Fig. 9.19, I) and horizontal (Fig. 9.19, II) center-line of cavity. At low Rayleigh number ($Ra = 10^4$), for air as working fluid, linear increase in temperature is observed. For vertical center-line ($X = 0.5$) of temperature For other two fluids, temperature is observed to very less because of higher momentum diffusivity and weak convection. The increase in convection effect causes rise of fluid temperature as discussed before. Thus for higher Rayleigh number ($R \geq 10^5$), all fluids show rise in temperature along vertical center-line. The temperature variation along horizontal center-line of cavity is illustrated in Figure (9.19, II). From isotherm patterns, it can be seen that, at Y=0.5, temperature profile shows linear decrease and then become parallel to horizontal axis. Temperature becomes parallel to horizontal axis because of

elliptical quasi-motionless region. For higher Rayleigh number ($Ra = 10^6$), temperature distribution is nearly same along horizontal center-line, which is explained from isotherm distribution. Isotherm distribution for $Ra = 10^6$, is nearly same for all three fluids.

Figure 9.20 represents U_x plotted along horizontal ($X = 0.5$) axis (Fig. 9.20, I) and U_y plotted along vertical ($Y = 0.5$) axis (Fig. 9.20, II). In general, the horizontal velocity U_x plotted at $X = 0.5$ originates from zero and attains its minimum value. It is followed by the gradual increase until it reaches to a maximum value and which further drops down to the zero values, and therefore, representing the flow circulation, irrespective of the flow governing parameters. Out of three fluids chosen for study, air shows maximum circulation, followed by R-12 refrigerant and water. The increase in Rayleigh number causes shifting of maxima and minima peaks near west and east walls. This is due to increase in the size of quasi-motionless region. U_y profile along vertical center-line is shown in Figure (9.20,II). The U_y velocity profile shows maxima first then minima, which is reverse pattern of U_x at $X = 0.5$. It also shows the stronger as well as complex effect of different fluids (Prandtl number) at large values of Ra. The stronger and complex dependence of flow characteristics on the dimensionless flow governing and parameters shall also influence on the heat transfer rate. These are presented and discussed in the ensuing sections.

9.2.3.2 Heat transfer rate

The rate of heat transfer is delineated by analyzing the variation of local (Eqn. 3.29) and average Nusselt number (Eqn. 3.30) calculated at the heated wall. The Nusselt number (Nu) or local heat flux is considered as an important physical parameter signifying the heat transfer rate. Local as well as average Nusselt are plotted for open ended cavity with different fluids for Rayleigh number of $10^4 \leq Ra \leq 10^6$. Figure 9.21 represents the local Nusselt number variation along partially heated wall for range of conditions covered herein. At low Rayleigh number, as discussed in previous section isotherm distribution is thin with thick thermal boundary layer indicating low rate of heat transfer. The increase in Rayleigh number, thermal boundary layer becomes thin with dense and stratified isotherms along

hot wall, indicating higher temperature gradient, implying higher rate of heat transfer. For lowest considered Rayleigh number, Nusselt number values remain in the range of $0.2 - 0.4$ for three fluids implying weak convection and hence low rate of heat transfer. Nusselt number values shown proportional increase with Rayleigh number due to increased convection effect. The local Nusselt number (Nu) is seen to have a complex dependence over the ranges of the flow governing parameters accounted herein. A sharp peak can also be seen in Figure 9.21, which are clear representation of the sharp changes in thermal gradients at those spatial locations due to the sudden change in the temperature from a heating mode to ambient mode and vice versa. The sharp gradients ultimately leads to the higher heat transfer at such locations. The higher Nusselt number values are obtained for water followed by R-12 refrigerant and air. Further, average Nusselt

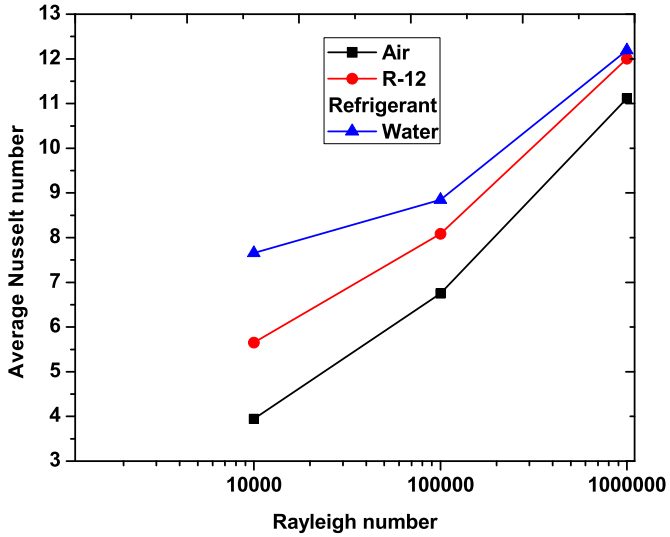

FIGURE 9.22: Average Nusselt number values estimated for different fluids and different Rayleigh numbers.

number values (Eq.(3.30)) can be obtained by integrating local Nusselt number values along active wall. Figure 9.24 shows average Nusselt number ($\overline{Nu}$) values estimated at partially heated wall ($X = 0$) for different Rayleigh number ($10^4 \leq Ra \leq 10^6$). It can be seen that the enclosure filled with water shows higher average Nusselt number values implying higher heat transfer rate than other two fluids. The cavity containing air shows lowest heat transfer rate. Further, average Nusselt number values of open ended cavity

TABLE 9.7: Estimated average Nusselt number ($\overline{Nu}$) values for different Prandtl and Rayleigh numbers.

Prandtl number	$Ra = 10^4$	$Ra = 10^5$	$Ra = 10^6$
0.71	2.921	5.385	9.308
1	3.018	5.446	9.505
2	3.124	5.504	10.01
3	3.201	5.746	10.17
4	3.251	5.788	10.27
4.5	3.743	6.149	10.32
5	3.899	6.309	10.34
6	4.371	6.555	10.38
7	5.170	6.744	10.45

with complete heated wall are also provided for comparing heat transfer rate. Thus, open ended cavity containing water facilitates the heat transfer. Besides this, simulations have been carried out to analyze the influence of Prandtl number variation ($0.71 \leq Pr \leq 7$) for range of Rayleigh number considered herein. Table 9.7 represents the average Nusselt number values for range of physical considered herein. It can be observed that $\overline{Nu}$ shows linear increase with both Prandtl and Rayleigh number.

9.2.3.3 Empirical correlation

For the scientific and engineering applications, it is worth to develop a simple closure empirical relationship presenting the functional dependence of the heat transfer rates (in case of heat transfer studies) on the dimensionless flow governing parameters.

Before presenting the empirical correlation for present work, a comparison of numerical results of the limiting case of present problem, i.e., the natural convection in open ended cavity with completely heated wall have analyzed. Table 9.8 represents the some empirical relationship of heat transfer rate with flow governing parameters from previous studies (Balaji and Venkateshan, 1994; Lal and Reji, 2009; Juarez et al., 2011; Prakash et al., 2012; Prakash, 2013). An analysis of Table 9.8 suggests that, for most of the studies of natural convection in open end cavity, the exponent of Rayleigh number is found to be close to ≈ 0.2.

TABLE 9.8: Empirical correlations developed in few previous studies of natural convection in open end cavity.

Source	Average Nusselt number ($\overline{Nu}$)		
	Correlation given	Correlation reduced to present domain	Range of parameters
Balaji and Venkateshan (1994)	$0.426Gr^{0.254}$	$0.426(Ra/Pr)^{0.254}$	$10^4 \leq Ra \leq 10^8$ $Pr = 0.71$
Lal and Reji (2009)	$0.95Ra^{0.19}(cos\delta)$	$0.95Ra^{0.19}$	$10^4 \leq Ra \leq 10^8$ $Pr = 0.7$ $0 \leq \delta \leq 60$
Juarez et al. (2011)	$-2.0926 + 0.5011Ra^{0.2584} - 0.1045\epsilon^{0.5916}$ $-0.0698Ra^{0.2584}\epsilon^{-0.1045}$	$-2.0926 + 0.5011Ra^{0.2584} - 0.1045$ $-0.0698Ra^{0.2584}$	$10^4 \leq Ra \leq 10^7$ $0.03 \leq \epsilon \leq 1.6$ $Pr = 0.7$
Prakash et al. (2012)	$0.0136Ra^{1/3}(1 + cos\theta)^{2.72}\left(\frac{d}{D}\right)^{0.72}$	$0.0136Ra^{1/3}$	$10^8 \leq Ra \leq 10^9$ $Pr = 0.7$ $0^o \leq \theta \leq 90^o$ $0.25 \leq (d/D)a \leq 1$
Prakash (2013)	$0.513Ra^{0.252}$	$0.513Ra^{0.252}$	$4.5 \times 10^5 \leq Ra \leq 1.5 \times 10^9$ $Pr = 0.7$

(ϵ: Non-dimensional temperature difference, δ: Tilt of cavity)
(θ: cavity inclination, d/D: opening ratio of cavity)

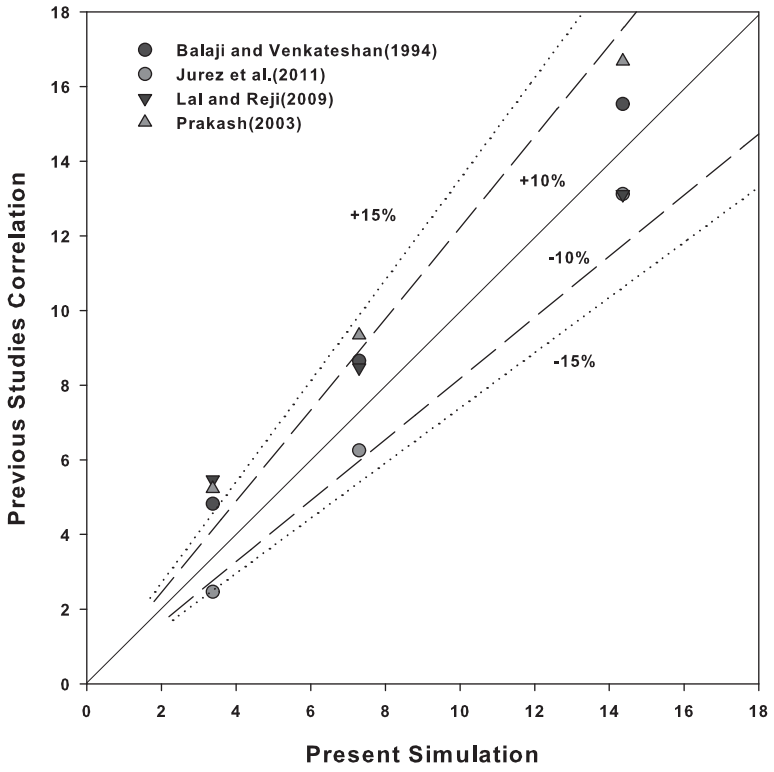

FIGURE 9.23: Comparison between simulated and predicted average Nusselt number values from previous studies correlations (as shown in Table 9.8).

Figure 9.23 shows the comparison between the present simulation data with previous studies. It can be observed that all correlations shown remarkable agreement with present simulation data of open ended cavity with complete heating. It gives us confidence to develop a empirical relationship encompassing heat transfer rate ($\overline{Nu}$) with Rayleigh (Ra) and Prandtl number (Pr). A standard closure relationship for present simulation results for heat transfer is given in the following form.

$$\overline{Nu} = 0.9276 Ra^{0.1733} Pr^{0.2157} \tag{9.8}$$

Figure 9.24 presents a parity plot between the average Nusselt number $\overline{Nu}$ obtained from simulation and predicted by Eq. (9.8). The results obtained from Eq. (9.8) is of an average error of 10.5%. Maximum deviation between predicted and simulated results is observed for highest considered Rayleigh number ($Ra = 10^6$), which is 17.8%. Further, the normalized percentage standard deviation ($\%\delta_N$) between simulation and correlation

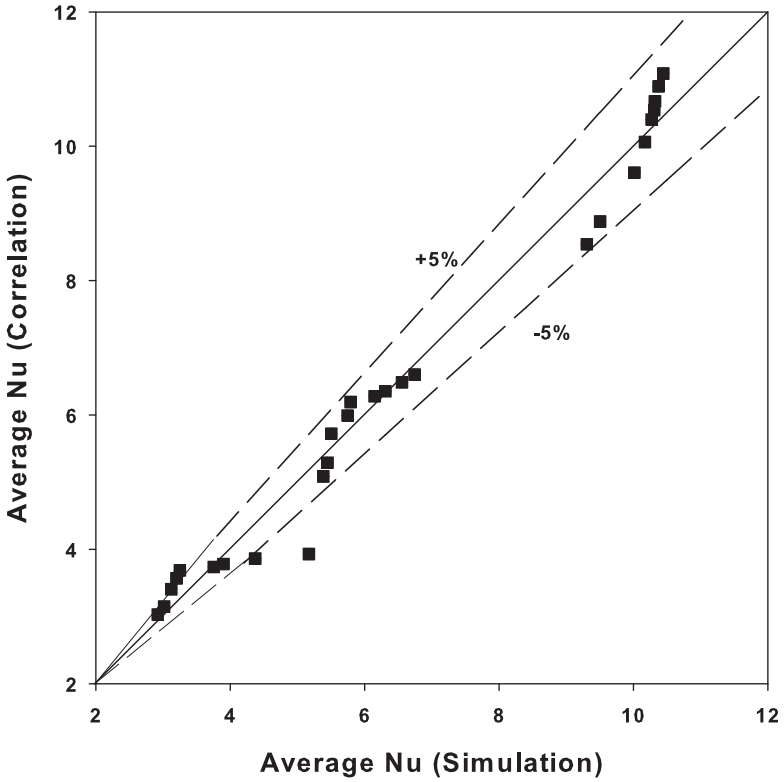

FIGURE 9.24: Comparison between simulated and predicted average Nusselt number values by Eq. 9.8.

values can be obtained by using following equation as given by Singh et al. (2008) as given below:

$$\%\delta_N = 100\sqrt{\frac{\sum\left[\frac{Nu_{simu}-Nu_{pred}}{Nu_{simu}}\right]^2}{N}} \tag{9.9}$$

where, Nu_{simu} and Nu_{pred} represents the average Nusselt number values obtained from simulation (as given in Table 9.7) and predicted by empirical correlation (Eq. 9.9). N represents the number of simulations performed (in present study, N=27). The normalized percentage standard deviation for present study is found to be $\%\delta_N = 7.427$, which is well within the permissible value of $\pm 10\%$.

9.3 Concluding remarks

The numerical investigation of laminar natural convection in an open ended square enclosure with partially heated wall by thermal lattice Boltzmann method (TLBM) is carried out. Natural convection effect on three different fluids viz., air ($Pr = 0.71$), R-12 refrigerant ($Pr = 4.5$) and water ($Pr = 7.0$) contained in partially heated enclosure have been investigated for range of Rayleigh number ($10^4 \leq Ra \leq 10^6$). The length of heater is kept constant at half of characteristic length ($L_h/2$) in mid of cavity. The validation of present numerical method with literature has shown excellent agreement. From this study, following conclusions can be drawn:

1. For a particular Rayleigh number (Ra), with the increase in Prandtl number, isotherm become confined to heated part of wall. The effect of different fluids (i.e., Prandtl number) on isotherms at higher Rayleigh numbers ($Ra \geq 10^5$) is nearly same. The visible difference is observed at lower horizontal half of the cavity.

2. At $Ra = 10^4$, streamline patterns remarkably vary for three chosen fluids. In particular, the quasi-motionless region formed due to clockwise circulation differs for fluids considered in this study. Air has elliptical quasi-motionless region. whereas, R-12 refrigerant and water has circular one, shifted towards the heated part of wall. This effect is observed due to higher momentum diffusivity for these two fluids than air.

3. For all considered fluids, at higher Rayleigh number ($Ra \geq 10^5$), the central quasi-motionless region elongates and formation of low temperature convection cell is formed at bottom of open end of cavity.

4. Linear increase in average Nusselt number ($\overline{Nu}$) is found with Rayleigh number for all three working fluids.

5. For all considered range of Rayleigh number, cavity filled with water shown higher heat transfer rate followed by R-12 refrigerant and air.

6. The functional dependence of average Nusselt number ($\overline{Nu}$) with Rayleigh number (Ra) and Prandtl number (Pr) is obtained by developing simple closure relationship.

7. The normalized percentage standard deviation for Nusselt number values for the range of Rayleigh and Prandtl number considered herein, is $\%\delta_N = 7.427$.

Chapter 10

NATURAL CONVECTION IN SQUARE CAVITY WITH BUILT-IN HEATED SQUARE BLOCK

In this chapter, the physical insights of the square cavity containing heated square body at its center is delineated for natural convection heat transfer. Numerical results are obtained for range of the Rayleigh ($10^4 \leq Ra \leq 10^6$) and Prandtl numbers ($Pr = 0.71, 5, 10$). The rate of heat transfer is expressed by calculating the average Nusselt number values.

10.1 Problem description

Consider natural convection heat transfer in a square cavity ($AR = 1$) with vertical walls ($X = 0, 1$) exposed to ambient (T_C) containing heated square block ($T_H > T_C$) at its center (as shown in Figure 10.1). The top and bottom walls are maintained adiabatically.

A heated square block is placed at the center of cavity with side length of $L_s = \beta H$. For solution of natural convective heat transfer phenomenon, the Boussinesq approximation is considered. The study is carried out for three cases, i.e., cavity containing different fluids with Prandtl numbers of $Pr = 0.71, 5$ and 10. The influence of Prandtl number on natural convection heat transfer have been explored for laminar range of Rayleigh number ($10^4 \leq Pr \leq 10^6$) and for $\beta = \frac{4}{25}$. The governing equations (in dimensional and

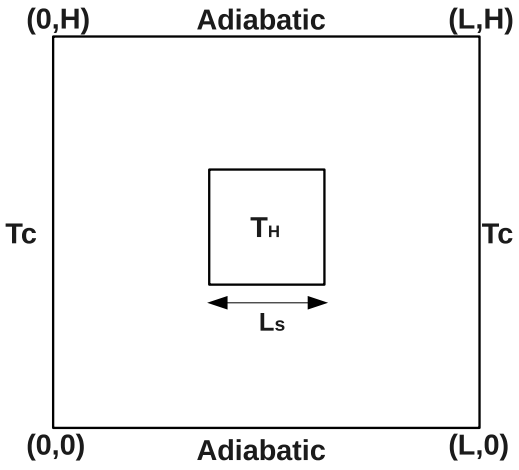

FIGURE 10.1: Schematic representation of the square cavity containing heated square block and boundary conditions.

dimensionless forms) along with general simplifications are expressed in Chapter 3. The physical realistic boundary conditions in non-dimensional form are expressed as below:

- At the west ($X = 0$) wall,

$$U_x = U_y = 0; \quad \theta = 0; \tag{10.1}$$

- At the east ($X = 1$) wall,

$$U_x = U_y = 0; \quad \theta = 0; \tag{10.2}$$

- At the bottom ($Y = 0$) and top ($Y = 1$) walls,

$$U_x = 0, U_y = 0; \quad \frac{\partial \theta}{\partial Y} = 0 \tag{10.3}$$

- Centrally placed heated square block,

$$U_x = U_y = 0; \quad \theta = 1; \tag{10.4}$$

10.2 Results and discussions

In this chapter, the influence of three Prandtl number (i.e., different fluids) $Pr = 0.71, 5, 10$ on natural convection heat transfer and fluid flow characteristics have been explored by using thermal lattice Boltzmann method for laminar range of Rayleigh numbers ($10^4 \leq Ra \leq 10^5$). For these broad ranges of flow governing parameters, the local and global convective flow characteristics such as the evolution of stream-lines, isotherms and average Nusselt number are obtained and discussed in the following sections.

10.2.1 Effect on flow field

In this section, the effect of Rayleigh number and Prandtl number (which are related to the development of boundary layer thickness) on streamline (Figure 10.2) and isotherms (Figure 10.3) is studied. It can be seen from Figure 10.2, the flow bifurcation take place from heated square block towards the opposite vertical cold wall. The fluid from half of heated block, approaches the top adiabatic wall, then it moves towards cold surface of wall due to buoyancy effect with continuous decrease in temperature of fluid. Again this cold fluid then approaches towards lower part of heated block, thus completing a circulation. Due to presence of two vertical cold walls, the fluid circulation looks like a mirror image on either side of heated block. Moreover, the circulation causes formation a single vortex. The position and size of this vortex structure differs for different Prandtl number. For instance, At lower Prandtl number ($Pr = 0.71$) and Ra=10^4, the convection effect starts dominating the conduction mode of heat transfer. The flow circulation is in elongated elliptical shape on the either side of square block (due to buoyancy effect). The further rise in Rayleigh number (Figure 10.2) increases the fluid circulation in enclosure

(rise in buoyancy effect). This causes the size of quasi-motionless region (vortex) to be reduced, due to larger circulation between hot and cold walls. From, Ra$\geq 10^5$, due to larger buoyancy effect, the streamline contours loses its symmetry about vertical center-line. The increase in Rayleigh number causes the shift of this vortex structure towards the top part of cavity. The increase in the Ra (heat intensity) significantly affects the size and position of vortex structure. At Ra=10^4, the vortex structure, formed on the either size of heated block, is vertical-elliptical shape and it is located slightly above the horizontal mid-plane of cavity. The increase in Prandtl number slightly affects the structure of the vortex structure. The increase in Prandtl number, fluid is more viscous, thus the thermal penetration is comparatively less as compared with low Pr fluids.

For, $Pr \geq 5$, due to increase in momentum thickness, the size of this vortex structure decreases, due to less thermal diffusion than viscous one. Similar effect (as of Pr=0.71) of Rayleigh numbers $Ra \geq 10^5$ on fluid pattern is observed at $Pr \geq 5$. The temperature con-

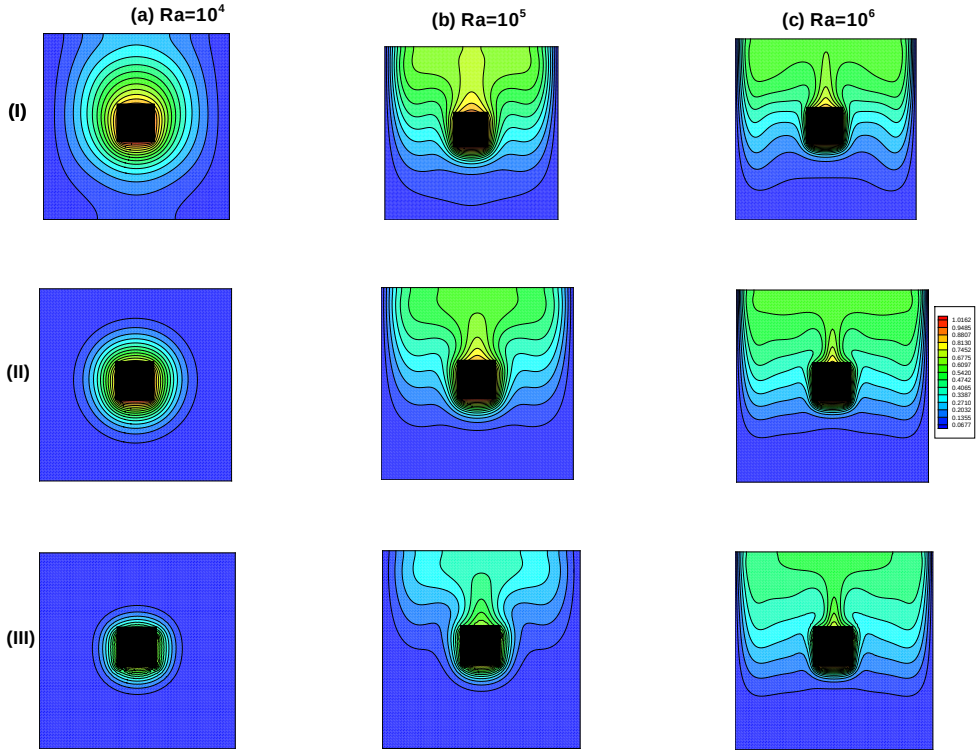

FIGURE 10.2: Influence of Prandtl numbers, (I) Pr=0.71, (II) Pr=5 and (III) Pr=10 on isotherm patterns for range of Rayleigh numbers.

tours (or isotherms) evaluated at different Prandtl and Rayleigh numbers are represented

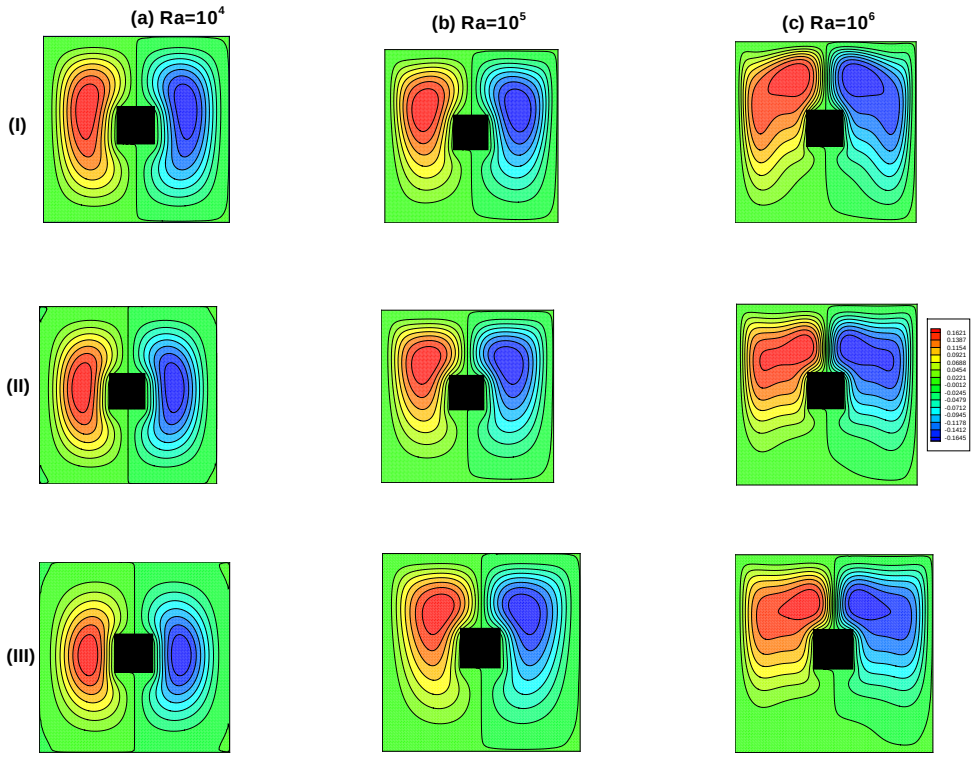

FIGURE 10.3: Influence of Prandtl numbers, (I) Pr=0.71, (II) Pr=5 and (III) Pr=10 on streamline patterns for range of Rayleigh numbers.

in Figure 10.2. At Ra= 10^4, convection effects just start dominating with symmetric fluid pattern along vertical center-line of cavity. For Prandtl number of Pr=0.71, the isotherm lines are in oval shape along the square block. It gets parallel to vertical walls from square body to vertical wall. For higher viscous fluids ($Pr \geq 5$), due higher momentum diffusivity, the isotherms become crowded along square body with dense clustering of isotherm lines, indicating higher temperature gradient (i.e., higher Nusselt number values).

The heated square body influences the shape of the isotherms and it is transferred to the fluid that carries it to the colder wall. It can be observed that isotherm lines change its value smoothly form hot square obstacle to cold vertical walls. Thus, the isotherms and streamlines are almost symmetric about the horizontal center-line As Rayleigh number increases, convection and hence buoyancy effect starts dominating. At $Ra = 10^5$ temperature distribution starts bifurcating with heated square block as center towards cold side walls. As buoyancy effect increase, it looks like temperature distribution in downwards direction from square object to side cold walls. As Ra increases, formation of a peak is

observed and is also found to be proportional to Ra. With increase in Ra, height of peak increases towards upper wall and width decreases. This phenomenon is result of increase in buoyancy effect.

With increase (Figure 10.2) in Prandtl number to 5 and 10, temperature distribution is uniform in circular shape surrounding the heated square block. This is because, higher the Prandtl number, more dominant is viscous diffusion rate than thermal diffusion rate or simply higher the Prandtl number, more is ratio of boundary layer thickness to that of thermal boundary layer. Buoyancy effect will be less, and hence the thermal distribution is along heat source in uniform pattern. At $Ra = 10^5$, isotherms are nearly same for Prandtl numbers of 5 and 10, except formation of corner eddies take place at Pr=10. At higher $Ra = 10^5$ and 10^6 , flow velocity increases, it causes stronger circulation near heated and cold walls. It can be observed that isotherms are more predominantly moving towards top walls. As discussed before, formation of peak near block in upward direction is not observed at $Ra = 10^4$ for Pr=5 and 10. As Ra increases the dominant heat transfer mechanism changes from conduction to convection and isotherms try to become horizontal near the center of cavity.

10.2.2 Average Nusselt number

The average Nusselt number ($\overline{Nu}$) estimated along each wall of built-in square block. Table 10.1 presents $\overline{Nu}$ for range of Rayleigh and Prandtl numbers. As expected the overall average Nusselt number (mean of $\overline{Nu}$) shows linear relationship with Rayleigh and Prandtl number. It can be observed that the walls of square blocks facing cold walls (left and right walls) show nearly same value of Nusselt numbers. The $\overline{Nu}$ of top and bottom walls are shows significant deviations with each other, which is due to buoyancy effect. The fluid movement takes place from heated square block in upward direction, after approaching cold wall with decrease in temperature. The drop in temperature continue till fluid comes in the vicinity of adiabatic wall, futher moves in downwards direction with

increase in temperature. Thus, higher heat transfer rate is observed at top wall of square block than bottom one.

TABLE 10.1: Average Nusselt number ($\overline{Nu}$) estimated at each wall of square body for range of Rayleigh and Prandtl numbers.

Ra	Pr	$\overline{Nu}_{west}$	$\overline{Nu}_{east}$	$\overline{Nu}_{top}$	$\overline{Nu}_{bottom}$	$\overline{Nu}_{overall}$
10^4	0.71	1.019	1.019	1.201	0.719	0.989
	5	1.312	1.312	1.439	1.166	1.307
	10	1.087	1.087	1.914	1.540	1.407
10^5	0.71	1.677	1.676	1.914	0.701	1.492
	5	1.823	1.312	1.971	0.913	1.633
	10	1.590	1.602	2.509	1.728	1.858
10^6	0.71	2.764	2.764	2.770	1.033	2.334
	5	2.821	2.821	2.716	1.369	2.433
	10	2.853	2.873	2.749	1.936	2.603

10.2.3 Empirical correlation

For present problem, the functional dependence of average Nusselt number with Prandtl and Rayleigh number is expressed in terms of an empirical correlation as given below. The mean of $\overline{Nu}$ of all four walls of heated square block is used for empirical correlation.

$$\overline{Nu}_{overall} = 0.3279 Pr^{0.1057} Ra^{0.1346} \quad (10^4 \leq Ra \leq 10^6; 0.71 \leq Pr \leq 10) \tag{10.5}$$

Figure 10.4 shows parity plot between average nusselt number values obtained by numerical simulations with that of developed empirical correlation (Eq. 10.5) from present results. It can be observed that match is excellent between two values. The average, maximum and minimum deviation between simulated and predicted values are found to be 0.47%, 23% and 0.20%. The empirical correlation can be useful for engineering applications for estimation of Nusselt number values at intermediate physical parameters (Prandtl and Rayleigh number).

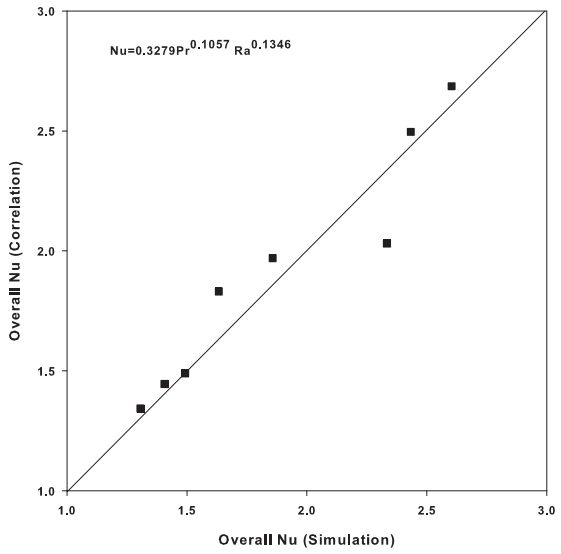

FIGURE 10.4: Comparison between simulated and predicted values (Eq. 10.5) of the average Nusselt number of heated square block.

10.3 Concluding remarks

Numerical simulations of natural convection in an enclosure containing heated square body are conducted. Passive scalar thermal lattice Boltzmann method (PS-TLBM) has been used as numerical tool for solving field equations. The numerical results are obtained for Rayleigh number $Ra = 10^4, 10^5, 10^6$ and Prandtl number of Pr=0.71,5 and 10. The results obtained can be summarized as follows:

1. For lower Prandtl numbers (Pr=0.71), temperature distribution is found to be uniform across an enclosure and is in oval shape around the heated square for $Ra = 10^4$.

2. As Prandtl number increases, isotherms becomes densely crowded along heated square block.

3. As Rayleigh number increases, isotherms become parallel to horizontal wall of enclosure with formation of a peak (a thermal plume) from top walls.

4. At higher Prandtl, isotherms pattern remains nearly same for given Rayleigh numbers, only change is observed in central peak of isotherms towards top wall.

5. Average Nusselt number shows linear variation with Rayleigh and Prandtl numbers.

6. An empirical correlation is developed and presented herein.

Chapter 11

WALL EFFECTS ON FORCE CONVECTIVE HEAT TRANSFER FROM HEATED BUILT-IN RECTANGULAR CYLINDER

In this chapter, the influences of wall confinement ($1/8 \leq \beta \leq 1/20$), Reynolds number ($5 \leq Re \leq 40$), aspect ratio of rectangular cylinder ($1 \leq a_r \leq 6$) on forced convection heat transfer characteristics of channel built-in rectangular cylinder are investigated.

11.1 Problem description and boundary conditions

Consider a two dimensional, steady, laminar flow of incompressible Newtonian fluid across a built-in rectangular cylinder with uniform velocity and temperature (U_∞, T_∞). The surface of square cylinder with side b is maintained at constant temperature of $T_W (> T_\infty)$ as shown in Figure 11.1. The blockage ratio is defined by the ratio of size of square cylinder (b) to the height of channel (H), i.e., $\beta = \frac{b}{H}$. The square cylinder is placed at a sufficient

distance from inlet ($L_u = 10$), such that it remains free from The thermo-physical properties of the fluid (thermal conductivity (k), density (ρ), heat capacity (c_p)) are considered to be a independent of the temperature and viscous heat dissipation effects are neglected (Bharti et al., 2008). The assumption of constant thermo-physical properties and neg-

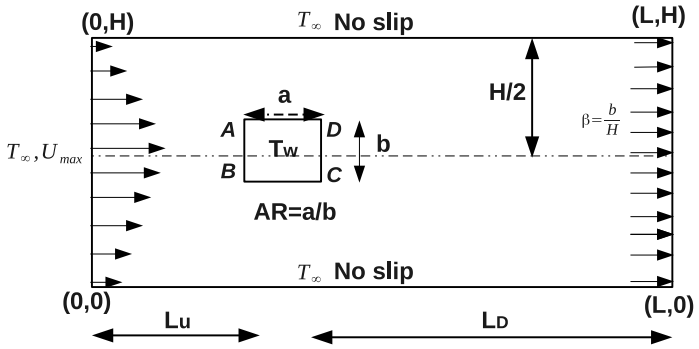

FIGURE 11.1: Schematic representation of confined flow past a square cylinder (physical as well as computational domain).

ligible viscous heat dissipation lead to decoupling of momentum and energy equations. These approximations restrict the applicability of the present numerical simulation to the situations where the temperature difference ($\Delta T = T_W - T_\infty$) is not too large and/or for moderate viscosity and/or shearing levels so that the viscous dissipation effects are negligible (Srinivas et al., 2009). The temperature difference is maintained small to justify the accountability of the variation of the fluid viscosity with temperature. The governing equations (in dimensional and dimensionless forms) along with general simplifications are expressed in Chapter 3. The boundary conditions are mentioned in Figure 11.1.

11.2 Choice of numerical parameters

It is very well known that numerical/computational parameters (such as mesh and domain sizes) have significant effects on the reliability and accuracy of the numerical results. Therefore, an accurate choice of the numerical parameters, namely, the upstream and downstream lengths and grid size is foremost before presenting the new results. In present work, the height of square cylinder (b) is used for characterizing the domain size. The choice of grid size and effect of upstream length are addressed in this section.

11.2.1 Grid independence study

In order to ensure the accuracy and reliability of present code, grid independence study is carried out based on drag coefficient as well as average Nusselt number ($\overline{Nu}$) of heated square cylinder. In this study, the adequacy of five uniform lattice sizes (grids) on side of square cylinder, ($G1 : 16$,$G2 : 18$,$G3 : 20$,$G4 : 30$,$G5 : 40$) have been examined (as shown in Figure 11.2). It is observed that relative error between coarsest grid ($G1 : 16$) with respect to finest grid ($G5 : 40$) is around $0.90\%, 0.76\%$ and $4.5\%, 2.62\%$ for drag coefficient (C_D) and mean Nusselt number values $\overline{Nu}_{mean}$, respectively for $\beta = 1/8, 1/20$. The relative error between grid sizes $G1$ to $G2$, $G2$ to $G3$, $G3$ to $G4$ and $G4$ to $G5$ in drag coefficient (C_D) values for blockage ratio of 1/8 and 1/20 are (0.6%0.06%0.08%0.09%) and (0.5%0.02%0.02%0.03%), respectively. Similarly, relative change in mean Nusselt number values for blockage ratio of 1/8 and 1/12 are (3.3%1.2%0.3%0.2%) and (0.6%, 0.9%, 0.45%, 0.5%), respectively. The results shown insignificant changes from grid size $G4$ onward with the enormous increase in computational time to get converged solution. Therefore, 30 lattice nodes on each side of cylinder is chosen in this study,which is found to be optimum with respect to computational time and mesh size, is chosen in this study, which is believed to be sufficiently refine enough to resolve thermal and hydrodynamic features within interested range of conditions.

11.2.2 Domain independence study

The proper choice of upstream and downstream length is very important in order to the keep numerical results free from entrance and end effects. In this section, the effects of upstream and downstream length on flow field have been investigated.

A detailed examination of choice of upstream length on pressure and viscous drag coefficients have been done. The adequacy of four upstream lengths ($L_u = 8, 10, 12, 15$) at Reynolds number of $Re = 5$ and $\beta = 1/8$ have been investigated as shown in Figure **??**. It can be observed that a very minor effect on C_{DP} and C_{DF} is observed for considered upstream lengths. The percent changes in C_{DP} and C_{DF} in upstream lengths of 8 to

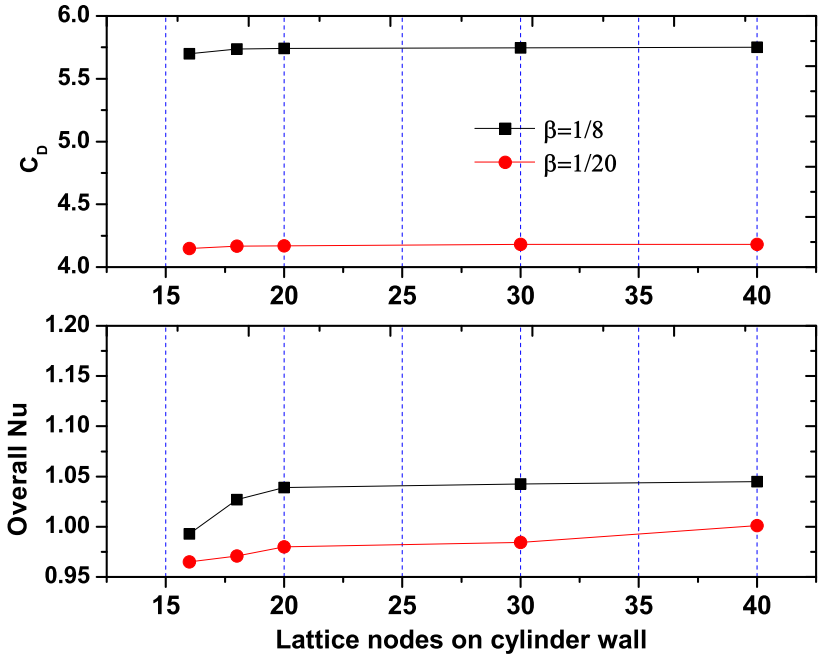

FIGURE 11.2: Grid independence results at $Re = 5$ and $\beta = 1/8, 1/20$ (a) total drag C_D and (b) overall Nusselt number for the cylinder

that of 15 is observed to be 1.2% and 2.6%. Hence, in present work, upstream length of $L_u = 10$ is used, which can be considered as sufficient enough to keep results free from entrance effects. An additional numerical experiments have been conducted to investigate the effect of uniform velocity profile at inlet. It is observed that at $L_u = 10$, insignificant changes are observed in the estimated values of C_D and $\overline{Nu}$. The total length of channel is assumed sufficiently large enough ($L = 50$) so that it does not affect flow characteristics near square cylinder. Hence, the downstream length, $L_d = 39$, which is much higher than previous studies (Dhiman et al., 2005, 2008a) is used for all considered range of conditions. The numerical parameters used in present study are: Upstream length, $L_u = 10$, downstream length $L_d = 39$, channel length, $L = L_u + b + L_d = 50$, the lattice size for domain, $50b \times b(1\ \beta)$. For present numerical simulation a uniform lattice size is chosen, which is believed to be refine enough to resolve the thermal and flow phenomenon within interested range of conditions.

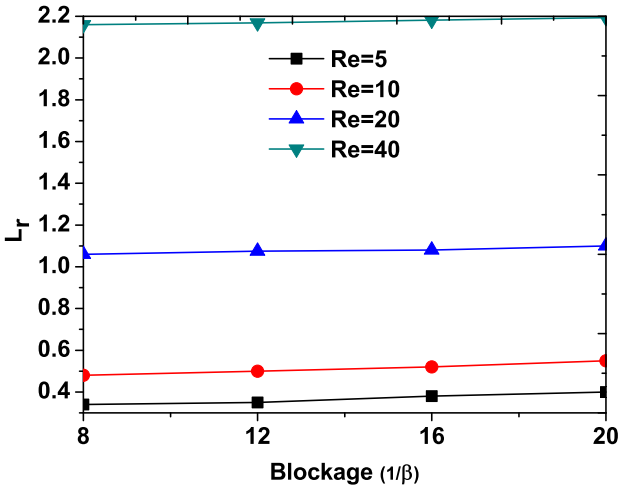

FIGURE 11.3: Estimated re-circulation length (L_r) as a function of blockage ratio (β) for different Reynolds number (Re)

11.2.3 Validation of results

The reliability and accuracy of present numerical simulation is examined by comparing the results obtained from present numerical procedure with previous reported studies. The validation is based on drag coefficient (C_D) and average Nusselt number ($\overline{Nu}$) values estimated along built-in square cylinder for all considered values of Reynolds numbers and blockage ratio ($\beta = 1/8$). For comparison purpose, $\overline{Nu}$ values are estimated at $Re = 5, 40$ and $Pr = 0.7$. Table 11.1 presents comparison between results obtained from present simulation with previous studies (Gupta et al., 2003; Dhiman et al., 2008b; Bouaziz et al., 2010).As can be seen from Table 11.1, present results show excellent agreement with literature. The minimum, maximum and average error of C_D and $\overline{Nu}$, between present

TABLE 11.1: Comparison of drag coefficient (C_D) values at different values of Re and $\beta = 1/8$ at Prandtl number $Pr = 0.71$.

Source	$Re = 5$	$Re = 10$	$Re = 20$	$Re = 40$
	C_D			
Present	5.601	3.642	2.395	1.699
Gupta et al. (2003)	5.549	3.511	2.448	1.871
Dhiman et al. (2008b)	5.849	3.633	2.442	1.752
Bouaziz et al. (2010)	-	-	2.372	1.752

results with that of literature are $(0.2\%, 8.1\%, 2.1\%)$ and $(2.1\%$ and $1.6\%)$, respectively. Moreover, the accuracy of flow past rectangular cylinder is ascertained by comparing the drag and Nusselt number values obtained by present numerical procedure at aspect ratio of $a_r = 2$, $\beta = 1/8$, Pr=1 and Re=5, 10, 20, 40 with results of Nitin and Chhabra (2005). Figure 11.4 presents the comparison between simulated and literature values of C_D and $\overline{Nu}$. It is evident that the present numerical results show excellent match with results of (Nitin and Chhabra, 2005). The present numerical simulation results are reliable in the

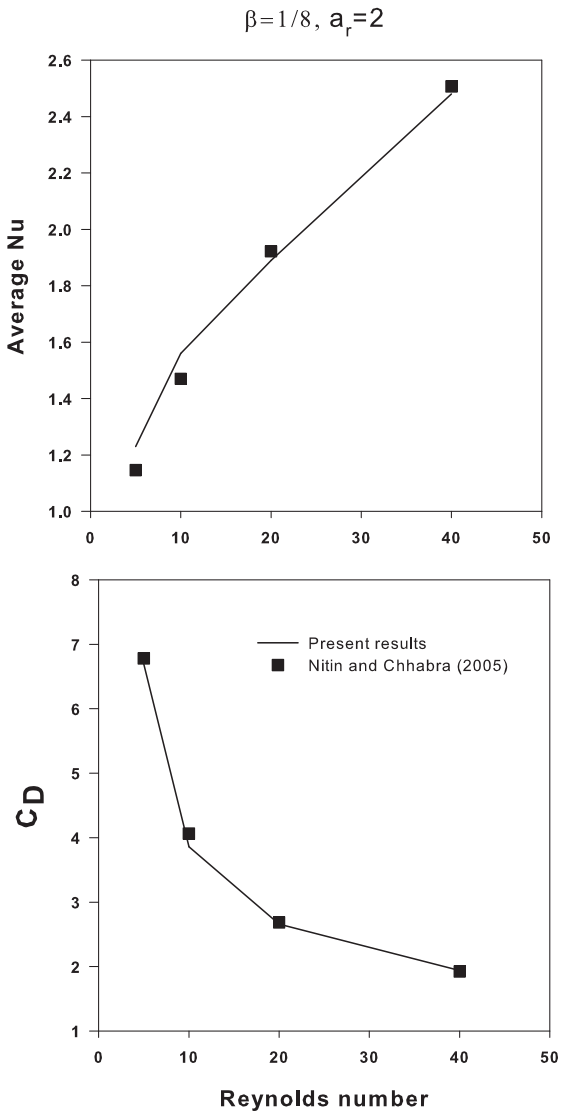

FIGURE 11.4: Comparison of present numerical results of total drag (C_D) and Nusselt numbe $\overline{Nu}$ at aspect ratio of rectangular cylinder $a_r = 2$, $\beta = 1/8$ for range of Reynolds numbers.

range of $\pm 4 - 5\%$. Such a minor errors tend to arise due to the factors such as numerical

method, grid size, convergence criterion, numerical errors (round up and programming) etc. Results presenting in this study are accurate and reliable in the range of $4-5\%$. With the above comparison between our developed code for channel flow with heated square cylinder in cross flow with the literature data, it is suffice to say that our results are quantified. This ascertains and inspires the confidence in accuracy and reliability of present in-house LBM solver. The effect of blockage ratio on forced convection heat transfer and fluid flow are discussed in next section.

11.3 Results and discussions

In the present work, the numerical computations have been carried out to investigate the steady forced convection flow and heat transfer characteristics of a channel confined rectangular cylinder by using in-house computational solver based on TLBM with D2Q9 lattice model (developed by the authors in C++ programming language) for the following ranges of the conditions: four values of Reynolds number ($5 \leq Re \leq 40$) varied as 5, 10, 20 and 40; four values of wall blockage ratio ($1/8 \geq \ \geq 1/20$, i.e.,$12.5\% \geq \ \geq 5\%$) varied as 1/8, 1/12, 1/16 and 1/20; four values of aspect ratio of rectangular cylinder ($AR = 1, 2, 4, 6$) and fixed Prandtl number (Pr = 1). Subsequently, the detailed analysis to elucidate the influences of dimensionless flow governing parameters on the the local and global convective flow and heat transfer characteristics such as the evolution of stream-function, isotherms and vorticity fields; pressure and friction coefficients; and the local and average Nusselt number has been presented and discussed herein the proceeding sections. The results and discussion section has been divided into two sections, viz., (a) forced convection from square cylinder (AR=1) and (b) forced convection from rectangular cylinder ($2 \leq AR \leq 6$).

11.3.1 Forced convection from square cylinder (a_r=1)

In this section, the flow and forced convection heat transfer characteristics of channel confined square cylinder is explored in details for wall effects and Reynolds numbers.

11.3.1.1 Effect on flow field

The local flow characteristics such as streamlines, vorticity profiles in the vicinity of the square cylinder, re-circulation length analyzed herein to gain the physical insights into the nature of the hydrodynamics features of heated built-in square cylinder in a plane channel. The influence of blockage ratio (β) on flow field in channel flow with heated

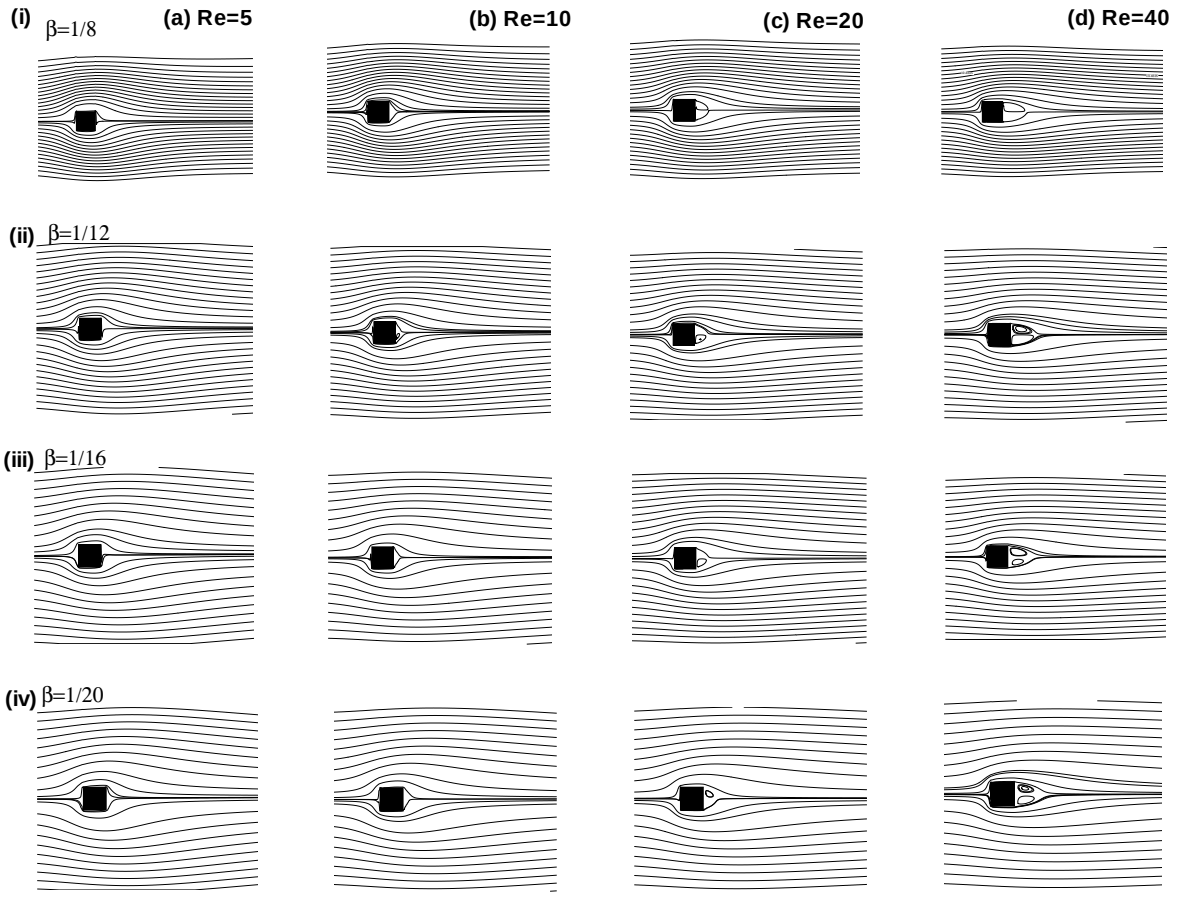

FIGURE 11.5: Streamline patterns for different Reynolds number (Re) and blockage ratio (β).

built-in square cylinder is delineated by evolution of isotherms, streamlines, vorticity,

drag coefficient, re-circulation length and pressure component variation along surface of square cylinder for interested range of conditions. Figure 11.5 represents the stream-line patterns in the vicinity of square cylinder for interested range of blockage ratio (β) and Reynolds number (Re). The blockage ratio variation slimy affects stream-line patterns for a constant Reynolds number. The increase in Reynolds number, as anticipated, increases the size of re-circulation length for a constant blockage ratio is observed. Reynolds number (Re) is parameter, implying the relative strength of inertial forces to the viscous forces. At low Reynolds number, i.e., $Re = 5$, the very little separation takes place behind the tailing edge of square cylinder due to dominant viscous forces. With the increase in Re, the flow become dominated by inertial forces. It results in the formation of a closed re-circulation zone, which compromises two symmetric vortices behind the rear face of square cylinder (Dhiman et al., 2005, 2008a; Dhiman, 2009b). For fixed values of Reynolds number (Re), the stream lines show slight change with blockage ratio. A little rise in re-circulation length is observed with the increase in blockage ratio (β) as shown in Figure 11.3. Thus, stream lines pattern show complex dependence with blockage ratio (β) and Reynolds number (Re). The stream lines pattern is more influenced by Reynolds number than blockage ratio.

The vorticity profile, as reported by (Dhiman et al., 2005, 2008a; Bharti et al., 2007) are used for locating the separation points and fluid behavior near the surface of square cylinder. Figure 11.6 shows the vorticity patterns for range of conditions considered herein. It can be observed that the increase in Reynolds number for fixed blockage ratio loss of symmetry is observed, which is consistent with previous study (Dhiman et al., 2005). For constant Reynolds number, increasing in blockage ratio results in increase in vorticity magnitude with vorticity pattern remain nearly same. At high Reynolds number, the blockage ratio variation has marginal effect on vorticity pattern. Thus, with the increase Reynolds number, blockage ratio influence becomes less pronounced.

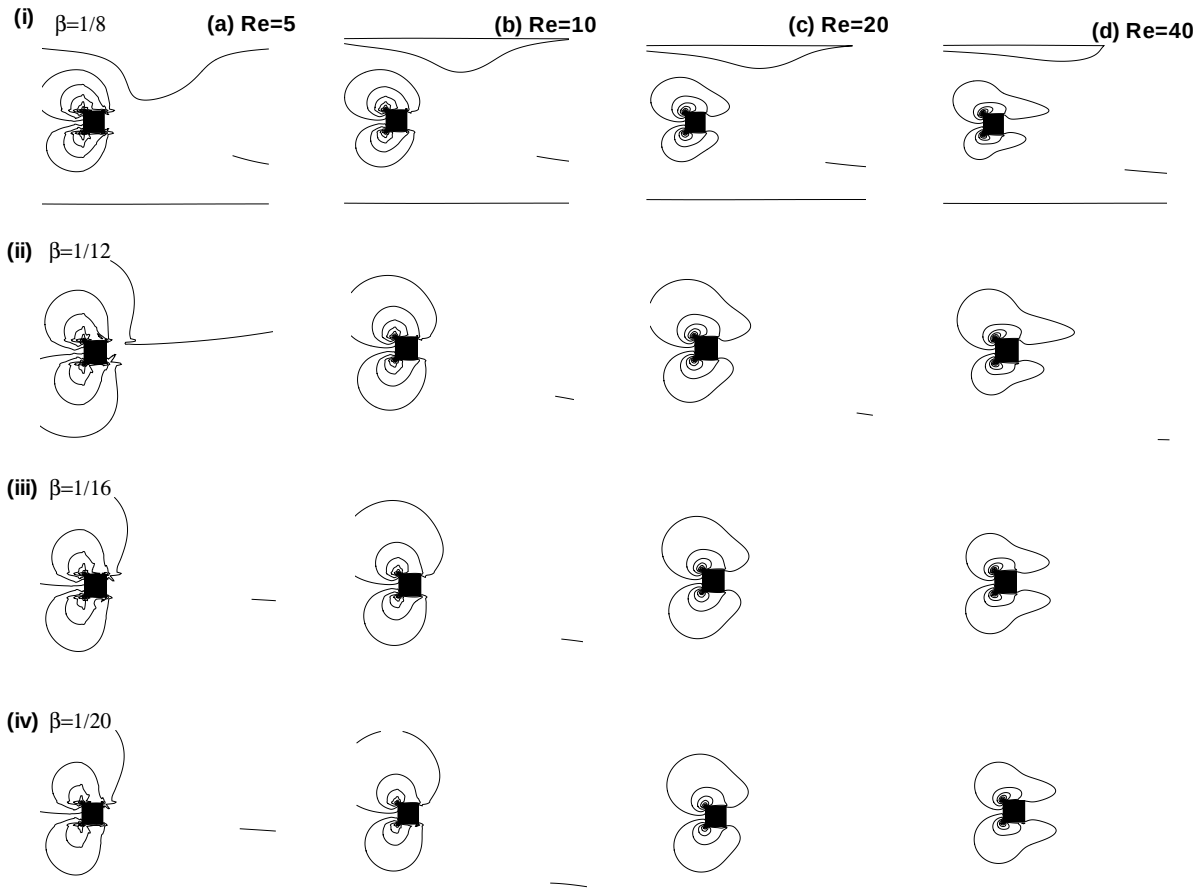

FIGURE 11.6: Vorticity patterns for different Reynolds number (Re) and blockage ratio (β).

11.3.1.2 Effect on isotherm patterns

Figure 11.7 depicts the variation of temperature distribution along the square cylinder surface. The isotherms pattern show complex dependence of the blockage ratio and Reynolds number. The nature of isotherm pattern along the heated square cylinder surface is dependent on the thickness of boundary layer. The development of boundary layer is inversely proportional to Reynolds number. At low Reynolds number, the isotherm pattern become uniformly crowded along the cylinder surface. With the increase in Reynolds number, isotherms become more confined to horizontal walls of square cylinder. Thus, due to low thickness of boundary layer, the isotherms crowding along the cylinder increases with the increase in blockage ratio, which is consistent with (Sharma and Eswaran, 2005). For the fixed value of Reynolds number, the increase in blockage ratio facilitates higher heat

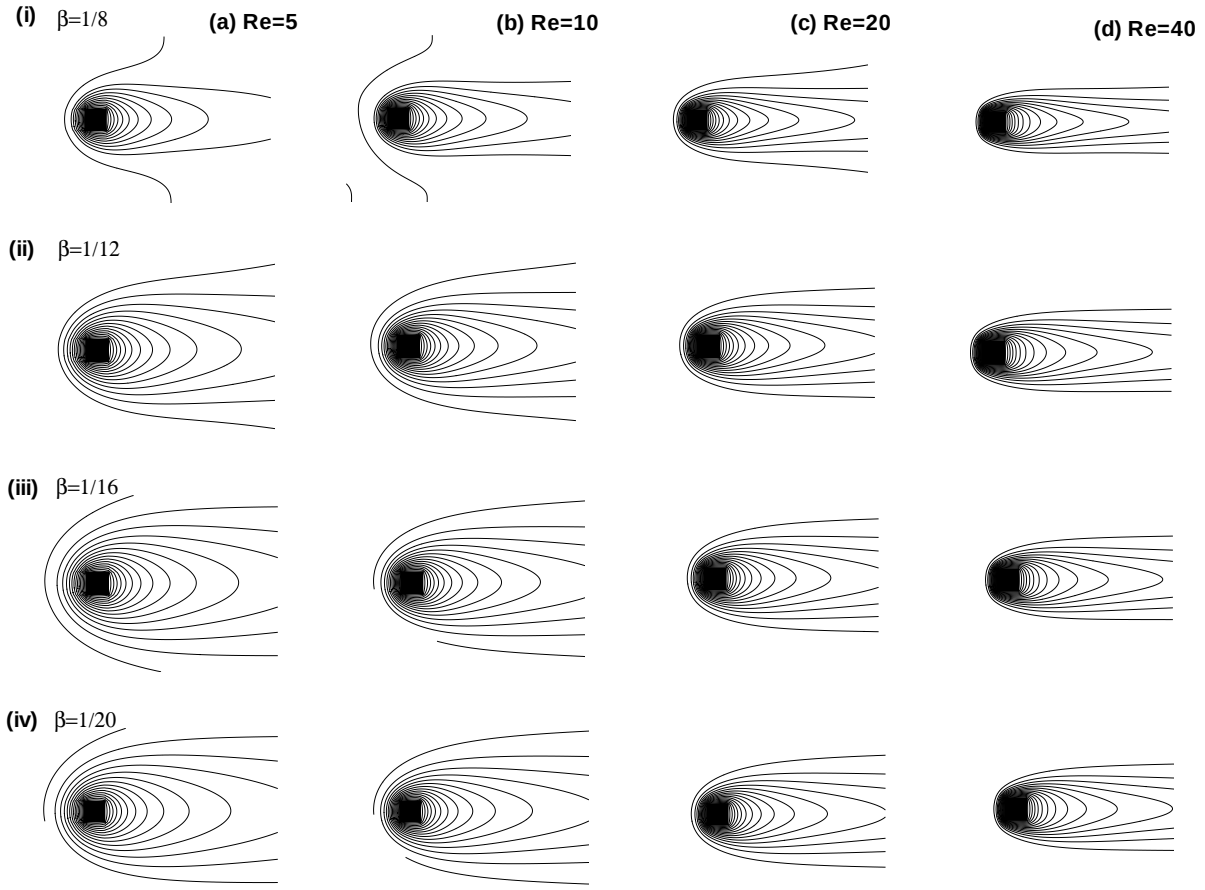

FIGURE 11.7: Isotherm patterns for different Reynolds number (Re) and blockage ratio (β).

transfer area as area between confining walls and square cylinder increases. It causes increase in the strength of isotherms. Thus, with the increase in blockage ratio causes increase in the strength of isotherm, which is also conformed by Nusselt number calculation (discussed in ensuing section).

11.3.1.3 Drag phenomenon

The drag force experienced by square cylinder in a cross flow is consist of two components, viz. pressure or form drag coefficient (C_{DP}) and viscous drag coefficient (C_{DF}). The summation of both coefficients comprise the total drag coefficient. The effect of blockage ratio (β) for different Reynolds number (Re) is represented in Table 11.2. The drag coefficient show complex dependence on blockage ratio and Reynolds number. As expected

the drag coefficient value for confined cylinder should be more than that of unconfined cylinder. Intuitively, with the increase in blockage ratio, flow behavior show more and more characteristics of unconfined cylinder flow. It can be seen that for fixed value of Reynolds number, the increase in blockage ratio (decrease in wall confinement) causes linear decrease in drag coefficient values. This is due to the fact that the increase in blockage ratio, the flow behavior become equivalent to unconfined flow causing decrease in pressure exerted on cylinder wall as well as viscous dissipation. For a constant blockage

TABLE 11.2: Drag coefficient results for square cylinder ($a_r = 1$), $Re = 5, 10, 20, 40$ at different values of blockage ratio (β) .

	$Re = 5$			$Re = 10$			$Re = 20$			$Re = 40$		
$1/\beta$	C_{DP}	C_{DF}	C_D	C_{DP}	C_{DF}	C_D	C_{DP}	C_{DF}	C_D	C_{DP}	C_{DF}	C_D
8	3.145	2.601	5.746	3.001	0.724	3.725	1.999	0.347	2.346	1.583	0.186	1.769
12	3.017	2.480	5.498	2.879	0.650	3.529	1.718	0.322	2.041	1.503	0.173	1.677
16	2.922	1.996	4.919	2.418	0.536	2.954	1.696	0.316	2.013	1.415	0.164	1.579
20	2.720	1.259	3.978	2.277	0.270	2.548	1.607	0.271	1.878	1.350	0.143	1.493

ratio, similar effect is observed in drag values with increase in Reynolds number. The increase in Reynolds number reduces the boundary layer thickness along square cylinder wall. So, it can be concluded that the Reynolds number (Re) and blockage ratio (β) have similar effect on drag values ,i.e. drag values varies in inverse manner with these two parameters. The values of pressure drag coefficient are always higher than that of viscous drag coefficient. This suggest dominant role of pressure force on square cylinder walls, which is similar with previous studies (Dhiman et al., 2006a; Dhiman, 2009b; Dhiman et al., 2005, 2008a). In order to elucidate the influence of the relative contributions of the individual components of the total drag coefficients is examined by through the drag ratio (C_{DR}) profiles.The effect of blockage ratio and Reynolds number on drag ratio ($C_{DR} = C_{DP}/C_{DF}$), is illustrated in Figure 11.8. For the fixed value of blockage ratio, the C_{DR} varies proportional with Reynolds number. In case of higher blockage ratio ($\beta \geq 1/12$), the influence of (C_{DR}) is nearly same for all Reynolds number. Hence, it can be observed that the low blockage ratio (β) has remarkable effect of normalized drag values.

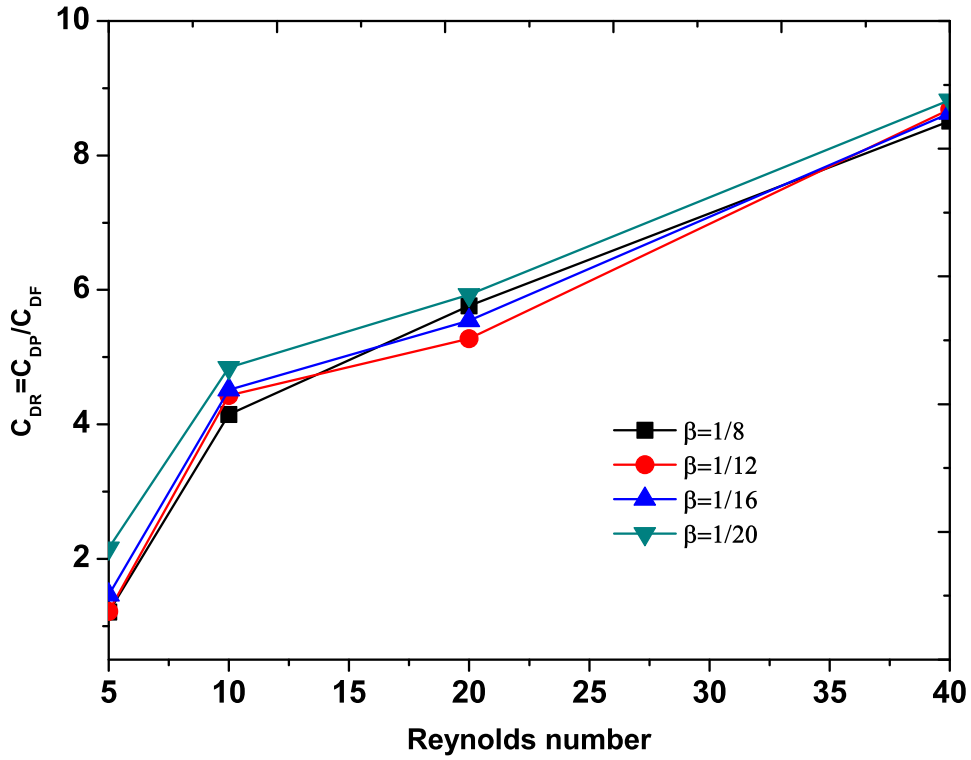

FIGURE 11.8: The variation of ratio of drag components with Reynolds number and blockage ratio.

11.3.2 Heat transfer rate

In this section variation of local as well as average Nusselt number along the surface of square cylinder is discussed. It is clear from dimensional analysis that the average Nusselt number is a function of Reynolds number (Re) and Prandtl number (Pr) and blockage ratio (β). The relationship between these parameters is explored in this section. The functional dependence between Reynolds numbering (Re), Prandtl number (Pr) and average Nusselt number ($\overline{Nu}$) is established by using the Colburn heat transfer factor (j_H).

11.3.2.1 Average Nusselt number

This is due to the fact that cold fluid first comes across front face initially than other faces, thus facilitating higher heat transfer. Low Nusselt number values are obtained at rear face of cylinder for interested range of conditions, as formation of wake impedes the rate of

heat transfer. For fixed values of Reynolds number, the Nu values decreases with the increase in blockage ratio. A monotonous trend in Nu values is observed for all Reynolds number and blockage ratio at the rear face of cylinder, which show nearly same value at rear face. As interaction of cold fluid with top and bottom surfaces of square cylinder is nearly of same magnitude, Nusselt number values along these faces of cylinder are nearly same.

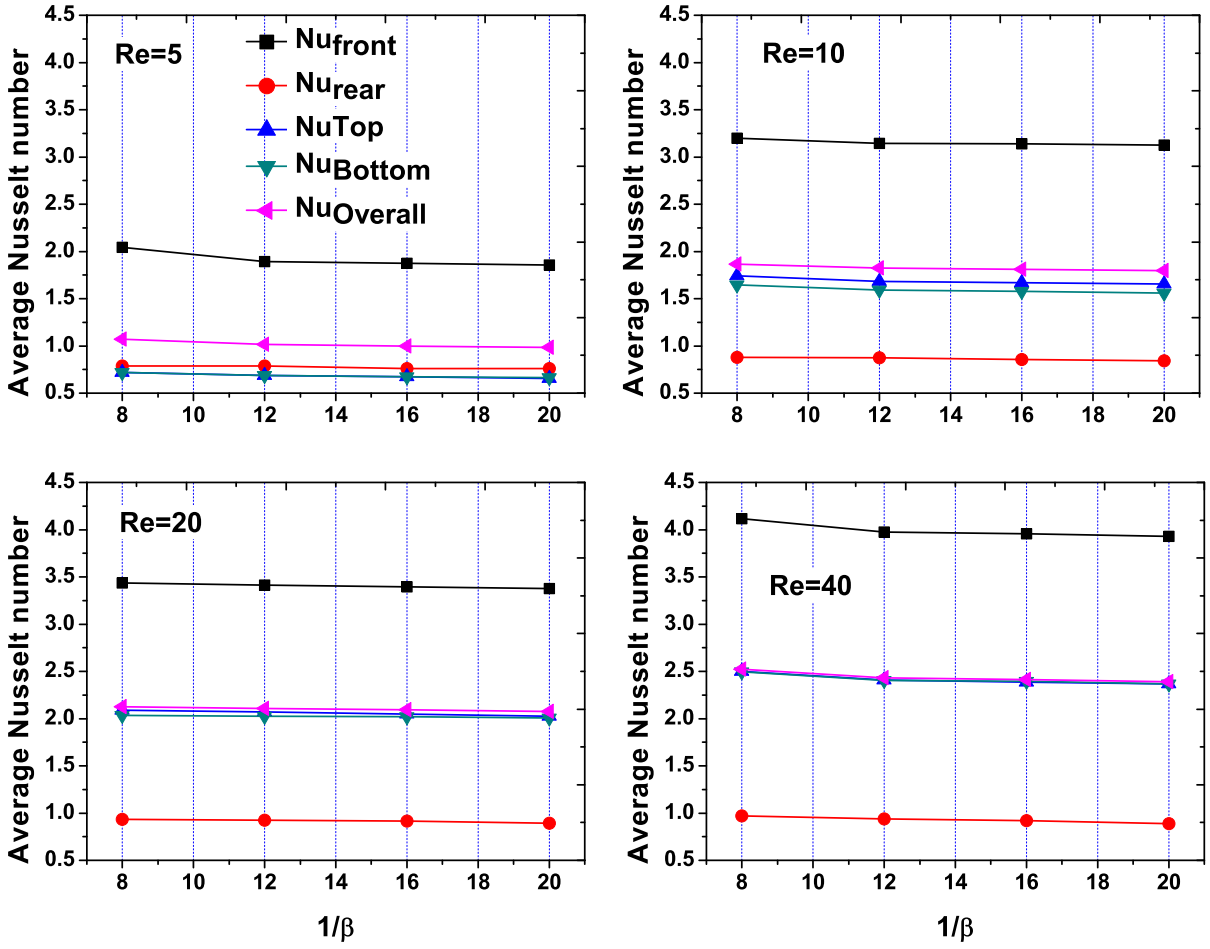

FIGURE 11.9: Average Nusselt number values estimated along each face of cylinder as well as overall Nusselt number as a function of blockage ratio (β) for different Reynolds number.

The average Nusselt number ($\overline{Nu}$) dependence on blockage ratio (β) and Reynolds number (Re) is shown in Figure 11.9. ($\overline{Nu}$) of all four sides of square cylinder along with average of all faces (overall ($\overline{Nu}$)) are represented in Figure 11.9. At constant blockage ratio, the average Nusselt number values were found to be increasing with Reynolds number. This is due to the fact that the increasing Reynolds number, contribution of convection to heat

transfer increases, which causes increase in average Nusselt number values (Bharti et al., 2007). For a fixed values of Reynolds number (Re), the average Nusselt number values marginal decline with increasing blockage ratio (decrease in wall confinement). This is due to the more heat is transferred from square cylinder to fluid for higher blockage ratio case than smaller one. But the difference in $\overline{Nu}$ values are so small, that effect of higher blockage ratios on $\overline{Nu}$ can be considered as insignificant. On the other hand, for fixed value of blockage ratio (β). ($\overline{Nu}$) is found to be vary proportionally with Reynolds number. At low Reynolds number, the heat transfer is dominated by conduction phenomenon. As expected, the increase in Reynolds number reduces the boundary layer thickness and increases convection heat transfer phenomenon.

11.3.2.2 The Colburn heat transfer factor (j_H)

In engineering practices, it is utile as well as common to use so-called the Colburn j-factor. It is expressed as given below:

$$j = \frac{Nu}{RePr^{1/3}} \tag{11.1}$$

The advantage of using Colburn factor (j_H) is that it can bring the range of values of Reynolds and Prandtl numbers in a single curve. The variation of (j_H) with the blockage ratio (β) and Reynolds number (Re) is shown in Figure 11.10. For better understanding, j_H is plotted as (a) function of Reynolds number and (b) as a function of blockage ratio. The Prandtl number chosen for present study is $Pr = 1$, due to this the $Pr^{1/3}$ vanishes and Colburn heat transfer factor becomes function of Nusselt number and Reynolds number only. As it is evident from Figure 11.10, j_H varies inverse proportion with Reynolds number and blockage ratio. It can be evident from Figure 11.10, at higher blockage ratio, i.e., lower wall confinement, j_H factor is nearly same for all interested range of Reynolds numbers. A strong dependence of Reynolds number on j_H is observed for lower blockage ratio of $\beta = 1/8$ for low Reynolds number range ($Re \leq 10$). For $Re > 10$, marginal change is observed in the value of j_H for all blockage ratio. In short, it can be concluded that the

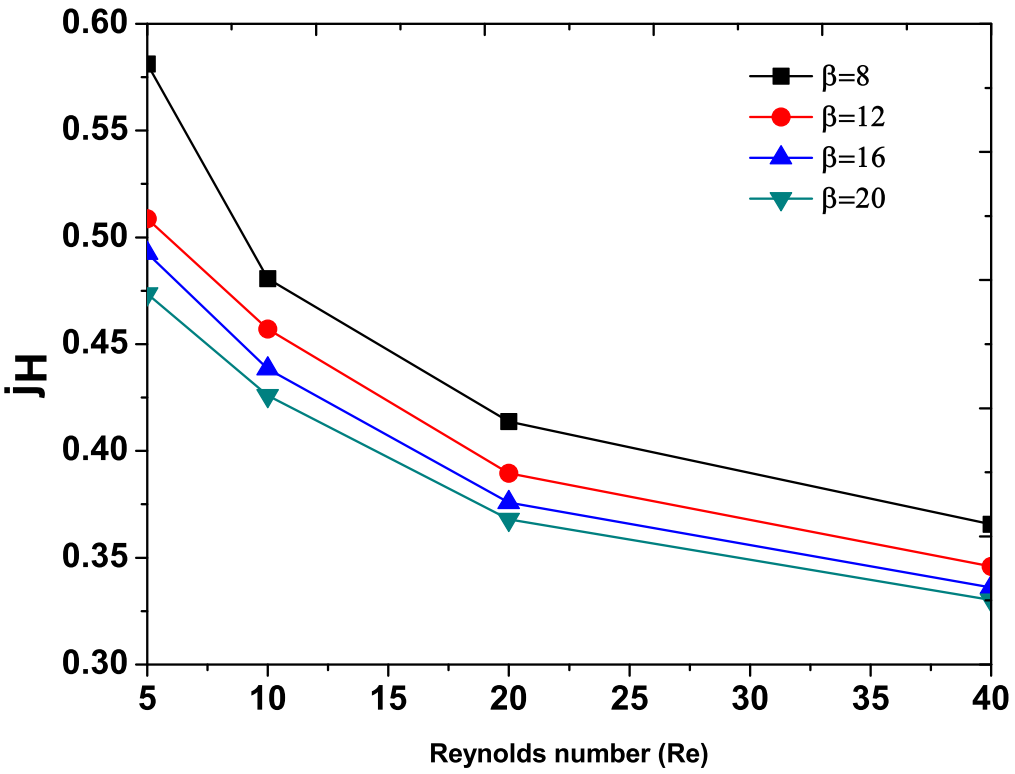

FIGURE 11.10: Variation of the Colburn factor for heat transfer (j_H) with blockage $1/\beta$ for different Reynolds number.

Colburn j_H heat transfer factor has strong dependence on blockage ratio than Reynolds number.

11.3.3 Forced convection from rectangular cylinder ($a_r > 1$)

In this section, combined influence of blockage ratio, aspect ratio of cylinder and Reynolds number on flow and thermal fields have been studied and presented herein.

11.3.3.1 Flow and temperature field: Effect of a_r

The effect of aspect ratio of rectangular cylinder (a_r) on local flow and thermal fields is examined through the contour profiles of the streamline, vorticity and temperature isotherms. The kinematic viscosity (ν) and thermal diffusivity (α) are the two significant

fluid properties which are evidently responsible for the development of hydrodynamic and thermal boundary layers, respectively.

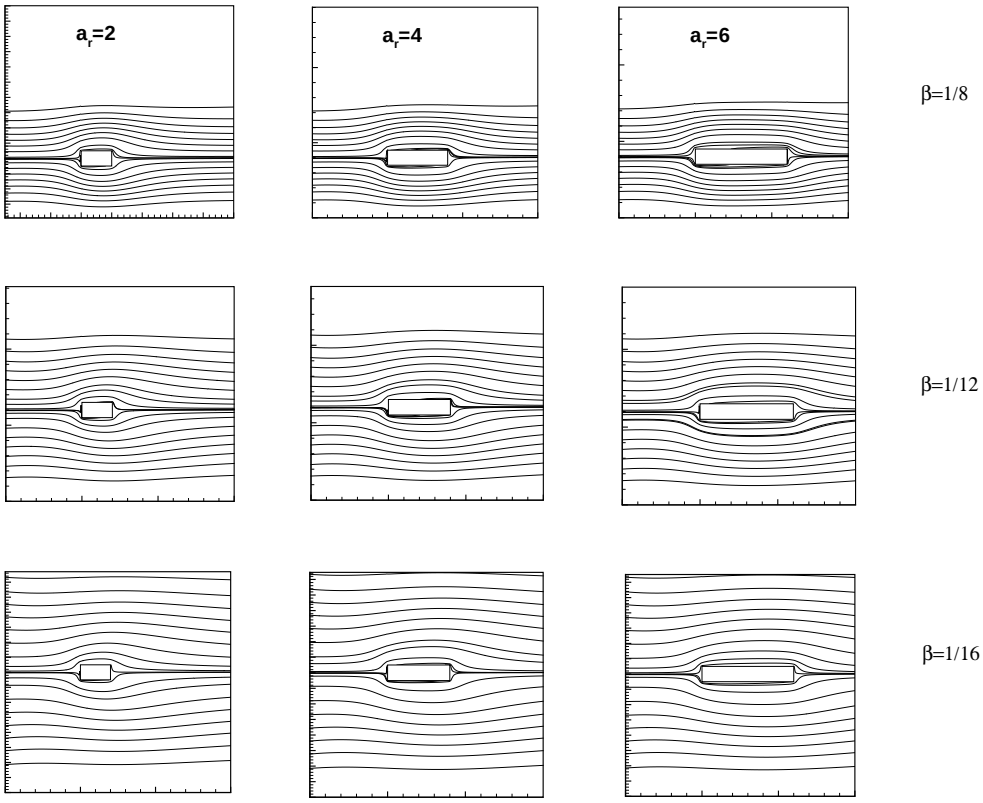

FIGURE 11.11: Streamline patterns for different aspect ratio of rectangular cylinder (a_r) and blockage ratio (β) at Reynolds number of Re=5.

In this section, the effect of aspect ratio (a_r) of rectangular cylinder on flow and thermal fields have been elucidated by means of streamline, vortices and isotherm contours (Figures 11.11 to 11.16). As expected and discussed in section 11.3.1, the inertial forces becomes dominant than viscous forces with the increase in Reynolds number. It is well represented by streamline (Figure 11.11) and vorticity patterns (Figure 11.12). The increase in Re causes increase in re-circulation length. The contours profiles are shown for only extreme values of Reynolds number (Re=5 and 40) for range of aspect ratio ($a_r = 2, 4, 6$) and blockage ratio ($\beta = 1/8, 1/12, 1/16$).

The increase in a_r causes insignificant change in the re-circulation length. Further, the blockage ratio also have very marginal influence on the size of wake. It slightly decreases

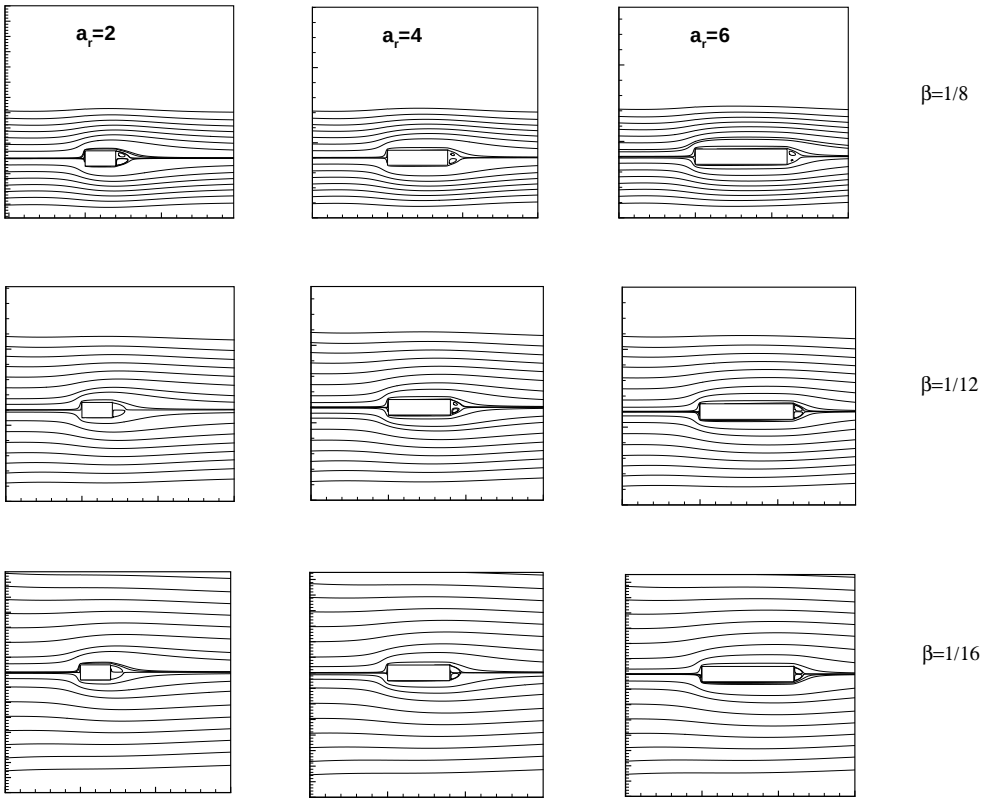

FIGURE 11.12: Streamline patterns for different aspect ratio of rectangular cylinder (a_r) and blockage ratio (β) at Reynolds number of Re=40.

with blockage ratio. Thus, Reynolds number has dominant influence on the flow characteristics than aspect ratio a_r of cylinder and blockage ratio (β).

Further, Figure 11.15 and Figure 11.16 decipt isotherm profiles. The increase in a_r causes increase in available surface area, thus increasing isotherm crowding and increasing heat transfer rate. The increase in the β causes marginal decrease in the wake region, which in turn increases isotherms crowding and hence facilitating higher heat transfer rate. At Re=5, isotherms are uniformly crowded along the cylinder surface due to dominating viscous force and having lower boundary layer thickness. The increase in Re causes isotherms to be more stratified around the cylinder surface with the increase in boundary layer. It causes increase in the temperature gradient along the cylinder surface, thus facilitating higher heat transfer rate.

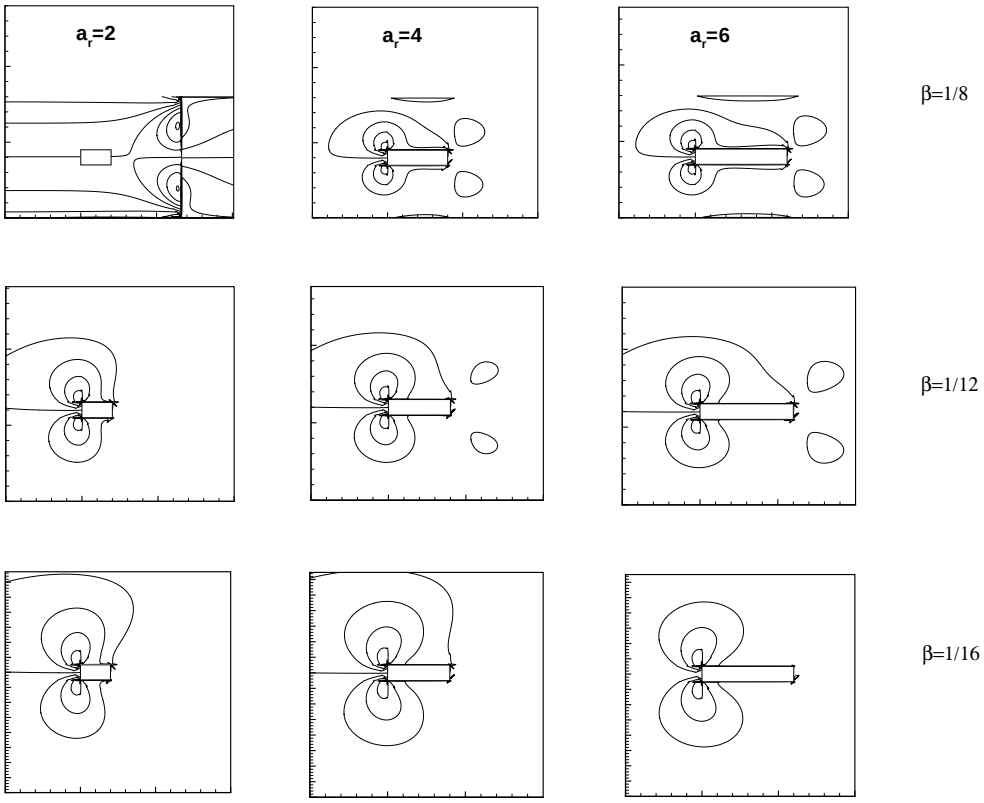

FIGURE 11.13: Vorticity patterns for different aspect ratio of rectangular cylinder (a_r) and blockage ratio (β) at Reynolds number of Re=5.

11.3.3.2 Drag values

The combined influence of aspect ratio of cylinder (a_r), blockage ratio (β) and Reynolds number is shown in Table 11.3. In this section, the influence of a_r on drag values have been explored. The increase in a_r causes increase in cylinder length in horizontal direction. The friction drag component is strong effect on horizontal walls of cylinder, which increases C_{DF} values for top and bottom walls of rectangular cylinder. The increase in a_r causes gradual rise in the value of pressure drag coefficient (C_{DP}). Thus a_r has linear dependence on drag values. The influence of Reynolds number and blockage ratio β, as discussed earlier, decreases the drag values. Table 11.3 presents values of drag coefficients (pressure (C_{DP}), viscous (C_{DF}) and total (C_D)) estimated for range of aspect ratio of rectangular cylinder ($a_r = 2, 4, 6$), blockage ratio ($\beta = 1/8, 1/12, 1/16$) and Reynolds number ($Re = 5, 10, 20, 40$). A similar trend of drag values as discussed in square cylinder section is

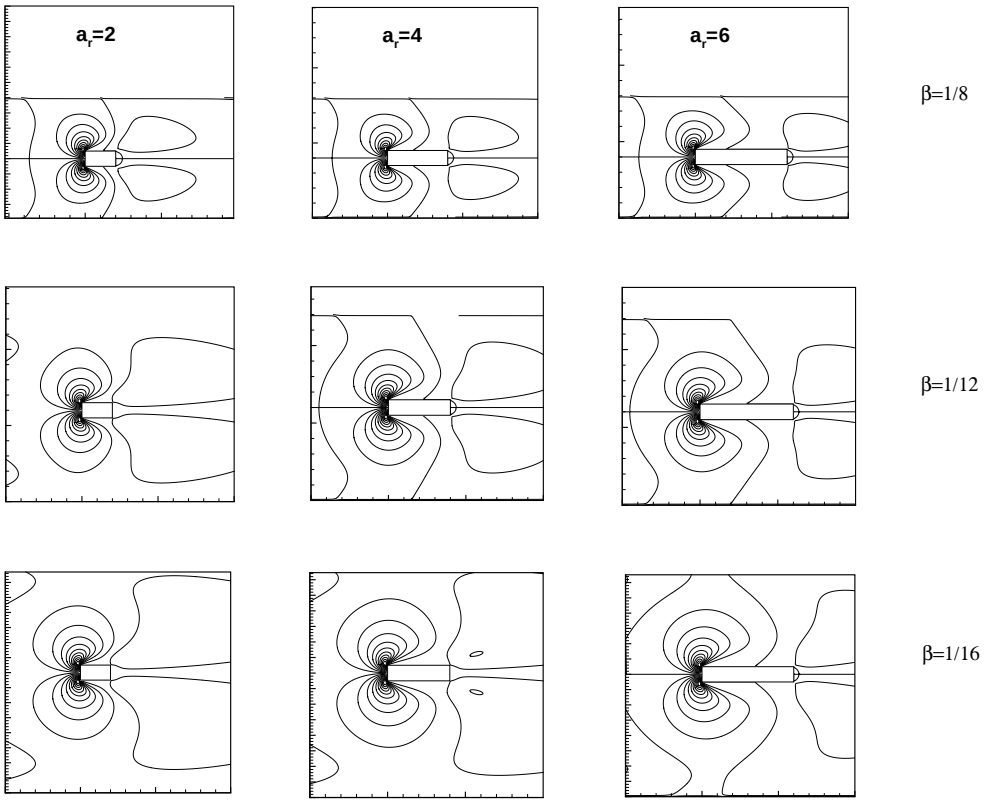

FIGURE 11.14: Vorticity patterns for different aspect ratio of rectangular cylinder (a_r) and blockage ratio (β) at Reynolds number of Re=40.

TABLE 11.3: Drag coefficient results for $Re = 5, 10, 20, 40$ at different values of aspect ratio of rectangular cylinder (a_r) and blockage ratio (β).

β	Re	C_{DP}	C_{DF}	C_D	C_{DP}	C_{DF}	C_D	C_{DP}	C_{DF}	C_D
		$a_r = 2$			$a_r = 4$			$a_r = 6$		
1/8	5	4.98	1.72	6.70	7.05	7.05	11.6	7.61	7.09	16.5
	10	3.49	0.37	3.86	4.69	1.02	5.71	4.86	1.39	6.26
	20	2.36	0.30	2.66	2.61	2.96	2.954	2.96	0.48	3.44
	40	1.68	0.27	1.94	1.31	1.52	2.548	1.35	0.21	1.57
		$a_r = 2$			$a_r = 4$			$a_r = 6$		
1/12	5	3.46	0.37	3.86	4.26	3.04	7.3	4.68	4.6	9.28
	10	2.62	0.31	2.93	2.95	0.34	3.29	2.9	0.86	3.77
	20	2.21	0.37	2.48	2.23	0.23	2.56	2.4	0.43	2.82
	40	1.45	0.24	1.69	1.10	0.18	1.28	0.91	0.41	1.32
		$a_r = 2$			$a_r = 4$			$a_r = 6$		
1/16	5	3.60	1.31	4.91	3.69	2.63	6.32	3.98	3.82	7.80
	10	2.37	0.28	2.65	3.31	0.36	3.67	3.35	1.01	4.36
	20	2.16	0.23	2.39	2.12	0.31	2.44	2.10	0.39	2.49
	40	1.37	0.23	1.60	0.88	0.16	1.05	1.19	0.17	1.36

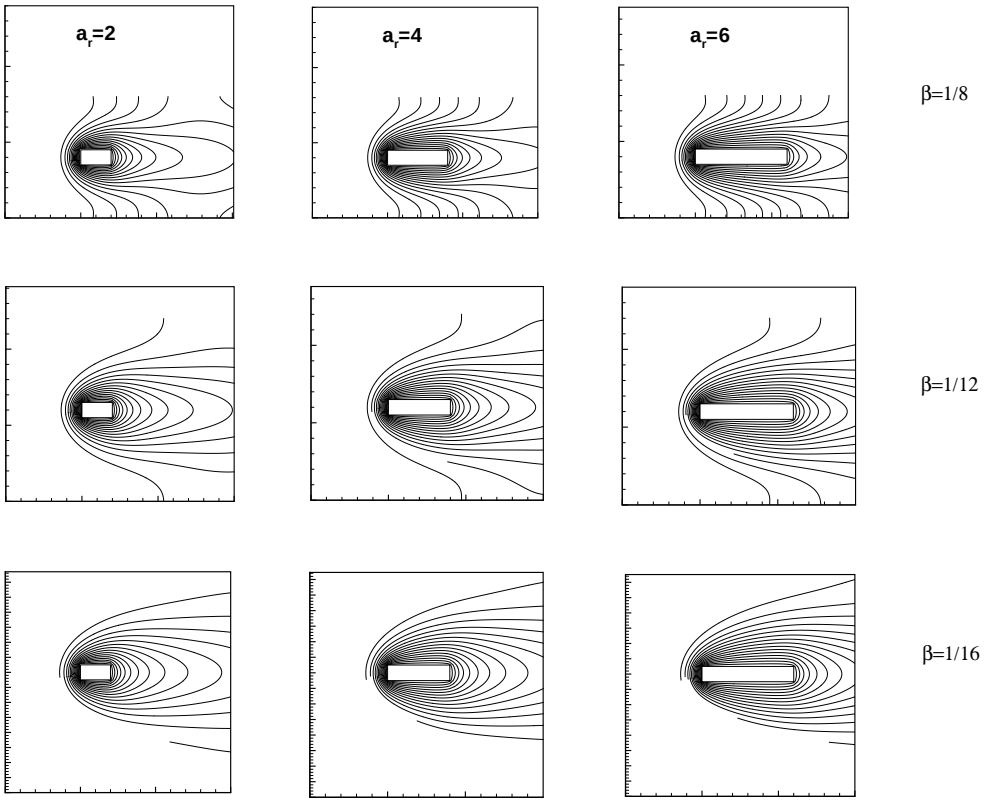

FIGURE 11.15: Isotherm patterns for different aspect ratio of rectangular cylinder (a_r) and blockage ratio (β) at Reynolds number of Re=5.

visible from analysis of Table 11.3. The increase in Reynolds number (inertial force) causes reduction in shear forces as well as normal stresses between rectangular cylinder and fluid. For constant blockage value, the increase in a_r values, the total as well as pressure and viscous components of drag increases. This is due to increase in a_r causes more available surface area. With the increase in a_r, amount of shearing increases as comparison to normal stress. Moreover, it can be seen that increase in C_{DF} is more predominant than C_{DP}, as with increase in a_r the length of horizontal wall increases.

The increase in blockage ratio, as expected, causes reduction in the drag values. This is due to reduction in pressure drop due to increase in the distance between channel and cylinder wall. Thus, drag values seen to have complex dependence on aspect ratio (a_r), blockage ratio (β) and Reynolds number (Re). Moreover, the influence of a_r and Re is much stronger than β.

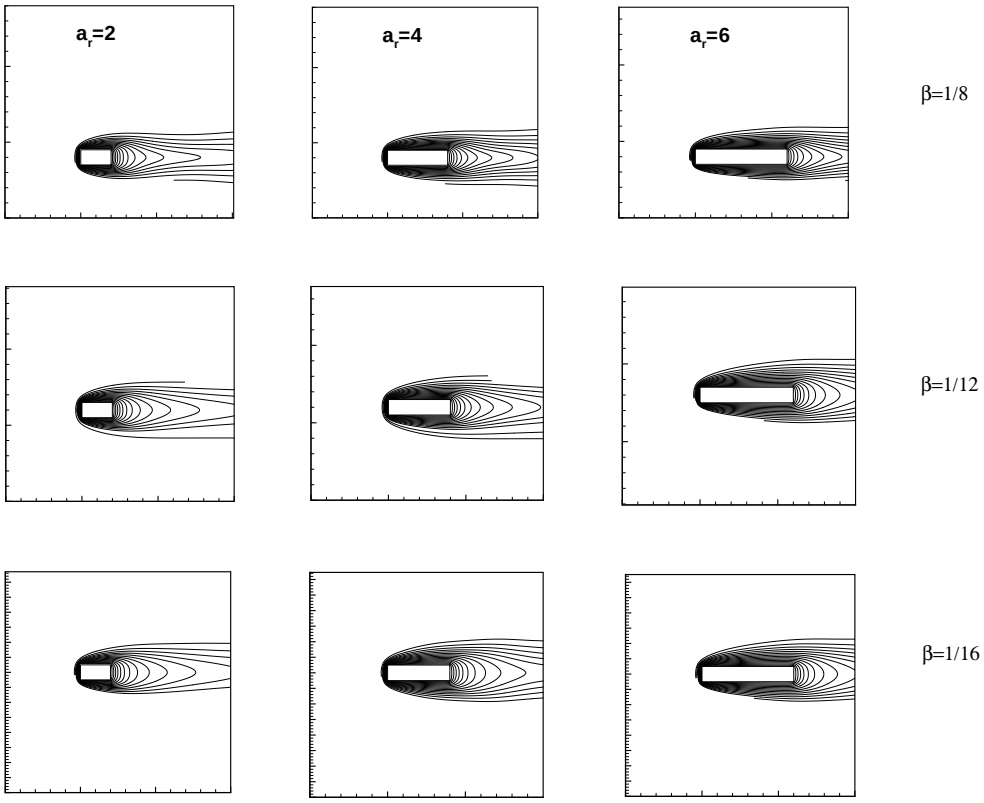

FIGURE 11.16: Isotherm patterns for different aspect ratio of rectangular cylinder (a_r) and blockage ratio (β) at Reynolds number of Re=40.

11.3.3.3 Average Nusselt number

The average Nusselt number for each surface of the rectangular cylinder is estimated by averaging the local Nu values over the each face of the cylinder. Finally, the overall mean value of the cylinder Nusselt number (Nu) is obtained by averaging the averaged Nusselt number for each face of the rectangular cylinder. Table 11.4 presents the average Nusselt number values estimated at all faces of rectangular cylinder, along with overall Nu values for range of aspect ratio (a_r), blockage ratio β and Reynolds number (Re). It can be seen from Table 11.4, the increase in a_r, as expected, causes more area available for heat transfer. Thus average Nusselt number $\overline{Nu}$ increases with a_r. The highest heat transfer rate ($\overline{Nu}$ values) are obtained for top and bottom (horizontal walls), followed by front and rear surface of cylinder. The lowest Nusselt number values are obtained for rear surface, due to presence of wake. Similar effect is observed on $\overline{Nu}$ values with blockage ratio (β)

TABLE 11.4: Average nusselt number results for $Re = 5, 10, 20, 40$ at different values of aspect ratio of rectangular cylinder (a_r) and blockage ratio (β).

β	Re	Nu_{front}	Nu_{rear}	Nu_{top}	Nu_{bottom}	$Nu_{overall}$
				$a_r = 2$		
1/8	5	1.30	0.50	1.51	1.51	1.23
	10	1.75	0.75	1.88	1.88	1.56
	20	2.01	0.83	2.36	2.36	1.89
	40	2.41	0.98	3.27	3.27	2.48
				$a_r = 4$		
	5	1.61	0.49	1.77	1.77	1.41
	10	1.93	0.64	2.17	2.18	1.73
	20	2.10	0.72	2.56	2.55	1.98
	40	2.34	1.00	3.42	3.43	2.54
				$a_r = 6$		
	5	1.64	0.42	1.85	1.84	1.44
	10	2.03	0.57	2.29	2.29	1.80
	20	2.15	0.66	2.71	2.71	2.05
	40	2.43	0.63	3.77	3.78	2.65
				$a_r = 2$		
1/12	5	1.27	0.45	1.44	1.45	1.15
	10	1.68	0.62	2.11	2.12	1.63
	20	1.96	0.78	2.42	2.42	1.89
	40	2.35	0.87	3.21	3.22	2.41
				$a_r = 4$		
	5	1.57	0.44	1.74	1.75	1.37
	10	1.87	0.62	2.09	2.08	1.67
	20	2.05	0.68	2.44	2.45	1.90
	40	2.29	0.97	3.38	3.39	2.50
				$a_r = 6$		
	5	1.61	0.39	1.80	1.81	1.40
	10	1.99	0.52	2.25	2.26	1.76
	20	2.11	0.58	2.68	2.67	2.01
	40	2.39	0.61	3.74	3.75	2.62
				$a_r = 2$		
1/16	5	1.25	0.43	1.42	1.43	1.13
	10	1.66	0.58	2.08	2.09	1.60
	20	1.93	0.75	2.38	2.38	1.86
	40	2.32	0.84	3.18	3.18	2.38
				$a_r = 4$		
	5	1.53	0.41	1.71	1.72	1.34
	10	1.84	0.59	2.06	2.06	1.64
	20	2.01	0.64	2.40	2.40	1.86
	40	2.27	0.94	3.35	3.36	2.48
				$a_r = 6$		
	5	1.58	0.36	1.78	1.78	1.38
	10	1.95	0.48	2.22	2.22	1.72
	20	2.09	0.55	2.64	2.65	1.98
	40	2.35	0.58	3.71	3.72	2.59

and Reynolds number (Re) as that for square cylinder ($a_r = 1$). The rise in the Reynolds number increases $\overline{Nu}$ values, while reverse effect is observed of blockage ratio on $\overline{Nu}$. Thus a_r, β and Re has complex dependence on $\overline{Nu}$ values.

11.3.3.4 The Colburn heat transfer factor (j_H)

The influence of Reynolds number (as Prandtl number values is Pr=1, it vanishes) on The Colburn heat transfer factor (j_H) is presented in Figure 11.17. Figure 11.17 shows j_H values as a function of Reynolds number estimated at various blockage ratio β and aspect ratio (a_r). It can be observed that the increases in Re causes decrease in j_H values for range of β and a_r considered herein. Aspect ratio of cylinder has remarkable effect on j_H values. The j_H values increases with a_r for all blockage ratios. Further, blockage ratio has negligible influence on the j_H values, which is evident from previous discussion. Thus, Reynolds number and aspect ratio has more dominant effect on j_H values than blockage ratio. Figure 11.17 shows representative variation of the Colburn factor $'j'_H$ at various blockage ratio $\beta = 1/8, 1/12, 1/16$ for different aspect ratio of cylinder ($a_r = 2, 4, 6$) as a function of Reynolds number ($Re = 5, 10, 20, 40$).

11.3.4 Empirical correlation

The present numerical calculations can be summarized by using an empirical correlations of drag coefficient (C_D) and average Nusselt number ($\overline{Nu}$). The dependence of drag, heat transfer rate i.e., average Nusselt number ($\overline{Nu}$) on the range of Reynolds number (Re), blockage ratio (β) and aspect ratio of rectangular cylinder (a_r) are expressed by using following correlations, which were found to fit the present simulation data satisfactorily:

$$C_D = \exp -9.24 \times 10^{-2} Re + 10.02\beta + 0.161 a_r + 0.909 \quad R^2 = 0.925 \tag{11.2}$$

$$\overline{Nu} = 3.21 \times 10^{-2} Re + 1.05\beta + 4.56 \times 10^{-2} + 0.982 \quad R^2 = 0.97 \tag{11.3}$$

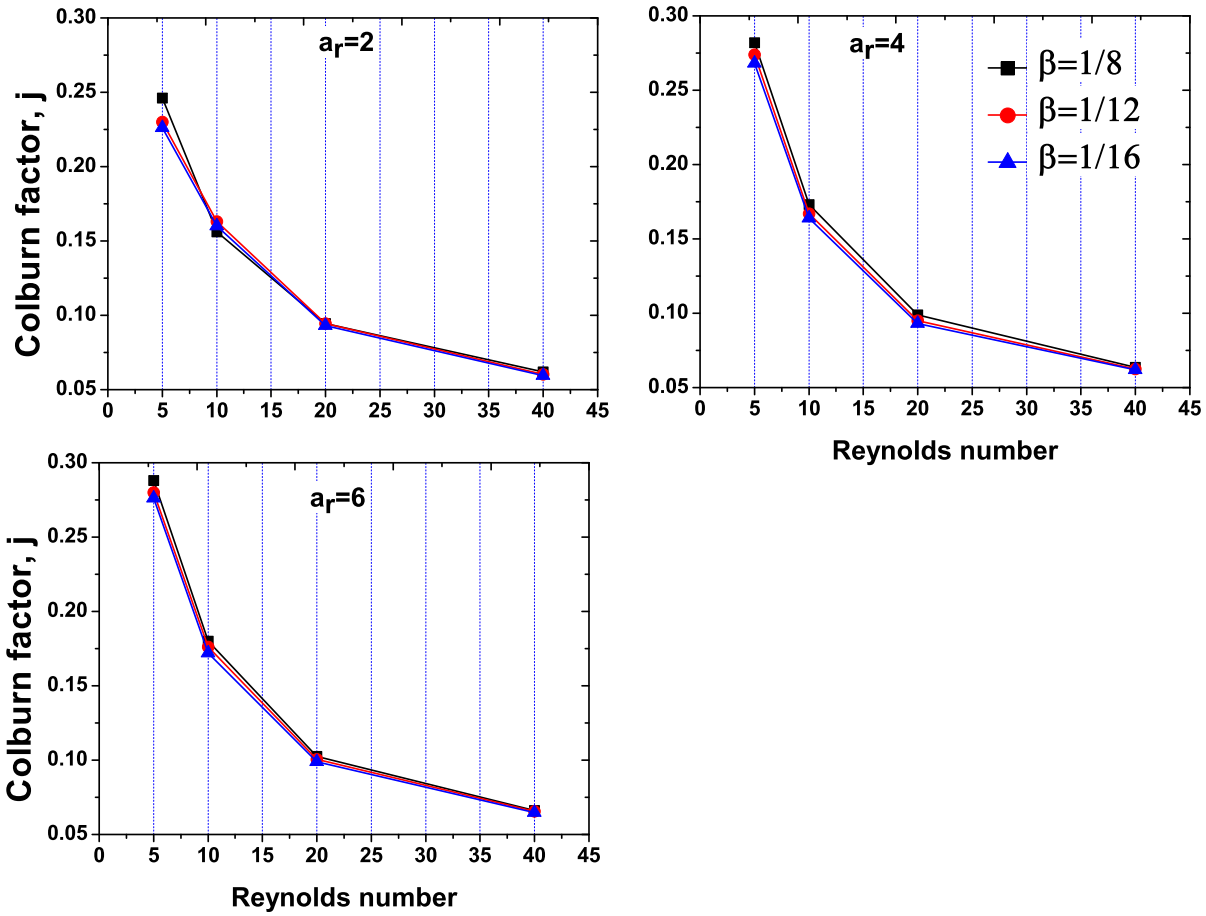

FIGURE 11.17: The Colburn j factor as a function of Reynolds number at various blockage ratio (β) and aspect ratio of rectangular cylinder (a_r) for Prandtl number of Pr=1.

Figure 11.18 presents comparison between drag coefficient C_D and average Nusselt number $\overline{Nu}$ obtained from simulation and predicted by Eq. (11.2) and Eq. (11.3), respectively.

11.4 Concluding Remarks

The numerical study of the laminar forced convection from heated square cylinder in channel flow by passive scalar based lattice Boltzmann method (LBM) is done. The combined effects of aspect ratio of cylinder (a_r), blockage ratio ($1/8 \leq \beta \leq 1/20$) on heat and fluid flow characteristics have been elucidated for the range of Reynolds number ($5 \leq Re \leq 40$) and a constant Prandtl number of $Pr = 1$. The accuracy of present in-house LBM solver (developed in C++ language) is ascertained by grid and domain

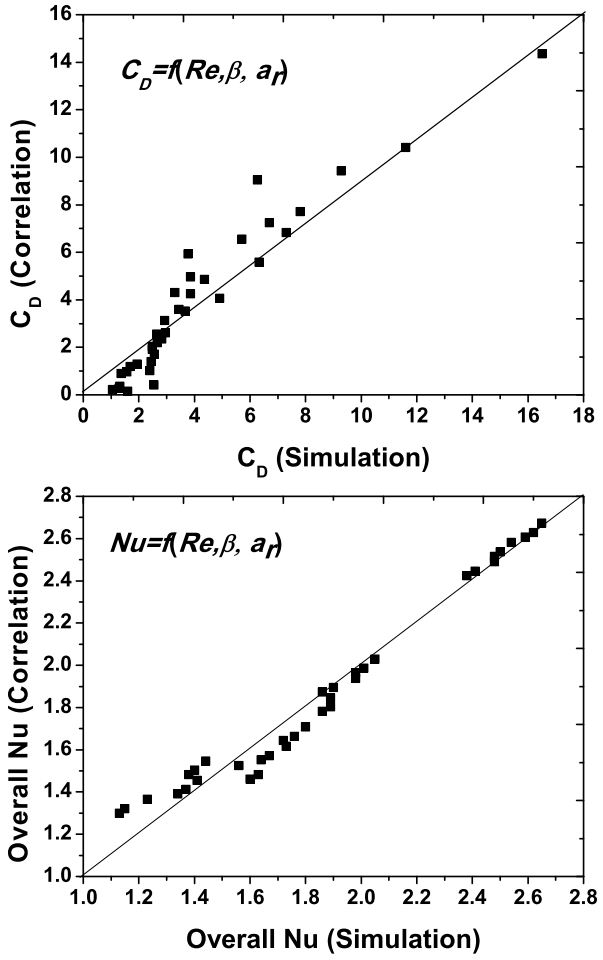

FIGURE 11.18: Comparison of the present drag C_D, average Nusselt number ($\overline{Nu}$) results with the prediction of proposed correlations (Eqs. 11.2, 11.3)

independence test and validation with literature. The validation of present numerical method with literature shown excellent agreement. The functional dependence of drag coefficient C_D and average Nusselt number ($\overline{Nu}$) with Reynolds number (Re) and blockage ratio (β) is obtained by developing simple closure relationship. From this work, following conclusions can be drawn:

1. The applicability of thermal lattice Boltzmann method for investigating the forced convection heat transfer from heated square cylinder is validated by this study.

2. The increase in blockage ratio causes marginal increase in re-circulation length for considered range of Reynolds number.

3. The drag values are found to be in inverse proportion with blockage ratio and Reynolds number.

4. At a constant Reynolds number, increase in blockage ratio causes crowding isotherms along cylinder.

5. Linear increase in average Nusselt number ($\overline{Nu}$) is observed with Reynolds number and lower blockage ratio. increase in blockage ratio impedes rate of heat transfer.

6. The Colburn heat transfer factor j_H is dominated more by blockage ratio than Reynolds number.

7. Empirical correlations relating total drag coefficient (C_D) and average Nusselt number ($\overline{Nu}$) with aspect ratio of cylinder (a_r), blockage ratio (β) and Reynolds number (Re) have been developed for its possible use in engineering design purpose.

Chapter 12

CONCLUSIONS AND RECOMMENDATIONS

The key findings of the problems studied in this thesis have been summarized in this chapter. In particular, the influence of range of pertinent dimensionless flow governing parameters on two-dimensional, steady, laminar, incompressible flow and heat transfer from enclosures (differentially, partially, open ended enclosures) and channel confined rectangular cylinder have been studied numerically by using in house developed thermal lattice Boltzmann method (TLBM) in C++ programming language. The broad ranges of physical parameters considered here, in brief, are as follows: Rayleigh number ($10^3 \leq Ra \leq 10^6$), Prandtl number ($0.71 \leq Pr \leq 100$), heating location (bottom, middle, top), heater size ($L_h = 1, 1/2, 1/4, 1/6$), cooler size ($L_c = 1, 1/2, 1/4, 1/6$), Hartmann number ($0 \leq Ha \leq 120$), angle of magnetic field direction ($\theta_M = 0^o, 45^o, 120^o$), Reynolds number ($5 \leq Re \leq 40$), blockage ratio ($1/8 \leq \beta 1/20$) and aspect ratio of rectangular cylinder ($a_r = 1, 2, 4, 6$). The concluding summary of each of the problems considered in this work are as follows:

12.1 Natural convection in differentially heated cavity: Effect of Rayleigh and Prandtl number

The numerical simulations are performed to investigate the effects of Prandtl numbers ($0.71 \leq Pr \leq 100$) on natural convective heat transfer mechanism for three different Rayleigh numbers viz., $Ra = 10^4, 10^5$ and 10^6. Extensive results are obtained and presented in terms of the streamline and vorticity patterns, the center-line variations of the velocity and temperature, and local and average Nusselt numbers. The following conclusions are drawn from the results: Natural convection effect increases with the increase in Prandtl number (Pr) for all values of the Rayleigh number (Ra) due to the increased viscous force effect in comparison to inertial force. As thermal diffusion is inversely proportional to Prandtl number, velocity is more diffused than thermal energy. For $Ra = 10^4$, dominant heat transfer mechanism is conductive for $Pr \geq 10$. The average Nusselt number (dimensionless heat transfer coefficient) of isothermal wall ($x = 0$) is seen to increase with the Prandtl and Rayleigh numbers. Further, the functional dependence of average Nusselt number on dimensionless flow governing parameters is presented.

12.2 Natural convection in partially-simultaneously heated/ cooled square cavity

In this part, the influence of Rayleigh number ($10^3 \leq Ra \leq 10^6$) on natural convective heat transfer mechanism in a square cavity with one wall subjected to equally both hot and cold thermal conditions, have been elucidated. The upper part ($0.5 \leq H \leq 1$) of west wall of cavity is subjected to higher temperature (T_H) and lower part ($0 \leq H \leq 0.5$) is exposed to ambient ($T_C < T_H$). A thermal lattice Boltzmann method with passive scalar and D2Q9 lattice model is used as a numerical tool. The numerical results are obtained and presented in terms of the streamline and isotherm patterns, the center line variations of the velocity and temperature, and local and average Nusselt numbers. Formation of

convection cell near lower part of mixed heated wall ($X = 0$) of cavity is observed after $Ra \leq 10^4$, as low temperature fluid retained in that region. The size of convection cell increases with the increase in Rayleigh number (Ra). The average Nusselt number ($\overline{Nu}$) and overall Nusselt number ($\widehat{Nu}$) value show linear increase with Rayleigh number. At $Ra = 10^5$, the rate of heat transfer of both vertical walls is almost same, which is indicated by nearly same values of average Nusselt number ($\overline{Nu}$). Predictive correlation of Nusselt number is also presented.

12.3 Magneto-hydrodynamic natural convection in partially differentially heated cavity

In this part, lattice Boltzman simulations have been carried out to investigate the influence of cooler size ($L_c = 1, 1/2, 1/4$) on magneto-hydrodynamic (MHD) natural convective heat transfer characteristics in partially-differentially heated square cavity. The west wall (X=0) is partially heated with heater size ($L_h = 1/2$) and east wall is partially cooled with four cooler lengths of $L_c = 1, 1/2, 1/4$. Other parts of cavity are maintained at adiabatic condition. In particular, the effects of Rayleigh number ($Ra = 10^3, 10^4, 10^5$), Hartmann number ($Ha = 0, 60, 120$), angle of magnetic field ($\theta_M = 0^o, 45^o, 90^o$) on streamlines, isotherms and average Nusselt number have been studied and reported in this work. Fluid circulation in cavity creates formation of convection cell in central region of cavity. The size of convection cell varies proportionally with Rayleigh number, while it decreases with augmentation of Hartmann number. At $Ra = 10^5$, convection cell elongates and bifurcates with the formation of two eddies at the corner of cell. The size of these eddies reduces with decrease in cooler length. Increase in Ha controls the flow circulation in cavity. The decrease in cooler size, reduce buoyancy effect, thereby, fluid circulation. The change in the magnetic field direction from horizontal to vertical, slightly increases the flow circulation in cavity for Ha=60, 120. The decrease in cooler length from $L_c = 1$ to 1/2 and 1/4, helps to clear the dense crowding and isotherms pattern spread horizontally

in cavity. The average Nusselt number increases with Rayleigh number and decreases with Hartmann number. Empirical correlation has been developed for average Nusselt number.

12.4 Natural convection in partially heated open ended cavity

In this part, numerical experimentation of steady laminar natural convective heat transfer in an open ended square enclosure with partially heated wall is carried out by using in-house developed CFD solver based on the passive scalar thermal lattice Boltzmann method (PS-TLBM). In particular, the effects of heating location (bottom, middle and top) on the partially heated wall and heater size (L_h=0.25, 0.5 and 0.75) on the heat and fluid flow characteristics of an incompressible fluid have been investigated for the wide range of Rayleigh number ($10^3 \leq Ra \leq 10^6$) and Prandtl number ($0.71 \leq Pr \leq 100$). At lowest value of the Rayleigh number ($Ra = 10^3$), streamlines bifurcate for the bottom and top heating locations due to weak buoyancy driven flow. For middle heating location, such bifurcation is not observed due to comparatively higher buoyancy driven flow. Irrespective of the heating locations and heater sizes, the size of elliptical quasi-motionless region increase with increasing value of the the Rayleigh number (Ra). At highest value of the Rayleigh number ($Ra = 10^6$), the streamlines elongate and bifurcate for all heating location and heater sizes. It shows the clockwise circulation with formation of vortex near lower part of open end of cavity. The maximum size of the vortex is seen for the top heating location case. Linear dependence of the average Nusselt number ($\overline{Nu}$) on the Rayleigh number is observed, irrespective of the heating locations and heater size. However, average Nusselt number ($\overline{Nu}$) shows a proportional dependence for the bottom and middle locations and inversely proportional dependence for the top heating location on the heater size, i.e., an increasing value of L_h enhanced $\overline{Nu}$ for the bottom and middle locations and deteriorated $\overline{Nu}$ for the top heating location. Over the range of

Rayleigh number, middle partial heating location shows higher heat transfer rate followed by bottom and top heating locations. The significant convection losses are indicated in the top heating location as $\overline{Nu}$ decreased with increase in the heater size. Finally results of study are summarized in terms of Nusselt number correlation.

12.5 Natural convection in square cavity with built-in heated square block

Numerical simulations of natural convection in an enclosure containing heated square body are conducted. Passive scalar thermal lattice Boltzmann method (PS-TLBM) has been used as numerical tool for solving field equations. The numerical results are obtained for Rayleigh number $Ra = 10^4, 10^5, 10^6$ and Prandtl number of Pr=0.71,5 and 10. For lower Prandtl numbers (Pr=0.71), temperature distribution is found to be uniform across an enclosure and is in oval shape around the heated square for $Ra = 10^4$. As Prandtl number increases, isotherms becomes densely crowded along heated square block. As Rayleigh number increases, isotherms become parallel to horizontal wall of enclosure with formation of a peak (a thermal plume) from top walls. At higher Prandtl, isotherms pattern remains nearly same for given Rayleigh numbers, only change is observed in central peak of isotherms towards top wall. Average Nusselt number shows linear variation with Rayleigh and Prandtl numbers.

12.6 Wall effects on force convective heat transfer from heated built-in rectangular cylinder

The numerical study of the laminar forced convection from heated square cylinder in channel flow by passive scalar based lattice Boltzmann method (LBM) is done. The effect of blockage ratio ($1/8 \leq \beta \leq 1/20$) on heat and fluid flow characteristics have been

elucidated for the range of Reynolds number ($5 \leq Re \leq 40$) and a constant Prandtl number of $Pr = 1$. The accuracy of present in-house LBM solver (developed in C++ language) is ascertained by grid and domain independence test and validation with literature. The validation of present numerical method with literature shown excellent agreement. The functional dependence of drag coefficient C_D and average Nusselt number ($\overline{Nu}$) with Reynolds number (Re) and blockage ratio (β) is obtained by developing simple closure relationship. The applicability of thermal lattice Boltzmann method for investigating the forced convection heat transfer from heated square cylinder is validated by this study. The increase in blockage ratio causes marginal increase in re-circulation length for considered range of Reynolds number. The drag values are found to be in inverse proportion with blockage ratio and Reynolds number. At a constant Reynolds number, increase in blockage ratio causes crowding isotherms along cylinder. Linear increase in average Nusselt number ($\overline{Nu}$) is observed with Reynolds number and lower blockage ratio. Thus, increase in blockage ratio impedes rate of heat transfer. The Colburn heat transfer factor j_H is dominated more by blockage ratio than Reynolds number.

12.7 Summary of empirical correlations

The empirical correlations developed in different problems for global characteristics variables such as (Nusselt number and drag coefficient) with pertinent flow governing parameters are listed in Table 12.1.

TABLE 12.1: The empirical correlations developed for different problems studied herein for with the range of physical parameters.

Sr. No.	Problem	Correlation	Range
1	1 (Chapter 6)	(a) $\overline{Nu} = 0.1499Ra^{0.2977}Pr^{0.2528}$ (b) $\overline{Nu} = 0.394Ra^{0.111}Pr^{0.7255}$ $\overline{Nu} = 0.1965Ra^{0.1203}Pr^{0.8339} + 3.3205$	$0.71 \leq Pr \leq 30$ $30 \leq Pr \leq 100$ $0.71 \leq Pr \leq 100$ $10^4 \leq Ra \leq 10^6$
2	2 (Chapter 7)	$\widehat{Nu} = 0.07Ra^{0.31}$	$10^4 \leq Ra \leq 10^6; Pr = 0.71$
3	3 (Chapter 8)	At constant Ra and θ_M $\overline{Nu} = f(L_c, Ha)$ As given in Table 8.2 andTable 8.3	$10^3 \leq Ra \leq 10^6; Pr = 0.71$ $0 \leq Ha \leq 120; 0^o \leq \theta_M \leq 90^o$
4	4 (Chapter 9, I)	(a) Top heating:$0.1781Ra^{0.2114}L_h^{c\,-0.753}$ (b) Middle heating: $0.5237Ra^{0.2336}L_h^{c\,0.5704}$ (c) Bottom heating: $0.4282Ra^{0.2545}L_h^{c\,0.7857}$	$10^3 \leq Ra \leq 10^6; Pr = 0.71$ $L_h = 0.25, 0.5, 0.75$
	5 (Chapter 9, II)	(d): $\overline{Nu} = 0.9276Ra^{0.1733}Pr^{0.2157}$	$10^3 \leq Ra \leq 10^6; 0.71 \leq Pr \leq 7$
5	6 (Chapter 10)	$\overline{Nu_{overall}} = 0.3279Pr^{0.1057}Ra^{0.1346}$	$10^4 \leq Ra \leq 10^6$ $0.71 \leq Pr \leq 10$
6	7 (Chapter 11)	$C_D = \exp -9.24 \times 10^{-2}Re + 10.02\beta + 0.161a_r + 0.909$ $\overline{Nu} = 3.21 \times 10^{-2}Re + 1.05\beta + 4.56 \times 10^{-2} + 0.982$	$\beta = 1/8 - 1/20, a_r = 1 - 6, Re = 5 - 40, Pr = 1$

12.8 Recommendations for future work

The present work is focused on the natural convective heat transfer characteristics from enclosure containing Newtonian fluid of varying shapes (differentially heated, partially-differentially, partially heated open and enclosure with built-in heated block) and forced connection heat transfer from channel confined heated rectangular cylinder, by using thermal lattice Boltzmann method. The thermo-physical properties is assumed to be independent and viscous heat dissipation, compression work done by pressure are neglected. The following suggestions can be made for future work.

1. All considered problems can be studied for three-dimensional (3D) analysis by using TLBM.
2. Mixed convection heat transfer analysis in partially heated lid-driven cavity.
3. Mixed convection heat transfer from heated rectangular cylinder.
4. Lattice Boltzmann method can be extended to study non-Newtonian fluids.

Bibliography

Adlam, J. H., 1986. Computation of two-dimensional time-dependent natural convection in a cavity where there are internal bodies. Computers & Fluids 14 (2), 141–157. (Cited on page 35)

Aghajani Delavar, M., Farhadi, M., Sedighi, K., 2011. Effect of discrete heater at the vertical wall of the cavity over the heat transfer and entropy generation using lattice boltzmann method. Thermal Science 37, 1513–1519. (Cited on pages iv and 34)

Agrawal, A., Djenidi, L., Antonia, R., 2006. Investigation of flow around a pair of side-by-side square cylinders using the lattice boltzmann method. Computers & Fluids 35, 1093–1107. (Cited on pages 39 and 42)

Ahlers, G., Xu, X., 2001. Prandtl number dependence of heat transport in turbulent rayleigh-benard convection. Physical Review Letters 86, 3320–3323. (Cited on page 19)

Alexander, F. J., Chen, S., Sterling, J. D., 1993. Lattice boltzmann thermodynamics. Physical Review E 47, R2249–R2252. (Cited on page 68)

Anderson, J. D. J., 1995. Computational fluid dynamics: The basics with applications. McGraw Hill, Inc. (Cited on pages 2, 3, 5, and 6)

Andreozzi, A., Manca, O., 2010. Numerical investigation on the steady state natural convection in a horizontal open-rnded cavity with a heated upper wall. Numerical Heat Transfer, Part A: Applications 57, 453–472. (Cited on page 32)

Angirasa, D., Eggels, J. G. M., Nieuwstadt, F. T. M., 1995. Numerical simulation of transient natural convection from an isothermal cavity open on a side. Numerical Heat Transfer, Part A: Applications 28, 755–768. (Cited on page 30)

Arcidiacono, S., Ciofalo, M., 2001. Low-prandtl number natural convection in volumetrically heated rectangular enclosures iii. shallow cavity , ar=0.25. International Journal of Heat and Mass Transfer 44, 3053–3065. (Cited on page 19)

Arcidiacono, S., Piazza, I., Ciofalo, M., 2001. Low-prandtl number natural convection in volumetrically heated rectangular enclosures ii. square cavity ar=1.0. International Journal of Heat and Mass Transfer 44, 537–550. (Cited on page 19)

Aydin, O., Yang, W.-J., 2000. Natural convection in enclosures with localized heating from below and symmetrical cooling from sides. International Journal for Numerical Methods in Fluids 10 (5), 518–529. (Cited on pages 22 and 24)

Balaji, C., Venkateshan, S. P., 1994. Interaction of radiation with free convection in an open cavity. International Journal of Heat and Fluid Flow 15 (4), 317–324. (Cited on pages 186 and 187)

Basak, T., Roy, S., Balakrishnan, A., 2006. Effects of thermal boundary conditions on natural convection flows within a square cavity. International Journal of Heat and Mass Transfer 49, 4525–4535. (Cited on pages 17, 21, and 113)

Bejan, A., 2003. Convection heat transfer, Second Edition. Wiley. (Cited on pages 1 and 18)

Bejan, A., Tien, C. L., 1978. Laminar natural convection heat transfer in a horizontal cavity with different end temperatures. Journal of Heat Transfer 100 (4), 641–647. (Cited on page 17)

Ben-Cheikh, N., Campo, A., Ouertatani, N., Lili, T., 2010. Three-dimensional study of heat and fluid flow of air and dielectric liquids filling containers partially heated from below and entirely cooled from above. International Communications in Heat and Mass Transfer 37, 449–456. (Cited on page 22)

Ben-Cheikh, N., Ouertatani, N., Ben-Beya, B., Lili, T., Campo, A., 2011. Numerical study of the heat transfer of two fluid flow in partially heated enclosure. Heat and Mass Transfer 47, 743–749. (Cited on pages 22 and 24)

Benos, L. T., Kakarantzas, S. C., Sarris, I. E., Grecos, A. P., Vlachos, N. S., 2014. Analytical and numerical study of mhd natural convection in a horizontal shallow cavity with heat generation. International Journal of Heat and Mass Transfer 75, 19–30. (Cited on page 23)

Bharti, R. P., 2006. Steady flow of incompressible power law fluids a circular cylinder: A numerical study. PhD Thesis, Department of Chemical Engineering, IIT Kanpur. (Cited on pages 10, 11, 16, 92, and 93)

Bharti, R. P., Chhabra, R. P., Eswaran, V., 2006. Steady flow of power-law fluids across a circular cylinder. Canadian Journal of Chemical Engineering 84 (4), 406–421. (Cited on pages 67 and 156)

Bharti, R. P., Chhabra, R. P., Eswaran, V., 2007. A numerical study of the steady forced convection heat transfer from an unconfined circular cylinder. Heat and Mass Transfer 43, 639–648. (Cited on pages iv, 93, 99, 209, and 215)

Bharti, R. P., Sivakumar, P., Chhabra, R. P., 2008. Forced convection heat transfer from an elliptic cylinder to power-law fluids. International Journal of Heat and Mass Transfer 51, 1838–1853. (Cited on page 202)

Bhattacharyya, S., Maiti, D. K., 2006. Vortex shedding suppression for laminar flow past a square cylinder near a plane wall: a two-dimensional analysis. Acta Mechanica 184, 15–31. (Cited on page 40)

Bhoite, M. T., Narasimham, G. S. V. L., Krishna Murthy, M., 2005. Mixed convection in a shallow enclosure with a series of heat generating components. International Journal of Thermal Sciences 129, 357–363. (Cited on page 36)

Bhuvaneswari, M., Sivasankaran, S., J., K. Y., 2011. Effect of aspect ratio on convection in a porous enclosure with partially active thermal walls. Computers and Mathematics with Applications 62, 3844–3856. (Cited on page 34)

Bilgen, E., Muftuoglu, A., 2008. Cooling strategy by mixed convection of a discrete heater at its optimum position in a square cavity with ventilation ports. International Communications in Heat and Mass Transfer 35, 545–550. (Cited on pages iii, 15, and 29)

Bilgen, E., Oztop, H., 2005. Natural convection heat transfer in partially open inclined square cavities. International Journal of Heat and Mass Transfer 48 (8), 1470–1479. (Cited on pages 30, 156, 157, and 163)

Bin, G., Neng-Chao, W., Chang, B. S., Zhao-Li, G., 2003. Lattice bgk simulation of two dimensional channel flow around a square cylinder. Journal of Fluids and Strcutures 12 (1), 67–74. (Cited on page 39)

Biswas, G., Luschefski, H., Mitra, N. K., Fiebig, M., 1990. Two-dimensional laminar uid ow and heat transfer in a channel with a built-in heated square cylinder. Numerical Heat Transfer, Part A: Applications 54, 5674–5686. (Cited on pages 39 and 44)

Blazek, J., 2001. Computational fluid dynamics: Principles and applications. Elsevier. (Cited on pages 5 and 6)

Bouaziz, M., Kessentini, S., Turki, S., 2010. Numerical prediction of flow and heat transfer of power-law fluids in a plane channel with a built-in heated square cylinder. International Journal of Heat and Mass Transfer 53, 5420–5429. (Cited on page 205)

Breuer, M., Bernsdorf, J., Zeiser, T., Durst, F., 2000. Accurate computations of the laminar flow past a square cylinder based on two different methods: lattice-boltzmann and finite-volume. International Journal of Heat and Fluid Flow 21, 186–196. (Cited on pages 42 and 46)

Breyiannis, G., Valougeorgis, D., 2006. Lattice kinetic simulations of 3-d mhd turbulence. Computers & Fluids 35, 920–924. (Cited on page 25)

Bruno, L., Fransos, D., Coste, N., Bosco, A., 2010. 3d flow around a rectangular cylinder: A computational study. Numerical Heat Transfer, Part A: Applications 98, 263–276. (Cited on page 47)

Burattini, P., Agrawal, A., 2013. Wake interaction between two side-by-side square cylinders in channel flow. Computers & Fluids 77, 134–142. (Cited on page 43)

Calcagni, B., Marsili, F., Paroncini, M., 2005. Natural convective heat transfer in square enclosures heated from below. Applied Thermal Engineering 25, 2522–2531. (Cited on pages 9 and 10)

Cengel, Y. A., Afshin, J. G., 2011. *Heat and Mass Transfer*, 2nd Edition. McGraw Hill Higher Education. (Cited on page 9)

Chamkha, A. J., Hussain, S. H., Abd-Amer, Q. R., 2011. Mixed convection heat transfer of air inside a square vented cavity with a heated horizontal square cylinder. Numerical Heat Transfer, Part A: Applications 59, 58–79. (Cited on page 37)

Chan, Y. L., Tien, C. L., 1985. A numerical study of two-dimensional natural convection in square open cavities. Numerical Heat Transfer, Part A: Applications 8, 65–80. (Cited on pages 34, 58, 156, and 157)

Chatterjee, D., Biswas, G., 2011. The effects of reynolds and prandtl numbers on flow and heat transfer across tandem square cylinders in the steady flow regime. Numerical Heat Transfer, Part A: Applications 59, 421–437. (Cited on page 39)

Chatterjee, D., Biswas, G., Amiroudine, S., 2009. Numerical investigation of forced convection heat transfer in unsteady flow past a row of square cylinders. International Journal of Heat and Mass Transfer 30, 1114–1128. (Cited on pages iv and 16)

Chatterjee, D., Halder, P., 2014. Mhd mixed convective transport in square enclosure with two rotating circular cylinders. Numerical Heat Transfer, Part A: Applications 65, 802–824. (Cited on page 27)

Chatterjee, D., Mondal, B., 2011. Effect of thermal buoyancy on vortex shedding behind a square cylinder in cross flow at low reynolds numbers. International Journal of Heat and Mass Transfer 54, 5262–5274. (Cited on page 39)

Cheikh, N. D., Beya, B. B., Lili, T., 2007. Influence of thermal boundary conditions on natural convection in a square enclosure partially heated from below. International Journal of Heat and Mass Transfer 34, 369–379. (Cited on pages 22 and 24)

Chen, C., Doolen, G. D., 1998. Lattice-boltzmann method for fluid flows. Annual Reviews of Fluid Mechanics 30, 329–364. (Cited on pages v, 7, 56, 60, 61, 62, 63, 64, 71, 72, 73, 77, 78, 79, 82, 83, and 88)

Chen, H., Chen, S., Matthaeus, W. H., 1992. Recovery of navier-stokes equations using a lattice gas-boltzmann method. Physical Review A 45 (8), R5339–R5342. (Cited on pages 7, 64, and 72)

Chen, S., Chen, H., Martinez, D., Matthaeus, W., 1991a. Lattice boltzmann model for for simulation of magnetohydrodynamic. Physical Review E 67 (27), 3776–3779. (Cited on pages v and 25)

Chen, S., Doolen, G. D., Eggert, K., Grunau, D., Loh, E. Y., 1991b. Local lattice-gas model for immiscible fluids. Physical Review A 43 (12), 7053–7056. (Cited on page v)

Chen, S., Tian, Z., 2010. Simulation of thermal micro-flow using lattice boltzmann method with langmuir slip model. International Journal of Heat and Fluid Flow 31, 227–235. (Cited on pages 59, 69, 70, and 71)

Chen, T.-H., Chen, L.-Y., 2007. Study of buoyancy-induced flows subjected to partially heated sources on the left and bottom walls in a square enclosure. International Journal of Thermal Sciences 46, 1219–1231. (Cited on page 24)

Cheng, M., Whyte, D. S., Lou, J., 2007. Numerical simulation of flow around a square cylinder lbm in uniform-shear flow. Journal of Fluids and Strcutures 23, 207–226. (Cited on pages 42 and 46)

Cheng, T. S., 2011. Characteristics of mixed convection heat transfer in a lid-driven square cavity with various richardson and prandtl numbers. International Journal of Thermal Sciences 50, 197–205. (Cited on page 20)

Chhabra, R. P., 1996. Hydrodynamics of non-spherical particles in non-newtonian fluids. In: Cheremisinoff, N.P., Cheremisinoff, P.N. (Eds.), Handbook of Applied Polymer Processing Technology. Marcel Dekker,New York (Chapter 1). (Cited on pages iv, 38, and 93)

Chhabra, R. P., 1999. Heat and mass transfer in rheologically complex systems. In: Siginer, D., De Kee, D., Chhabra, R.P. (Eds.), Advances in the Rheology and Flow of Non-Newtonian Fluids. Elsevier, Amsterdam (Chapter 39). (Cited on pages iv and 38)

Chikatamarla, S. S., Karlin, I. V., 2009. Lattices for the lattice boltzmann method. Physical Review E 79 (046701), 1–18. (Cited on page 8)

Chopard, B., Dupuis, A., 2003. A mass conserving boundary condition for lattice boltzmann models. International journal of Modern Physics B 17, 103–107. (Cited on page 76)

Cianfrini, C., Corcione, M., Habib, E., Quintino, A., 2013. Convective transport in rectangular cavities partially heated at the bottom and cooled at one side. Journal of Thermal Science 22 (1), 55–63. (Cited on pages 22 and 24)

Cormack, D. E., Legal, L. G., Imberger, J., 1974a. Natural convection in a shallow cavity with differentially heated end walls. part 1. asymptotic theory. Journal of Fluid Mechanics 65 (2), 209–229. (Cited on page 17)

Cormack, D. E., Legal, L. G., Seinfeld, J. H., 1974b. Natural convection in a shallow cavity with differentially heated end walls.part 2. numerical solutions. Journal of Fluid Mechanics 65 (2), 231–246. (Cited on page 17)

Cowling, T. G., 1962. Magnetohydrodynamics. Reports on Progress in Physics 25, 244–268. (Cited on page 25)

Davis, G. D. V., 1968. Laminar natural convection in an enclosed rectangular cavity. International Journal of Heat and Mass Transfer 11, 1675–1693. (Cited on pages 9, 16, and 17)

Davis, R., Moore, E., 1982. A numerical study of vortex shedding from rectangles. Journal of Fluid Mechanics 116, 475–606. (Cited on page 45)

Davis, R., Moore, E., Purtell, L., 1983. A numerical study of vortex shedding from rectangles. Physics of Fluids 27 (1), 475–606. (Cited on page 45)

Dawson, S. P., Chen, S., Doolen, G. D., 1993. Lattice boltzmann computations for reaction-diffusion equations. Journal of Chemical Physics 98 (2), 1514–1523. (Cited on page v)

De, A. K., Dalal, A., 2006. A numerical study of natural convection around a square, horizontal, heated cylinder placed in an enclosure. International Journal of Heat and Mass Transfer 49, 4608–4623. (Cited on pages 35 and 36)

de Vahl Davis, G., 1983. Natural convection in a square cavity: a bench mark numerical solution. International Journal for Numerical Methods in Fluids 3, 249–264. (Cited on pages 16, 17, 99, and 133)

Dellar, P. J., 2002. Lattice kinetic schemes for magnetohydrodynamics. Journal of Computational Physics 179, 95–126. (Cited on page 25)

Dellar, P. J., 2003. Incompressible limits of lattice boltzmann equations using multiple relaxation times. Journal of Computational Physics 190, 351–370. (Cited on pages 99 and 155)

Dellar, P. J., 2011. Lattice boltzmann formulation for braginskii magnetohydrodynamics. Computers & Fluids 41, 201–205. (Cited on page 26)

Delouei, A. A., Nazari, M., Kayhani, M. H., Succi, S., 2014. Non-newtonian unconfined flow and heat transfer over a heated cylinder using the direct-forcing immersed boundarythermal lattice boltzmann method. Physical Review E 89 (053312), 1–13. (Cited on page v)

Deng, Q.-H., 2008. Fluid flow and heat transfer characteristics of natural convection in square cavities due to discrete sourcesink pairs. International Journal of Heat and Mass Transfer 51, 5949–5957. (Cited on page 22)

Dhiman, A., 2009a. Heat transfer to power law dilant fluids in a channel with heated built-in square cylinder. International Journal of Thermal Sciences 48, 1552–1563. (Cited on page 39)

Dhiman, A., 2009b. Heat transfer to power law dilant fluids in a channel with heated built-in square cylinder. International Journal of Thermal Sciences 48, 1552–1563. (Cited on pages 209 and 212)

Dhiman, A., Chhabra, R., Eswaran, V., 2005. Flow and heat transfer across a conned square cylinder in the steady ow regime: Eect of peclet number. International Journal of Heat and Mass Transfer 48, 4598–4614. (Cited on pages 39, 44, 204, 209, and 212)

Dhiman, A., Chhabra, R., Eswaran, V., 2006a. Steady flow of power law fluids across a square cylinder. Chemical Engineering Research and Design 84 (A4), 300–310. (Cited on pages iv, 16, 39, 57, and 212)

Dhiman, A., Chhabra, R., Eswaran, V., 2007. Heat transfer to power law fluids from a heated square cylinder. Numerical Heat Transfer, Part A: Applications 52, 185–201. (Cited on pages iv, 16, and 39)

Dhiman, A., Chhabra, R., Eswaran, V., 2008a. Steady flow across a confined square cylinder: Effect of power-law index and blockage ratio. International Journal of Heat and Mass Transfer 148, 141–150. (Cited on pages 40, 44, 204, 209, and 212)

Dhiman, A., Chhabra, R., Eswaran, V., 2008b. Steady mixed convection across a confined square cylinder. International Journal of Heat and Mass Transfer 52, 47–55. (Cited on pages 40, 44, and 205)

Dhiman, A., Chhabra, R., Sharma, A., Eswaran, V., 2006b. Effects of reynolds and prandtl numbers on heat transfer across a square cylinder in the steady flow regime. Numerical Heat Transfer, Part A: Applications 49 (A4), 717–731. (Cited on pages iv, 16, and 39)

Dhiman, A. K., 2006. Flow over and heat transfer to power-law fluids across a sqaure cylinder in steady regime: A numerical study. PhD Thesis, Department of Chemical Engineering, IIT Kanpur, India. (Cited on pages iv and 93)

Dixit, H., Babu, V., 2006. Lattice boltzmann simulation of natural convection heat transfer of al_2o_3 / water nanofluids in a square enclosure. International Journal of Heat and Mass Transfer 49, 727–739. (Cited on page 21)

Djebali, R., Ganaoui, M., Habib, S., 2009. Investigation of a side wall heated cavity by using lattice boltzmann method. European Journal of Computational Mechanics 18, 215–236. (Cited on pages 16, 17, and 21)

Dong, Y., Zhang, J., Yan, G., 2010. A higher-order moment method of the lattice boltzmann model for the conservation law equation. Applied Mathematical Modelling 34, 481–494. (Cited on page 72)

Du, S. Q., Bilgen, E., Vasseur, P., 1998. Mixed convection heat transfer in open ended channels with protruding heaters. International Journal of Heat and Mass Transfer 34, 263–270. (Cited on pages iii, 15, and 29)

DOrazio, A., Succi, S., 2003. Boundary conditions for thermal lattice boltzmann simulations. Lecture Notes in Computer Science 2657, 977–986. (Cited on page 81)

Ekundayo, C. O., 1994. Heat transfer in enclosures: Ovens. PhD Thesis, School of Mechanical Engineering, Department of Applied Energy, University of Cranfield. (Cited on page 10)

Elsasser, W. M., 1954. Dimensional relations in magnetohydrodynamics. The Physical Review 95 (1), 1–5. (Cited on page 25)

Etminan-Farooji, V., Ebrahimnia-Bajestan, E., Niazmand, H., Wongwises, S., 2012. Unconfined laminar nanofluid flow and heat transfer around a square cylinder. International Journal of Heat and Mass Transfer 55, 1475–1485. (Cited on page 39)

Fattahi, E., Farhadi, M., Sedighi, K., 2010. Lattice boltzmann simulation of natural convection heat transfer in eccentric annulus. International Journal of Thermal Sciences 49, 2353–2362. (Cited on page 56)

Fattahi, E., Farhadi, M., Sedighi, K., Nemati, H., 2012. Lattice boltzmann simulation of natural convection heat transfer in nanofluids. International Journal of Thermal Sciences 52, 137–144. (Cited on pages 56, 75, and 99)

Frisch, U., Hasslacher, B., Pomeau, Y., 1986. Lattice as automata for the navier-stokes equation. Physical Review Letters 56 (14), 1505–1508. (Cited on page 7)

Gallivan, M. A., Nobel, D. R., Georgiadis, J. G.and Buckius, R. O., 1997. An evaluation of the bounce-back boundary condition for lattice boltzmann simulations. International Journal for Numerical Methods in Fluids 25, 249–263. (Cited on page 81)

Gerrard, J. H., 1978. The wakes of cylindrical bluff bodies at low reynolds number. Philosophical Transactions of the Royal Society of London. Series A, Mathematical and Physical Sciences 288, 351–382. (Cited on page 38)

Ghazanfarian, J., Abbassi, A., 2010. Heat transfer and fluid flow in microchannels and nanochannels at high knudsen number using thermal lattice-boltzmann method. Physical Review E 82 (046312), 1–8. (Cited on page 101)

Ghia, U., Ghia, K. N., Shin, C. T., 1982a. High-re solutions for incompressible using the navier-stokes equations multigrid method. Journal of Computational Physics 48, 387–411. (Cited on page 90)

Ghia, U., Ghia, K. N., Shin, C. T., 1982b. High-re solutions for incompressible flow using the navier-stokes equations and a multigrid method. Computers & Fluids 48, 387–411. (Cited on page v)

Ginzbourg, I., d'Humieres, D., 2003. Multi reflection boundary conditions for lattice boltzmann models. Physical Review E 68, 066614. (Cited on page 76)

Grosan, T., Revnic, C., Pop, I., Ingham, D. B., 2009. Magnetic field and internal heat generation effects on the free convection in a rectangular cavity filled with a porous medium. International Journal of Heat and Mass Transfer 52, 1525–1533. (Cited on page 28)

Grossmann, S., Lohse, D., 2000. Scaling in thermal convection: a unifying. Journal of Fluid Mechanics 407, 27–56. (Cited on page 113)

Guo, Z., Shi, B., Zhen, C., 2002. A coupled lattice bgk model for the boussinesq equations. International Journal for Numerical Methods in Fluids 39 (4), 325–342. (Cited on pages 69 and 73)

Guo, Z., Zheng, C., Shi, B., Zhao, T. S., 2007. Thermal lattice boltzmann equation for low mach number flows: decoupling model. Physical Review E 75, 1–15. (Cited on pages 69, 70, and 101)

Gupta, A., Sharma, A., Chhabra, R., Eswaran, V., 2003. Two-dimensional steady flow of a power-law fluid past a square cylinder in a plane channel: Momentum and heat-transfer characteristics. Industrial & Engineering Chemistry Research 42, 5674–5686. (Cited on pages 39, 44, and 205)

Ha, M. Y., Jun, M. J., Kim, Y. S., 1999. Numerical study on transient heat transfer and fluid flow of natural convection in an enclosure with a heat-generating conducting body. Numerical Heat Transfer, Part A: Applications 35, 415–433. (Cited on page 35)

Habib, S., Surry, C., Belghith, A., 2005. Analysis of mixed convection at high temperature during the material processing in rotary-kiln. High Temperature Material Process 9, 483–507. (Cited on pages iii and 15)

Haghshenas, A., Nasr, M. R., Rahimian, M. H., 2010a. Numerical simulation of natural convection in an open-ended square cavity filled with porous medium by lattice boltzmann method. International Journal of Heat and Mass Transfer 53, 1513–1519. (Cited on pages 31, 163, and 179)

Haghshenas, A., Rafati Nasr, M., Rahimian, M. H., 2010b. Numerical simulation of natural convection in an open-ended square cavity filled with porous medium by lattice boltzmann method. International Communications in Heat and Mass Transfer 37 (10), 1513–1519. (Cited on page 34)

Han, S., Zhu, P., Lin, Z., 2007. Two-dimensional interpolation-supplemented and taylor-series expansion-based lattice boltzmann method and its application. Communications in Non-linear Science and Numerical Simulation 12, 1162–1171. (Cited on page 42)

Hart, J., 1983. Low prandtl number convection between differentially heated end walls. International Journal of Heat and Mass Transfer 26 (7), 1069–1074. (Cited on page 18)

Hasimoto, H., 1959. On the periodic fundamental solutions of the stokes equations and their application to viscous flow past a cubic array of spheres. Journal of Fluid Mechanics 5 (2), 317–328. (Cited on page 38)

He, X., Chen, S., Doolen, G. D., 1998. A novel thermal model for the lattice boltzmann method in incompressible limit. Journal of Computational Physics 146, 282–300. (Cited on pages v, 68, 69, 70, 71, and 73)

He, X., Luo, L.-S., 1997. A priori derivation of the lattice boltzmann equation. Physical Review E 55 (6), R6333–R6336. (Cited on pages 60 and 62)

He, X., Luo, L.and Dembo, M., 1996. Some progress in lattice boltzmann method. part i. nonuniform mesh grids. Journal of Computational Physics 44, 121135. (Cited on page 87)

He, Y., Qi, C., Hu, Y., Qin, B., Li, F., Ding, Y., 2011. Lattice boltzmann simulation of alumina-water nanofluid in a square cavity. Nanoscale Research Letters 6, 1–8. (Cited on page 155)

Henkes, R. A. W. M., Hoogendoorn, C., 1993. Scaling of the kminar natural-convection flow in a heated square cavity. International Journal of Heat and Mass Transfer 36 (11), 2913–2925. (Cited on page 18)

Heslot, F., Castaing, B., Libchaber, A., 1987. Transitions to turbulence in helium gas. Physical Review A 36, 5870–5873. (Cited on page 113)

Heubes, D., Bartel, A., Ehrhardt, M., 2014. Characteristic boundary conditions in the lattice boltzmann method for fluid and gas dynamics. Journal of Computational and Applied Mathematics 262, 51–61. (Cited on page 76)

Higuera, F., Succi, S., Benzi, R., 1989. Boltzmann approach to lattice gas simulations. Europhysics letter 9, 633. (Cited on page 60)

Hiller, W. J., Koch, S., Kowalewski, T. A., 1989. Three-dimensional structures in laminar natural convection in a cubic enclosure. Experimental Thermal and Fluid Science 2 (1), 34–44. (Cited on pages 16, 17, and 21)

Hinojosa, J. F., Cabanillas, R. E., Alvarez, G., Estrada, C. E., 2005. Nusselt number for the natural convection and surface thermal radiation in a square tilted open cavity. International Communications in Heat and Mass Transfer 32 (9), 1184–1192. (Cited on page 30)

Hobbi, A., Siddiqui, K., 2009. Experimental study on the effect of heat transfer enhancement devices in at-plate solar collectors. International Journal of Heat and Mass Transfer 52, 4650–4658. (Cited on pages iii, 15, and 29)

Hoffman, P., 1998. The man who loved only numbers: The story of paul erdos and the search for mathematical truth. New York: Hyperion, 238–239. (Cited on page 8)

Hossain, M. S., Alim, M. A., 2013. Effects of heat flow patterens for mhd free convection within trapezoidal cavity based on heatline concept. International Journal of Mathematics and Computer Applications Research 3 (2), 87–102. (Cited on page 28)

Hou, S., Zou, Q., Chen, S., Doolen, H., Cogley, A. C., 1995. Simulation of cavity flow by the lattice boltzmann method. Journal of Computational Physics 118, 329–347. (Cited on page 71)

House, J. M., Beckermann, C., Smith, T. F., 1990. Effect of a centered conducting body on natural convection heat transfer in an enclosure. Numerical Heat Transfer, Part A: Applications 18, 213–225. (Cited on page 35)

Howard, L., 1963. Heat transport by turbulent convection. Journal of Fluid Mechanics 17, 405–432. (Cited on page 113)

Hsiao, K. L., 2007. Conjugate heat transfer of magnetic mixed convection with radiative and viscous dissipation effects for second-grade viscoelastic fluid past a stretching sheet. Applied Thermal Engineering 27, 1895–1903. (Cited on pages iii, 15, and 29)

Hsu, T. H., Wang, S. G., 2000. Mixed convection in a rectangular enclosure with discrete heat sources. Numerical Heat Transfer, Part A: Applications 38, 627–652. (Cited on pages iii, 15, and 29)

Hussein, A. K., Ashorynejad, H. R., Shikholeslami, M., Sivasankaran, S., 2014. Lattice boltzmann simulation of natural convection heat transfer in an open enclosure filled with cuwater nanofluid in a presence of magnetic field. Nuclear Engineering and Design 268, 10–17. (Cited on page 33)

Imberger, J., 1974a. Natural convection in a shallow cavity with differentially heated end walls. part 3. experimental results. Journal of Fluid Mechanics 65 (2), 247–260. (Cited on page 17)

Imberger, J., 1974b. Natural convection in a shallow with differentially heated end walls. part 3. experimental results. Journal of Fluid Mechanics 65 (2), 247–260. (Cited on page 18)

Islam, S., Zhou, C., Shah, A., Xie, P., 2012. Numerical simulation of flow past rectangular cylinders with different aspect ratios using the incompressible lattice boltzmann method. Journal of Mechanical Science and Technology 26 (4), 1027–1041. (Cited on page 47)

Jafari, M., Farhadi, M., Sedighi, K., 2014. Single walled carbon nanotube effects on mixed convection heat transfer in an enclosure: a lbm approach. Journal of Transport Phenomena in Nano and Micro Scales 2 (1), 14–28. (Cited on page v)

Jami, M., Mezrhab, A., Bouzidi, M., Lallemand, P., 2007a. Lattice boltzmann method applied to the laminar natural convection in an enclosure with a heat-generating cylinder conducting body. International Journal of Thermal Sciences 46, 38–47. (Cited on pages 20 and 101)

Jami, M., Mezrhab, A., Bouzidi, M., Lallemand, P., 2007b. Lattice boltzmann method applied to the laminar natural convection in an enclosure with a heat-generating cylinder conducting body. International Journal of Thermal Sciences 46, 38–47. (Cited on page 37)

Janssen, R., Armfield, S., 1996. Stability properties of the vertical boundary layers in differentially heated cavities. International Journal of Heat and Fluid Flow 17 (6), 547–556. (Cited on page 18)

Janssen, R. J. A., Henkes, R. A. W. M., J., H. C., 1993. Transition to time-periodicity of a natural-convection flow-in a 3d differentially heated cavity. International Journal of Heat and Mass Transfer 36 (11), 2927–2940. (Cited on page 18)

Jmai, R., Ben-Beya, B., T., L., 2013. Heat transfer and fluid flow of nanofluid-filled enclosure with two partially heated side walls and different nanoparticles. Superlattices and Microstructures 53, 130–154. (Cited on pages iv and 34)

Juarez, J. O., Hinojosa, J. F., Xaman, J. P., Tello, M. P., 2011. Numerical study of natural convection in an open cavity considering temperature-dependent fluid properties. International Journal of Thermal Sciences 50, 2184–2197. (Cited on pages 186 and 187)

Kahveci, K., Oztuna, S., 2009. Mhd natural convection flow and heat transfer in a laterally heated partitioned enclosure. European Journal of Mechanics B / Fluids 28, 744–752. (Cited on page 28)

Kakarantzas, S. C., Sarris, I. E., Grecos, A. P., Vlachos, N. S., 2009. Magnetohydrodynamic natural convection in a vertical cylindrical cavity with sinusoidal upper wall temperature. International Journal of Heat and Mass Transfer 52, 250–259. (Cited on page 25)

Kaluri, R. S., Basak, T., 2010. Heatline analysis of thermal mixing due to natural convection in discretely heated porous cavities filled with various fluids. Chemical Engineering Science 65, 2132–2152. (Cited on pages 31 and 34)

Kandaswamy, P., Kumar, K., 1999. Buoyancy-driven non-linear convection in a square cavity in the presence of magnetic field. Act Mechanica 136, 29–39. (Cited on page 25)

Kandaswamy, P., Sundari, S. M., Nithyadevi, N., 2008. Magnetoconvection in an enclosure with partially active vertical walls. International Journal of Heat and Mass Transfer 51, 1946–1954. (Cited on page 22)

Kandhai, D., Vidal, D. J., Hoekstrah, A. G., Hoefsloot, H., Iedema, H. P., Sloot, P. M. A., 1998. A comparison between lattice-boltzmann and finite-element simulations of fluid flow in static mixer reactors. International journal of Modern Physics C 9 (8), 1123–1128. (Cited on pages 87 and 88)

Kao, P., Chen, Y., Yang, R., 2006. Simulations of the macroscopic and mesoscopic natural convection flows within rectangular cavities. International Journal of Thermal Sciences 51, 3776–3793. (Cited on pages 99 and 133)

Kao, P., Ren, T., Yang, R., 2007. An investigation into fixed-bed microreactors using lattice boltzmann method simulations. International Journal of Thermal Sciences 50, 4243–4255. (Cited on page v)

Kao, P., Yang, R., 2007. Simulating oscillatory flows in rayleigh-benard convection using the lattice boltzmann method. International Journal of Thermal Sciences 50, 3315–3328. (Cited on pages 20, 21, 99, 101, 113, and 133)

Kareem, A., Cermak, J. E., 1984. Pressure fluctuations on square building model in boundary-layer flows. Journal of Wind Engineering and Industrial Aerodynamics 16, 17–41. (Cited on page 38)

Kefayati, G., Gorji-Bandpy, M., Sajjadi, H., 2012a. Investigation of prandtl number effect on natural convection mhd in an open cavity by lattice boltzmann method. International Journal of Thermal Sciences 30 (1), 97–116. (Cited on pages 21, 28, 32, 34, and 75)

Kefayati, G. R., 2013a. Effect of a magnetic eld on natural convection in an open cavity subjugated to water/alumina nanouid using lattice Boltzmann method. International Journal of Heat and Mass Transfer 40, 67–77. (Cited on pages 33, 76, 156, and 157)

Kefayati, G. R., 2013b. Lattice boltzmann simulation of natural convection in nanofluid-filled 2d long enclosures at presence of magnetic field. Theoretical and Computational Fluid Dynamics 27, 865–883. (Cited on pages 23 and 28)

Kefayati, G. R., 2013c. Mhd natural convection flow and heat transfer in a laterally heated partitioned enclosure. International Communications in Heat and Mass Transfer 40, 67–77. (Cited on page 28)

Kefayati, G. R., Hosseinizadeh, S. F., Gorji, M., Sajjadi, H., 2012b. Lattice boltzmann simulation of natural convection in an open enclosure subjugated to water/copper nanouid. International Communications in Heat and Mass Transfer 52, 147–168. (Cited on page 34)

Khanafer, K., Vafai, K., 2000. Buoyancy-driven fow and heat transfer in open-ended enclosures: elimination of the extended boundaries. International Journal of Heat and Mass Transfer 43, 4087–4100. (Cited on page 30)

Khanafer, K., Vafai, K., 2002. Effective boundary conditions for buoyancy-driven flows and heat transfer in fully open-ended two-dimensional enclosures. International Journal of Heat and Mass Transfer 45, 2527–2538. (Cited on pages 30 and 34)

Kim, B. S., Lee, D. S., Ha, M. Y., Yoon, H. S., 2008. A numerical study of natural convection in a square enclosure with a circular cylinder at different vertical locations. International Journal of Heat and Mass Transfer 51, 1888–1906. (Cited on page 37)

Koca, A., Oztop, H. F., Varol, Y., 2007. The effects of prandtl number on natural convection in triangular enclosures with localized heating from below. International Communications in Heat and Mass Transfer 34, 511–519. (Cited on page 20)

Koteswara Rao, P., Sasmal, C., Sahu, A., Chhabra, R., Eswaran, V., 2011. Effect of power-law fluid behavior on momentum and heat transfer characteristics of an inclined square cylinder in steady flow regime. International Journal of Heat and Mass Transfer 54, 2854–2867. (Cited on pages 16 and 124)

Kuznik, F., Vareilles, J., Rusaouen, G., Krauss, G., 2007. A double-population lattice boltzmann method with non-uniform mesh for the simulation of natural convection in a square cavity. International Journal of Heat and Fluid Flow 28 (4), 862–870. (Cited on pages 21, 51, 56, 69, 70, 71, and 101)

Lai, F. H., Yang, Y. T., 2011. Lattice boltzmann simulation of natural convection heat transfer of al_2o_3 / water nanofluids in a square enclosure. International Journal of Thermal Sciences 50, 1930–1941. (Cited on page 20)

Lal, S. A., Reji, C., 2009. Numerical prediction of natural convection in vented cavities using restricted domain approach. International Journal of Heat and Mass Transfer 52, 724–734. (Cited on pages 186 and 187)

Lallemand, P., Luo, L.-S., 2003. Theory of the lattice boltzmann method: Acoustic and thermal properties in two and three dimensions. Physical Review E 68 (036706), 1–25. (Cited on page 70)

Lee, B. E., 1975. The effect of turbulence on the surface pressure field of a square prism. Journal of Fluid Mechanics 69 (2), 263–282. (Cited on page 38)

Lee, J. M., Ha, M. Y., Yoon, H. S., 2010. Natural convection in a square enclosure with a circular cylinder at different horizontal and diagonal locations. International Journal of Heat and Mass Transfer 53, 5905–5919. (Cited on pages 37 and 101)

Lee, Y., Kim, J., Hur, J., 2014. Study on the empirical design of open-ended coaxial cavity resonator. Microwave and Optical Technology Letters 56 (3), 606–610. (Cited on page 33)

Li, H., Braun, M. J., Paudel, G., 2006. Flow structure and heat transfer in a lower half heated and upper half cooled rectangular enclosure. International Journal of Heat and Mass Transfer 49, 3462–3476. (Cited on page 22)

Li, Q., He, Y. L., Tang, G. H., Tao, Q., 2004. Lattice boltzmann model for axisymmetric thermal flows. Physical Review E 70 (016703), 1–9. (Cited on page 71)

Like, L., Renwei, M., James, F. K., 2013. Boundary conditions for thermal lattice boltzmann equation method. Journal of Computational Physics 237, 366–395. (Cited on pages 76 and 81)

Lin, D. S., Nansteel, M., 1987. Natural convection heat transfer in a square enclosure containing water near its density maximum. International Journal of Heat and Mass Transfer 30 (11), 2319–2329. (Cited on pages 16, 17, and 21)

Lu, J., Shi, B., Guo, Z., Chai, Z., 2009. Numerical study on natural convection in a square enclosure containing a rectangular heated cylinder. Frontiers of Energy and Power Engineering in China 3 (4), 373–380. (Cited on page 37)

Luo, X.-H., Li, B.-W., Zhang, J.-K., Hu, Z.-M., 2014. Simulation of thermal radiation effects on mhd free convection in a square cavity using the chebyshev collocation spectral method. Numerical Heat Transfer, Part A: Applications 66, 792–815. (Cited on page 27)

Mahmoudi, A., Mejri, I., Abbassi, M. A., Omri, A., 2014. Lattice boltzmann simulation of mhd natural convection in a nanofluid-filled cavity with linear temperature distribution. Powder Technology256, 257–271. (Cited on pages 28 and 136)

Manca, O., Nardini, S., 2010. Composite correlations for air natural convection in tilted channels. Heat Transfer Engineering 20 (3), 64–72. (Cited on pages iii and 15)

Manca, O., Nardini, S., Khanafer, K., Vafai, K., 2003. Effect of heated wall position on mixed convection in a channel with an open cavity. Numerical Heat Transfer, Part A: Applications 43, 259–282. (Cited on page 30)

Markatos, N., Pericleous, K., 1984. Laminar and turbulent natural convection in enclosed cavity. Journal of Fluid Mechanics 27 (5), 755–772. (Cited on pages 17 and 113)

Matida, Y., Kuwahara, K., Takami, H., 1975. Numerical study of steady two dimensional flow past a square cylinder in a channel. Journal of the physical society of Japan 38 (5), 1682–1702. (Cited on page 38)

Mc Namara, G. R., Zanetti, G., 1988. Use of the soltzmann equation to simulate lattice-gas automata. Physical Review Letters 61 (20), 2332–2335. (Cited on pages 60, 64, and 83)

Mcdonough, J., Catton, I., 1982. Accuracy of the mean field approximation and the physical effect of prandtl number in bnard convection. Physics of Fluids 25, 1502–1505. (Cited on page 18)

Metropolis, N., Ulam, S., 1949. The monte carlo method. Journal of the American Statistical Association 44, 335–341. (Cited on page 8)

Mezrhab, A., Amine, M., Jami, M., Naji, H., Bouzidi, M., 2010. Double mrt thermal lattice boltzmann method for simulating convective flows. Physical Review A 374, 3499–3507. (Cited on pages 21, 101, and 102)

Mezrhab, A., Bouali, H., Amaoui, H., Bouzidi, M., 2006. Computation of combined natural-convection and radiation heat-transfer in a cavity having a square body at its center. æ83, 1004–1023. (Cited on page 36)

Miller, W., 1995. Flow in the driven cavity calculated by the lattice boltzmann method. Physical Review E 51 (4), 3659–3669. (Cited on pages 7 and 60)

Minewitsch, S., Frank, R., Rodi, W., 1994. Numerical investigation of laminar vortex shedding flow past a square cylinder oscillating in line with the mean flow. Journal of Fluids and Strcutures 8, 787–802. (Cited on page 39)

Mishra, S. C., Kumar, T. B. P., Mondal, B., 2008. Lattice boltzmann method applied to the solution of energy equation of a radiation and non-fourier heat conduction problem. Numerical Heat Transfer, Part A: Applications 54, 798–818. (Cited on page iv)

Mishra, S. C., Lankadasu, A., N., B. K., 2005. Application of the lattice boltzmann method for solving the energy equation of a 2-d transient conductionradiation problem. International Journal of Heat and Mass Transfer 48, 3648–3659. (Cited on page iv)

Mishra, S. C., Roy, H. K., 2007. Solving transient conduction and radiation heat transfer problems using the lattice boltzmann method and the finite volume method. Journal of Computational Physics 223, 89–107. (Cited on page iv)

Mohamad, A. A., 1995. Natural convection in an open cavities and slots. Numerical Heat Transfer, Part A: Applications 27, 705–716. (Cited on pages 29, 156, 157, and 163)

Mohamad, A. A., 2011. Lattice Boltzmann Method:Fundamentals and Engineering Applications with Computer Codes. Springer . (Cited on pages 3, 60, 61, 62, 64, 67, 71, 72, 77, 78, 79, 80, 81, 82, 83, and 87)

Mohamad, A. A., Bennacer, R., El-Ganaoui, M., 2010. Double dispersion, natural convection in an open end cavity simulation via lattice boltzmann method. International Journal of Heat and Mass Transfer 49, 1944–1953. (Cited on page 34)

Mohamad, A. A., El-Ganaoui, M., Bennacer, R., 2009. Lattice boltzmann simulation of natural convection in an open ended cavity. International Journal of Thermal Sciences 48 (10), 1870–1875. (Cited on pages v, 31, 34, 56, 156, 157, 163, and 179)

Mondal, B., Li, X., 2010. Effect of volumetric radiation on natural convection in a square cavity using lattice boltzmann method with non-uniform lattices. International Journal of Heat and Mass Transfer 53, 4935–4948. (Cited on page 21)

Mondal, B., Mishra, S. C., 2009. Simulation of natural convection in the presence of volumetric radiation using the lattice boltzmann method. Numerical Heat Transfer, Part A: Applications 55, 18–41. (Cited on page v)

Montiel-Gonzaleza, M., Hinojosab, J., Villafan-Vidalesc, H., Bautista-Orozcoc, A., Estrada, C., 2014. Theoretical and experimental study of natural convection with surface thermal radiation in a side open cavity. Applied Thermal Engineering 10.1016/j.applthermaleng.2014.05.047. (Cited on page 33)

Moussaoui, M. A., Mezrhab, A., Naji, H., 2011. A computation of flow and heat transfer past three heated cylinders in a vee shapeby a double distribution mrt thermal lattice boltzmann model. International Journal of Thermal Sciences 50, 1532–1542. (Cited on page 42)

Muftuoglu, A., Bilgen, E., 2008. Natural convection in an open square cavity with discrete heaters at their optimized positions. International Journal of Thermal Sciences 47, 369–377. (Cited on page 31)

Murlidhar, K., Sundararajan, T., 2003. Computational Fluid Flow and Heat Transfer. IIT Kanpur Lecture series, Narosa Publishers, N. Delhi, second edition. (Cited on page 1)

Muthtamilselvan, M., Doh, D.-H., 2014. Magnetic field effect on mixed convection in a lid-driven square cavity filled with nanofluids. Journal of Mechanical Science and Technology 28 (1), 137–143. (Cited on page 27)

Nasr, K. B., Chouikh, R., Kerkeni, C., Guizani, A., 2006. Numerical study of the natural convection in cavity heated from the lower corner and cooled from the ceiling. Applied Thermal Engineering 26, 772–775. (Cited on page 31)

Nazari, M., Mohebbi, R., Kayhani, M. H., 2014. Computation of transitional flow past a circular cylinder using multiblock lattice boltzmann method with a dynamic subgrid scale model. Journal of Non-Newtonian Fluid Mechanics 204, 38–49. (Cited on pages 43 and 46)

Nazari, M., Ramzani, S., 2014. Cooling of an electronic board situated in various configurations inside an enclosure: lattice boltzmann method. Meccanica 49, 645–658. (Cited on page v)

Niemela, J., Skrbek, L., Sreenivasan, K., Donnelly, R., 2000. Turbulent convection at very high rayleigh numbers. Nature 404, 837–840. (Cited on page 113)

Nikbakhti, R., B., R. A., 2012. Double-diffusive natural convection in a rectangular cavity with partially thermally active side walls. Journal of the Taiwan Institute of Chemical Engineers 43, 535–541. (Cited on pages iv and 34)

Nithyadevi, N., Kandaswamy, P., Lee, J., 2007. Natural convection in a rectangular cavity with partially active side walls. International Journal of Heat and Mass Transfer 50, 4688–4697. (Cited on pages 22 and 24)

Nitin, S., Chhabra, R., 2005. Non-isothermal flow of a power law fluid past a rectangular obstacle (of aspect ratio 1:2) in a channel:drag and heat transfer. International Journal of Engineering Science 43, 707–720. (Cited on pages 47 and 206)

Noble, C., Chen, S., Georgiadis, J. G., Buckius, R. O., 1995. A consistent hydrodynamic boundary condition for the lattice boltzmann method. Physics of Fluids 7, 203–209. (Cited on page 76)

Norberg, C., 1993. Flow around rectangular cylinders: Pressure forces and wake frequencies. Journal of Wind Engineering and Industrial Aerodynamics 49, 187–196. (Cited on page 45)

Obasaju, E. D., 1979. On the effects of end plates on the mean forces on square sectioned cylinders. Journal of Industrial Aerodynamics 5, 179–186. (Cited on page 38)

Oh, J. Y., Ha, M. Y., Kim, K. C., 1997. Numerical study of heat transfer and flow of natural convection an enclosure with a heat generating conducting body. Numerical Heat Transfer, Part A: Applications 31, 289–303. (Cited on page 35)

Okajima, A., 1982. Strouhal numbers of rectangular cylinders. Journal of Fluid Mechanics 123, 379–398. (Cited on page 45)

Ostrach, S., 1972. Natural convection in enclosures. Adv. Heat Transfer 8, 161–227. (Cited on page 18)

Oztop, H. F., 2007. Natural convection in partially cooled and inclined porous rectangular. International Journal of Thermal Sciences 46, 149–156. (Cited on pages 22 and 24)

Oztop, H. F., Abu-Nada, E., 2008. Numerical study of natural convection in partially heated rectangular enclosures filled with nanofluids. International Journal of Heat and Fluid Flow 29, 1326–1336. (Cited on page 22)

Paliwal, B., Sharma, A., Chhabra, R., Eswaran, V., 2003. Power law fluid flow past a square cylinder: momentum and heat transfer characteristics. Journal of Fluids and Strcutures 58, 5315–5329. (Cited on pages 39 and 57)

Park, S., Chung, Y., Cheon, C., 2013. Simple technique for measurement of complex permittivity and detection of small permittivity change using partially open cavity. Journal of Electrical Engineering & Technology 8, 742–746. (Cited on page 33)

Park, T. S., 2013. Effects of an inserted square cylinder on wall heat transfer in laminar channel flows. Journal of Mechanical Science and Technology 27 (5), 1501–1508. (Cited on page 41)

Park, Y., Sik, H., Yeong, M., 2012. Lattice boltzmann simulation of natural convection heat transfer of al_2o_3 / water nanofluids in a square enclosure. International Journal of Heat and Mass Transfer 55, 7911–7925. (Cited on page 21)

Patil, P. P., Tiwari, S., 2008. Effect of blockage ratio on wake transition for flow past square cylinder. Fluid Dynamics Research 40, 753–778. (Cited on pages 40 and 44)

Patterson, J., Imberger, J., 1980. Unsteady natural convection in a rectangular cavity. Journal of Fluid Mechanics 100 (1), 66–86. (Cited on page 17)

Pattison, M. J., Premnath, K. N., Morley, N. B., Abdou, M. A., 2008. Progress in lattice boltzmann methods for magnetohydrodynamic flows relevant to fusion applications. Fusion Engineering and Design 83, 557–572. (Cited on page 25)

Peng, Y., 2005. Thermal lattice boltzmann two phase flow model for fluid dynamics. PhD ThesisUniversity of Pittsburgh. (Cited on page 70)

Peng, Y., Shu, C., Chew, Y. T., 2003a. A 3d incompressible thermal lattice boltzmann model and its application to simulate natural convection in a cubic cavity. Journal of Computational Physics 193, 260–274. (Cited on pages 51, 70, and 73)

Peng, Y., Shu, C., Chew, Y. T., 2003b. Simplified thermal lattice boltzmann model for incompressible thermal flow. Physical Review E 68 (026701), 1–8. (Cited on pages v, 21, 70, 71, and 75)

Perumal, D. A., Kumar, G. V. S., Dass, A. K., 2012. Numerical simulation of viscous flow over a square cylinder using lattice boltzmann method. ISRN Mathematical Physics , 1–16. (Cited on pages 43 and 46)

Petty, D., 1979. The effect of turbulence intensity and scale on the flow past square prism. Journal of Industrial Aerodynamics 4, 247–252. (Cited on page 38)

Phillips, T. N., 1984. Natural convection in an enclosed cavity. Journal of Computational Physics 54, 365–381. (Cited on page 17)

Piazza, I. D., Ciofalo, M., 2000. Low-prandtl number natural convection in volumetrically heated rectangular enclosures i. slender cavity , ar = 4. International Journal of Heat and Mass Transfer 43, 3027–3051. (Cited on page 19)

Pirmohammadi, M., Ghassemi, M., 2009. Effect of magnetic field on convection heat transfer inside a tilted square enclosure. International Journal of Heat and Mass Transfer 36, 776–780. (Cited on page 28)

Podvin, B., Quere, P., 2001. Low-order models for the flow in a differentially heated cavity. Physics of Fluids 13 (11), 3204–3214. (Cited on page 19)

Polat, O., Bilgen, E., 2002. Laminar natural convection in inclined open shallow cavities. International Journal of Thermal Sciences 41, 360–368. (Cited on page 30)

Poots, G., 1961. Laminar natural convection flow in magneto-hydrodynamics. International Journal of Heat and Mass Transfer 3, 1–25. (Cited on page 25)

Prakash, M., 2013. Numerical studies on natural convection heat losses from open cubical cavities. Journal of Engineering 320647, 1–9. (Cited on pages 186 and 187)

Prakash, M., Kedare, S. B., Nayak, J. K., 2012. Numerical study of natural convection loss from open cavities. International Journal of Thermal Sciences 51, 23–30. (Cited on pages 32, 186, and 187)

Prasianakis, N. I., Karlin, I. V., 2007. Lattice boltzmann method for thermal flow simulation on standard lattices. Physical Review E 76 (016702), 1–11. (Cited on page 71)

Premnath, K. N., J., P. M., Banerjee, S., 2013. Computation of transitional flow past a circular cylinder using multiblock lattice boltzmann method with a dynamic subgrid scale model. Fluid Dynamics Research 45, 1–26. (Cited on pages 43 and 46)

Qi-Hong Deng, Q.-H., Tang, G.-F., Li, Y., Ha, M. Y., 2002. Interaction between discrete heat sources in horizontal natural convection enclosures. International Journal of Heat and Mass Transfer 45, 5117–5132. (Cited on page 36)

Qian, Y. H., 1990. Lattice gas and lattice kinetic theory applied to the navier-stokes equations. PhD Thesis. (Cited on pages 64, 65, 68, and 73)

Qian, Y. H., d'Humieres, D., Lallemand, P., 1992. Lattice bgk models for navier-stokes equation. Europhysics letter 17, 479–484. (Cited on pages 64, 65, 68, 72, and 99)

Qian, Y. H., d'Humieres, D., Lallemand, P., 1993. Simulating thermohydrodynamics with lattice bgk model. Journal of Scientific Computing8, 231–241. (Cited on pages 64, 65, and 73)

Qiana, S., Bau, H. H., 2009. Magneto-hydrodynamics based microfluidics. Mechanics Research Communications 36 (1), 10–21. (Cited on page 23)

Quere, P. L., Behnia, M., 1998. From onset of unsteadiness to chaos in a differentially heated square cavity. Journal of Fluid Mechanics 359, 81–107. (Cited on page 18)

Rahman, M. M., Oztop, H. F., Ahsan, A., Kalam, M. A., Billah, M. M., 2012. Mixed convection in a channel with a triangular cavity. Numerical Heat Transfer, Part A: Applications 61, 268–282. (Cited on page 26)

Rahman, M. M., Parvin, S., Saidur, R., Rahim, N. A., 2011a. Magnetohydrodynamic mixed convection in a horizontal channel with an open cavity. International Communications in Heat and Mass Transfer 138, 184–193. (Cited on page 28)

Rahman, M. M., Saidur, R., Rahim, N. A., 2011b. Conjugated effect of joule heating and magneto-hydrodynamic on double-diffusive mixed convection in a horizontal channel with an open cavity. International Journal of Heat and Mass Transfer 54, 3201–3213. (Cited on pages 23 and 28)

Rahman, M. M. R., Mamunc, M. A. H., Saidur, R., 2011c. Analysis of magnetohydrodynamic mixed convection and joule heating in lid-driven cavity having a square block. Journal of the Chinese Institute of Engineers 34 (5), 585–599. (Cited on page 38)

Rao, K. P., Sahu, A. K., Chhabra, R. P., 2010. Momentum and heat transfer from a square cylinder in power-law fluids. International Journal of Heat and Mass Transfer 54, 390–403. (Cited on page 40)

Rashidi, S., Bovand, M., Pop, I., Valipour, M. S., 2014. Numerical simulation of forced convective heat transfer past a square diamond-shaped porous cylinder. Transport in Porous Media 102, 207–225. (Cited on page 41)

Reyes, M., Velazquez, A., Martin, E., Arias, J. R., 2013. Experimental study on the conned 3d laminar ow past a square prism with a high blockage ratio. International Journal of Heat and Mass Transfer 44, 444–457. (Cited on pages 41 and 44)

Roberts, P. H., Soward, A. M., 1972. Magnetohydrodynamics of the earth's core. Annual Reviews of Fluid Mechanics 4, 117–154. (Cited on page 25)

Robertson, J. M., Wedding, J. B., Peterka, J., Cermak, J., 1978. Wall pressures of seperation- reattachment flow on a square prism in uniform flow. Journal of Industrial Aerodynamics 2, 345–359. (Cited on page 38)

Rockwell, D. O., 1977. Organized fluctuations due to flow past a square cross section cylinder. Journal of Fluids Engineering 99 (3), 511–516. (Cited on page 38)

Roshko, A., 1993. Perspectives on bluff body aerodynamics. Journal of Wind Engineering and Industrial Aerodynamics 49, 79–100. (Cited on page 38)

Rowghani, S., Mirzaei, M., Kamali, R., 2010. Numerical simulation of fluid flow past a square lbm cylinder using a lattice boltzmann method. Journal of Aerospace Science and Technology 7 (1), 9–17. (Cited on pages 42 and 46)

Roy, S., Basak, T., 2005. Finite element analysis of natural convection flows in a square cavity with non-uniformly heated wall(s). International Journal of Engineering Science 43, 668–680. (Cited on pages iii, 19, and 21)

Sahu, A., Chhabra, R., Eswaran, V., 2009. Effects of reynolds and prandtl numbers on heat transfer from a square cylinder in the unsteady ow regime. International Journal of Heat and Mass Transfer 52 (3-4), 839–850. (Cited on pages 16 and 39)

Sahu, A. K., 2010. Power law fluid flow across a square cylinder in unsteady laminar flow regime. PhD Thesis, Department of Chemical Engineering, IIT Kanpur, India. (Cited on page iv)

Sahu, A. K., Chhabra, R. P., Eswaran, V., 2010. Two-dimensional laminar ow of a power-law uid across a conned square cylinder. Journal of Non-Newtonian Fluid Mechanics 165, 752–763. (Cited on pages 40 and 44)

Sajjadi, H., Gorji, M., Kefayati, G. R., Ganji, D. D., Shayannia, M., 2010. Simulation of natural convection flow in an inclined open cavity using lattice boltzmann method. World Academy of Science, Engineering and Technology 55, 265–271. (Cited on pages 32 and 156)

Saleem, M., Md. Hossain, A., Mahmud, S., Pop, I., 2011. Entropy generation in marangoni convection flow of heated fluid in an open ended cavity. International Journal of Heat and Mass Transfer 54, 4473–4484. (Cited on page 32)

Sankar, M., Bhuvaneswari, M., Sivasankaran, S., Do, Y., 2011. Buoyancy induced convection in a porous cavity with partially thermally active sidewalls. International Journal of Heat and Mass Transfer 54, 5173–5182. (Cited on pages iv and 34)

Sankaranarayanan, K., Shan, X., Kevrekidis, I. G., Sundaresan, S., 2002. Analysis of drag and virtual mass forces in bubbly suspensions using an implicit formulation of the lattice boltzmann method. Journal of Fluid Mechanics 452, 61–96. (Cited on page v)

Sathiyamoorthy, M., Basak, T., Roy, S., Pop, I., 2007. Investigation of prandtl number effect on natural convection mhd in an open cavity by lattice boltzmann method. International Journal of Heat and Mass Transfer 50 (1), 766–775. (Cited on page 19)

Shankar, P., Deshpande, M., 2000. Fluid mechanics in the driven cavity. Annual Reviews of Fluid Mechanics 32, 93–136. (Cited on page 90)

Sharma, A., Eswaran, V., 2004. Heat and fluid flow across a square cylinder in the two-dimensional laminar flow region. Numerical Heat Transfer, Part A: Applications 45, 247–269. (Cited on pages 11 and 39)

Sharma, A., Eswaran, V., 2005. Effect of channel confinement on the two dimensional laminar flow and heat trasfer across a square cylinder. Numerical Heat Transfer, Part A: Applications 47, 79–107. (Cited on pages iv, 39, 44, and 210)

Sharma, A., Eswaran, V., 2010. Heat and fluid flow across a square cylinder in the two dimensional laminar flow regime. Numerical Heat Transfer, Part A: Applications 45, 247–269. (Cited on page 39)

Sharma, N., Dhiman, A., Kumar, S., 2012. Numerical investigation of forced convection heat transfer in unsteady flow past a row of square cylinders. International Journal of Heat and Mass Transfer 55, 1–8. (Cited on pages iv and 16)

Sheikholeslami, M., Gorji-Bandpy, M., Ganji, D. D., Soleimani, S., Seyyedi, S. M., 2012. Natural convection of nanofluids in an enclosure between a circular and a sinusoidal cylinder in the presence of magnetic field. International Journal of Heat and Mass Transfer 39 (9), 1435–1443. (Cited on page v)

Sheikholeslami, M., Gorji-Bandpy, M., Pop, I., Soleimani, S., 2013a. Numerical study of natural convection between a circular enclosure and a sinusoidal cylinder using control volume based finite element method. International Journal of Thermal Sciences 72, 147–158. (Cited on page 38)

Sheikholeslami, M., Gorji-Bandpy, M., Seyyedi, S., Ganji, D., Rokni, H., Soleimani, S., 2013b. Application of lbm in simulation of natural convection in a nanofluid filled square cavity with curve boundaries. Powder Technology247, 87–94. (Cited on pages 32 and 34)

Sheikholeslami, M. amd Gorji-Bandpy, M., Ganji, D. D., 2014. Lattice boltzmann method for mhd natural convection heat transfer using nanofluid. Powder Technology254, 82–93. (Cited on page 28)

Sheikhzadeh, G. A., Arefmanesh, A., Kheirkhah, M. H., Abdollahi, R., 2011a. Natural convection of cuwater nanofluid in a cavity with partially active side walls. European Journal of Mechanics B / Fluids 30, 166–176. (Cited on page 23)

Sheikhzadeh, G. A., Fattahi, A., Mehrabian, M. A., 2011b. Numerical study of steady magneto-convection around an adiabatic body inside a square enclosure in low prandtl numbers. Heat and Mass Transfer 47, 27–34. (Cited on page 26)

Shim, J. W., Gatignol, R., 2011. Thermal lattice boltzmann method based on a theoretically simple derivation of the taylor expansion. Physical Review E 83 (046710), 1–5. (Cited on page 71)

Shin, C., Economou, D., 1990. Mass transfer by natural and forced convection open cavities. International Journal of Heat and Mass Transfer 33 (10), 2191–2205. (Cited on page 29)

Singh, A. K., Roy, S., Basak, T., 2012. Visualization of heat transport during natural convection in a tilted square cavity: Effect of isothermal and nonisothermal heating. Heat and Mass Transfer 61, 417–441. (Cited on page 23)

Singh, R. K., Kumar, S., Kumar, S., Kumar, A., 2008. Development of parthenium based activated carbon and its utilization for adsorptive removal of p-cresol from aqueous solution. Journal of Hazardous Materials 155, 523–535. (Cited on pages 114 and 189)

Siscoe, G. L., 1983. Solar system magnetohydrodynamics. Solar-Terrestrial Physics, Astrophysics and Space Science Library Volume 104, 11–100. (Cited on page 25)

Sivakumar, P., Bharti, R. P., Chhabra, R. P., 2006. Effect of power-law index on critical parameters for power-law flow across an unconfined circular cylinder. Chemical Engineering Science 61 (18), 6035–6046. (Cited on pages 67 and 156)

Sivakumar, P., Bharti, R. P., Chhabra, R. P., 2007. Steady flow of power-law uids across an unconned elliptical cylinder. Chemical Engineering Science 62, 1682–1702. (Cited on pages 56 and 58)

Sivakumar, V., Sivasankaran, S., Prakash, P., Lee, J., 2010. Effect of heating location and size on mixed convection in lid-driven cavities. Computers and Mathematics with Applications 59, 3053–3065. (Cited on page 34)

Sivasankaran, S., Bhuvaneswar, M., 2011. Effect of thermally active zones and direction of magnetic field on hydromagnetic convection in an enclosure. Thermal Science 15 (2), S367–S382. (Cited on page 24)

Skok, H., Ramadhyani, S., Schoenhals, R. J., 1990. Natural convection in a side-facing open cavity. International Journal of Heat and Fluid Flow 12 (1), 36–45. (Cited on pages iii and 15)

Skordos, P. A., 1993. Initial and boundary conditions for the lattice boltzmann method. Physical Review A 48, 4823–4842. (Cited on page 76)

Sofone, V., Sekerka, R. F., 2005. Diffuse-reflection boundary conditions for a thermal lattice boltzmann model in two dimensions: Evidence of temperature jump and slip velocity in microchannels. Physical Review E 71 (066709), 1–10. (Cited on page 76)

Sohankar, A., Norberg, C., Davidson, L., 1997. Numerical simulation of unsteady low-reynolds number flow around rectangular cylinders at incidence. Journal of Wind Engineering and Industrial Aerodynamics 69-71, 189–201. (Cited on page 45)

Spall, R. E., 1996. Unsteady mixed convection in horizontal ducts with applications to chemical vapor deposition processes. International Journal of Heat and Mass Transfer 23, 115–122. (Cited on pages iii, 15, and 29)

Sparrow, E. M., Cess, R. D., 1961. The effect of a magnetic field on free convection heat transfer. International Journal of Heat and Mass Transfer 3 (4), 267–274. (Cited on page 25)

Srinivas, A. T., Bharti, R. P., Chhabra, R. P., 2009. Mixed convection heat transfer from a cylinder in power-law fluids: effect of aiding buoyancy. Industrial & Engineering Chemistry Research 48, 9735–9754. (Cited on pages 51, 67, 156, and 202)

Stevens, R., Van Der Poel, E., Grossmann, S., Lohse, D., 2013. The unifying theory of scaling in thermal convection: the updated prefactors. Journal of Fluid Mechanics 730, 295–308. (Cited on page 113)

Succi, S. Benzi, R., Higuera, H., 1991. The lattice boltzmann equation: A new tool for computational fluid-dynamics. Physica D: Nonlinear Phenomena 47, 219–230. (Cited on page 61)

Succi, S., Foti, E., Higuera, F., 1989. Three-dimensional flows in complex geometries with the lattice boltzmann method. Europhysics letter 10, 433–443. (Cited on page v)

Sukop, M. C., Throne, D. T., 2005. Lattice Boltzmann Modeling. Springer . (Cited on pages 3, 7, 61, 77, 78, 79, 80, 83, and 88)

Taghikhani, M. A., Najafkhani, H., 2013. Investigation of magnetic field effect on natural convection flow using fast $\psi - \omega$ method. International Research Journal of Applied and Basic Sciences 4 (10), 2939–2949. (Cited on page 27)

Tang, G. H., Tao, W. Q., He, Y. L., 2005. Thermal boundary condition for the thermal lattice boltzmann equation. Physical Review E 72 (016703), 1–6. (Cited on page 70)

Teamah, M., Dawood, M., El-Maghlany, W., 2011. Double diffusive natural convection in a square cavity with segmental heat sources. European Journal of Scientific Research54 (2), 287–301. (Cited on pages 17 and 21)

Tian, F. B., Bharti, R. P., Xu, Y. Q., 2014. Deforming-spatial-domain/stabilized space-time (dsd/sst) method in computation of non-newtonian fluid flow and heat transfer with moving boundaries. Computational Mechanics 53 (2), 257–271. (Cited on page 156)

Tuhkala, M., Juuti, J., Jantunen, H., 2014. Determination of complex permittivity of surfactant treated powders using an open-ended coaxial cavity resonator. PhD Thesis256, 140–145. (Cited on page 33)

Turki, S., Abbassi, H., Nasrallah, S., 2003a. Effect of the blockage ratio on the flow in a channel with a built-in square cylinder. Computational Mechanics 33, 22–29. (Cited on pages 39 and 44)

Turki, S., Abbassi, H., Nasrallah, S., 2003b. Numerical simulation of mixed convection heat transfer in a horizontal channel with built-in square cylinder. International Journal of Thermal Sciences 42, 1105–1113. (Cited on pages 39 and 44)

Vafai, K., Ettefagh, J., 1990a. The effects of sharp corners on buoyancy-driven flows with particular emphasis on outer boundaries. International Journal of Heat and Mass Transfer 33 (10), 2311–2328. (Cited on page 29)

Vafai, K., Ettefagh, J., 1990b. Thermal and fluid flow instabilities in buoyancy-driven flows in open-ended cavities. International Journal of Heat and Mass Transfer 33 (10), 2329–2344. (Cited on page 29)

Vahala, G., Pavlo, P., Vahala, L., Martys, N. S., 1998. Thermal lattice-boltzmann model (tlbm) for compressible flows. International journal of Modern Physics C 9 (8), 1247–1261. (Cited on page 70)

Varol, Y., Koca, A., Oztop, H. F., Avci, E., 2008. Analysis of adaptive-network-based fuzzy inference system (anfis) to estimate buoyancy-induced flow field in partially heated triangular enclosures. Expert Systems with Applications 35, 1989–1997. (Cited on pages iv and 34)

Varol, Y., Oztop, H., Koca, A., 2010. Effects of inclination angle on conduction-natural convection in divided enclosures filled with different fluids. International Communications in Heat and Mass Transfer 37, 182–191. (Cited on pages 24 and 34)

Varol, Y., Oztop, H. F., Koca, A., Ozgen, F., 2009a. Lattice boltzmann simulation of natural convection in an open ended cavity. International Journal of Heat and Mass Transfer 29, 340–350. (Cited on page 31)

Varol, Y., Oztop, H. F., Pop, I., 2009b. Natural convection in a diagonally divided square cavity filled with a porous medium. International Journal of Thermal Sciences 48, 1405–1415. (Cited on pages 20 and 22)

Watari, M., Tsutahara, M., 2004. Possibility of constructing a multispeed bhatnagar-gross-krook thermal model of the lattice boltzmann method. Physical Review E 70 (016703), 1–9. (Cited on page 70)

Wittwer, J., 2004. Monte carlo simulation basics. http://vertex42.com/ ExcelArticles/mc/MonteCarloSimulation.html. (Cited on page 8)

Wolfram, S., 1986. Cellular automaton fluids. 1: Basic theory. Journal of Statistical Physics 71 (1), 471–526. (Cited on page 77)

Yang, S., Fu, W.-S., 2001. Numerical investigation of heat transfer from a heated oscillating rectangular cylinder in a cross flow. Numerical Heat Transfer, Part A: Applications 39, 569–591. (Cited on page 45)

Yang, Z., 2013. Lattice boltzmann outflow treatments: Convective conditions and others. Computers and Mathematics with Applications 65, 160–171. (Cited on page 76)

Yesiloz, G., Aydin, O., 2011. Natural convection in an inclined quadrantal cavity heated and cooled on adjacent walls. Experimental Thermal and Fluid Science 51, 1169–1176. (Cited on pages 22 and 23)

Yoon, D.-H., Yang, K.-S., Choi, C.-B., 2012. Three-dimensional wake structures and aerodynamic coefficients for flow past an inclined square cylinder. Journal of Wind Engineering and Industrial Aerodynamics 101, 34–42. (Cited on page 41)

Yu, H., Zhao, K., 2000. Lattice boltzmann method for compressible flows with high mach numbers. Physical Review E 61 (4), 3867–3870. (Cited on page v)

Yu, P. X., Qiu, J. X., Qin, Q., Tian, Z. F., 2013. Numerical investigation of natural convection in a rectangular cavity under different directions of uniform magnetic field. International Journal of Heat and Mass Transfer 67, 1131–1144. (Cited on page 25)

Yu, Z., Hu, Y., Fan, L. W., Cen, K. F., 2010a. A parametric study of prandtl number effects on laminar natural convection heat transfer from a horizontal circular cylinder to its coaxial triangular enclosure. International journal of Computation and Methodology 58, 37–41. (Cited on page 20)

Yu, Z., Hu, Y., Fan, L. W., Cen, K. F., 2010b. Prandtl number dependence of laminar natural convection heat transfer in a horizontal cylindrical enclosure with an inner coaxial triangular cylinder. International journal of Computation and Methodology 53, 1333–1340. (Cited on page 20)

Yu, Z., Wang, W., Fan, L., Hu, Y.C.and Cen, K., 2011. A numerical investigation of transient natural convection heat transfer of aqueous nanofluids in a differentially heated square cavity. International Journal of Heat and Mass Transfer 38, 585–589. (Cited on page 113)

Yucel, N., Turkoglu, H., 1994. Natural convection in rectangular enclosures with partial heating and cooling. Heat and Mass Transfer 29, 471–477. (Cited on pages 22, 24, and 29)

Zamora, B., Kaiser, A. S., 2014. 3d effects in numerical simulations of convective flows in cubical open cavities. International Journal of Thermal Sciences 77, 172–185. (Cited on page 33)

Zdravkovich, M. M., 1997a. Flow around circular cylinders: Fundamentals. Oxford University Press, New York vol.1. (Cited on pages iv and 38)

Zdravkovich, M. M., 1997b. Flow around circular cylinders: Fundamentals. Oxford University Press, New York vol.2. (Cited on pages iv and 38)

Zhang, R., Chen, H., 2003. Lattice boltzmann method for simulations of liquid-vapor thermal flows. Physical Review E 67 (066711), 1–6. (Cited on page 70)

Zhi-Qiang, Z., Jie, P., 2005. Simulation of non-newtonian (power-law) fluid flow past a row of square cylinders. Computational Mechanics 35, 342–351. (Cited on page 47)

Ziegler, D. P., 1993. Boundary conditions for lattice boltzmann simulations. Journal of Statistical Physics 71, 1171–1177. (Cited on pages 76 and 77)

Zou, Q., He, X., 1997. On pressure and velocity boundary conditions for the lattice boltzmann BGK model. Physics of Fluids 9, 1591–1598. (Cited on pages 76, 79, and 80)